

# Epigenetic analysis of human $\gamma\delta$ T lymphocytes



## Dissertation

Zur Erlangung des Doktorgrades  
der Mathematisch-Naturwissenschaftlichen Fakultät  
der Christian Albrechts Universität  
zu Kiel

vorgelegt von

**Jaydeep Bhat**

Kiel, 2017

First referee: Prof. Dr. Dr. Thomas Bosch

Second referee: Prof. Dr. Dieter Kabelitz

Date of the oral examination: 14.03.2017

Approved for publication: 14.03.2017

***Dedicated to...***

My parents, family members and teachers (Guru)...

*“I have no special talents. I am only passionately curious.”*

- Albert Einstein

## Content

<b>1. Introduction</b>	<b>1 - 32</b>
1.1 The immune system: Basics and disease-associated dysfunction	1
1.1.1 Conventional and non-conventional human T lymphocytes	1
1.1.2 T-cell development and TCR repertoire	1
1.1.3 Antigen recognition and functional diversity	3
1.1.4 Receptors and ligands of human $\gamma\delta$ T lymphocytes	7
1.1.5 NKG2D receptor - ligand system	8
1.1.5.1 NKG2D ligand-mediated tumor immune escape mechanisms	9
1.1.5.2 Clinical implications and therapeutic aspects of NKG2D ligand release and shedding	11
1.2 Epigenetics of T-cells	12
1.2.1 Basic overview of epigenetic regulation	12
1.2.2 ‘Millions of minorities’ constitute epigenetic landscape	12
1.2.2.1 Chromatin packaging and nucleosome positioning	13
1.2.2.2 Chromatin remodeling and histone proteins	14
1.2.2.3 Histone modifications	16
1.2.2.3.1 Histone acetylation - deacetylation	16
1.2.2.3.2 Histone (de)methylation and other PTM	18
1.2.3 DNA methylation and hydroxymethylation	19
1.2.4 Gene regulation at the level of RNA expression	21
1.3 Technological advancements in T cell epigenetic research	23
1.3.1 (Epi)genome-wide analysis using chip-arrays and sequencing technology	24
1.3.2 Analysis of (epi)genomic data	27
1.3.2.1 Bioinformatic workflow and tools	27
1.3.2.2 Epigenomic features and CpG Island features	29
1.3.2.3 Integrated analysis: The multi-omic approach	31
<b>2. Aims and objectives of the thesis</b>	<b>33</b>

<b>3. Materials</b>	<b>34 - 53</b>
3.1 Biological materials	34
3.1.1 Tumor cells	34
3.1.2 Peripheral blood from healthy individuals	34
3.1.3 Peripheral blood samples from $\gamma\delta$ -HSTCL patient	37
3.1.4 T-cell subset purification and purity	38
3.2 Reagents, chemicals and culture mediums	40
3.2.1 Reagents	40
3.2.1 Culture mediums and kits	42
3.2.2 Antibodies for western blotting, flow cytometry, immunoprecipitation and Imaging	43
3.3 Primers used	47
3.4 Buffers and biochemical solutions	50
3.5 Laboratory consumables, equipment and software	52
<b>4. Methods</b>	<b>54 - 69</b>
4.1 Cell biological and immunological methods	54
4.1.1 Cell cultures	54
4.1.1.1 Maintenance of tumor cells	54
4.1.1.2 Tumor cell culture	54
4.1.1.3 Isolation of peripheral blood mononuclear cells and preparation of antigen-activated T-cell lines	54
4.1.1.4 Isolation of T-cell subsets	55
4.1.2 Functional assay set-up	55
4.1.2.1 Co-culture assays and assays for soluble versus immobilized NKG2D ligands	55
4.1.2.2 Assay for H3K9ac analysis	56
4.1.2.3 Cell death analysis assays	56
4.1.3 Proliferation assay by $^3\text{H}$ -thymidine incorporation	56
4.1.4 Flow cytometry	57
4.1.4.1 Basic flow cytometry protocol	57

4.1.4.2	NKG2D ligand expression on tumor cells by flow cytometry	58
4.1.4.3	Immunophenotyping of cultured cells	58
4.1.4.4	Annexin-PI staining for cell death analysis	58
4.1.4.5	Flow cytometric sorting of T-cell populations for ATAC-seq	59
4.1.5	Analysis of culture supernatants for NKG2D ligand shedding (ELISA)	59
4.2	Biochemical methods	60
4.2.1	Isolation of exosomes	60
4.2.2	(s)MICA/B immunoprecipitation	60
4.2.3	Immunoblotting	60
4.3	ImageStream analysis	61
4.4	Molecular biological and epigenetic methods	62
4.4.1	Quantification of mRNA expression	62
4.4.2	ATAC-seq library preparation	62
4.4.3	DNA extraction, bisulfite conversion and DNA methylation analysis	63
4.4.4	RNA extraction, quality control and library preparation	63
4.5	Bioinformatic analysis	64
4.5.1	Bioinformatics analysis of IL-4, CASP3, MLKL and HDAC1	64
4.5.2	Analysis of ATAC-seq data	64
4.5.3	Analysis of DNA methylation data	65
4.5.4	Healthy T cell methylome	66
4.5.5	$\gamma\delta$ -HSTCL methylome	66
4.5.6	Analysis of RNA-seq	67
4.5.6.1	Transcriptome analysis	67
4.5.6.2	Long non-coding RNA analysis	67
4.5.6.3	miRNA analysis	67
4.5.7	Integrated analysis of ATAC-seq, DNA methylation and RNA-seq data	68
4.5.8	Functional annotation	69
4.6	Statistical analysis	69

	<b>Content</b>
<b>5. Results</b>	<b>70 - 141</b>
5.1 Release of NKG2D ligands from tumor cells: <i>Exosomes versus shedding</i>	70
5.1.1 Expression and release of MICA depends on origin of tumor cell type	70
5.1.2 MICA antibody specifically detects full-length (truncated) form of protein	71
5.1.3 Pancreatic carcinoma shed MICA in culture supernatant	72
5.1.4 Prostate cancer cell lines release MICA through exosomes	73
5.2 Epigenetic modulation of NKG2D receptor and ligands:	
<i>Mechanism of NKG2D ligand release and functional effects</i>	75
5.2.1 Epigenetic modifiers differentially modulate NKG2D ligand surface expression and release from pancreatic carcinoma and prostate carcinoma cells	75
5.2.2 VPA affects NKG2D receptor expression differentially on the cell surface of activated $\gamma\delta$ T-cells and freshly isolated PBMC	80
5.2.3 VPA regulates mRNA expression of the NKG2D receptor and its ligands	82
5.2.4 Flow cytometric analysis of H3K9 acetylation at the single cell level	85
5.3 Functional implications of epigenetic modulators on healthy human $\gamma\delta$ T-cells:	
<i>Modulation of human <math>\gamma\delta</math> T-cell activation and phenotype by histone deacetylase inhibitors</i>	89
5.3.1 Dose-dependent inhibition of T-cell proliferation by VPA	89
5.3.2 Inhibitory concentrations of VPA induce cell death	92
5.3.3 Subset specific cytotoxicity of VPA for human $\gamma\delta$ T lymphocytes	93
5.3.4 Toxic concentrations of VPA selectively down-regulate T-cell surface markers	94
5.3.5 Cell death-inducing concentrations of VPA modulate histone acetylation in human $\gamma\delta$ T-cells	96
5.4 Functional implications of epigenetic modulators on healthy human $\gamma\delta$ T-cells:	



<i>Generation of intracellular cytokine variants and association with cell death</i>	98
5.4.1 HDACi induces IL-4 $\delta_{13}$ in human $\gamma\delta$ T-cells	98
5.4.2 Differential changes in secretory vs non-secretory forms of IL-4	101
5.4.3 Cell death pathway inhibitors modulate IL-4 $\delta_{13}$ induction and histone modification	104
5.4.4 Interplay of IL-4 $\delta_{13}$ with c-Jun expression and histone acetylation	105
5.5 Comprehensive epigenetic landscape of human $\gamma\delta$ T-cells:	
<i>Chromatin accessibility, DNA methylation and total RNA analysis</i>	109
5.5.1 DNA methylome segregates T-cell subsets	109
5.5.2 $\gamma\delta$ T cells share distinct DNA methylation patterns with $\alpha\beta$ T cells	113
5.5.3 Genomic and epigenomic features form the basis for the $\gamma\delta$ T-cell methylation pattern	114
5.5.4 Functional validation of T cell-specific DNA methylome	116
5.5.5 Gene expression profile represents differential regulation of $\gamma\delta$ T cells	118
5.5.6 $\gamma\delta$ T cells share a discrete regulatory RNA (miRNA and lncRNA) profile	119
5.5.7 Nucleosome positioning and differential chromatin accessibility support $\gamma\delta$ T-cell subset specification	124
5.5.8 A set of genes integrating $\gamma\delta$ T cell-specific DNA methylation and the RNA expression profile forms the basis for $\gamma\delta$ T cell immune function	127
5.6: Epigenetic modification of human $\gamma\delta$ T-cells in malignancy:	
<i>A case report of an hepatosplenic gamma/delta T-cell lymphoma patient responding to Interferon-<math>\alpha</math> treatment</i>	133
5.6.1 Clinical representation of a $\gamma\delta$ -HSTCL patient	133
5.6.2 Time-dependent changes in DNA methylation	135
5.6.3 Interferon- $\alpha$ therapy induces differential methylation over time	135
5.6.4 Genomic- and CpG Island (CGI) - features support changes in malignant $\gamma\delta$ T cell DNA methylome due to Interferon- $\alpha$ therapy	137
5.6.5 Biological association of differential methylation pattern upon IFN $\alpha$ 2c-treatment	139

	<b>Content</b>
<b>6. Discussion and conclusion</b>	<b>142 - 163</b>
6.1 Release of NKG2D ligands from tumor cells: <i>Exosomes versus shedding</i>	142
6.2 Epigenetic modulation of NKG2D receptor and ligands: <i>Mechanism of NKG2D ligand release and functional effects</i>	144
6.3 Functional implications of epigenetic modulators on healthy human $\gamma\delta$ T-cells: <i>Modulation of human <math>\gamma\delta</math> T-cell activation and phenotype by histone deacetylase Inhibitors</i>	148
6.4 Functional implications of epigenetic modulators on healthy human $\gamma\delta$ T-cells: <i>Generation of intracellular cytokine variants and association with cell death</i>	152
6.5 Comprehensive epigenetic landscape of human $\gamma\delta$ T-cells: <i>Chromatin accessibility, DNA methylation and total RNA analysis</i>	156
6.6 Epigenetic modification of human $\gamma\delta$ T-cells in malignancy: <i>A case report of an hepatosplenic gamma/delta T-cell lymphoma patient responding to Interferon-<math>\alpha</math> treatment</i>	162
<b>7. Future perspectives</b>	<b>164</b>
<b>8. Summary</b>	<b>165</b>
<b>9. Zusammenfassung</b>	<b>166</b>
<b>10. References</b>	<b>168</b>
<b>11. Appendix</b>	<b>193 - 198</b>
11.1 Acknowledgement	193
11.2 Curriculum vitae	195
11.3 Declaration	198

## Abbreviations

<sup>3</sup> H-TdR	3H-thymidine
5hmC	5-hydroxymethylcytosine
5mC	5-methylcytosine
ADAM	A disintegrin and metalloproteases
ATAC-seq	Assay for Transposase-Accessible Chromatin using sequencing
BrHPP	Bromohydrin pyrophosphate
BTN3A1	Butyrophilin, subfamily 3, member A1
CASP3	Caspase 3
CD	Cluster of differentiation
CDP-ME	4-diphosphocytidyl-2-C-methyl-D-erythritol
CDP-MEP	4-diphosphocytidyl-2-C-methyl-D-erythritol 4-phosphate
CGI	CpG Island
DEG	Differentially expressed genes
DMAPP	Dimethylallyl pyrophosphate
DMG	Differentially methylated genes
DANN	Deoxyribonucleic acid
DNMT	DNA methyltransferases
DOXP	1-deoxy-D-xylulose 5-phosphate
ELISA	Enzyme-linked immunosorbent assay
FPP	Farnesyldiphosphate
GO	Gene ontology
HAT	Histone acetyl transferase
HDAC1	histone deacetylase 1
HDACi	histone deacetylase inhibitor
HLA	Human Luekocyte antigen
HMB-PP	(E)-4-hydroxy-3-methyl-but-2-enyl-pyrophosphate
HMG-CoA	3-hydroxy-3-methylglutaryl-coenzyme A
HSTCL	Hepatosplenic T-cell lymphoma
IFNa2c	Interferon- $\alpha$ 2c
IFNg	Interferon- $\gamma$
Ig	Immunoglobulin
IL	Interleukin
IU	International Unit
JMJD	Jumonji Domain containing protein
Kb	Kilo bases
KDa	Kilo Dalton
lncRNA	Long non-coding RNA
MAPK1	Mitogen-activated protein kinase 1

## Abbreviations

MDS	Multidimensional scaling
MEcPP	2-C-methyl-D-erythritol 2,4-cyclopyrophosphate
MEP	2-C-methyl-D-erythritol 4-phosphate
MICA	MHC class I chain-related protein A
MICB	MHC class I chain-related protein B
miRNA	MicroRNA
MLKL	Mixed lineage kinase domain like protein
MMP	Matrix metalloproteases
N-BP	Nitrogen-containing bisphosphonates
NCR	Natural cytotoxicity receptor
Nec1	Necrostatin-1
NFR	Nucleosome free regions
NGS	Next-Generation sequencing
NK cell	Natural killer cell
NKG2D	Natural-killer group 2, member D (receptor protein)
NKG2DL	Ligands for Natural-killer group 2, member D protein receptor
NSA	Necrosulfonamide
P	Phosphate
pAg	Phosphoantigen
PBMC	Peripheral Blood Mononuclear Cells
PCA	Principal component analysis
PHA	Phytohaemagglutinin
PI	Propidium Iodide
PTM	Post-translational modification
RNA	Ribonucleic acid
s.c.	Sub-cutaneous
SDS-PAGE	Sodium dodecyl sulfate-Polyacrylamide gel electrophoresis
SE	Staphylococcal Enterotoxin
SNP	Single-nucleotide polymorphisms
TCR	T-cell receptor
TET	Ten eleven translocation
TLR	Toll-like receptor
TSA	Trichostatin A
TSS	Transcription start site
ULBP	UL16-binding proteins
VPA	Valproic acid
VPM	Valpromide
zVAD	Z-Val-Ala-DL-Asp-fluoromethylketone

## 1. Introduction

### 1.1 The immune system: Basics and disease-associated dysfunction

#### 1.1.1 Conventional and non-conventional human T lymphocytes

Hematopoietic stem cells (HSC) have the capacity to undergo lineage commitment producing myeloid cells (monocytes, macrophages) through common myeloid progenitors (CMP) or lymphoid cells (T cells, B cells and NK cells) through common lymphoid progenitors (CLP). Broadly, humoral immunity provided by B cells and cell-mediated immunity provided by T cells are collectively termed '*adaptive*' immunity. The cells involved in primary immune responses or first line of defense like NK cells, mast cells and other leukocyte subsets including monocytes and dendritic cells are considered as '*innate*' immune cells. Usually, '*conventional T cells*' are T cells expressing the  $\alpha\beta$  T-cell receptor (TCR) repertoire. Peptide antigen recognition and major histocompatibility complex (MHC) restriction of  $\alpha\beta$  T cells have been studied in depth and were initially found to be central to immune responses. In the mid-1980s, T cells with distinct  $\gamma\delta$  TCR rearrangements, non-peptide antigen recognition and non-MHC restriction were discovered and termed '*non-conventional T cells*'. In addition to this classification of T cells based on the TCR repertoire and MHC restriction, another immune subset of importance are invariant natural killer T (iNKT) cells, which share phenotypic and functional characteristics of T cells and features of NK cells (Roberts and Girardi, 2008).  $\gamma\delta$  T cells links functional immune responses of innate and adaptive cells (Holtmeier and Kabelitz, 2005). To define T-cell subsets, they are usually characterized based on their '*cluster of differentiation*' (CD) antigen profile.

#### 1.1.2 T-cell development and TCR repertoire

In the thymus, nurse cells select lymphocytes to differentiate them into T cells. Through a series of developmental checkpoints and commitment events, mature T cells are generated. Thus, only after education and training (positive and negative selection), T cells are ready to leave the thymus "school". Following the process of intrathymic TCR gene rearrangement, mature T cells express a diverse TCR repertoire, which categorizes them as  $\alpha\beta$  T cells or  $\gamma\delta$  T cells. However, the process of T cell development and TCR gene rearrangement gives rise to three functionally distinct T cell subsets including,  $CD4^+\alpha\beta$  T cells,  $CD8^+\alpha\beta$  T cells and  $\gamma\delta$  T cells.

Thymocyte development is divided into four stages (Fig. 1.1A) according to the expression of surface markers: double negative (DN), immature single positive (ISP), double positive (DP) and

single positive (SP). The DN stage is separated into 4 populations (I-IV), where early thymocytes acquire differential expression of CD34, CD38 and CD1a. Following CD1a expression for T cell lineage commitment, cells pass through the CD4<sup>+</sup> ISP stage. Next, CD3<sup>-</sup> cells enter the CD4<sup>+</sup>CD8 $\alpha$ <sup>+</sup> early DP and CD4<sup>+</sup> CD8 $\alpha$ <sup>+</sup>CD8 $\beta$ <sup>+</sup> DP blast stage. Soon after,  $\beta$  selection occurs leading to the rearrangement of the TCR $\alpha$  locus and giving rise to the TCR $\alpha\beta$ <sup>+</sup> DP stage. TCR $\alpha\beta$ <sup>+</sup>DP cells develop into SP with mature CD4 and CD8 cells and undergo positive and negative selection.  $\gamma\delta$  T cells are DN T cells and have the potential to emerge from the DN, ISP or early DP stage of T-cell development (Joachims *et al*, 2006).  $\beta$ -selection is the process, by which a rearranged nascent TCR $\beta$  chain successfully pairs with the pre-TCR $\alpha$  (pT $\alpha$ ) protein and CD3 molecules forming the pre-TCR complex allowing for the transmission of a selective signal for survival, expansion and allelic exclusion (Spits 2002; Michie *et al*, 2002).

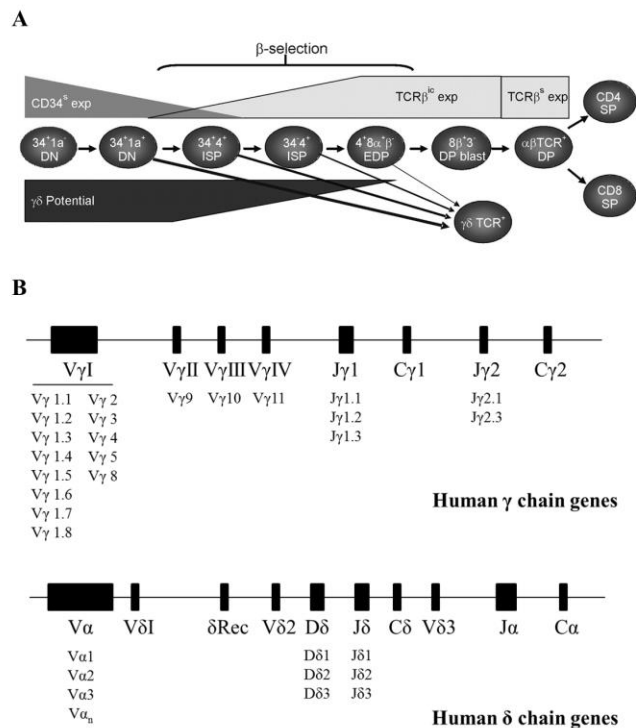


**Figure 1.1: Stages of T-cell development and germline organization of the human TCR  $\gamma$  and  $\delta$  gene loci.** (A) Four distinct stages (DN, ISP, DP and SP) through which immature thymocytes develop and give rise to either TCR $\alpha\beta$ <sup>+</sup> CD4 and CD8 T cells or TCR $\gamma\delta$ <sup>+</sup> T cells (Figure adopted from Joachims *et al*, 2006). (B) Recombination of individual gene segments from variable (V), constant (C), diversity (D) and joining (J) elements leads to the rearrangement of a distinct TCR  $\gamma$  or  $\delta$  chain. This TCR  $\gamma\delta$  rearrangement gives rise to functionally diverse  $\gamma\delta$  T cell subsets.

The diversity of TCR gene rearrangement in  $\alpha\beta$  or  $\gamma\delta$  T cells occurs in the third complementary determining region (CDR3) and is generated due to the possibility of V(D)J recombination at genomic region of diverse variable (V), constant (C), diversity (D) and joining (J) segments. Human  $\alpha$ ,  $\beta$ ,  $\gamma$  and  $\delta$  chain gene segments are located on chromosome 7 and 14 ( $\delta$  chain within  $\alpha$  chain gene segments). Three completely different models have been proposed to explain the role of TCR gene rearrangement during T-cell development. The ‘instructive model’ is based on the formation of TCR $\gamma\delta$  to develop into  $\gamma\delta$  T cells from bipotent  $\alpha\beta/\gamma\delta$  T cell precursors and similarly formation of pre-TCR complex for  $\alpha\beta$  T cells. The ‘stochastic’ or ‘separate lineage’ model uses predefined rearrangement of the TCR genes with lineage commitment defined by other factors such as IL-7R expression or Notch signaling. The most widely accepted model is the ‘signal strength’ model. According to this model, the choice of  $\alpha\beta$  or  $\gamma\delta$  T cells depends on the strength of the pre-TCR signal. Stronger signals lead to  $\gamma\delta$  T-cell development, while weaker signals generate  $\alpha\beta$  T cells (Joachims *et al*, 2006).

The peripheral T-cell compartment comprise of  $\alpha\beta$  T cells (~95 %) and  $\gamma\delta$  T cell (~5 %) of total CD3<sup>+</sup> T cells. Depending on the further usage of gene segments during TCR $\gamma\delta$  gene rearrangement (as illustrated in Figure 1.1B) and tissue-localization (Vroom *et al*, 1991),  $\gamma\delta$  T cells are further classified as V $\delta$ 1, V $\delta$ 2 or V $\delta$ 3 T cells, pairing with various V $\gamma$  gene elements (Vantourout and Hayday, 2013). V $\delta$ 2 T cells are predominantly found in peripheral blood and V $\delta$ 2 often pairs with V $\gamma$ 9 (so called V $\gamma$ 9V $\delta$ 2 T cells), while V $\delta$ 1 and V $\delta$ 3 T cells are localized in mucosal tissues such as intraepithelial lymphocytes (IELs).

### **1.1.3 Antigen recognition and functional diversity**

$\alpha\beta$  or  $\gamma\delta$  T cells follow completely different antigen recognition and activation pathways. The TCR complex in association with other coreceptors leads to T-cell activation. Typically, the TCR $\alpha\beta$  forms a complex with CD3 $\epsilon\gamma$  and CD3 $\epsilon\delta$  heterodimers, and a TCR $\zeta\zeta$  homodimer. Depending on the presence of CD4 or CD8 coreceptor, the T cell interacts with peptide- MHC class I or II molecules present on antigen-presenting cells (APC). Followed by this ‘signal 1’, a costimulatory ‘signal 2’ is provided by respective B7 (CD80/CD86) or CD40 proteins on APC which are ligands for CD28 or CD40L on T cells. ‘Signal 3’ by cytokines activates a cascade of downstream signaling events, ultimately culminating in  $\alpha\beta$  T-cell activation (Lenschow *et al*, 1996; Davis, 2002; Choudhuri *et al*, 2005; Han *et al*, 2012).

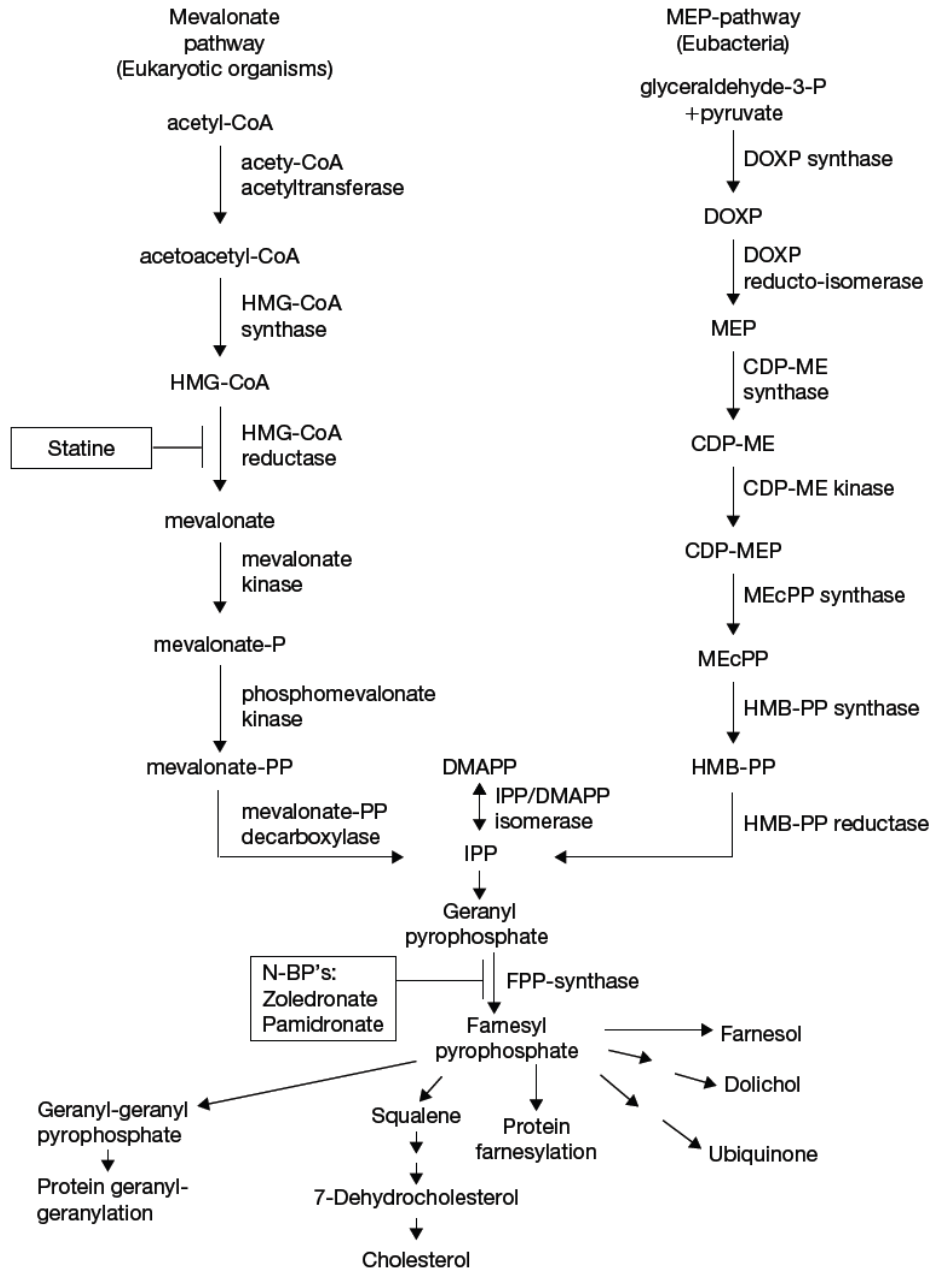


**Figure 1.2: Classical isoprenoid biosynthesis pathway.** In eukaryotic organisms, isopentenyl pyrophosphate (IPP) is generated using the classical mevalonate pathway, while its corresponding pathway in eubacteria is referred to as the non-mevalonate or Rohmer or DOXP pathway. IPP generation through further enzymatic reactions is required for additional biochemical processes such as cholesterol biosynthesis, protein geranyl-geranylation. (Figure adopted from Holtmeier and Kabelitz, 2005).

As  $\gamma\delta$  T cells do not recognize peptide antigens in an MHC-dependent manner, they do not follow the classical T-cell activation process as described above. Moreover, antigen-presenting



proteins mediating  $\gamma\delta$  T-cell activation are under investigation.  $\gamma\delta$  T cells recognize and are activated by non-peptide ligands including isopentenyl pyrophosphate (IPP), nitrogen-containing bisphosphonates and alkylamines. The “classical” mevalonate pathway (MVA pathway; Fig. 1.2) is used in eukaryotes, archaeobacterial and certain eubacteria for IPP generation. Another pathway called non-mevalonate, Rohmer, the 2-C-methyl-d-erythritol 4-phosphate (MEP) or DOXP pathway is used in many eubacteria, the plastids of algae and higher plants. Naturally occurring agonists for  $\gamma\delta$  T cells like, IPP and dimethylallyl pyrophosphate (DMAPP) are collectively called phosphoantigens (pAg). However, HDMAPP or its synthetic compound, cHDMAPP (or ‘picostim’) are the most potent  $\gamma\delta$  T-cell activators with bioactivity around 100 pM, which is 30,000 times higher than that of endogenously produced IPP.  $\gamma\delta$  T-cell activation can also be induced by the clinically used nitrogen-containing bisphosphonates, such as zoledronic acid. Nonetheless, the statins, inhibitors of HMG-CoA reductase do substantially decrease  $\gamma\delta$  T cell activation (Holtmeier and Kabelitz, 2005).

Although  $\gamma\delta$  T cells do not require MHC molecules for antigen presentation, a related function has recently been shown for butyrophilin 3A (BTN3A) or CD277 molecule present on antigen-presenting cells or tumor cells. CD277 is absolutely required for pAg-dependent  $\gamma\delta$  T cell activation and anti-tumor immune responses (Harly, *et al*, 2012). Of note, the molecular mechanism that governs BTN3A-mediated pAg presentation is not yet completely clear. Genomic organization also supports the role of BTN3A molecules, as BTN genes are located in the extended MHC region on human chromosome 6 (Rhodes, *et al*, 2001; Riano *et al*, 2014). Reports on the role of BTN3A in  $\gamma\delta$  T cell activation have proposed three hypothetical models (Harly *et al*, 2015). In an outside-in model (Fig. 1.3A-a), internal pAg or external pAg that are brought in by transporters interact with the intracellular B30.2 domain of BTN3A1 (Sandstrom *et al*, 2014). Contradicting results indicate an inside-out model (Fig. 1.3A-b) that proposes that pAg are produced inside and are transported out through transporters (Vavassori *et al*, 2013 *Nat Immunol*). In this model, the extracellular domain of BTN3A1 serves as antigen-presenting molecule. A third model (Fig. 1.3A-c) is hypothetically based on the combination of both inside-out and outside-in signaling. Despite these alternate models, it is clear that pAg produced by microbes and tumor cells are recognized by  $\gamma\delta$  T cells.

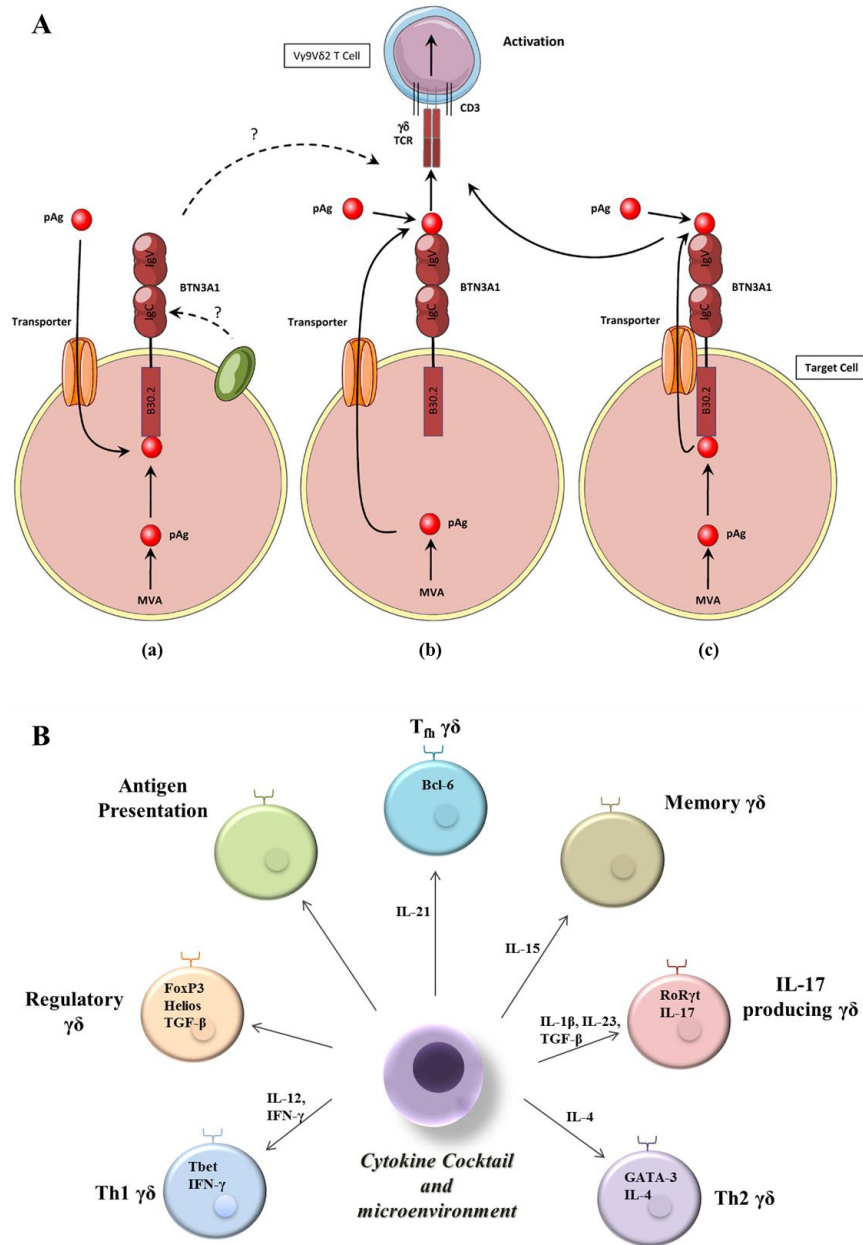


**Figure 1.3: Proposed models for CD277/BTN3A-mediated human  $\gamma\delta$  T cell activation and  $\gamma\delta$  T cell functional plasticity.** (A) Three different hypothetical models have been proposed to explain the basis for phosphoantigen-recognition and activation of  $\gamma\delta$  T cells. Phosphoantigens are shown to be recognized by possibly three different modes (a) - (c) of signaling mediated by CD277/BTN3A1  $\gamma\delta$  T cell surface proteins (Figure adopted from Harly *et al*, 2015). (B) Upon antigen recognition and depending on the microenvironment provided,  $\gamma\delta$  T cells can be further differentiated into functional subsets including Th1-, Th2-, Th17-, follicular-, antigen presenting-, memory- and regulatory-  $\gamma\delta$  T cells based on supplemented cytokines and microenvironment.

The intrinsic property of pAg recognition by  $\gamma\delta$  T cells translates into potent anticancer activity against leukemias/lymphomas and various epithelial tumor cells, and thus has emerged as a promising tool for cancer immunotherapy (Kabelitz *et al*, 2013). Apart from their antitumor response,  $\gamma\delta$  T cells possess a surprising functional plasticity which includes follicular B-cell helper activity but also regulatory activity. T-cell subset differentiation is governed by a set of specific transcription factors and the local cytokine milieu. Under appropriate microenvironmental conditions, human  $\gamma\delta$  T cells can thus differentiate *in vitro* into Th1, Th2, Th17, Tfh and Treg lineages as similar to  $\alpha\beta$  T cells (Fig. 1.3B; Wesch *et al*, 2001; Ness-Schwickerath *et al*, 2010; Caccamo *et al*, 2012; Peters *et al*, 2014; Bansal *et al*, 2012; Brandes *et al*, 2009).

#### **1.1.4 Receptors and ligands of human $\gamma\delta$ T lymphocytes**

The capability to sense cellular stress and transformation events make  $\gamma\delta$  T cells an important component of immunosurveillance. In this scenario,  $\gamma\delta$  T cells recognize ligands on tumor or ‘transformed’ cells. These ‘self-ligands’ expressed on tumor cells include heat shock proteins (HSP) and F1-ATPase. For instance, human V $\gamma$ 9V $\delta$ 2 T cells recognize HSP60 expressed on oral tumor cells and show specific cytotoxicity against them (Laad *et al*, 1999). Mitochondrial F1-ATPase proteins expressed on tumor cells together with the delipidated form of apolipoprotein A-I (apo A-I) is also recognized by TCR V $\gamma$ 9V $\delta$ 2, which promotes tumor cell recognition and  $\gamma\delta$  T cell activation (Scotet *et al*, 2005). Though the antigens for V $\delta$ 1 activation are as yet largely unknown, a subset of V $\delta$ 1 T cells is reactive to CD1d- $\alpha$ -galactosylceramide ( $\alpha$ -GalCer; Uldrich *et al*, 2013).

Apart from these potent ligands expressed on target tumor cells, other costimulatory molecules like natural cytotoxicity receptors (NCR) and toll-like receptors (TLR) are known to affect immunomodulatory functions of  $\gamma\delta$  T cells. V $\delta$ 1 T cells derived from peripheral blood express NKp30, NKp44 and NKp46. Out of these NCR, NKp30-expressing V $\delta$ 1 T cells are specialized for the killing of leukemic cells (Correia *et al*, 2011). Moreover, TLR2, TLR3, TLR4, TLR7/9 and TLR 8 are expressed on  $\gamma\delta$  T cells and contribute to diverse immune cell functions (Dar *et al*, 2014).

### 1.1.5 NKG2D receptor - ligand system

Immune cells have the capacity to recognize not only infectious non-self and non-infectious self-antigens, but also ‘abnormal self’ antigens. Usually these abnormal self-antigens are proteins upregulated in response to viral infection, DNA damage or tumor transformation. Upon recognition, the functional response of T-cells results from the coordinated activity of a number of interconnected signaling molecules and pathways which are controlled by activating or inhibiting receptors and the release of cytokines and chemokines (Pegram *et al*, 2011). KIR/CD158, encoding killer Ig-like receptors and the NKG2A/CD94 heterodimers are inhibitory receptors expressed on NK cells, CD8 cells and  $\gamma\delta$  T-cells. NKG2D is one of the activating receptors involved in recognition of such induced self-proteins. NKG2D is a C-type, lectin-like, type II transmembrane glycoprotein, expressed on all human NK cells, NKT cells, CD8,  $\gamma\delta$  T cells and a small subset of CD4 T cells in humans (Spear *et al*, 2013). Apart from human and mice, they are also widely expressed in other mammals. Human NKG2D receptors recognize two families of NKG2D ligand proteins (Fig. 1.4 lower panel): the highly polymorphic MHC class I chain-related protein A (MICA) and B (MICB) family, the family of UL16-binding proteins (ULBP1-6). The NKG2D receptor - ligand axis plays an important role in  $\gamma\delta$  T cell-mediated cytotoxicity against a broad range of tumor cells (Wrobel *et al*, 2007; Nedellec *et al*, 2010) and immune cell development (Zafirova *et al*, 2011).

Depending on the interaction of activating or inhibitory receptors, a signal is transduced through intracellular immune-receptor tyrosine-based inhibitory motifs (ITIMs) or immune-receptor tyrosine-based activation motifs (ITAMs). Thus, in humans, NKG2D receptor - ligand binding sends a signal via the associated transmembrane adapter protein DAP10 using ITAMs (Pegram *et al*, 2011). DAP10 activates Grb2-Vav and activates phosphoinositide-3-kinase (PI3K), which delivers activation signals to enhance survival, cytotoxicity and co-stimulation of T cells. However, overstimulation by DAP10 leads to Fas/FasL-dependent Caspase-3/-7 activation. Activation of Caspase-3/-7 induces CD3 $\zeta$  degradation, which delivers inhibitory signals through FcR $\gamma$ , NCR and TCR molecules (Chitadze *et al*, 2013).

### 1.1.5.1 NKG2D ligand-mediated tumor immune escape mechanisms

In a typical immune editing process, immunosurveillance by effector cells such as NK cells or T cells leads to the elimination of malignant cells. Tumor cells that escape immunosurveillance might develop an immune-resistance phenotype. This further orchestrates tumor immune escape mechanisms to overcome the complete anti-tumor capacity of effector cells (Dunn *et al*, 2004). As the NKG2D receptor - ligand axis is one of the key signaling mechanisms for  $\gamma\delta$  T cell-mediated anti-tumor responses, tumors have also established the ability to express and release NKG2D ligands from the cell surface, referred to as 'shedding' (Waldhauer *et al*, 2008), as an escape mechanism. The release of NKG2D ligands in humans mainly differs among different tumor entities and uses different molecular mechanisms (Chitadze *et al*, 2013; Chitadze *et al*, 2013; Liu *et al*, 2010). Nevertheless, it is still under extensive investigation whether shedding of NKG2D ligands is beneficial or not for anti-tumor responses (Groh *et al*, 2002; Deng *et al*, 2015).

NKG2D ligand shedding is primarily mediated by three mechanisms (Fig. 1.4). In a first scenario, proteolytic cleavage is mediated by proteases (Fig. 1.4A) such as matrix metalloproteases-9 (MMP-9) and 'A disintegrin and metalloproteases'- 10/-17 (ADAM-10/-17). Substrate cleavage results both in a decrease of surface expression and the release of a soluble portion of the substrate. Moreover, ligands or proteins can be released through subcellular organelles like exosomes (Fig. 1.4B). Exosomes decorated with NKG2D ligands are released into outer microenvironment and further binds to effector cells, which could downregulate NKG2D receptor signaling. The prostate carcinoma cell line PC-3 (Chitadze *et al*, 2013), leukemia/lymphoma cells (Hedlund *et al*, 2011) and mature human DCs (Viaud *et al*, 2009) are reported to release NKG2D ligands via exosomes. In a human gastric cancer cell line model, ULBP1-3 are cleaved by phosphatidylinositol-specific phospholipase C (PI-PLC; Song *et al*, 2006; Fig. 1.4C). PI-PLC is specific to GPI-anchored ULBP-1, -2 and -3, which as an effect downregulate NKG2D-mediated cytotoxicity of effector cells.

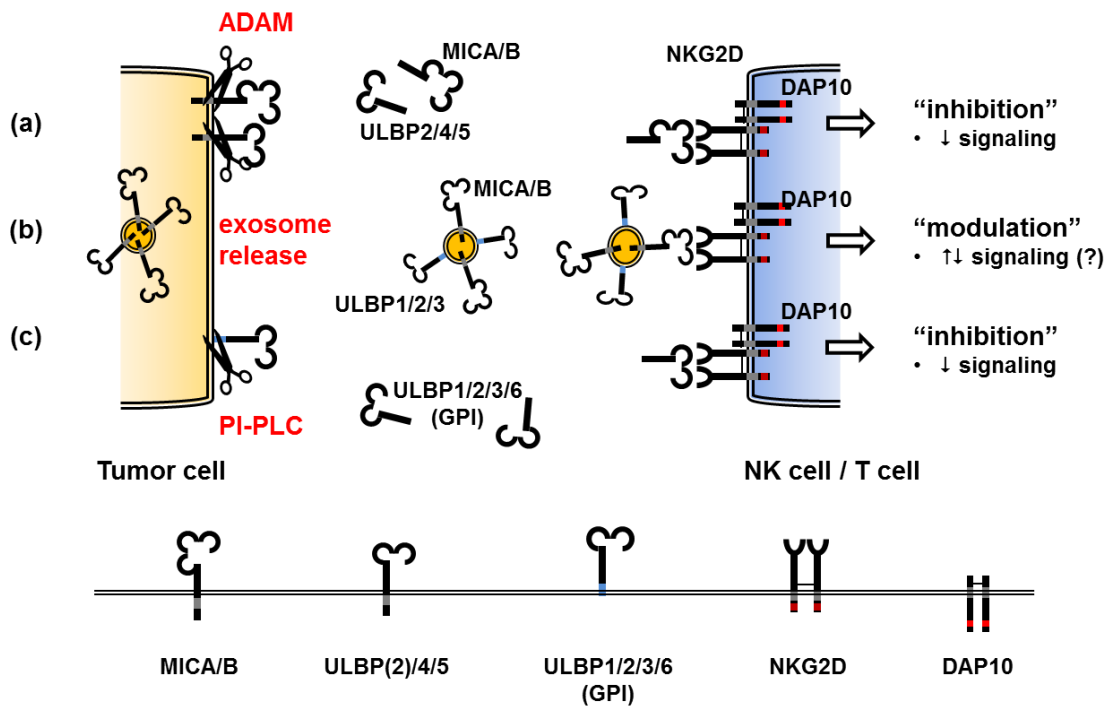


**Figure 1.4: Mechanisms of NKG2D ligand release from tumor cells.** NKG2D ligands can be released by any of the three mechanisms represented in the figure; NKG2D ligand cleavage by ADAM proteases (A), via exosomes (B) or by phosphatidylinositol-specific phospholipase C (PI-PLC) activity (C). The binding to the NKG2D receptor modulates functional activity of respective effector cells (Figures adopted from Chitadze *et al*, 2013).

Though shedded and soluble NKG2D ligands play a major role, other mechanisms might also contribute to the downregulation of NKG2D receptor signaling. For example, transforming growth factor- $\beta$ 1 (TGF- $\beta$ 1), interferon- $\beta$ 1 (IFN- $\beta$ 1), interleukin-21 (IL-21) all downregulate NKG2D receptor expression, while IL-2, IL-7, IL-12 and IL-15 trigger NKG2D upregulation (Lanier 2015). The modulation of NKG2D receptor signaling by these cytokines is also controlled by post-transcriptional modification. TGF- $\beta$ 1 upregulates miRNA-1245 expression, resulting in NKG2D receptor downregulation in NK cells and impaired cytotoxicity (Espinoza *et al*, 2012).

### 1.1.5.2 Clinical implications and therapeutic aspects of NKG2D ligand release and shedding

Persistent down-modulation of the NKG2D receptor leads to impaired effector cell activity. Apart from *in vitro* experiments, the impact of NKG2D ligand release has been very well corroborated in patients suffering from various types of cancer. Clinical data clearly underscores the association of tumor-derived or soluble NKG2D ligands with poor prognosis and disease outcome in patients with pancreatic cancer (Duan *et al*, 2011), prostate cancer (Wu *et al*, 2004), hepatocellular carcinoma (Kumar *et al*, 2012) and leukemia (Hilpert *et al*, 2012). To overcome this negative impact of NKG2D ligand(s) release in patient sera, a number of potential therapeutic approaches have been suggested. To this end, a super-agonist antibody targeting IL-15 and soluble MIC is shown to enhance the anti-tumor effect (Basher *et al*, 2016). In a clinical trial with melanoma patients, anti-MICA autoantibodies were induced as an effect of anti-CTLA-4 immunotherapy (Jinushi *et al*, 2006). Other suggested potential strategies include therapeutic agents targeting proteases such as ADAM-10/17 or ERp5 molecules. Also, antibodies opsonizing antigen presenting DCs to enhance cross presentation and antibody-dependent cell cytotoxicity (ADCC) to target membrane bound NKG2D ligand (Zhang *et al*, 2015). Recently, histone deacetylase inhibitors (HDACi) have emerged as potential anticancer drugs, which also serve as possible therapeutic approach to modulate NKG2D ligand expression and release in patients (Fionda *et al*, 2015).

## **1.2 Epigenetics of T-cells**

### **1.2.1 Basic overview of epigenetic regulation**

In 1892, the German biologist August Weismann proposed that genetic inheritance occurs through germ cells (concept of genotype and phenotype), while the famous French biologist, Jean-Baptiste Lamarck proposed the theory of inheritance of acquired characteristics. The theory of inheritance of acquired characteristic, also called “soft inheritance”, Lamarckism or theory of adaptation supports modern era ‘epigenetics inheritance’. It describes the phenomenon of inheritance of acquired features which can increase the adaptation of an organism to its environment (Haig, 2004; Haig, 2007). Addressing the view on classical controversies in embryology, Conrad Waddington wrote in his book, ‘An introduction to Modern Genetics’, “... *but equally it is clear the interaction of these constituents (of the fertilized eggs) gives rise to new type of tissue and organ which were not present originally, and in so far development must be considered as ‘epigenetics’*” (Waddington, 1939 [p.156]). Thus, he introduced the term ‘epigenetics’ for such non-genetic mechanisms as “*the branch of biology which studies the causal interactions between genes and their products, which bring the phenotype into being*” (Waddington, 1942).

Throughout the last decades scientists have come up with different views on and various definitions of epigenetics. The current definition of epigenetics has evolved as, “*the study of changes in gene function that are mitotically and/or meiotically heritable and that do not entail a change in DNA sequence*” (Wu and Morris, 2001). Nonetheless, epigenetics, in a broader sense, is a bridge between genotype and phenotype. For instance, multicellular organisms exhibit identical genotypes, but the functional diversity of processes specifies a unique cell-type depending on the context. This vast capacity of (cellular differentiation by) epigenetic mechanisms controls heritable changes in gene expression or cellular phenotype and is described as “epigenetic landscape” (Goldberg *et al*, 2007).

### **1.2.2 ‘Millions of minorities’ constitute epigenetic landscape**

To understand Waddington’s ‘epigenetic landscape’, it is important to familiarize with various processes involved. Thus, the following sections will give a comprehensive overview of the most widely studied processes (hence titled ‘millions of minorities’) involved in the control of epigenetic mechanisms.



### 1.2.2.1 Chromatin packaging and nucleosome positioning

The major breakthrough came during 1869 to 1951, when Miescher, Flemming, Kossel, Heitz, Muller and McClintock laid the foundation of modern era of epigenetics, by providing early hints for non-Mendelian inheritance. Specifically, the pioneering work of the German scientist Emil Heitz formed the cytological basis for the distinction between euchromatin (genetically active) and heterochromatin (genetically inactive) (Passarge, 1979). So, he further classified heterochromatin as constitutive heterochromatin, where both maternal as well as paternal chromosomes respond in similar way during development; and as facultative heterochromatin, where both homologous chromosomes behave differently (one becomes heterochromatic and another remains euchromatic) (Brown, 1966). Thus, it is very interesting how chromatin organization is structured in the cell!

A cell is the most basic building unit of life and holds all the genetic information in a total of 6 million base pairs of DNA. A 2 nm wide DNA double helical structure is called chromatin. Typically, chromatin is made up of octamer histone proteins (H2A, H2B, H3 and H4) wrapped around 146 bp of DNA (or 1.7 turns of DNA) and linker DNA of about 20-60 bp forming the nucleosome (Kornberg, 1974). This structure is often referred to as 'string-of-beads'. A nucleosome with an H1 histone forms a 'chromatosome', an 11 nm size structure. Next, these chromatosomes fold up together to produce a 30 nm fiber that forms loops of 300 nm average length. These 300-nm fibers are further coiled to produce 'the chromatid of a chromosome' (schematically represented in Fig.1.5). Coiling of 'string-of-beads' and fibers is important to compact 2 meter long DNA into the microscopic space of the eukaryotic nucleus. Positively charged small histone proteins bind very tightly to negatively charged DNA (because of the phosphate group within the phosphate-sugar backbone) by providing the energy mainly in the form of electrostatic interactions (Annunziato *et al*, 2008).

It is widely accepted that the euchromatin status in the cell reflects 'active' gene expression, because of accessible chromatin with distinct nucleosome positioning, which facilitates interaction with the transcriptional and accessory machinery. *Vice versa*, thus, it is also true for heterochromatin leading to 'inactive' gene with inaccessible chromatin. Chromatin accessibility and nucleosome remodeling are primary regulators of gene expression (Ramachandran and Henikoff, 2016).

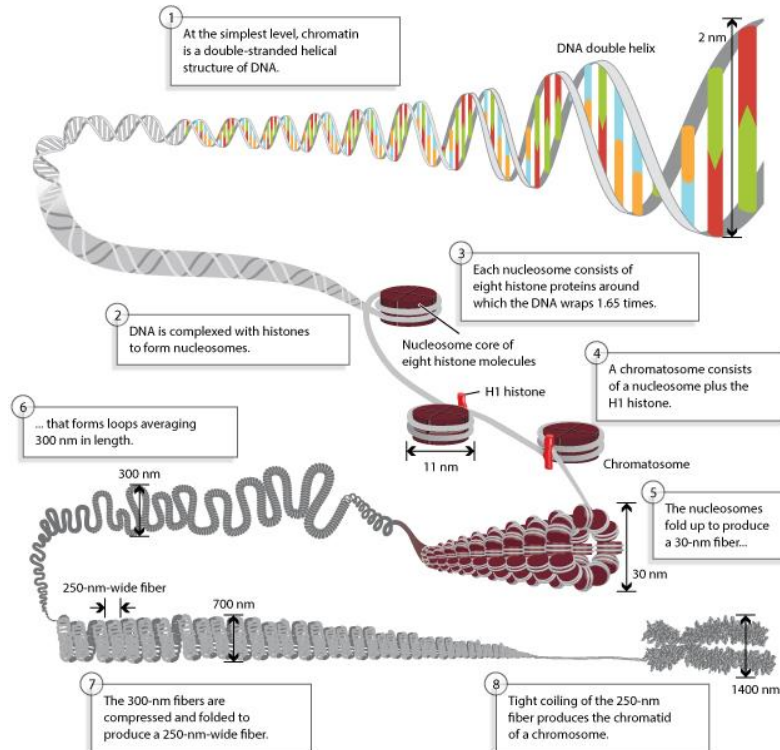


**Figure 1.5: Structural organization of chromatin and nucleosomes within a cell.** Nucleosomes, the basic unit of chromatin, are formed from histone-bound DNA. The spatial orientation of nucleosomes, also called as nucleosome positioning, further compacts to loops to produce the chromatid of a chromosome. Thus, a human chromosome of 1400 nm size contains 6 million base pairs of DNA per cell (figure adopted from Annunziato *et al*, 2008).

### 1.2.2.2 Chromatin remodeling and histone proteins

The organization of chromatin and nucleosome is a structurally dynamic process. This dynamic process is not only important for the packaging of DNA, but also for the regulation of DNA accessibility for transcription, recombination, DNA repair and replication, which ultimately leads to the cumulative effect of gene expression during health and/or disease progression. These complex processes are mainly regulated by energy-dependent chromatin remodellers, histone chaperons and histone-modifying enzymes. Based on structural and functional domain outside the enzymatic core, the so called SWI/SNF, ISWI, CHD and inositol-requiring 80 (INO80) protein families are the four groups of chromatin remodellers (Petty and Pillus, 2013). Chromatin remodellers use the energy of ATP hydrolysis to drive a DNA translocase. This allows nucleosome repositioning by sliding, eviction, assembly, spacing or histone replacement in order

to maintain higher-order chromatin organization and to modulate its accessibility. These accessible regions are possibly available for histone chaperones to carry out nucleosome assembly or for histone exchange of variants to regulate (post-) transcriptional processes. Histone chaperones are histone-interacting proteins that play a crucial role in transcriptional regulation, histone storage, transport, nucleosome stability, assembly and disassembly. They are classified based on the type of substrate they bind. Histone chaperones are shown to bind to H3-H4, H2A-H2B oligomers or both hetero-oligomers. Depending on their location and/or function, they can bind to specific canonical or variant histones alone. Serving as important linkers with chromatin remodellers, they cooperate to act as ‘histone sinks’ or also known as ‘histone acceptors’ (Venkatesh and Workman, 2015). But, the basic question is, ‘what are histones?’

Basically histones are highly alkaline proteins found in eukaryotic cells, which serve as main components of chromatin. Histone proteins are distinguished in two distinct ways, one being canonical (or core) histones (H2A, H2B, H3 and H4) and another are their histone variants. The core center of the nucleosome is an H3/H4 tetramer, due to strong four helix bundle interaction between the two H3 proteins. These H3/H4 tetramer interact with H2A/H2B and thus provides docking site for entry-exit of DNA via H2A C terminus domain. H2A and H2B turnover are higher than those of H3/H4 due to weaker intranucleosomal contacts, sensitivity to transient unwrapping and DNA exposure (Weber and Henikoff, 2014). Gene expression of histone genes is very important and highly regulated, but different for canonical and variant histones. Canonical histone synthesis and deposition is dependent on DNA synthesis. These genes are clustered and transcribed during the S phase of cell cycle. A unique feature is that mRNA lacks introns and poly A tails, which are replaced with special regulatory stem-loop structure to stimulate translation. Fully synthesized canonical histones are deposited into nucleosome behind the replication fork, at the site of DNA repair. Histone variant gene expression is DNA-independent and employs RNA polymerase II transcripts. As per evolutionary analysis, all H3 and H2A can be considered as histone variants too (Talbert and Henikoff, 2016). Histone variants possess distinct amino acid sequences, which influence the physical properties of nucleosome dynamics and transcriptional processes around *cis*-regulatory and coding regions (Weber and Henikoff, 2014). This swapping mechanism, by which the entire or parts of the nucleosome are removed or replaced with new histones (canonical or variants) or their

components, is known as ‘histone turnover’ (Venkatesh and Workman, 2015). Thus, histone turnover plays an indispensable role in maintaining or altering the chemical, physical nature and functional properties of nucleosomes, ultimately affecting regulatory processes like cell death.

### 1.2.2.3 Histone modifications

As mentioned above, histone-modifying enzymes are one of the three important regulators of higher-order chromatin conformation and nucleosome positioning, which eventually also control the regulation of gene expression. These histone-modifying enzymes are responsible for the covalent post-translational modifications (PTM) of histone proteins. These PTM or ‘epigenetic marks’ have been found in both flexible tails and globular domains of the canonical/core and linker histones. The extensive characterization of histone modifications has detected more than 550 post-translational modifications, broadly categorized as epigenetic ‘writer’, ‘reader’ and ‘eraser’. Epigenetic ‘writers’ lay down specific modification on histone tail, which includes histone acetyltransferases (HATs), histone methyltransferases (HMT), protein arginine methyltransferases (PRMTs) and kinases. To read these marks and facilitate the binding of the transcriptional machinery, epigenetic ‘readers’ are generated, including for example, bromodomains, chromodomains and tudor domains. The removal of particular marks is performed by epigenetic ‘erasers’, such as histone deacetylases (HDACs), lysine demethylases (KDMs) and phosphatases (Falkenberg and Johnstone, 2014; Andrews et al, 2016). As proposed by C. David Allis and coworkers, the ‘*histone code hypothesis*’ is based on these PTM through addition/removal or reading of covalent histone modifications to generate a remarkable diversity of combinatorial patterns, which govern biological specificity and downstream events (Strahl and Allis, 2000). An extension of this famous hypothesis is proposed to represent a broader ‘*epigenetic code*’, which along with other factors also includes histone cassettes, binary switches and the multivalency of effector-ligand binding reactions (Allis and Jenuwein, 2016).

#### 1.2.2.3.1 Histone acetylation - deacetylation

Histone modifications are directed by histone-modifying enzymes, including histone acetyltransferases (HAT) and histone deacetylases (HDAC), sharing potential cross-talk between different modifications (Kouzarides, 2007). HAT proteins are divided into two main classes, type-A and type-B. Type-A class HAT are further grouped as General control non-derepressible 5 (Gcn5)-related N-acetyltransferases (GNATs), p300/CBP and MYST proteins, which are the

three major families of HAT described so far. Class type-B HATs are conserved, predominantly cytoplasmic, acetylating free histones, which are newly synthesized (Bannister and Kouzarides, 2011). More than 18 HDACs have been shown to have non-redundant functions. They are primarily grouped as class I (HDAC1, 2, 3, 8), class II (HDAC4, 5, 7, 9), class IIa (HDAC6, 10), class IV (HDAC11; sharing class I and II deacetylases) and NAD<sup>+</sup>-dependent class III (sirtuins) (Dokmanovic *et al*, 2007). The simplified version of reversible histone acetylation - deacetylation is represented in Fig. 1.6. Generally, HATs and HDACs are embedded into a large multimolecular complex along with other cofactors and subunits of this complex. These subunits are strictly specific for corresponding acetylation sites. HATs utilize acetyl CoA as a cofactor and catalyze the transfer of an acetyl group to the  $\epsilon$ -amino group of a lysine side chain. In turn, it neutralizes the positive charge of a given lysine, which leads to a weak interaction between histones and DNA. Thus, the enzymatic property of HATs and inhibition of HDACs mechanistically modulate genome-wide turnover of acetyl group on histones. Finally, acetyl marks on histones (eg., H3K9ac, H4K20ac) lead to an open chromatin state, leaving nucleosome-free accessible DNA and help to physically interact with sequence-specific transcription factors in target-specific regulatory genomic regions, such as promoters or enhancers (Legube and Trouche, 2003).

In a cellular context-dependent manner, any of the following six different mechanisms are sought to be responsible for the interplay between HATs and HDACs with other regulators of gene expression. First, the  $\epsilon$ -amino group of a lysine residue can be marked with other modifications in addition to acetylation; second, lysine acetylation could affect the modification of a neighboring residue; third, HAT and HDAC are physically linked to the catalytic activities of other proteins; fourth, association of HATs and HDACs with modification-specific modules for sequential actions with different modifications; fifth, some HATs physically interact with non-coding RNAs (ncRNA) and other HDACs with microRNAs (miRNA); sixth and the last, different HATs and HDACs may target the same substrate (Yang and Seto, 2007). Considering these possibilities, it would be more efficient to use pan-HDAC inhibitors for further studies to investigate cellular responses. In this regard, pharmacological inhibitors specific for the respective epigenetic enzymes are already in clinic or in pre-clinical phase. The HAT inhibitor Curcumin and the HDAC inhibitors Valproic acid (VPA), Trichostatin A (TSA), 4-Phenylbutric

acid (4-PBA) are already in clinics or in clinical trials for the treatment of various diseases (West and Johnstone 2014).

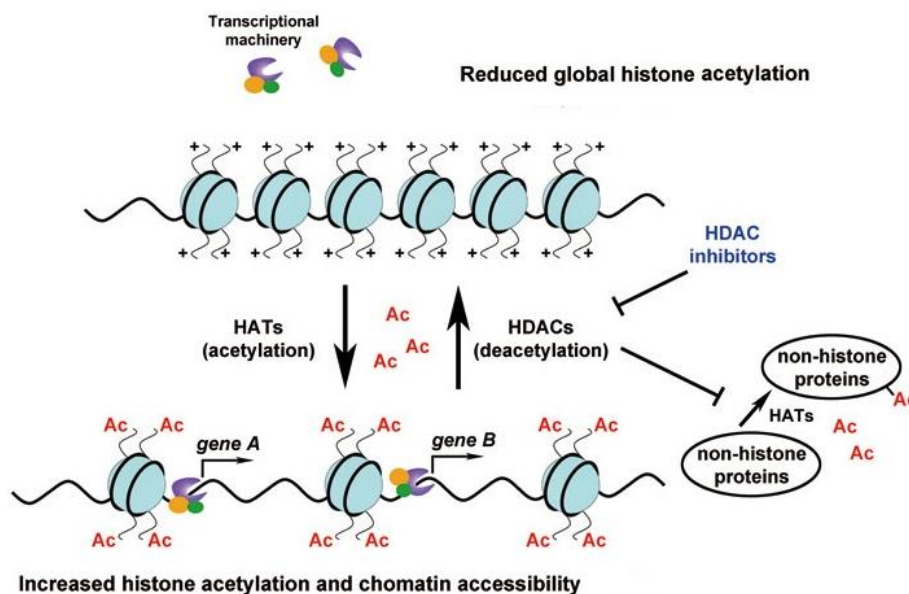


**Figure 1.6: Interplay between histone acetylation and deacetylation controlling gene expression.** Important epigenetic writer (HAT) and erasers (HDAC) work reversibly, which leads to DNA accessibility, differential global histone acetylation levels and transcriptional control of gene expression. Inhibition of HDAC induces expression of proteins of interest and also non-histone proteins, which in turn inhibit acetylation of non-histone proteins (figure modified from Wang *et al*, 2014).

### 1.2.2.3.2 Histone (de)methylation and other PTM

With detailed insight into the biological importance a number of PTMs are being incorporated into the growing list of modifications. Usually some PTMs like histone phosphorylation, acetylation, GlcNAcylation, palmitoylation and methylation are ‘simple’ modifications as they are reversible and binary, while some PTMs are more ‘complex’ as they regulate important cellular responses like ubiquitination for protein degradation or poly-ADP-ribosylation for DNA damage responses (Prabakaran *et al*, 2012). The most widely studied PTM in cellular immunology is histone methylation. It occurs on the side chains of lysine and arginine residues. Like histone acetylation, it does not simply change charges of histones, but it adds more methylation groups. It means lysine side chain of histones can be mono-, di- or tri- methylated,

whereas arginine can be mono-, or di- methylated (symmetrically or asymmetrically) (Bannister and Kouzarides, 2011). Thus, based on presence of these histone modifications, functional feature of the regulatory elements, such as enhancers can be represented. For example, H3K27ac (acetylation on 27<sup>th</sup> lysine residue of histone 3) with H3K4me1 (monomethylation 4<sup>th</sup> lysine side chain of histone 3) marks represent active enhancer region, while only H3K4me1 represents poised enhancers (Creyghton *et al*, 2010). Likewise, H3K4me3 marks active promoter and H3K27me3 marks repressed promoter (Bernstein *et al*, 2006 Cell). Thus, as these examples illustrate the presence of histone marks on different epigenetic features (Transcription Start Site or TSS, gene body, etc. will be described later in following sections) contributes to differential regulatory mechanisms that govern gene expression (Pekowska *et al*, 2010).

In the context of arginine and lysine methyltransferases, they structurally possess distinct catalytic site from DNA methyltransferases (DNMTs), but methyl group transfer is S-adenosylmethionine (SAM)-dependent. The histone methylations are considered more stable and static modifications. However, the emergence of histone demethylation showed very important role in transcription control of gene expression and respective cellular processes. The bifunctional arginine demethylase and lysyl-hydroxylase, jumonji protein (JMJD6) represents an example involved in the reversal of arginine methylation on H3R2me and H4R3me (Bannister and Kouzarides, 2011). However, findings on functional significant JMJD6-like modifications need to be reiterated in both healthy and disease conditions. Thus, other newly discovered PTM, including lysine crotonylation (Kcr) and lysine 2-hydroxyisobutyrylation (Khib) are of interest for the functional characterization and specificity for epigenetic readers.

### **1.2.3 DNA methylation and hydroxymethylation**

The most widely studied 5-methylcytosine (5mC) and the relatively newly discovered 5-hydroxymethylation (5hmC) are more dynamic and chemically stable chromatin modifications along with histone modifications (PTM as above discussed). DNA methylation mostly occurs at 5' position of the cytosine ring within CG dinucleotides (CpG) (thus, also known as '*CpG methylation*'), except for stem cells, in which methylation occurs on cytosine rings within CA dinucleotide (Schuebeler, 2009). The methylation reaction is catalyzed by DNA methyltransferase enzymes (DNMT1, DNMT3a, DNMT3b) generating 5mC (step 1, Fig. 1.7), which have variable affinities for unmethylated and hemimethylated DNA. The covalent addition

of a methyl group to the 5' position involves SAM as the methyl donor. Next, 2-oxoglutarate (2OG-) and Fe(II)-dependent dioxygenase ten eleven translocation (TET) enzymes catalyze the reaction of 5mC to 5hmC (step 2, Fig. 1.7). In this DNA 5mC/hmC cycle, step 3 and 4 in Fig. 1.7 are responsible for reversal of DNA methylation or DNA demethylation. Thus, during DNA demethylation, 5-formylcytosine (5fC) and 5-carboxycytosine (5caC) are likely excised by thymine-DNA glycosylase (TDG) enzymes and repaired by base excision repair mechanism (step 3 and 4, Fig. 1.7) (Leoni *et al*, 2015). The step 2 in Fig. 1.7, TET-mediated catalysis of 5mC to 5hmC is also reported to be carried out by other mechanisms such as UV irradiation of 5mC in aerated aqueous solution and DNA methyltransferase reaction of cytosine with formaldehyde, while activation-induced deaminase and DNA glycosylase also mediate DNA demethylation as shown in step 3 and 4 of Fig. 1.7 (Godderis *et al*, 2015). Such additional mechanisms emphasize the role of environmental factors in the modification of DNA methylation and hydroxymethylation.

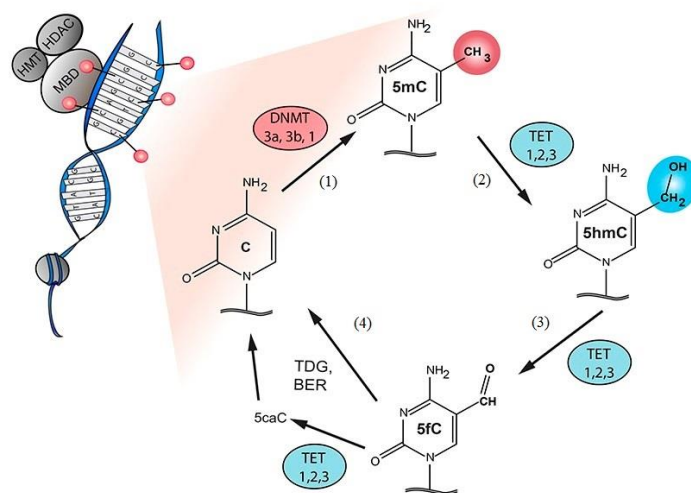


**Figure 1.7: DNA methylation (5mC) and hydroxymethylation (5hmC) cycle of DNA modification.** Two important classes of enzymes, methyltransferases and dioxygenases regulate the formation of CpG clusters on DNA. Methylated clusters are recognized by methyl-CpG-binding domain (MBD) proteins, which in turn recruit other histone modifying enzymes like HMT and HDAC. This ultimately impacts on chromatin accessibility and transcriptional control of gene expression (figure slightly modified from Leoni *et al*, 2015).



Chemically synthesized DNMT inhibitors are available and have been used in the clinic. These DNMT inhibitors, including 5-azacytidine and 5-aza-2'-deoxycytidine were tested as nucleoside antimetabolites, but later showed effects also on DNA methylation (Christman, 2002). Though these chemical compounds are of more clinical choice for treatment, epigenetic modifications like DNA methylation can be induced by environment and diet. Environment and nutrition are interconnected entities, playing an important role in healthy individuals. For instance, derivatives of folate (vitamin B) are crucial for the generation of SAM, while vitamin C acts as an antioxidant that helps to maintain activity of TET enzymes (Leoni *et al*, 2015). Moreover, other types of DNA modifications such as 5-formylcytosine (5fC), and 5-carboxycytosine (5caC) (Plongthongkum *et al*, 2014) are also under intensive investigation. Of note, one of the indispensable characteristic of DNA modifications is their association with single-nucleotide polymorphisms (SNPs) in coding and non-coding regions (Zaina *et al*, 2010; Tak and Farnham, 2015) and its interplay with miRNA (Leoni *et al*, 2015), which certainly complements the entire complexity to the epigenetic landscape of the cell.

### 1.2.4 Gene regulation at the level of RNA expression

Regulation of gene expression occurs at three different stages: first at the level of transcriptional regulation during the generation of mRNA from DNA, second at the level of translational regulation during the generation of gene product from mRNA and third by post-transcriptional or post-translational regulation through various modifications. RNA synthesis or transcription is a highly coordinated process including four different steps, *viz.*, recognition, initiation, elongation and termination. This transcriptional program is often regulated through the interplay between chromatin modifying proteins and other epigenetic elements, their binding specificity to DNA (coding and non-coding) sequences (Chowdhury and Novina, 2005). Traditionally, the promoter regions are considered to play important role in the binding of transcription factors and regulatory proteins. Enhancers located in non-coding DNA are gaining more importance in the very same steps of recognition and initiation (Nguyen *et al*, 2015). As epigenetic modifications play a central role in the control of gene expression, H3K4me3 (representing active state) are positively correlated with gene expression, while negatively correlated with H3K27me3 (representing repressive state) in T cells. Interestingly, based on these correlations, gene expression together with histone methylations are further divided in four distinct forms: active,

repressive, poised and bivalent. When considering only gene expression, three distinct patterns are identified: active, repressed and poised (Araki *et al.*, 2009). Further addition to the complexity, it was found that the process of transcription elongation is highly regulated by RNA polymerase II (pol II) pausing mechanisms, which coordinate other potential epigenetic mechanisms like nucleosome positioning and non-coding RNA (Jonkers and Lis, 2015; Zorca *et al.*, 2015). Pol II pausing may govern a primary role in co-expression co-regulation of genes. Thus, considering the abundance of pol II at promoter regions of specific gene(s) and expression/regulation of other active gene(s), these specific genes are also called as ‘immediate early genes’, ‘late response genes’ (further divided as delayed-primary response genes and secondary response genes) and ‘universal amplifier genes’. Some examples of these genes are as follow: immediate early genes (c-Jun, c-Fos), delayed-primary response genes (VCL, PLOD2), secondary response genes (MMP3, MMP13) and universal amplifier genes (c-Myc) (Nie *et al.*, 2012; Tullai *et al.*, 2007).

Fully functional mRNA transcripts are produced by passing through above said essential steps and additional RNA processing steps such as splicing, capping and polyA tail addition. This mRNA can be used to construct proteins, hence is referred to as protein-coding RNA. However, this coding region represents merely 3% of the total genome. Importantly, the big portion (~ 62 %) is transcribed into regulatory non-coding RNA (ncRNA) (Derrien *et al.*, 2012). Based on their dimension, regulatory ncRNA are classified as “small” ncRNA (< 200 nucleotides) and “long” ncRNA (> 200 to > 1000 nucleotide). These families of regulatory ncRNA are summarized in Table 1.1 (Panzeri *et al.*, 2015; Kowalczyk and Higgs, 2012). The role of ncRNA has been described in a context-dependent manner during events of chromatin conformation, histone modification, post-transcriptional processing, localization and degradation (Yang and Seto, 2007; Quinn and Chang, 2016).

More than 100 types of post-transcriptional RNA modifications have been identified, of which N6-methyladenosine (m6A) RNA methylation is one of the most prevalent modifications of mRNA, also mediated by miRNA (Chen *et al.*, 2015). In addition, the alternative splicing and expression quantitative trait loci (eQTL) play pivotal roles in the context-dependent regulation of mRNA expression (Pai *et al.*, 2012).

Table 1.1: Main classes of regulatory ncRNA

<i>Abbreviation</i>	<i>ncRNA</i>	<i>Length (nt)</i>	<i>No. of known transcripts</i>
<b>Short ncRNA</b>			
miRNA	Micro RNA	21-23	1756
snoRNA	Small nucleolar RNA	60-300	1521
snRNA	Small nuclear RNA	150	1944
piRNA	Piwi-interacting RNA	25-33	-
PASR	Promoter-associated short RNA	22-200	-
TASR	Termini-associated short RNA	22-200	-
siRNA	Short interfering RNA	21-23	-
tiRNA	Transcription initiation RNA	15-30	-
tRNA	Precursors to short Transfer RNA	73-93	497
<b>Long ncRNA</b>			
NAT	Natural antisense transcripts	>200	5446
PALR	Promoter-associated long RNA	200-1000	-
PROMT	Promoter upstream transcript	200-600	-
T-UCR	Transcribed ultraconserved regions	>200	-
Intronic RNA	Intronic RNA	>200	-
eRNA	Enhancer-derived RNA	>200	>2000
LincRNA	Long intervening/intergenic RNA	>200	6742
uaRNA	3'UTR-derived RNA	<1000	12
circRNA	Circular RNA	100 to >4000	-

### 1.3 Technological advancements in T cell epigenetic research

New technological developments and the advent of computational biology enable us to investigate the role of immune cells, specifically T cells with high resolution and in different conditions such as health and disease, or human and mice. Most of the (epi)genetic studies over decades have been based on sequencing approaches. However, the use of microarrays over sequencing is still a popular choice, due to less complex bioinformatics analysis. In the following

sub-sections, I will introduce the most widely used chip-based arrays and sequencing techniques. The bottleneck of these advanced techniques is the complex bioinformatics analysis, which will also be discussed in brief.

### 1.3.1 (Epi)genome-wide analysis using chip-arrays and sequencing technology

Microarrays are developed from the raw sequences and their expression, which were systematically combined by tiling probes across the genome. This tiling capacity allows researchers to generate a (epi)genome-wide comprehensive map of the cell. For DNA methylation analysis, the most extensively used microarrays are the Infinium<sup>®</sup> Human Methylation 450 Bead Chip (450k) from Illumina Inc. Nowadays, 850k (EPIC) arrays, which have deeper methylation coverage, are also commercially available. Basically, the 450k array uses target-specific probes to interrogate more than 480,000 of 28 million CpG sites in the human methylome. They are designed based on two different chemistries, type 1 and 2. Type 1 has two probes per locus where the 3' terminus is designed to match either methylated cytosine or converted thymine base, while the chemistry for type 2 has a single probe per locus where the 3' terminus complements the base directly upstream of the query site. Methylation levels are the ratio between the methylated probe intensity to the combined methylated and unmethylated intensity (Walker *et al*, 2015; Bibikova *et al*, 2011).

Until the introduction of the first next-generation sequencers (NGS) like massively parallel signature sequencing (MPSS) in 2000 and Roche/454 FLX pyrosequencer in 2004, bacterial artificial chromosome (BAC) clone-based sequencing was routinely used. This so called 'first generation' sequencing technology is based on the Sanger method of chain-terminating dideoxynucleotides (Mardis, 2008; Metzker 2010). Thus early in the 1980s, using such first-generation methods, TCR genes had been discovered both in mice and humans identifying distinct V(D)J rearrangements (Patten *et al*, 1984; Yoshikai *et al*, 1986). In the Next-Generation Sequencing (NGS) era, five different platforms for massively parallel systems available are Roche/454 FLX, Illumina/Solexa Genome Analyzer, Applied Biosystem SOLiD<sup>™</sup> System, Helicos Heliscope<sup>™</sup>, Pacific Biosciences SMRT instruments. All platforms are based on a common approach, i.e. first to obtain single strand of fragment library, amplify it and then to perform the sequencing reactions on amplified strand. The Applied Biosystems SOLiD sequencer uses the ligase-mediated sequencing approach, while the Illumina sequencing platform

uses the sequencing-by-synthesis (SBS) approach. In Illumina platform, single strand of fragment library is generated by annealing Illumina-specific ‘adapters’ with DNA sequence or genome of interest. Afterwards bridge amplification, i.e. *in situ* amplification of highly selective and specific library on the oligo-decorated cluster fragments on the solid surface of flow cell is carried out by automated device called ‘Cluster station’, using DNA polymerase and all four fluorescently labeled 3’-OH chemically blocked nucleotides. Thus, each cluster has around a million copies of original fragment and each cluster strand is extended by one nucleotide. Then unused reagents are washed away and a scan buffer is added to the flow cell. Followed by this step, the image of emitted fluorescence from each lane of the flow cell is recorded in three 100-tile segments by the instrument optics using laser excitation at a cluster density per tile of 30,000. ‘Tiles’ is an imaging unit used by scanner of the optical system. After this step, chemicals effecting cleavage of the fluorescence labels and the 3’-OH blocking group are added to the flow cell, so that it is prepared for the next round of fluorescent nucleotide incorporation. This continues to perform the user-defined number of cycles that permits usually 25-35 bases read length. At this point, a base-calling alignment assigns sequences and associated quality to each read. Thus, raw data from each run is ready for further steps of analysis. Each flow cell is an 8-channel sealed glass microfabricated device (called ‘lane’). This way, 8 different samples can be loaded and sequenced at the same time (Mardis, 2008).

Thus, in the recent years, several technologies have been developed to analyze the regulatory gene networks at the epigenetic level by coupling with different molecular, biochemical, biophysical and imaging approaches. These combined approaches have resulted in the epigenetic analysis even up to the single cell level. For example, the assay for transposase-accessible chromatin using sequencing (ATAC-seq) developed based on Tn5 transposases by the Greenleaf lab at Stanford University has the potential to jointly analyze all of three facets of epigenetic regulations, i.e. chromatin accessibility, nucleosome positioning and transcription factor occupancy in a single sequencing run from small numbers of CD4 T cells (Buenrostro *et al*, 2013). Recently, ATAC-seq has been extended to single cell analysis, also referred to as scATAC-seq (Buenrostro *et al*, 2015), or with the possibility of visualization, termed ATAC-see (Chen *et al*, 2016). Table 1.2 summarizes the representative landmark reports on the epigenetic processes controlling diversity of T-cell populations.

**Table 1.2: Sequencing and/or array-based technical approaches to study diverse epigenetic processes in T cells**

<i>Epigenetic process</i>	<i>Techniques</i>	<i>T cells</i>	<i>References</i>
<b>Chromatin accessibility</b>	ATAC-seq	CD4, CD8	Buenrostro <i>et al</i> , 2013; Sen <i>et al</i> , 2016
	MNase-seq	CD4	Schones <i>et al</i> , 2008
	DNase-seq	CD4	Boyle <i>et al</i> , 2008
<b>Nucleosome positioning</b>	ATAC-seq	CD4	Buenrostro <i>et al</i> , 2014
	NOMe-seq	CD4	Durek <i>et al</i> , 2016
	MNase-seq	CD4	Schones <i>et al</i> , 2008
<b>Transcription factor occupancy</b>	ATAC-seq	CD4	Buenrostro <i>et al</i> , 2014
	DNase -seq	CD4	Boyle <i>et al</i> , 2008
<b>Enhancer activity quantification</b>	CapStarr-seq	CD4 <sup>+</sup> CD8 <sup>+</sup>	Vanhille <i>et al</i> , 2015
<b>Histone modifications</b>	ChIP-seq	CD4, $\gamma\delta$	Barski <i>et al</i> , 2007; Schmolka <i>et al</i> , 2013
<b>DNA methylation</b>	450k arrays	CD4, CD8	Zilbauer <i>et al</i> , 2013
	EPIC arrays	-	-
	NOMe-seq	CD4	Durek <i>et al</i> , 2016
	WGBS	CD4, CD8	Ziller <i>et al</i> , 2015
	MeDIP-seq	CD4, CD8	Zilbauer <i>et al</i> , 2013
<b>DNA hydroxymethylation</b>	CMS-IP-coupled sequencing	CD4, CD8	Tsagaratou <i>et al</i> , 2014
<b>RNA expression</b>	Gene arrays	$\gamma\delta$ , $\alpha\beta$	Pont <i>et al</i> , 2012
	RNA-seq	CD4, Treg	Birzele <i>et al</i> , 2011; Ranzani <i>et al</i> , 2015
<b>Polymerase pausing</b>	GRO-seq	CD4	Zorca <i>et al</i> , 2015

### 1.3.2 Analysis of (epi)genomic data

When it comes to the Next-Generation-Sequencing (NGS) experiments, library preparation is relatively easy. The most challenging part is the complex bioinformatics analysis. Thus, while deciphering the epigenomic regulation of the cell, it is important to understand typical workflow of the analysis, distinct (epi)genomic features and the integration of generated information about multiple regulatory mechanisms to interpret the biological meaning behind this complexity.

#### 1.3.2.1 Bioinformatic workflow and tools

Depending on the use of array- or sequencing-based methods, the analysis pipeline differs substantially. As represented schematically in Fig. 1.8, these analyses are typically divided into four stages. The first stage is the pre-analysis, where suitable sample libraries are prepared and sequencing or array hybridization are performed. Once data is generated from the NGS platform, quality checking is required to remove poor-quality sequences and platform-specific adapters. In the second stage i.e. core analysis-1, raw data is generated and subjected to basic processing. That includes the quality control (QC) of sequencing or arrays. QC of raw sequencing data can be easily done by specific software like FastQC, which is freely available. (<http://www.bioinformatics.babraham.ac.uk/projects/fastqc/>). Another important step is the alignment of DNA/RNA sequences to organism-specific whole-genome like UCSC database (hg19). Next is the core analysis-2 stage, which has very crucial steps, including peak calling, generation of sequence-specific read counts from NGS data or probe-specific methylation values from methylation array data (termed as ‘ $\beta$ -value’ or ‘beta-value’). In this stage, the analysis can be complemented by addressing different levels of epigenetic regulations. For instances in the ATAC-seq, together with differential accessibility, transcription factor footprint analysis can be done using RSAT, HOMER tools (Medina-Rivera, *et al*, 2015; Heinz *et al*, 2010).

The last stage of analysis is the advanced analysis or also referred to as ‘downstream analyses’. In the advanced analysis, data from the different levels of regulation is integrated. It must be supplemented with statistical modeling approaches. Furthermore, biological interpretation of all the complex data is an indispensable part of any epigenetic method. This biological interpretation is often based on functional annotation of the data. Functional annotation reveals gene ontological features, association with various signaling pathways and even involvement of epigenetic regulators like transcription factors and regulatory elements. A number of tools and

algorithms are available for functional annotation analysis including InnateDB, Enrichr, Panthor (Breuer *et al*, 2013; Mi *et al*, 2016; Kuleshov *et al*, 2016).

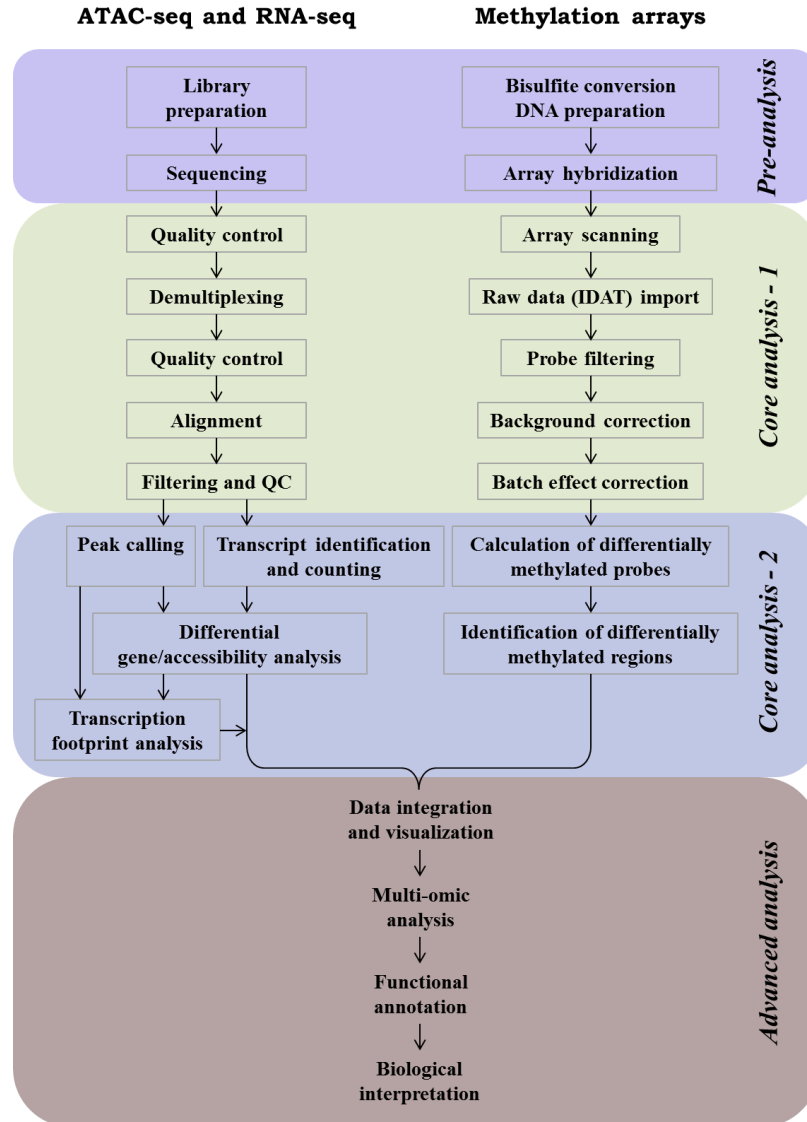


**Figure 1.8: Combined overview of workflow for ATAC-seq, RNA-seq and methylation arrays data analysis.** As mentioned above, the epigenetic analysis is typically divided into four parts. From library preparation and sequencing- or hybridization- run of pre-analysis stage, the analysis pipeline flows through core analysis-1 and -2 up to the advanced analysis stage. The workflow represented is in generalized form and can be modified according to objective of the epigenetic analysis.



Any of the epigenetic analyses can easily be influenced by a number of factors during chromatin, DNA/RNA preparation. These contribute to the introduction of biases. Thus, comprehensive information is available about different techniques, analytical tools, packages, algorithms and related methods, which is encouraged to be considered for the best practices of NGS methods for chromatin biology (Tsompana and Buck, 2014; Meyer and Liu, 2014), RNA-seq (Conesa *et al*, 2016) and Infinium human methylation Bead Chip (450k) data (Morris and Beck, 2015; Du *et al*, 2010).

### 1.3.2.2 Epigenomic features and CpG Island features

In order to understand the complex network of epigenetic processes and perform epigenome-wide data analysis, it is important to know various structural and functional properties of the gene and associated regulatory elements (Fig. 1.9A). In a *cis*-regulation of gene expression, promoter regions play important roles. A *promoter region* is composed of the core promoter and proximal promoter elements and spans nearly – 1 kb pairs. Traditionally, the promoter region is considered as the key region controlling gene expression as it facilitates the binding of the preinitiation complex and the transcriptional machinery. However, recent reports on the involvement of distal regulatory elements show that these elements play more active roles in a spatial- or temporal- manner, independent of distance and orientation, which leads to *cis*- and/or *trans*-regulation of gene expression. *Distal regulatory elements* are enhancers, silencers, insulators and locus control regions. Enhancer regions have clusters of transcription factor binding sites and functionally work similar to proximal promoter elements, which cordially enhance transcription. Silencers are sequence-specific elements, which allow binding of transcriptional repressors, resulting in repressed transcription. Insulators or boundary elements are ~0.5 - 3 kb pairs length and function in position-dependent, orientation independent manner to block genes from being affected by transcriptional activity of neighboring genes and thus partition the genome. Insulators possess two main properties: one, enhancer-binding activity and second, heterochromatin-barrier activity. Locus control regions (LCRs) are the multiple regulatory elements, including *cis*-acting elements like enhancers, silencers, insulators and nuclear-matrix or chromosome scaffold-attachment regions (MARs or SARs). LCRs function together to regulate the entire locus or gene cluster (Maston *et al*, 2006). Thus, the promoters and

distal regulatory elements control expression of an mRNA transcript, encoding exon-spanning sequences of genomic region.

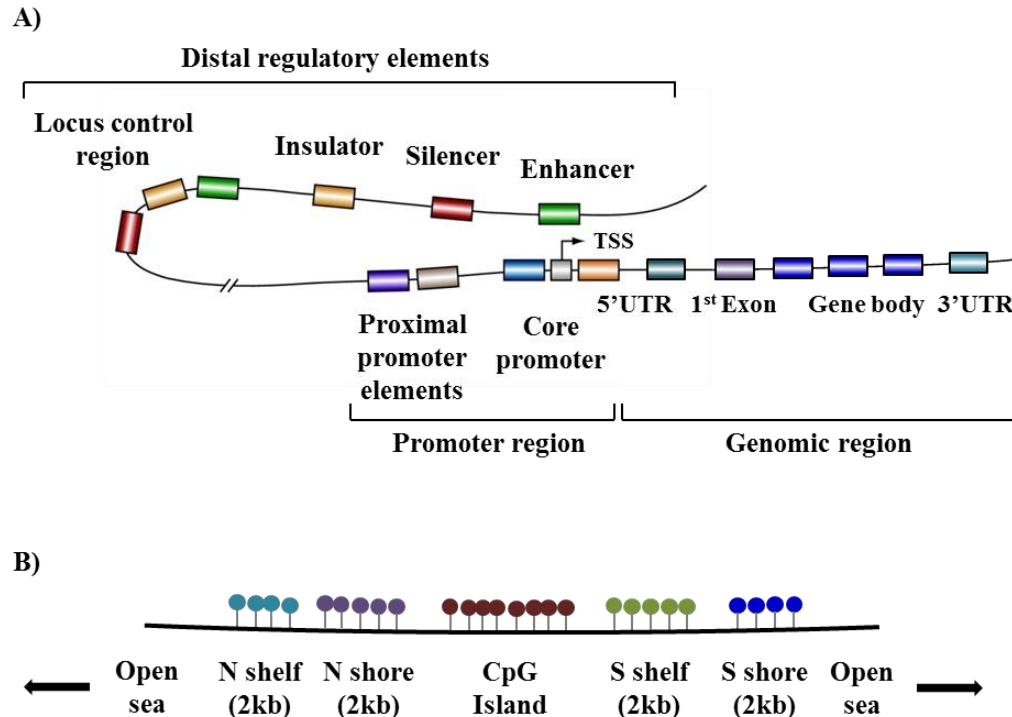


**Figure 1.9: Structural organization of genes, regulatory elements and CpG island features.** A) Transcriptional control of genes is mediated by the activity of promoter regions and distal regulatory elements. *Cis*-regulation functions mainly through epigenetic modifications at promoter regions and transcription start sites (TSS), while distal regulatory elements are involved in both *cis*- and *trans*- regulation of gene expression. Thus, the use of epigenetic techniques like ATAC-seq helps researchers to get more insight into regulatory regions like enhancers (Figure modified from Maston *et al.*, 2006). B) DNA methylation around promoter and TSS regions leads to transcriptional activation or repression. The structure of this CpG Island (CGI) cluster is distributed based on the density of CpG sites across genomic locations. The non-CGI associated CpG sites are considered to be isolated or also referred as ‘open sea’.

DNA modifications such as cytosine methylation (5mC) on these regulatory regions also play a greater role in deciding the fate of transcription. As described before, 5mC usually occurs in CpG dinucleotides. Hence, CpG islands (CGI) are defined as regions with a high G + C content ( $\geq 0.5$ ), high observed to expected CpG dinucleotides ratio ( $\geq 0.6$ ), and within sequence window

of length more than 200 bp (Fazzari and Greally, 2004). CGI ‘shore’ is defined as the 2 kb of sequence flanking a CGI on upstream and downstream (designated ‘N’ and ‘S’, respectively); while 2 kb beyond the shores are CGI ‘shelves’ and then ‘open sea’ (Fig. 1.9 B). Recently, DNA methylation ‘ravines’, ‘valleys’ and ‘canyons’ of low methylation are also described (Edgar *et al*, 2014). In fact, the methylation patterns are more dynamic at CGI shores than CGI itself. Though initially the methylation status of most CpG islands was unknown, the increase of CpG island density in the promoter region of the gene (also known as ‘promoter methylation’) now helps to predict transcriptional permissiveness in human CD4 T cells (Hughes *et al*, 2010).

### **1.3.2.3 Integrated analysis: The multi-omic approach**

‘Multi-omic’ stands for the multiple types of datasets that originate from high-throughput technologies used for genome-wide analyses, including RNA-seq (transcriptomics), methylation or histone modifications (epigenomics) or even mass spectrometry protein data (proteomics). Data integration and its analysis using multi-omic approach is gaining interest in the field of epigenetics. Though it is still at its infancy, a number of methods are described for such complex integration of data. These integration methods are primarily based on the concept, concatenation, the model, transformation and an advanced statistics (Ritchie *et al*, 2015). For example, a pairwise DNA methylation and RNA-seq integration has been reported to be done among other modelling approaches using general linear models (Conesa *et al*, 2016). General linear models (GLM) are an advanced statistical analysis approach based on regression and correlation methods, where generalization of multiple linear regression to the dataset with one dependent variable (univariate) or to multiple sets of quantitative and qualitative dependent variables (multivariate). GLM is considered as the foundation for the t-test, Analysis of Variance (ANOVA), Analysis of covariance (ANCOVA), regression analysis and many of the multivariate methods such as cluster analysis, multidimensional scaling (MDS), factor analysis, canonical correlation, principal component analysis (PCA) and others. Using a multivariate approach, integration of multi-omic datasets is described for multiple high dimensional datasets. Multi-omic approaches thus, need to be supported through powerful statistical analysis, to address each omic data independently, and also to integrate these data for exploratory analysis and the generation of predictive models such that, regulatory gene network can be inferred. In support of this

possibility, Angelini and Costa (2014) have recently proposed the potential for statistical data integration methods and tools using ChIP-seq and RNA-seq data.

## 2. Aims and objectives of the thesis

$\gamma\delta$  T cells share characteristics of both innate and adaptive immune responses.  $\gamma\delta$  T cells are a unique T cell subset, possessing the capacity of antigen-presentation, immunosurveillance, anti-tumor cytotoxicity and HLA-independent antigen recognition.  $\gamma\delta$  T cells mediate anti-tumor responses through the T-cell receptor and the NKG2D receptor and their respective ligands expressed on tumors. They also play an important role in various diseases including autoimmune diseases and cancer. In general, genetic factors and the environment play a major role in shaping the composition and the function of immune cells. Along this line, a recent study showed the importance of environmental factors such as microbiome and diet in the control of the immune homeostasis of leukocyte subsets including  $\gamma\delta$  T cells (Mangino *et al*, 2017). Likewise the presence of tumor-infiltrating leukocytes in the tumor microenvironment is related to therapeutic responses. Thus, using *in silico* systems immunology approaches,  $\gamma\delta$  T cells have emerged as the prognostically most favorable tumor-infiltrating leukocyte population in different human cancer types (Gentles *et al*, 2015). More than 30 years of research has shed light on the peculiar features of  $\gamma\delta$  T cells. Of note, they have the potential to differentiate into functionally distinct subsets depending on microenvironmental signals. The response of leukocytes to the (micro)environment is regulated by distinct molecular programs, most likely by epigenetic mechanisms. Thus, the aim of this thesis was to elucidate the epigenetic landscape of human  $\gamma\delta$  T-cells.

Specifically, the following objectives have been investigated:

- Using epigenetic inhibitors, the possible modulation of the expression and release of NKG2D ligands, and its implication on NKG2D receptors, was studied.
- The effect of HDAC inhibitors on the cell surface marker expression, intracellular cytokines and transcription factors in human  $\gamma\delta$  T cells were investigated.
- Using systems immunology approach, (epi)genome-wide epigenetic processes in  $\gamma\delta$  T cells in comparison to CD4, Treg and CD8 cells were analyzed. Specifically, I characterized DNA methylation, gene expression and its regulation by miRNA and long non coding RNA, chromatin accessibility and nucleosome positioning in  $\gamma\delta$  T cells.

**3. Materials:****3.1 Biological materials****3.1.1 Tumor cells**

The pancreatic ductal adenocarcinoma cell line PancTu-I kindly provided by Prof. Holger Kalthoff (Institute for Experimental Cancer Research, UKS-H, Campus Kiel, Germany) and the prostate cancer cell line PC-3 (ATCC number CRL-1435<sup>TM</sup>) was from ATCC, Manassas, VA, USA.

**3.1.2 Peripheral blood from healthy individuals**

PBMC were obtained by either from 60 ml peripheral blood drawn from healthy individuals in heparinized tube or from leukocyte concentrates obtained from the Department of Transfusion Medicine, UKS-H, Campus Kiel, Germany. Informed consent was obtained from all donors, and the study was approved by the local Ethics Committee (D405/10 and D515/15). The details of donors and corresponding cell populations are summarized in the Tables 3.1 and 3.2.

Table 3.1: Details of donors used for experiments performed in section 5.5 of results and discussions

Method	Donor Number	Gender	Age
ATAC-seq	1	Female	58
	2	Male	26
	3	Female	20
	4	Female	58
450k arrays	1	Male	42
	2	Male	48
	3	Male	30
	4	Male	27
Pyrosequencing	1	Male	24
	2	Male	41
	3	Male	23
	4	Male	32
RNA-seq	1	Male	26
	2	Male	52
	3	Female	23
	4	Male	50

Table 3.2: Donor-wise number of cells used and other information for ATAC-seq method

Donor	T-cell subsets	Number of cells used	Purity of T-cell (%)	Lane	Barcode
1	CD4	100,000	99.2	1	Ad2_1
1	CD8	100,000	99.5	1	Ad2_2
1	Treg	100,000	99.0	1	Ad2_3
1	V $\delta$ 1	100,000	99.3	2	Ad2_1
1	V $\delta$ 2	100,000	99.0	2	Ad2_2
2	CD4	100,000	97.9	2	Ad2_3
2	CD8	100,000	99.0	3	Ad2_1
2	Treg	36,000	98.1	3	Ad2_2
2	V $\delta$ 1	96,000	98.2	3	Ad2_3
2	V $\delta$ 2	100,000	99.6	4	Ad2_1
3	CD4	100,000	99.7	4	Ad2_2
3	CD8	100,000	99.9	4	Ad2_3
3	Treg	75,000	100	5	Ad2_1
3	V $\delta$ 1	94,000	97.5	5	Ad2_2
3	V $\delta$ 2	100,000	99.9	5	Ad2_3
4	CD4	100,000	99.2	6	Ad2_1
4	CD8	100,000	99.2	6	Ad2_2
4	Treg	88,000	99.2	6	Ad2_3
4	V $\delta$ 1	100,000	97.9	7	Ad2_1
4	V $\delta$ 2	100,000	99.0	7	Ad2_2



### 3.1.3 Peripheral blood samples from $\gamma\delta$ -HSTCL patient for experiments performed in section 5.6 of results and discussions

**Table 3.3: Time-dependent clinical information of  $\gamma\delta$ -HSTCL patient**

<i>Visit number</i>	<i>Date</i>	<i>Leukocyte counts (per <math>\mu</math>l of blood)</i>	<i>Phenotype (% <math>\gamma\delta</math>)</i>	<i>Treatment</i>
1	09.01.1990	18,700	92.9	Prednisolone (5 mg) every 2 <sup>nd</sup> day; IFN $\alpha$ 2c with 1 million IU s.c. once daily
2	20.04.1990	20,000	87.2	IFN $\alpha$ 2c with 1 million IU s.c. once daily
3	27.07.1990	12,000	89.3	IFN $\alpha$ 2c with 1 million IU s.c. once daily
4	21.02.1991	7,700	93.2	IFN $\alpha$ 2c with 1 million IU s.c. once daily
5	30.08.1991	7,200	92.5	IFN $\alpha$ 2c with 1 million IU s.c. once daily

### 3.1.4 T-cell subset purification and purity

As described previously, highly purified T-cell populations were used. Thus, the purity of the T-cell subsets used in various experiments according to methods is summarized in Tables 3.4 and 3.5.

**Table 3.4: Purity of healthy T-cell populations used for DNA methylation analysis**

<i>Methylation analysis</i>	<i>Donor Number</i>	<i>T-cell subset</i>	<i>Purity (%)</i>
450k arrays	1	CD4	96.18
		CD8	88.47
		Treg	98.21
		$\gamma\delta$	99.42
	2	CD4	93.47
		CD8	96.91
		Treg	99.41
		$\gamma\delta$	95.84
	3	CD4	98.09
		CD8	92.67
		Treg	98.42
		$\gamma\delta$	99.7
	4	CD4	97.11
		CD8	95.7
		Treg	98.66
		$\gamma\delta$	99.98
Pyrosequencing	1	CD4	98.27
		CD8	94.4
		Treg	99.34
		$\gamma\delta$	97.68
	2	CD4	97.86
		CD8	92.09

		Treg	99.34
		$\gamma\delta$	99.03
	3	CD4	97.72
		CD8	99.72
		Treg	94.75
		$\gamma\delta$	98.72
	4	CD4	98.72
		CD8	99.04
		Treg	97.88
		$\gamma\delta$	98.35

Table 3.5: Purity of T-cell populations used for RNA-seq analysis

<i>Donor Number</i>	<i>T-cell subset</i>	<i>Purity (%)</i>
1	CD4	97.95
	CD8	98.05
	Treg	95.08
	$\gamma\delta$	99.31
2	CD4	99.00
	CD8	97.65
	Treg	97.54
	$\gamma\delta$	99.34
3	CD4	98.63
	CD8	97.24
	Treg	97.41
	$\gamma\delta$	97.92
4	CD4	97.51
	CD8	97.15
	Treg	98.58
	$\gamma\delta$	99.01

### 3.2 Reagents, chemicals and culture mediums

#### 3.2.1 Reagents

**Table 3.6: List of fine chemicals and their concentrations**

<i>Reagent</i>	<i>Used concentration</i>	<i>Company</i>
Trypsin-EDTA	0.05 % - 0.02 % (w/v)	Biochrom AG, Berlin, Germany
penicillin	100 U/ml	Biochrom AG, Berlin, Germany
streptomycin	100 µg/ml	Biochrom AG, Berlin, Germany
zoledronate	2.5 µM	Novartis, Basel, Switzerland
Bromohydrin pyrophosphate (BrHPP)	300 nM	Innate Pharma, Marseille, France
human recombinant IL-2	50 IU/ml	Novartis, Basel, Switzerland
Staphylococcal Enterotoxin A (SEA)	1 ng/ml	Toxin Technology, Florida, USA
Staphylococcal Enterotoxin C-1 (SEC1)	1 ng/ml	Toxin Technology, Florida, USA
Staphylococcal Enterotoxin D (SED)	1 ng/ml	Toxin Technology, Florida, USA
Staphylococcal Enterotoxin E (SEE)	1 ng/ml	Toxin Technology, Florida, USA
Phytohaemagglutinin (PHA)	0.5 µg/ml	Remel Europe, Dartford, Kent, UK
Monensin	3 µM	EMD Millipore/Calbiochem, Darmstadt, Germany
Etoposide	0.425 mM	Sigma–Aldrich Chemie, Munich, Germany
Protease and phosphatase inhibitors (aprotinin, leupeptin, phenylmethanesulfonylfluoride (PMSF), sodium pyrophosphate, sodium orthovanadate and sodium fluoride)	1:100	Sigma–Aldrich Chemie, Munich, Germany

## Materials

FcR blocking reagent	1:10	Miltenyi Biotec GmbH, Bergisch Gladbach, Germany
Valproic acid (VPA)	Depending on experiments	Sigma–Aldrich Chemie, Munich, Germany
Trichostatin A (TSA)	Depending on experiments	Sigma–Aldrich Chemie, Munich, Germany
5-Aza-2'-deoxycytidine (Decitabine)	Depending on experiments	Sigma–Aldrich Chemie, Munich, Germany
4-Phenylbutyric acid (4-PBA)	Depending on experiments	Sigma–Aldrich Chemie, Munich, Germany
Curcumin	Depending on experiments	Sigma–Aldrich Chemie, Munich, Germany
Epigallocatechin gallate (EGCG)	Depending on experiments	Sigma–Aldrich Chemie, Munich, Germany
Phorbol 12-myristate 13-acetate (PMA)	100 ng/ml	Sigma-Aldrich Chemie, Munich, Germany
<sup>3</sup> H-TdR	1 μCi/well	Hartmann Analytic, Braunschweig, Germany
Z-Val-Ala-DL-Asp-fluoromethylketone (zVAD)	10 μM	Bachem, Weil am Rhein, Germany
Necrosulfonamide (NSA)	0.5 μM	EMD Millipore/Calbiochem, Darmstadt, Germany
Necrostatin-1 (Nec-1)	50 μM	Sigma–Aldrich Chemie, Munich, Germany
Unmethylated DNA	-	EpigenDX Inc., Hopkinton, MA, USA

**3.2.1 Culture mediums and kits**

X-vivo 15 medium (Lonza, Cologne, Germany)

RPMI-1640 medium (Gibco<sup>®</sup>, Life Technologies, Darmstadt, Germany)

Fetal calf serum (FCS; Gibco<sup>®</sup>, Life Technologies)

Ficoll-Hypaque (Biochrom)

Hanks' Balanced Salt Solution (HBSS; Biochrom)

Dulbecco's PBS (Cell Concepts, Umkirch, Germany)

Human CD4<sup>+</sup> T-cell isolation kit (Miltenyi Biotec GmbH, Bergisch Gladbach, Germany)

Dynabeads<sup>®</sup> Regulatory CD4<sup>+</sup>/CD25<sup>+</sup> T-cell kit (Thermo Fischer Scientific, Rockford, Illinois, USA)

Human CD8 T-cell microbeads kit (Miltenyi Biotec)

Human TCR $\gamma\delta$  microbeads kit (Miltenyi Biotec)

Cytofix/Cytoperm fixation/permeabilization kit (BD Biosciences, Heidelberg, Germany)

BD Pharmingen Transcription Factor Buffer set (BD Biosciences)

LEGENDplex<sup>™</sup> human Th cytokine panel kit (13-plex; BioLegend, London, UK)

MICA ELISA kit (R&D Systems)

MICB ELISA kit (R&D Systems)

ULBP-1 ELISA kit (R&D Systems)

ULBP-2 ELISA kit (R&D Systems)

Cell Titer-Glo Luminescent Cell Viability Assay (Promega GmbH, Mannheim, Germany)

ExoQuick<sup>™</sup> Exosome Precipitation solution (System Biosciences, Mountain View, USA)

NuPAGE 4-12% Bis-Tris Gel (1.5 mm X 15 well; Life Technologies)

Enhanced chemiluminescence (ECL) western blot detection reagent (GE Healthcare)

QIAzol lysis solution (Qiagen Inc., Valencia, USA)

peqGOLD TriFast Isolation procedure (Peqlab, Erlangen, Germany)

cDNA synthesis kit (AmpTec, Hamburg, Germany)

Nextera sample preparation kit (Illumina Inc., San Diego, USA)

Qiagen MinElute kit (Qiagen)

NEB next high fidelity 2X PCR master mix (New England BioLabs GmbH, Frankfurt am Main, Germany)

Ampure XP beads (Beckman Coulter)  
 Agilent High Sensitivity DNA kit (Agilent Technologies, Waldbronn, Germany)  
 Gentra purification kit (Qiagen)  
 Qubit dsDNA BR Assay kit (Life Technologies, Darmstadt, Germany)  
 EZ-DNA Methylation kit (Zymo Research Europe GmbH, Frieberg, Germany)  
 Infinium HumanMethylation450 BeadChip Kit (Illumina)  
 EpiTect Bisulfite kit (48) (Qiagen)  
 PyroMark kit (800) (Qiagen)  
 miRNeasy mini kit (Qiagen)  
 RNase-free DNase set (Qiagen)  
 TruSeq stranded total RNA library preparation kit (Illumina)  
 TruSeq small RNA library preparation kit (Illumina)

**3.2.2 Antibodies for western blotting, flow cytometry, immunoprecipitation and Imaging**

**Table 3.7: List of antibodies, their clones and application**

<i>Antibody</i>	<i>Clone</i>	<i>Origin</i>	<i>Company</i>	<i>Application</i>
Anti-MICA/B	BAM01	Mouse	BAMOMAB GmbH, Gräfelfing, Germany	Western blot
Anti-human H3K9ac	C5B11	Rabbit	Cell Signaling Technology, Beverly, MA, USA	Western blot
Anti-human c-Jun	60A8	Rabbit	Cell Signaling Technology, Beverly, MA, USA	Western blot
Anti-human phospho-Jun	D47G9	Rabbit	Cell Signaling Technology, Beverly, MA, USA	Western blot

## Materials

Anti-human Bcl-11B	D6F1	Rabbit	Cell Signaling Technology, Beverly, MA, USA	Western blot
Anti-human $\beta$ -actin	AC-15	Mouse	Sigma-Aldrich	Western blot
Anti-human MICA	2C10	Mouse	Santa Cruz Biotechnology, Inc. Heidelberg, Germany	Immunoprecipitation
Anti-human MICA	159233	Mouse	R&D Systems, Wiesbaden, Germany	Immunoprecipitation
Anti-human V $\delta$ 2 FITC	IMMU389	Mouse	Beckman Coulter, Krefeld, Germany	Flow cytometry
Anti-human CD3 PE	SK7	Mouse	BD Biosciences, Heidelberg, Germany	Flow cytometry
Anti-human TCR $\alpha\beta$ FITC	WT31	Mouse	BD Biosciences, Heidelberg, Germany	Flow cytometry
Anti-human CD25 PE	2A3	Mouse	BD Biosciences, Heidelberg, Germany	Flow cytometry
Anti-human CD95 PE	DX2	Mouse	BD Biosciences, Heidelberg, Germany	Flow cytometry
Anti-human HLA-DR PE	L243	Mouse	BD Biosciences, Heidelberg, Germany	Flow cytometry
Anti-human CCR5 PE	2D7/CCR5	Mouse	BD Biosciences, Heidelberg, Germany	Flow cytometry
Anti-human CD40 PE	HB14	Mouse	BioLegend, London, UK	Flow cytometry
Anti-human CD54 PE	84H10	Mouse	Beckman Coulter, Krefeld, Germany	Flow cytometry
Anti-human CD86 PE	2331	Mouse	R&D Systems, Wiesbaden, Germany	Flow cytometry



## Materials

Anti-human NKG2D PE	149810	Mouse	R&D Systems, Wiesbaden, Germany	Flow cytometry
Annexin V-FITC	-	-	MabTag GmbH, Friesoythe, Germany	Flow cytometry
Propidium Iodide (PI)	-	-	Serva, Heidelberg, Germany	Flow cytometry
Anti-human CD3 Alexa Fluor 647	SK7	Mouse	BioLegend, London, UK	Flow cytometry
Anti-human CD4 Brilliant Violet 510	OKT4	Mouse	BioLegend, London, UK	Flow cytometry
Anti-human CD8 APC-Cy7	SK1	Mouse	BioLegend, London, UK	Flow cytometry
Anti-human V $\delta$ 2 PerCp	B6	Mouse	BioLegend, London, UK	Flow cytometry
Anti-human CD25 Brilliant Violet 421	M-A251	Mouse	BD Biosciences, Heidelberg, Germany	Flow cytometry
Anti-human CD127 PE	hIL-7R- M21	Mouse	BD Biosciences, Heidelberg, Germany	Flow cytometry
Anti-human V $\delta$ 1 FITC	TS8.2	Mouse	Thermo Fisher Scientific, Rockford, Illinois, USA	Flow cytometry
Anti-human IL-4 Brilliant Violet	MP4-25D2	Rat	BioLegend, London, UK	Flow cytometry
Anti-human IFN- $\gamma$ PE	4S.B3	Mouse	BD Biosciences, Heidelberg, Germany	Flow cytometry
Anti-human MICA PE	159227	Mouse	R&D Systems, Wiesbaden, Germany	Flow cytometry
Anti-human MICB Alexa Fluor 700	236511	Mouse	R&D Systems, Wiesbaden, Germany	Flow cytometry

## Materials

Anti-human ULBP-1 PerCp	170818	Mouse	R&D Systems, Wiesbaden, Germany	Flow cytometry
Anti-human ULBP2/5/6 APC	165903	Mouse	R&D Systems, Wiesbaden, Germany	Flow cytometry
Anti-human IL-4 $\delta_{13}$ PE	8D4-8	Mouse	BD Biosciences, Heidelberg, Germany	Flow cytometry and Imaging
Anti-human IL-4R $\alpha$	Sc-684	Rabbit	Santa Cruz Biotechnology, Heidelberg, Germany	Flow cytometry and Imaging
Anti-rabbit IgG (H+L) Alexa Fluor 488	-	Donkey	Life Technologies GmbH, Darmstadt, Germany	Flow cytometry and Imaging
DRAQ5 <sup>TM</sup>	-	-	Abcam plc, Cambridge, UK	Imaging
Anti-human H3K9ac Pacific Blue	C5B11	Rabbit	Cell Signaling Technology, Beverly, MA, USA	Imaging
Anti-human CD107a FITC	H4A3	Mouse	BioLegend, London, UK	Imaging

### 3.3 Primers used

**Table 3.8: PCR primers (TIB Molbiol GmbH, Berlin, Germany; Bhat *et al*, 2016; Chitadze *et al*, unpublished work) used in methods from results and discussion section 5.2 and 5.4**

<i>Gene name</i>	<i>Primer</i>	<i>Sequence</i>
NKG2D receptor		
FL_NKG2D	Forward	GCTGTATTCCTAAACTCATTATTCAACC
	Reverse	CTGCCAAGATCCATTTGTTG
Tr_NKG2D	Forward	TTCTGCTGCTTCATCGCTGT
	Reverse	TGGACTAATAGCAAAAATGTGACAA
Both_NKG2D	Forward	CCTCTCTGCGGTAGACGTG
	Reverse	GACATCTTTGCTTTTGCCATC
NKG2D ligands		
MICA	Forward	AGGGTCTGTGAGATCCATGAAGAC
	Reverse	CCTGACGTTTCATGGCCAAGG
MICB	Forward	ACCTTGGCTATGAACGTCACA
	Reverse	CCCTCTGAGACCTCGC
ULBP-2	Forward	GCAAGGATGTCTTGTGAGCA
	Reverse	GGCCACAACCTTGTCATTCT
Cytokines		
IL-4	Forward	GCCACCATGAGAAGGACT
	Reverse	ACTCTGGTTGGCTTCCTTCA
IFN- $\gamma$	Forward	TCAGCTCTGCATCGTTTTGG
	Reverse	GTTCCATTATCCGCTACATCTGAA
Housekeeping genes		
$\beta$ 2-microglobulin	Forward	GGGTTTCATCCATCCATCCGACA
	Reverse	ACACGGCAGGCATACTCATC
$\beta$ -actin	Forward	CTGAACCCCAAGGCCAAC
	Reverse	CAGAGGCGTACAGGGATAGC
18S RNA	Forward	GACTCAACACGGGAAACCTC
	Reverse	AGACAAATCGCTCCACCAAC

**Table 3.9: A list of oligos used for PCR from Biomers GmbH, Ulm, Germany (Buenrostro *et al*, 2013)**

<i>Name of oligos</i>	<i>Sequence</i>
Ad1_noMX:	AATGATACGGCGACCACCGAGATCTACACTCGTCGGCAGCG TCAGATGTG
Ad2.1_TAAGGCGA	CAAGCAGAAGACGGCATAACGAGATTCGCCTTAGTCTCGTGG GCTCGGAGATGT
Ad2.2_CGTACTAG	CAAGCAGAAGACGGCATAACGAGATCTAGTACGGTCTCGTGG GCTCGGAGATGT
Ad2.3_AGGCAGAA	CAAGCAGAAGACGGCATAACGAGATTTCTGCCTGTCTCGTGGG CTCGGAGATGT

Table 3.10: A list of primers used for pyrosequencing-PCR

<i>CpG site Gene Name</i>	<i>Primers</i>	<i>Sequence</i>	<i>Primer Modification</i>	<i>Temp. (°C)</i>	<i>PCR Product size (bp)</i>
cg04437762 IL-6R	Forward	GAAGTATGGAGTAAATGATT GTG	-	60	190
	Reverse	CCTAAAAAATCCTAACAACTC C	Biotin		
	Sequencing	AGTTGGTTGAGAGGGGA	-		
cg20235075 EOMES	Forward	GAGGTTTAGAGGTGTTAGTAT GAG	Biotin	55	181
	Reverse	TTCCACCTAAAAAATTATA AC	-		
	Sequencing	ATTAACAAACAAAAAATC	-		
cg00014104 MAPK1	Forward	GTTTTTTAAAGTGTTGGGATT ATAG	-	60	101
	Reverse	TTCTCCTCAATATAACTA CTC	Biotin		
	Sequencing	GTTGATGGTAGTTTTTATTA	-		
cg00344178 NMNAT2	Forward	GTTAAAAATTTTATGGAAAG AATATAG	-	55	104
	Reverse	AAAATAACTATCTCTCAACCT CC	Biotin		
	Sequencing	AAATTTTATGGAAAGAATAT A	-		
cg00556515 TNFRSF1A	Forward	TTTATTGAGGTAGAGGTTGTA A	-	55	118
	Reverse	AATCTCTTCTTACACAATAAA CC	Biotin		
	Sequencing	AGTATTGGAAAAGGTTTTTA	-		

### 3.4 Buffers and biochemical solutions

#### MACS buffer

PBS  
0.5 % BSA (w/v)  
2 mM EDTA

#### Dynal buffer

PBS  
0.1 % BSA (w/v)  
2 mM EDTA

#### Washing buffer

PBS  
1 % BSA (w/v)  
0.1 % NaN<sub>3</sub> (v/v)

#### Annexin V binding buffer

10 mM HEPES  
140 mM NaCl  
5 mM CaCl<sub>2</sub>  
MilliQ water

#### 1 % NP40 lysis buffer

1 % NP-40 (v/v)  
20 mM Tris-HCl (pH 7.4)  
150 mmol/l NaCl  
5 mM ethylenediaminetetraacetate (EDTA)

#### 1X TNE cell lysis buffer

1 % NP-40 (v/v)  
50 mM Tris  
150 mM NaCl  
2 mM EDTA

#### 5X sample loading buffer

50 mM Tris

10 % SDS (w/v)

25 % Glycerol (v/v)

10 %  $\beta$ -mercaptoethanol (v/v)

0.005 % Bromophenol blue stain

2X sample loading buffer

125 mM Tris

4 % SDS (w/v)

20 % Glycerol (v/v)

10 %  $\beta$ -mercaptoethanol (v/v)

0.005 % Bromophenol blue stain

Hanks' Balanced Salt Solution (HBSS) supplemented with 1% FCS

HBSS supplemented with 10 % FCS

10% polyacrylamide gel

Stacking gel

30 % Acrylamide (1.67 ml)

1 M Tris-HCl, pH 6.8 (1.25 ml)

10 % SDS (0.1 ml)

MilliQ water (7.03 ml)

20 % APS (50  $\mu$ l)

TEMED (10  $\mu$ l)

10 % running gel

30 % Acrylamide (10 ml)

1 M Tris-HCl, pH 8.8 (11.2 ml)

10 % SDS (0.3 ml)

MilliQ water (8.7 ml)

20 % APS (100  $\mu$ l)

TEMED (20  $\mu$ l)

5 % BSA blocking solution

1 g of BSA

20 ml 0.05 % PBS with tween-20

5 % non-fat dry milk blocking solution

1 g of non-fat dry milk powder

20 ml 0.05 % PBS with tween-20

Cold lysis buffer

1 M Tris-HCl, pH 8 (Rockland Inc, USA)

10 mM NaCl (Merck KGaA, Darmstadt, Germany)

3 Mm MgCl<sub>2</sub> (Merck KGaA, Darmstadt, Germany)

0.1 % IGEPAL CA-630 (Sigma-Aldrich, Steinheim, Germany)

Transposition reaction mix (Nextera sample preparation kit, Illumina Inc., San Diego, USA)

25 µl 2X TED buffer

2.5 µl TDE1 transpose enzyme

22.5 µl water

### **3.5 Laboratory consumables, equipment and software**

12 well cell culture plate (CELLSTAR, Greiner Bio-One GmbH, Frickenhausen, Germany)

V-bottom 96 well plate (nerbe plus GmbH, Winsen (Luhe), Germany)

Flat-bottom 96-wells Maxisorp Nunc Immunoplate (Thermo Fischer Scientific)

Cellulose acetate filters (0.2 µm ; Whatman GmbH, Dassel, Germany)

Amicon Ultra-15 centrifugal filters (100 kDa, Merck/Millipore GmbH, Schwalbach am Taunus, Germany)

Hybond C Extra nitrocellulose membranes (GE Healthcare, Munich, Germany)

Bio-Rad SmartSpec 3000 (Bio-Rad Laboratories GmbH, Munich, Germany)

Scintillation counter (PerkinElmer, Rodgau, Germany)

BD LSRFortessa (BD Biosciences, Heidelberg, Germany)

BD Calibur (BD Biosciences, Heidelberg, Germany)

FACSAria (BD Biosciences, Heidelberg, Germany)

ImageStreamX Mark II imaging flow cytometry (Merck Millipore)

Tecan Infinite-200 microplate reader (Tecan Group Ltd., Maennedorf, Germany)

Agilent Bioanalyzer 2100 (Agilent Technologies, Waldbronn, Germany)

Illumina HiSeq 2000 platform (Illumina, San Diego, USA)



Illumina HiSeq 2500 platform (Illumina)

NanoDrop ND-1000 spectrophotometer (Thermo Fisher Scientific, Pittsburg, USA)

Qubit Fluorometer (Life Technologies, Darmstadt, Germany)

PyroMark Q96 ID pyrosequencer (Qiagen)

Agilent 4200 TapeStation system (Agilent Technologies, Waldbronn, Germany)

CellQuest Pro software (BD Biosciences, USA)

BD FACSDiva™ (BD Biosciences, Heidelberg, Germany)

FlowJo software (FlowJo LLC, Ashland Or, USA)

IDEAS software (v6.0, Amnis)

PyroMark Assay Design software (Qiagen)

PyroMark CpG software (Qiagen)

GenomeStudio software (v2011.1; Illumina)

Qlucore Omics Explorer (v2.3(45), 64-bit; Qlucore, Lund, Sweden)

PrismGraph (GraphPad Software, Inc. La Jolla, CA, USA)

R (3.3.1) and Bioconductor packages

## **4 Methods:**

### **4.1 Cell biological and immunological methods**

#### **4.1.1 Cell cultures**

##### **4.1.1.1 Maintenance of tumor cells (for results and discussion in section 5.1 and 5.2)**

Experiments were performed with the pancreatic ductal adenocarcinoma cell line PancTu-I and the prostate cancer cell line PC-3, which were kept in culture for less than 3 months. PancTu-I and PC-3 cells were grown in RPMI-1640 medium supplemented with 10 % heat-inactivated fetal calf serum (FCS), 100 U/ml penicillin and 100 µg/ml streptomycin. All cell lines were kept at 37°C in a humidified atmosphere with 5 % CO<sub>2</sub>. Subsequent passaging of tumor cells was done by using Trypsin-EDTA (0.05 % - 0.02 % (w/v); Biochrom).

##### **4.1.1.2 Tumor cell culture (for results and discussion in for section 5.1)**

For all experiments regarding the analysis of tumor cells and culture supernatant for soluble MICA, 3.5 x 10<sup>6</sup> tumor cells were cultured for 4 days in 50 ml X-vivo 15 medium (Lonza) without additional serum supplementation in the presence or absence of 100 ng/ml Phorbol 12-myristate 13-acetate (PMA; Sigma-Aldrich).

##### **4.1.1.3 Isolation of peripheral blood mononuclear cells and preparation of antigen-activated T-cell lines (for results and discussion in section 5.2, 5.3 and 5.4)**

PBMC were isolated by Ficoll-Hypaque (Biochrom) density gradient centrifugation. Cell cultures were set up in RPMI-1640 medium (Life Technologies) supplemented with 10 % heat inactivated FCS and 100 U/ml penicillin and 100 µg/ml streptomycin antibiotics mix (Biochrom). PBMC were stimulated either with 2.5 µM zoledronate (Novartis) or with bromohydrin pyrophosphate (300 nM BrHPP; Innate Pharma) in the presence of 50 IU/ml human recombinant IL-2 (Novartis). IL-2 was repeatedly added every second day. After 12 days, respective cultures usually contained > 90 % Vγ9Vδ2-expressing γδ T cells. αβ T-cell lines were generated by stimulating PBMC with a mixture of staphylococcal enterotoxins (1 ng/ml each; SEA, SEC1, SED, SEE; hereafter referred as SE-Mix; Toxin Technology) for 7 days. For experiments using PHA blasts, PBMC were stimulated with 0.5 µg PHA (Remel) for 5 days, and PHA blasts were maintained in RPMI supplemented with 10 % FCS and IL-2 following depletion of dead cells by Ficoll-Hypaque (Biochrom) density gradient centrifugation. In some experiments, serum-free X-vivo 15 medium (Lonza) was used.

#### 4.1.1.4 Isolation of T-cell subsets (for results and discussion in section 5.5)

PBMC were subjected to purification of individual human T cell populations by the following MACS kits: CD4 T cells were first negatively isolated using human CD4<sup>+</sup> T-cell isolation kit (Miltenyi); responder (referred to hereafter as CD4 T cells; CD4<sup>+</sup>CD25<sup>-</sup>) and regulatory T cells (CD4<sup>+</sup>CD25<sup>hi</sup>) were then separated from negatively isolated CD4 T cells using Dynabeads<sup>®</sup> Regulatory CD4<sup>+</sup>/CD25<sup>+</sup> T-cell kit (Thermo Fischer Scientific); CD8 T cells were positively isolated using human CD8 T-cell microbeads kit (Miltenyi); for  $\gamma\delta$  T-cells, PBMC were first blocked with FcR blocking reagent (Miltenyi) for non-specific binding of antibodies and then positively isolated using anti-human TCR $\gamma\delta$  microbeads kit. Purified human T-cell subset populations were washed once with PBS (Cell Concepts) and counted microscopically.  $2 \times 10^6$  -  $4 \times 10^6$  cells of each cell subsets were stored immediately as dry cell pellet at  $-80^\circ\text{C}$  until further use for DNA methylation analysis, or lysed into QIAzol lysis solution (Qiagen) for RNA-seq analysis and kept in  $-80^\circ\text{C}$  until total RNA extraction.

#### 4.1.2 Functional assay set-up

##### 4.1.2.1 Co-culture assays and assays for soluble versus immobilized NKG2D ligands (for results and discussion in section 5.2)

For co-culture assays,  $0.8 \times 10^6$  tumor cells per ml of growth medium were treated with 2.5 mM valproic acid (VPA) for 24 hrs in 12 well cell culture plate (CELLSTAR, Greiner Bio-One). Afterwards,  $1 \times 10^6$  effector cells (PBMC or  $\gamma\delta$  T cells) were added to the culture for another 24 hrs, without changing medium. Cells were then harvested for gene expression and flow cytometric analysis.

A mixture of recombinant MICA, MICB and ULBP-2 proteins were prepared from commercially available standard proteins from ELISA kits (DY1300, DY1599, and DY1298 respectively; all from R&D Systems) at the concentration 2000, 2500, 2000 pg/ml, respectively. For immobilized NKG2DL (imNKG2DL) treatment, 100  $\mu\text{l}$  of mixture at respective concentrations was coated on flat-bottom 96-wells Maxisorp Nunc Immunoplate (Thermo Fischer Scientific) for overnight at room temperature. Prior to addition of cells, imNKG2DL solution was removed from wells and plates were washed once with PBS (Cell Concepts). Alternatively, 100  $\mu\text{l}$  NKG2D ligands (sNKG2DL) mixture at respective concentrations was added together with 2.5 mM VPA and  $0.1 \times 10^6$  effector cells (PBMC or  $\gamma\delta$  T cells). After 24 hrs

of treatment with 2.5 mM VPA and sNKG2DL or imNKG2DL treatment, effector cells were harvested and used for the analysis of protein expression using flow cytometry. Cell culture supernatants were collected and stored at  $-20^{\circ}\text{C}$  until further use.

#### **4.1.2.2 Assay for H3K9ac analysis (for results and discussion in section 5.2 and 5.3)**

Total H3K9ac in human  $\gamma\delta$  T cells were analyzed by western blot and flow cytometry as described previously (Bhat *et al*, 2015; 2016). Briefly,  $1 \times 10^6$  per ml of  $\gamma\delta$  T cells were either treated with 5 mM, 2.5 mM, 1 mM VPA, valpromide, DMSO (as solvent control) or left untreated. After 24 hrs of treatment, cells were harvested carefully and washed once with Dulbecco's PBS (Cell Concepts). Cells were either lysed and subjected to blotting or harvested for analysis by flow cytometry.

#### **4.1.2.3 Cell death analysis assays (for results and discussion in section 5.4)**

$\alpha\beta$  T cells or  $\gamma\delta$  T cells were cultured at  $1 \times 10^6$  per ml for 24 hrs in the absence or presence of Valproic acid (VPA), Trichostatin A (TSA), or 5-Aza-2'-deoxycytidine (Decitabine; all from Sigma-Aldrich). Where indicated,  $\gamma\delta$  T cells were first pretreated with cell death inhibitors Z-Val-Ala-DL-Asp-fluoromethylketone (zVAD, Bachem) for 30 mins, and Necrosulfonamide (NSA, Merck Chemicals), and/or Necrostatin-1 (Nec-1, Sigma-Aldrich) for 2 hrs. While zVAD is a pan-caspase inhibitor which blocks apoptosis, Nec-1 inhibits RIPK1, and NSA MLKL, thereby blocking programmed necrosis/necroptosis (Philipp *et al*, 2015; Sosna *et al*, 2013). Cell death analysis for VPA-induced toxicity of  $\gamma\delta$  T cells was performed by combined annexin-V FITC/ PI staining and also additionally by ATP release using the Cell Titer-Glo Luminescent Cell Viability Assay according to the manufacturer's protocol (Promega). Luminescence was measured by Tecan Infinite-200 microplate reader (Tecan). Briefly, after 24 hrs treatment of  $\gamma\delta$  T cells with VPA and cell death inhibitors (zVAD, Nec1, NSA), cells were harvested for annexin V-FITC/PI staining as described (Bhat *et al*, 2015).

#### **4.1.3 Proliferation assay by $^3\text{H}$ -thymidine incorporation (for results and discussion in section 5.3)**

Proliferation of PBMC, PHA blasts or short-term cultured  $\gamma\delta$  T cells was measured by  $^3\text{H}$ -thymidine ( $^3\text{H}$ -TdR) incorporation as described previously (Falk *et al*, 2004). Shortly,  $0.1 \times 10^6$  PBMC per well were seeded in round bottom 96-well culture plates and stimulated with mitogen or phosphoantigen. For mitogen stimulation, PHA was used and proliferation was measured after

72 hrs, while for phosphoantigen stimulation, BrHPP in X-vivo 15 medium with IL-2 was used and  $^3\text{H-TdR}$  uptake was measured at the end of 7 days. In some experiments,  $\gamma\delta$  T-cell lines were generated by stimulating PBMC with zoledronate plus IL-2, and purity was screened at around day 12. Cell lines with  $> 90\%$   $\gamma\delta$  T cells were used for restimulation with BrHPP and IL-2 in the presence or absence of 5 mM VPA. Proliferation was measured after additional 72 hrs.  $0.5 \times 10^6$  PHA blasts per well on day 11 were kept in IL-2 free medium 24 hrs before use, and the effect of VPA on  $^3\text{H-TdR}$  incorporation was quantitated after 72 hrs in the presence of exogenous IL-2. In each case, cells were labeled with 1  $\mu\text{Ci/well}$   $^3\text{H-TdR}$  (Hartmann Analytic) during the last 16 hrs. After incubation, cells were harvested on glass-fiber filters, and radioactivity was counted in a scintillation counter (PerkinElmer). Data are represented as mean counts per minute (cpm)  $\pm$  S.E. of triplicate cultures.

#### **4.1.4 Flow cytometry**

##### **4.1.4.1 Basic flow cytometry protocol**

For analysis of cell surface proteins, cells were harvested into V-bottom 96 well plate (nerbe plus). Cells were washed once with 200  $\mu\text{l}$  of 1X wash buffer. Respective antibodies for surface staining were incubated for 30 mins at 2-8°C. Afterwards, cells were again washed twice with 200  $\mu\text{l}$  of 1X wash buffer. After the second wash, cells were either resuspended in 1% paraformaldehyde (PFA; for surface staining) or in 200  $\mu\text{l}$  of 1X wash buffer (for intracellular or intranuclear staining). Surface stained cells were measured immediately by flow cytometry (BD LSRFortessa or BD Calibur). For the intracellular or intranuclear staining, 3  $\mu\text{M}$  monensin (EMD Millipore/Calbiochem) was added to the cultures for last 4 hrs. Depending on the experiment, cells with or without surface staining and with or without dead cell exclusion by live/dead fixable far-red dead cell stain kit (Life Technologies) were further subjected to the staining of intracellular or intranuclear proteins. Subsequently, cells were permeabilized using either Cytofix/Cytoperm fixation/permeabilization kit (BD Biosciences) for 30 mins or by BD Pharmingen Transcription Factor Buffer set (BD Biosciences) for 45 mins at 2-8°C. Fixed and permeabilized cells were further stained with respective antibodies for 30-45 mins at 2-8°C. Afterwards cells were washed twice with 200  $\mu\text{l}$  of 1X perm-wash buffer. Stained cells were resuspended in 100  $\mu\text{l}$  of 1X wash buffer and measured immediately by flow cytometry (BD LSRFortessa or BD Calibur). Flow cytometry data was analyzed using CellQuest Pro software

(BD Biosciences) or FlowJo software (FlowJo LLC, Ashland Or, USA). Median fluorescence intensity was calculated by subtracting median intensity of isotype control staining for the respective test antibody staining.

#### **4.1.4.2 NKG2D ligand expression on tumor cells by flow cytometry (for results and discussion in section 5.2)**

Epigenetic inhibitors i.e. Valproic acid (VPA), Trichostatin (TSA), 4-Phenylbutyric acid (4-PBA), Epigallocatechin gallate (EGCG), 5-Aza-2'-deoxycytidine (Decitabine), Curcumin were used at indicated concentration to study modulation of NKG2D ligand expression and release from tumor cells.  $0.8 \times 10^6$  tumor cells in growth medium were seeded in 12-well plate, either treated with respective epigenetic inhibitors, DMSO as solvent control or left untreated. Cells were harvested, washed and surface stained with respective NKG2D ligand antibodies as per method 4.1.4.1. The following anti-human antibodies were used: PE-conjugated anti-human MICA, Alexa Fluor 700-conjugated anti-human MICB, PerCp-conjugated anti-human ULBP-1 and APC-conjugated anti-human ULBP2/5/6 together with respective isotype controls.

#### **4.1.4.3 Immunophenotyping of cultured cells (for results and discussion in section 5.3)**

$0.1 \times 10^6$  PBMC per well in 96-well plates were stimulated with BrHPP or zoledronate and IL-2 in the presence or absence of VPA for 7 days. In experiments involving the analysis of various cell surface marker expression, epigenetic inhibitors were added during the last 24 hrs of 7 day zoledronate-stimulated or staphylococcal enterotoxin mixture-stimulated PBMC. Cultured cells from both experimental set-ups were analyzed by flow cytometry using monoclonal antibodies for human V $\delta$ 2 (Beckman Coulter) FITC, CD3 PE, TCR $\alpha\beta$  FITC, CD25 PE, CD95 PE, HLA-DR PE, CCR5 PE (all from BD Biosciences), CD40 PE (BioLegend), CD54 PE (Beckman Coulter), CD86 PE and NKG2D PE (R&D Systems) as additional surface markers together with PI. Activated lymphocytes were identified based on scatter properties and further gated on PI-negative population.

#### **4.1.4.4 Annexin-PI staining for cell death analysis (for results and discussion in section 5.3 and 5.4)**

PBMC cultured for 7 days with zoledronate plus IL-2 or  $\gamma\delta$  T cells with and without VPA were analyzed for cell death by Annexin V and PI staining. Cells were harvested and washed once with cold PBS. Annexin V-FITC (MabTag GmbH) and propidium iodide (PI; Serva) were added

as per manufacturer's protocol. After 25 mins of incubation at room temperature in the dark, cells were washed with 250  $\mu$ l of Annexin V binding buffer. Stained cells were immediately acquired on FACSCalibur flow cytometer (BD Biosciences) with FL1–FL3 channels. Data analysis was done using the CellQuest Pro software (BD Biosciences).

#### **4.1.4.5 Flow cytometric sorting of T-cell populations for ATAC-seq (for results and discussion in section 5.5)**

T-cell subsets were sorted using flow sorting with FACS Aria device (BD Biosciences). PBMC were stained with fluorophore-labelled antibodies as follows: CD3 Alexa Fluor 647, CD4 Brilliant Violet 510, CD8 APC-Cy7, V $\delta$ 2 PerCp (BioLegend), CD25 Brilliant Violet 421, CD127 PE (BD Biosciences), V $\delta$ 1 FITC (Thermo Fisher Scientific). Flow staining was done in Hanks' Balanced Salt Solution (HBSS, Biochrom) supplemented with 1% heat inactivated fetal calf serum (FCS) and finally resuspended in 500  $\mu$ l volume of the same buffer. T-cell subset populations were defined based on surface markers as follow: CD3<sup>+</sup>CD4<sup>+</sup>CD8<sup>-</sup>CD25<sup>-</sup>CD127<sup>+</sup>V $\delta$ 1<sup>-</sup>V $\delta$ 2<sup>-</sup> for Responder T-cells (referred everywhere as CD4), CD3<sup>+</sup>CD4<sup>+</sup>CD8<sup>-</sup>CD25<sup>hi</sup>CD127<sup>-</sup>V $\delta$ 1<sup>-</sup>V $\delta$ 2<sup>-</sup> for regulatory T-cells (referred everywhere as Treg), CD3<sup>+</sup>CD4<sup>-</sup>CD8<sup>+</sup>CD25<sup>-</sup>CD127<sup>-</sup>V $\delta$ 1<sup>-</sup>V $\delta$ 2<sup>-</sup> for CD8 T-cells, CD3<sup>+</sup>CD4<sup>-</sup>CD8<sup>+/-</sup>CD25<sup>-</sup>CD127<sup>-</sup>V $\delta$ 1<sup>+</sup>V $\delta$ 2<sup>-</sup> for V $\delta$ 1 T cells and CD3<sup>+</sup>CD4<sup>-</sup>CD8<sup>-</sup>CD25<sup>-</sup>CD127<sup>-</sup>V $\delta$ 1<sup>-</sup>V $\delta$ 2<sup>+</sup> for V $\delta$ 2 T cells. After sorting, T-cell subset populations were checked for purity, which was around 98-100 %. All the procedure of FACS sorting and collection of purified T cells were performed in HBSS with 10 % FCS at 4°C. T-cell subsets were then washed once with cold PBS (Cell Concepts), counted microscopically and immediately subjected to ATAC-seq library preparation.

#### **4.1.5 Analysis of culture supernatants for NKG2D ligand shedding (ELISA) (for results and discussion in section 5.2)**

Culture supernatants were harvested employing an experimental setup analogous to the only used to analyze NKG2D ligand expression. Supernatant were quickly spun down to remove debris. Flat-bottom 96-wells Maxisorp Nunc Immunoplates (Thermo Fischer Scientific) were used to quantitate soluble MICA, MICB, ULBP-1, ULBP-2 (DY1300, DY1599, DY1380, DY1298 respectively; all from R&D Systems) by ELISA according to manufacturer's protocol.

## 4.2 Biochemical methods

### 4.2.1 Isolation of exosomes (for results and discussion in section 5.1)

Exosomes were isolated using the ExoQuick™ Exosome Precipitation solution (System Biosciences). Briefly, the cell culture supernatant was centrifuged at 3000g for 15 min to remove cellular debris. Supernatants were filtered through 0.2 µm cellulose acetate filters (Whatman) and the ExoQuick Exosome Precipitation Solution was added at a 1:1 (v/v) ratio. The solution was kept overnight at 4°C. Afterwards, the mixture was centrifuged at 1500 g for 30 min to precipitate exosomes.

Alternatively, exosomes were isolated by differential centrifugation as described previously by Ashiru et al. with slight modifications (Ashiru *et al.*, 2010). Here, 50 ml of culture supernatant was centrifuged for 5 min at 1,400 rpm to remove cellular debris and then filtered through Amicon Ultra-15 centrifugal filters (100 KDa, Merck/Millipore). Subsequently, the media was ultracentrifuged at 100,000g for 2 hrs and the pellet was washed with phosphate buffered saline (PBS) at 80,000 g for 1.5 hrs. The pelleted exosomes were resuspended in 1% NP40 lysis buffer for analysis of MICA expression and subjected to MICA immunoprecipitation.

### 4.2.2 (s)MICA/B immunoprecipitation (for results and discussion in section 5.1)

Exosomes or tumor cells were lysed using 1 % NP40 lysis buffer with inhibitor cocktail. After centrifugation at 14,000 rpm for 10 min at 4°C, MICA protein was immunoprecipitated with anti-human MICA (R&D systems) and protein G sepharose beads (GE Healthcare). For precipitation of soluble MICA, 50 ml of filtered (0.2 µm) culture supernatant was rotated with anti-human MICA antibody and protein G beads overnight at 4°C. The beads were washed thrice with 1 % NP40 buffer and twice with PBS and then subjected to deglycosylation using PNGase F (New England BioLabs).

### 4.2.3 Immunoblotting

Proteins were obtained either from exosome experiments or from proteins on beads from immunoprecipitation experiments for experiments (in section 5.1) or from cultured cell lysates for experiments (all sections). For preparation of proteins, either 1 % NP40 lysis with protease inhibitors (in section 5.1) or 1X TNE cell lysis buffer with protease and phosphatase inhibitors (all sections except section 5.1) was used. Protein concentration was estimated on a spectrophotometer using Bradford's method (Bio-Rad SmartSpec 3000). For immunoblotting



methods in section 2 - 5, 10  $\mu\text{g}$  of protein together with 5X sample loading buffer were run on NuPAGE 4-12 % Bis-Tris Gel (1.5 mm X 15 well) commercially available from Life Technologies. In section 1, all the obtained protein was loaded with 2X SDS sample buffer on 10 % freshly prepared polyacrylamide gels (in section 5.1) with appropriate prestained markers. Proteins were transferred to Hybond C Extra nitrocellulose membranes (GE Healthcare). The membrane was blocked with 5 % BSA or non-fat dry milk and appropriate antibodies against protein of interest or anti-human  $\beta$ -actin as loading control (Sigma-Aldrich) were detected with respective horseradish peroxidase-conjugated secondary antibodies. Proteins were visualized using enhanced chemiluminescence (ECL) western blot detection reagent (GE Healthcare). Details about combination of primary antibodies, blocking and secondary antibodies are mentioned in the following table 4.1.

**Table 4.1: List of antibodies used in the study**

<i>Primary antibody</i>	<i>Blocking</i>	<i>Secondary antibody</i>	<i>Used in section</i>
Anti-MICA/B (BAMO1)	5% BSA	Anti-mouse HRP	5.1
Anti-human H3K9ac	5% non-fat dry milk	Anti-rabbit HRP	5.2, 5.3, 5.4
Anti-human c-Jun	5% non-fat dry milk	Anti-rabbit HRP	5.4
Anti-human phospho-Jun	5% non-fat dry milk	Anti-rabbit HRP	5.4
Bcl-11B	5% non-fat dry milk	Anti-rabbit HRP	5.5
Anti-human $\beta$ -actin	5% BSA	Anti-mouse HRP	5.2, 5.3, 5.4, 5.5

### **4.3 ImageStream analysis (for results and discussion in section 5.2 and 5.4)**

Shortly,  $1 \times 10^6/\text{ml}$  of  $\gamma\delta$  T cells were treated with 5 mM VPA or left untreated as control. After 24 hrs of treatment,  $\gamma\delta$  T-cells were harvested and stained for PE-conjugated Anti-human IL-4 $\delta_{13}$  and Alexa Fluor 488-labelled IL-4R $\alpha$  or FITC-labelled CD107a together with live/dead fixable dye (section 4) or for Pacific Blue-labeled anti-human H3K9ac antibody and DRAQ5<sup>TM</sup> (1  $\mu\text{M}$ ; Abcam plc, Cambridge, UK; section 2 of results). Intracellular or intranuclear staining of cells was performed as per method described in methods section 4.1.4.1. Cells were measured immediately on an ImageStreamX Mark II imaging flow cytometry device (Merck Millipore).

IDEAS software (v6.0, Amnis) was used for analysis. The co-localization wizard implemented in the IDEAS software was applied for single cell analysis (Bhat *et al*, 2016; Fritsch *et al*, 2014).

#### **4.4 Molecular biological and epigenetic methods**

##### **4.4.1 Quantification of mRNA expression (for results - discussion in section 5.2 and 5.4)**

mRNA expression was quantified by real time PCR employing primers specific for the major form of human IL-4, IFN- $\gamma$  and NKG2D receptor-ligands mRNA. RNA was isolated from PBMC,  $\gamma\delta$  T cells or tumor cells using the peqGOLD TriFast Isolation procedure (PepLab). RNA (200 ng) was transcribed into cDNA using the cDNA synthesis kit (AmpTec). PCR amplification for respective genes (Table 3.8) was done at 60°C. qPCR data were analyzed according to the  $\Delta\Delta C_t$  method or the relative quantitation method using the mean  $C_t$  value of the housekeeping genes ( $\beta$ -actin,  $\beta$ 2-microglobulin and 18S). Fold changes of expression levels were calculated and the obtained values were used for further statistical analysis (Quabius *et al*, 2012).

##### **4.4.2 ATAC-seq library preparation (for results and discussion in section 5.5)**

ATAC-seq libraries were prepared as described by Buenrostro *et al* (2013) and Buenrostro *et al* (2015) with slight modifications. Flow sorted T cells (CD4, CD8, Treg, V $\delta$ 1, V $\delta$ 2) in cold PBS were centrifuged at 500 g and 4°C for 5 mins. 50  $\mu$ l of cold lysis buffer was added to cell pellet of 36,000 - 100,000 T cells and was centrifuged immediately for 10 min at 500 g and 4°C. 50  $\mu$ l transposition reaction mix (25  $\mu$ l 2X TED buffer, 2.5  $\mu$ l TDE1 transposase enzyme, 22.5  $\mu$ l water) was added to the nuclei pellet and resuspended several times. The transposition reaction was carried out on thermomixer (Eppendorf) at 37°C with 300 rpm for 30 min, immediately followed by purification using Qiagen MinElute kit (Qiagen) and eluted in 20  $\mu$ l final volume of water.

With the transposed DNA, PCR amplification was carried out by adding 25  $\mu$ l NEB next high fidelity 2X PCR master mix (New England BioLabs), 2.5  $\mu$ l of 25  $\mu$ M PCR primer 1 (Ad1\_noMx; to all reactions) and 2.5  $\mu$ l of 25  $\mu$ M PCR primer 2 (Ad2\_barcode; according to cell-types and individual donors, as details are given in the Table 3.9; Biomers). For PCR the following conditions were applied: 72°C for 5 mins, 98°C for 30 sec followed by 10 cycles of thermocycling at 98°C for 10 sec, 63°C for 30 sec and 72°C for 1 min. Amplified PCR library was purified using Qiagen MinElute kit (Qiagen).

To eliminate DNA fragments more than 800 bp, ATAC-seq library was subjected to size selection using Ampure XP beads (Beckman Coulter) and were again purified using Qiagen

MinElute kit (Qiagen). The quality and concentration of the ATAC-seq library was determined by Agilent High Sensitivity DNA kit on an Agilent Bioanalyzer 2100 (Agilent Technologies). Resulting successful libraries were sequenced for 3 samples per lane with 50 paired end reads on the Illumina HiSeq 2000 platform (Illumina) at BGI-Europe Co. Ltd., Copenhagen, Denmark.

#### **4.4.3 DNA extraction, bisulfite conversion and DNA methylation analysis (for results and discussion in section 5.5 and 5.6)**

Genomic DNA was extracted from T-cell subsets using the commercially available Genra purification kit (Qiagen) following manufacturer's standard protocol. The quality of DNA was determined by NanoDrop ND-1000 spectrophotometer (Thermo Fisher Scientific) and Qubit Fluorometer using the Qubit dsDNA BR Assay kit (Life Technologies). The bisulfite conversion of 1 µg of DNA from each sample was performed using EZ-DNA Methylation kit (Zymo Research) according to the protocol provided by the manufacturer. DNA methylation analysis was performed using hybridization to the Infinium HumanMethylation450 BeadChip (also known as '450k arrays'; Illumina), which covers 99 % of RefSeq genes and 96 % of CpG islands that are more than 485,577. Arrays were scanned using the Illumina iScan (Bibikova *et al*, 2011). DNA methylation data of T cells from healthy donors from 450k microarrays was validated by the bisulfite pyrosequencing (BPS) method (Ammerpohl *et al*, 2016). Briefly, 1 µg of DNA was bisulfite converted using EpiTect Bisulfite kit (48) (Qiagen). PCR amplification of the bisulfite-converted DNA was done using the PyroMark kit (800) (Qiagen) for amplification of DNA sequences around selected CpG loci. The primers used for PCR (Table 3.10) were designed by the PyroMark Assay Design software (Qiagen). As a control, fully methylated DNA, unmethylated DNA (commercially available from EpigenDX Inc., Hopkinton, MA, USA) and genomic control (Non- bisulfite-converted DNA; a pool of DNA isolated from peripheral blood of healthy individuals) were used. BPS and DNA methylation analysis was performed with the PyroMark Q96 ID pyrosequencer and PyroMark CpG software (Qiagen).

#### **4.4.4 RNA extraction, quality control and library preparation (for results and discussion in section 5.5)**

Total RNA including miRNA was extracted from each T-cell population from 4 healthy donors using miRNeasy mini kit (Qiagen) in combination with RNase-free DNase set (Qiagen), according to the manufacturer's protocol with slight modifications. Eluted RNA was stored at -

20°C and shipped on dry ice to the Institute of Clinical Molecular Biology, Christian-Albrechts-University, Kiel, Germany. The quality of RNA was checked using Agilent high sensitivity RNA ScreenTape assay on the Agilent 4200 TapeStation system (Agilent Technologies). Purified RNA was divided into two parts; one part was used for RNA-seq analysis of total RNA (mRNA and lncRNA), while the other part was used for the analysis of miRNA by RNA-seq. cDNA libraries for mRNA and lncRNA analysis were prepared using TruSeq stranded total RNA library preparation kit without enrichment (Illumina). For miRNA analysis, TruSeq small RNA library preparation kit was used. The resulting libraries were sequenced on an Illumina HiSeq 2500 platform using a paired-end run (2 x 125 bp for mRNA and lncRNA; 2 x 50 bp for miRNA). An average of ~26 million 125-nt paired-end reads was sequenced for each sample.

#### **4.5 Bioinformatic analysis**

##### **4.5.1 Bioinformatics analysis of IL-4, CASP3, MLKL and HDAC1 (for results and discussion in section 5.4)**

IL-4, CASP3, MLKL, HDAC1 genes were analyzed in UCSC Genome Browser (hg19 assembly). A list of transcription factors associated with respective genes from CHIP-seq ENCODE database with factorbook motifs was derived. The unique set of transcription factors involved in the regulation of all 4 genes was further analyzed using String database for protein-protein interaction and association studies. All prediction methods, viz. neighborhood, gene fusion, co-occurrence, co-expression, experiments, databases and text mining were used with high confidence score (0.700), showing direct interaction through links for each type of method as described by Szklarczyk *et al* (2015).

##### **4.5.2 Analysis of ATAC-seq data (for results and discussion in section 5.5)**

To analyze the accessibility of the DNA in the CD4, CD8, Treg and  $\gamma\delta$  T cells of four human donors, ATAC-seq was performed as described by Buenrostro *et al* (2013). Paired-end 100 bp reads were each trimmed to 50 bp with fastx\_trimmer (v0.0.13; [http://hannonlab.cshl.edu/fastx\\_toolkit](http://hannonlab.cshl.edu/fastx_toolkit)) to prevent adapter contamination of DNA fragments smaller than 100 bp. Then, reads were aligned to human genome version hg19 using bowtie (v2.1.0, Langmead *et al*, 2012) with parameters “-X 3000” and “-no-discordant”. Those parameters ensure that fragments up to 3,000 bp are allowed to align (“-X 3000”) and that no contradictory alignments of a read pair are allowed (“-no-discordant”). The Picard tool (v2.1.1;

<http://broadinstitute.github.io/picard>) MarkDuplicates was used to remove duplicated DNA fragments to account for PCR artifacts. To calculate DNA fragment coverage for browser display, deepTools' bamCoverage was used (v2.7; Ramirez *et al*, 2014). Specifically, three distinct tracks of genome-wide fragment coverage were generated as bigWig files: (i) The coverage for all mapped fragments with the command line options “-bs 5 --normalizeUsingRPKM --minMappingQuality 30”; (ii) the coverage for fragments with a size between 180bp and 247bp, i.e. mono-nucleosome coverage (see also Buenrostro *et al*, 2013), with command line options “-bs 5 --normalizeUsingRPKM --minMappingQuality 30 --minFragmentLength 180 --maxFragmentLength 247 -e 220”; and (iii) the coverage for fragments with a size up to 100bp, i.e. nucleosome free regions (NFR), with command line options “-bs 1 --minMappingQuality 30 -e 1”. The read starts in the NFR coverage tracks were adjusted to represent the center of the Tn5 transposase binding event (Gangadharan *et al*, 2010) by offsetting read starts that align to the + strand by +4 bp and those that align to the – strand by –5 bp. To identify regions of significant DNA accessibility, peaks were called on offset read starts using MACS (v2.1.1.20160309; Zhang *et al*, 2008). To obtain a hierarchical clustering of samples based on Pearson's r, reads with mapping quality greater than 10 were quantified in 1,000bp non-overlapping genomic windows using bamsignals' bamProfile() function (v1.4.2; <http://bioconductor.org/packages/bamsignals>). For the mono-nucleosomal fraction, the center of a DNA fragment was counted. For the NFR fraction, the start and end of a DNA fragment was counted because they represent to independent transposition (cutting) events.

#### **4.5.3 Analysis of DNA methylation data (for results and discussion in section 5.5 and 5.6)**

Raw hybridization signals were processed using GenomeStudio software (v2011.1; Illumina) in methylation analysis module (v1.9.0; Illumina), applying default settings. The intrinsic controls present on the array were used for data normalization. To exclude technical and biological biases, we used several filters including sex-specific CpG and ‘rs-tags’ non-CpG probes. As analyzed by 450k arrays, we further excluded polymorphisms with an allele frequency > 5 % in the population, which are located within a distance of 0-3 bp next to cytosine. A detection p-value below 0.01 per CpG site was set as internal quality control criteria considering the technical results of hybridization. A total of 470,183 CpG sites were further annotated to

HumanMethylation450 v1.2 Manifest file (Illumina) using the UCSC Genome Browser database (hg19 version) (Kent *et al*, 2002).

#### 4.5.4 Healthy T cell methylome (for results and discussion in section 5.5)

The methylation level at each CpG is represented by the  $\beta$  value, defined as the proportion of the methylated signal to the total signal and calculated from normalized intensity values. Statistical analysis was performed on the list of CpG sites passing above mentioned criteria using Qlucore Omics Explorer (v2.3(45), 64-bit; Qlucore). CpG sites were considered statistically significant for the p-value 0.01 and were adjusted with q-value 0.01803 (also interpreted as false discovery rate; FDR). These statistically significant CpG sites and an absolute difference in the mean  $\beta$  value  $|\Delta\beta|$  (also referred as ‘delta beta’)  $\geq 0.2$  between  $\alpha\beta$  T-cell subset group (includes CD4, CD8 and Treg) and  $\gamma\delta$  T-cell group were defined as differentially methylated probes (DMPs), further divided as ‘hypomethylated in  $\gamma\delta$ ’, ‘hypermethylated in  $\gamma\delta$ ’, or ‘partially methylated in  $\gamma\delta$ ’. Partially methylated in  $\gamma\delta$  are the all CpG sites between +0.2 to -0.2 delta beta values. The location of CpG sites in relation to the genomic region with the possibility of alternative TSS and regions containing more than one gene was defined as follow: TSS1500 (from 201 to 1500 bp upstream of the TSS), TSS200 (from 1 to 200 bp upstream of the TSS), 5' UTR, 1<sup>st</sup> Exon, gene body and 3' UTR. Relation of CpG site to CpG islands (CGI) was defined as CGI (within CpG Islands), CGI shore (0-2 kb from CGI edge), CGI shelf (>2 kb to 4 kb from CGI edge) and outside CGI (Kulis *et al*, 2015). Wherever indicated, adjusted p-values were calculated using non-parametric Wilcoxon signed-rank test with the multiple hypothesis testing correction by the Benjamini-Hochberg method. Statistical analysis and graphs were generated using R (3.3.1) and Bioconductor packages. Alternatively, RnBeads package were used for DNA methylation analysis. Briefly, idat file from respective hybridization arrays were loaded into RnBeads package in R (Assenov *et al*, 2104). Furthermore, vanilla analysis mode was used. Beta values for each CpG sites were converted to M-value using default options. The comparison between beta values from RnBeads and GenomeStudio was performed.

#### 4.5.5 $\gamma\delta$ -HSTL methylome (for results and discussion in section 5.6)

As described above for the methylome of healthy T cells, bioinformatics analysis was done using similar pipeline and annotations with slight modifications. Briefly, the list of CpG sites after all exclusion, quality control and detection p-value <0.01 were imported into Qlucore Omic

Explorer. In this study, only one sample per group was investigated for global DNA methylation. Hence we used 0.25 filter by variance ( $\sigma/\sigma_{\max}$ ) criteria. Beta value per CpG was used to calculate  $|\Delta\beta|$  ('delta beta')  $\geq 0.2$  between methylation level of visit 5 and visit 1. DMPs were further divided as 'hypomethylated on visit 5', 'hypermethylated on visit 5', or 'partially methylated on visit 5'. All other genomic features and CGI features were analyzed as described above.

#### **4.5.6 Analysis of RNA-seq (for results and discussion in section 5.5)**

##### **4.5.6.1 Transcriptome analysis**

Raw reads were pre-processed using cutadapt (Martin *et al*, 2011) to remove adapter and low quality sequences and were then aligned to the human genome (GrCh38) reference genome with Ensemble gene annotation using TopHat2 (Trapnell *et al*, 2012). HTSeq was used to compute gene expression values of transcripts (Anders *et al*, 2015). Differential gene expression levels were analyzed and visualized by the Bioconductor package DESeq2 (Love *et al*, 2014). DESeq2 was used to perform principal component analysis (PCA) that illustrate a separation according to the first principal component between CD4, CD8, Treg and  $\gamma\delta$  T-cells. Differential expression of genes between T-cell subsets was determined using Wald tests to calculate the significance of differential expression for each gene in a pair-wise comparison between CD4, CD8 and Treg versus  $\gamma\delta$  subtypes.

##### **4.5.6.2 Long non-coding RNA analysis**

The long non-coding RNA was identified and quantified using PLAR (Hezroni *et al*, 2015) for the same set of comparisons as described above. Application of PLAR allowed us to combine multiple complementary filters for the potential protein-coding to distinguish between coding and non-coding transcripts (Hezroni *et al*, 2015). Different types of transcripts identified by PLAR for the pair-wise comparison between CD4, CD8 and Treg versus  $\gamma\delta$  T cells that they are assigned to protein coding, long non-coding RNA (lncRNA), long intervening non-coding RNA (lincRNA) and small RNA. Differential expression analyses of long non-coding RNA were done by Cufflinks and Cuffdiff (Trapnell *et al*, 2012).

##### **4.5.6.3 miRNA analysis**

miRNA profiling was performed using Illumina sequencing technology. After adapter trimming using cutadapt v1.3 (Martin, 2011), reads mapping to viral genomes, human non-miRNA short RNA and non-human miRNA were excluded. Subsequently, count data was generated

employing miRDeep2 (Friedländer *et al*, 2012). Finally, unexpressed miRNAs (with counts not being  $> 20$  in  $> 50\%$  of the samples per trait) were discarded.

For exploratory analysis, raw counts were subjected to a variance-stabilizing transformation (VST) as implemented in DESeq2 (Love *et al*, 2014) and projected on the 2-dimensional space employing multidimensional scaling (MDS) with a distance based on Spearman correlation. Differential expression (DE) analysis then was performed conducting statistical hypothesis testing (likelihood ratio (LR) test) based on generalized linear models (GLMs as implemented in DESeq2) for all pairs of cell types (Treg vs.  $\gamma\delta$ , CD4 vs.  $\gamma\delta$ , CD8 vs. Treg, CD4 vs. CD8, CD8 vs.  $\gamma\delta$ , CD4 vs. Treg). Furthermore, a combined analysis was performed to compare  $\alpha\beta$  to  $\gamma\delta$  cells. For a given comparison miRNAs were considered as being significantly DE in case of adjusted p-values  $< 0.05$  and absolute logarithmic fold changes  $|\log_2(\text{FC})| > 1$ . Thereby correction for multiple testing was conducted according to Benjamini and Hochberg (Benjamini and Hochberg, 1996). For illustrative purpose heatmap of expression patterns were generated for miRNAs that were differentially expressed with respect to any of the cell type comparisons. Thereby a distance based on Spearman correlation and complete linkage was used.

#### **4.5.7 Integrated analysis of ATAC-seq, DNA methylation and RNA-seq data (for results and discussion in section 5.5)**

To integrate the data from 450k DNA methylation arrays, transcriptome and lncRNA profiling, we used standard gene symbols (hg19, UCSC genome database). The genes from respective datasets were merged by simple merged command in R program. To determine association between these three levels of epigenetic processes, Fitting Linear Regression Model was used. The gene expression level was considered as dependent variable on methylation and lncRNA expression levels (independent variables; van Eijik *et al*, 2012). For the regression analysis between methylation and lncRNA, DNA methylation was considered as dependent variable and lncRNA expression level as independent variable. Furthermore, correlation analyses based on Pearson method and principal component analyses were done on each possible combination of dataset comparisons. The integrated analysis data was represented by biplot and heatmap with clusters.



**4.5.8 Functional annotation (for results and discussion in section 5.5 and 5.6)**

Functional annotation was performed using the online available databases either by PANTHOR (Mi *et al*, 2016), by Enrichr (Kuleshov *et al*, 2016) or by InnateDB (Breuer *et al*, 2013) using default parameters.

**4.6 Statistical analysis**

Data were analyzed using PrismGraph (GraphPad Software) either with analysis of variance (ANOVA) with repeated measures or student's t-test. For comparison of samples with controls, multiple comparison tests were applied. p-values <0.05 were considered significant and displayed as \* for p-value < 0.05, \*\* for p-value < 0.01, \*\*\* for p-value < 0.001.

## 5 Results

### 5.1 Release of NKG2D ligands from tumor cells: *Exosomes versus shedding*

*Associated publication:*

The results presented in this chapter are already published in the manuscript: Guranda Chitadze\*, Marcus Lettau\*, **Jaydeep Bhat**, Daniela Wesch, Alexander Steinle, Daniel Fuerst, Joannis Mytilineos, Holger Kalthoff, Ottmar Janssen, Hans-Heinrich Oberg\* and Dieter Kabelitz\*. (2013) Shedding of endogenous MHC class I-related chain molecules A and B from different human tumor entities: Heterogenous involvement of the “a disintegrin and metalloproteases” 10 and 17. *International Journal of Cancer*, 133:1557-1567. (\* equally contributing authors)

Cellular differentiation and functional responses to the external environment are controlled by genetic and epigenetic mechanisms. In comparison to  $\alpha\beta$  T-cells, human  $\gamma\delta$  T-cells exhibit a surprising extent of functional plasticity. The primary function of  $\gamma\delta$  T-cells is the control of cellular integrity and stress surveillance. As a consequence,  $\gamma\delta$  T-cells have a broad anti-tumor activity. Key mediators involved in the execution of such responses are NKG2D receptor - ligands which are not expressed on normal cells but are induced by cellular stress and are constitutively expressed on transformed cells (Raulet 2003; Raulet *et al*, 2013; Wrobel *et al*, 2007). Cytotoxic cells including  $\gamma\delta$  T-cells, recognize NKG2D ligands expressed on the surface of tumor cells. However, tumor cells also have the capacity to escape from recognition by immune cells, by releasing soluble NKG2D ligands. This immune escape mechanism broadly affects cytokine production and cytotoxicity of human  $\gamma\delta$  T-cells. Thus, within the scope of this PhD thesis, I first addressed this important mechanism of tumor immune escape, which also affects human  $\gamma\delta$  T-cell function.

#### 5.1.1 Expression and release of MICA depends on origin of tumor cell type

Previously it was reported that tumor cells have the capacity to proteolytically release NKG2D ligands, a phenomenon termed ‘shedding’ (Groh *et al*, 2002), through distinct cleavage activity of cell surface enzymes. With this background information, we sought to investigate the shedding activity of tumor cells of different origin, specifically pancreatic ductal adenocarcinoma (PancTu-I, Panc89), prostate carcinoma (PC-3) and breast carcinoma (MDA-MB-231). All tested cancer cell lines expressed differential amounts of MICA protein on the cell surface as revealed by flow cytometry (Fig. 5.1.1). Panc89, PancTu-I and MDA-MB-231 showed

high surface expression of MICA/B while PC-3 expressed lower levels. Release of MICA and MICB present in 24 hrs cell culture supernatants were quantified by ELISA. MICA was detected in cell culture supernatants of all tested tumor cell lines except PC-3. From PC-3 cells, only MICB release was detectable, despite MICA cell surface expression. Thus, preliminary results obtained from cell surface protein expression and culture supernatants prompted us to investigate this diversity of MICA shedding from different tumor entities in more detail.

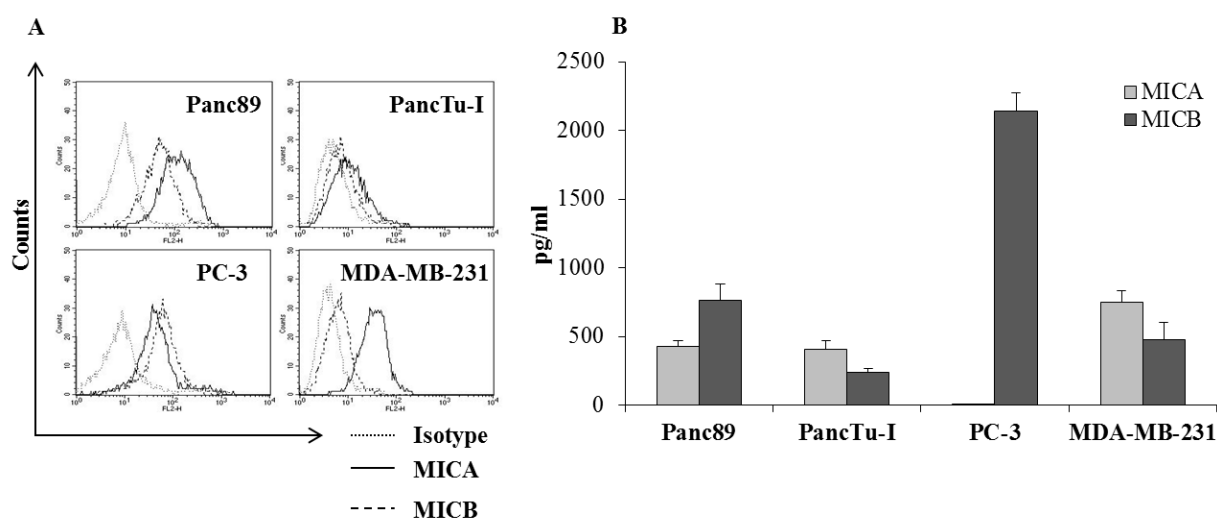


**Figure 5.1.1: Different epithelial cancer cell lines express and release soluble MICA and MICB into the supernatant.** Cells were cultivated for 24 hrs. (A) Cell surface expression of MICA (solid lines) and MICB (thick dotted lines) was determined by flow cytometry. Thin dotted lines represent the isotype control. (B) The amount of sMICA (light gray) and sMICB (dark gray) from harvested supernatant was determined by ELISA. Data are represented as mean values of three independent experiments  $\pm$  standard error of the mean (SEM). Data and figure is adapted from Chitadze, Lettau, Bhat *et al.*, (2013) published in International Journal of Cancer, 133:1557-1567.

### 5.1.2 MICA antibody specifically detects full-length (truncated) form of protein

PC-3 cells fail to shed MICA despite the fact that it is expressed on the cell surface. As the allelic variant MICA\*008, which results in a protein with a truncated intracellular part, is described to be released in association with exosomes (Ashiru *et al.*, 2010), we addressed MICA protein expression biochemically via Western blot analysis. MICA was immuno-precipitated from cellular lysates and, after deglycosylation by PNGase F, subjected to SDS-PAGE and transferred to nitrocellulose (Fig. 5.1.2). As expected, deglycosylated MICA migrated at 42 KDa in the case

of Panc89, PancTu-I and MDA-MB-231 cells, whereas MICA was detected as a 33-KDa band in lysates from PC-3 cells. This clearly indicated that these cells might express a truncated form of MICA as described for the allelic variants MICA\*008, MICA\*023, MICA\*028 and MICA\*054 (Huovila *et al*, 2005). Consequently, MICA from PC-3 cells comigrated with MICA precipitated from HeLa cells (not shown), which are homozygous for MICA\*008 (Ashiru *et al*, 2010).

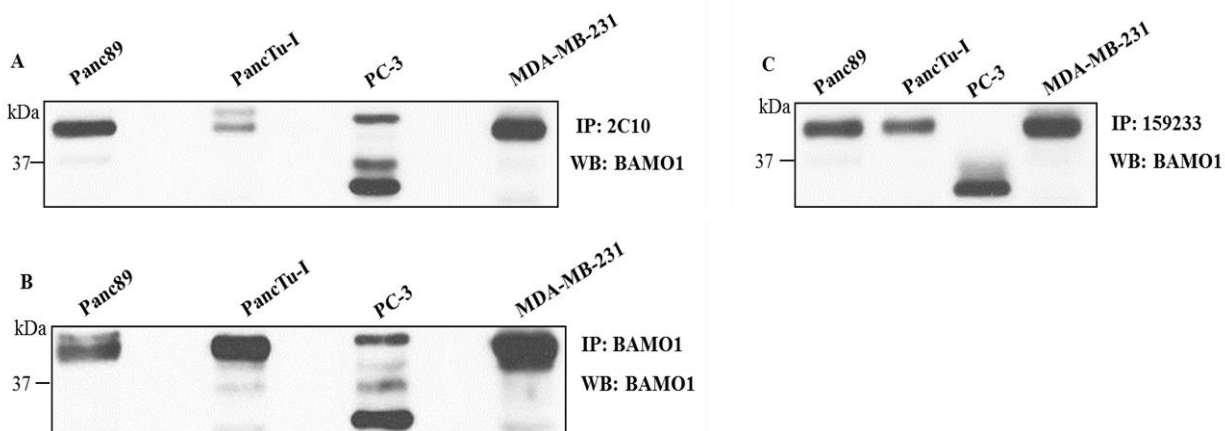


**Figure 5.1.2: MICA allelic variation is associated truncated protein expression in PC-3.** MICA from tumor cell lysates was immunoprecipitated by anti-MICA mAb, deglycosylated by PNGase F, separated by SDS-PAGE and detected by Western blot using anti-MICA mAb BAMO1. Three different clones *viz.* A) 2C10 from Santa Cruz Biotech, B) 159233 from R&D Systems, C) BAMO1 from BAMOMAB GmbH, Germany were tested for immunoprecipitation of MICA protein.

### 5.1.3 Pancreatic carcinoma shed MICA in culture supernatant

After establishing a biochemical read-out for the analysis of MICA variants in cell lysates, we employed this approach for culture supernatants along with cell lysate to analyze soluble MICA. Cultures were grown for 4 days or until they reached a confluency of more than 90 %. Culture supernatant was harvested and cell lysate from the same experiment was used for MICA analysis by immunoprecipitation and western blot. Further, we precipitated the cleaved ectodomain of MICA from supernatants of PancTu-I cells and detected it as a faint band at about 32 KDa, which migrated slightly beneath full-length MICA of PC-3 cells (Fig. 5.1.3). Interestingly, a MICA fragment that resembles sMICA in size is also detected in cellular lysates of PancTu-I cells, indicating that cleavage might occur within an intracellular compartment.

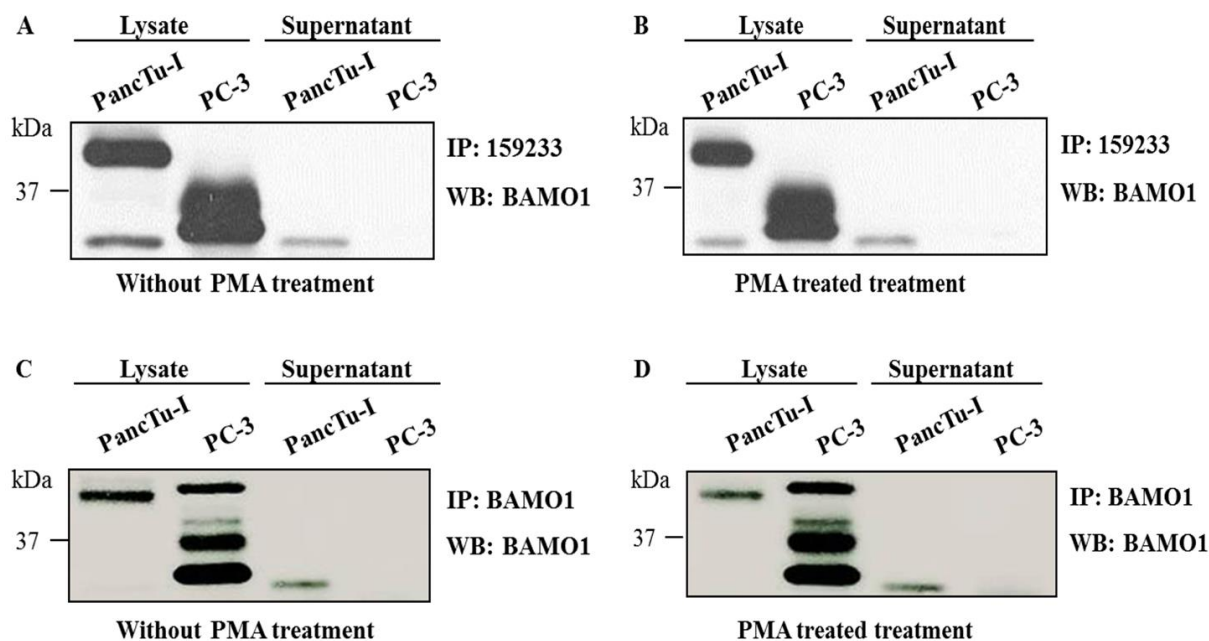


**Figure 5.1.3: MICA shedding in the PancTu-I cell line.** PancTu-I and PC-3 cells were cultured for 4 days and cells were harvested to prepare lysate. Simultaneously culture supernatants were harvested for the analysis of MICA protein release without (A, C) and with PMA treatment (B, D) for 24 hrs. Cell lysates and supernatants were subjected to immunoprecipitation with 159233 from R&D Systems (A, B) or with BAMO1 from BAMOMAB GmbH, Germany (C, D). After deglycosylation with PNGase F, protein was analyzed by western blot with clone BAMO1 (BAMOMAB GmbH, Germany) for detection of human MICA.

We also tried to enhance shedding by PMA treatment. However, we failed to detect significant changes in expression levels of any of the MICA protein. In line with our previous results, we failed to detect sMICA released from PC-3 cells.

#### 5.1.4 Prostate cancer cell lines release MICA through exosomes

In a similar experiment, we precipitated MICA from exosomes isolated from the supernatants of PancTu-I and PC-3 cells using a commercial exosome precipitation kit. We detected the truncated full-length form of the MICA\*008 variant expressed in PC-3 cells in exosomes, but not in PancTu-I-derived exosomes (Fig. 5.1.4). The same results were obtained with exosomes isolated by a classical ultracentrifugation protocol (Fig. 5.1.4C - F). Of note, MICA was also

absent from Panc89- and MDA-MB-231-derived exosomes. MICA was also detected in cellular lysates of PancTu-I, Panc89 and MDA-MB-231 cells (data not shown).

Based on the results of culture supernatant, use of different antibody clones, alternative methods of exosome isolation and PMA treatment did not induce any change in MICA protein expression analyzed from supernatant-derived exosomes. Taken together, these data clearly indicate that endogenous MICA\*008 expressed in PC-3 cells is released in association with exosomes, while absence of MICA\*008 expression from PancTu-I, Panc89 and MDA-MB-231 doesn't result in such exosomal release.

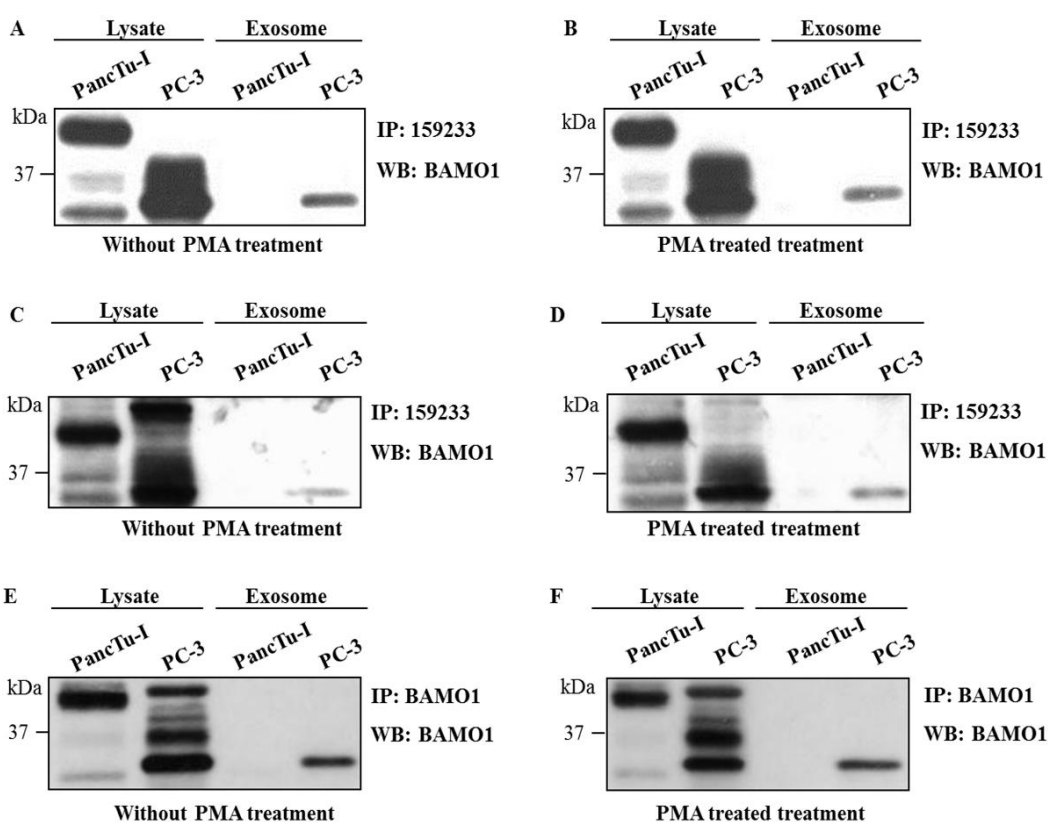


**Figure 5.1.4: Release of MICA through exosomes by PC-3 cells.** PancTu-I and PC-3 cell lines were left untreated (A, C, E) or treated with PMA for 24 hrs (B, D, F). Exosomes were isolated either by using ExoQuick™ Exosome precipitation (System Biosciences, USA) method (A, B) or by using traditional ultracentrifugation (C - F). In each case, deglycosylation by PNGase F, immunoprecipitation by anti-human MICA mAb clone 159233 from R&D Systems (A - D) or with anti-human MICA mAb BAMO1 from BAMOMAB GmbH, Germany (C, D), detection by anti-human MICA/B mAb (BAMOMAB GmbH, Germany) was performed using SDS-PAGE.

## 5.2 Epigenetic modulation of NKG2D receptor and ligands: *Mechanism of NKG2D ligand release and functional effects*

*Associated manuscript:*

The results presented in this chapter will be part of a manuscript (in preparation): **Jaydeep Bhat**, Samuel Dubin, Alexandra Dananberg, Elgar Susanne Quabius, Guranda Chitadze, Jürgen Fritsch, Marie Dowds, Marcus Lettau and Dieter Kabelitz.

The detection of soluble MICA in the sera of patients has emerged as an important prognostic marker (Holdenrieder *et al*, 2006; Holdenrieder *et al*, 2006; Kumar 2012). In addition to its soluble form, allelic and single nucleotide polymorphisms of MICA were shown to be associated with several diseases, including cancer and inflammation-associated diseases (Kumar 2012; Frigoul and Lefranc, 2005). Hence, it is of interest to investigate the effect of therapeutic agents on NKG2D ligand release. Out of several other mechanisms that modulate NKG2D ligand expression and release, epigenetic mechanisms are of special interest due to the availability of epigenetic modifiers/inhibitors. Thus, in this section, the effect of various epigenetic inhibitor(s) on the modulation of NKG2D ligand shedding and the functional consequences on immune cells such as activated  $\gamma\delta$  T cells in comparison to freshly isolated PBMC will be addressed.

### 5.2.1 Epigenetic modifiers differentially modulate NKG2D ligand surface expression and release from pancreatic carcinoma and prostate carcinoma cells

As shown in the previous section and also indicated by further findings from our group, the pancreatic carcinoma cell line PancTu-I are heterozygous for MICA\*002:01 (A9), MICA\*009:01 (A6) and the prostate carcinoma cell line PC-3 are heterozygous for MICA\*008:01:01 (A5.1), MICA\*012:01:01 (A4). Based on these differences of MICA alleles, PancTu-I cells shed MICA/B directly, whereas PC-3 cells release MICA via exosomes (Chitadze *et al*, 2013). To address the potential role of epigenetic mechanisms, I used 6 different epigenetic inhibitors specific for 3 different important epigenetic processes. Trichostatin A (TSA), Valproic acid (VPA) and 4-Phenylbutric acid (4-PBA) targeting histone deacetylation by HDAC, Epigallocatechin gallate (EGCG) and 5-Aza-2'-deoxycytidine (Decitabine) targeting DNA methylation by DNMT and Curcumin targeting histone acetylation by HAT were used.

The experimental strategy to investigate the effect of epigenetic inhibitors on PancTu-I and PC-3 cells is schematically represented in Figure 5.2.1. All epigenetic modifiers were titrated for their cell-type dependent effective dose concentrations (Bhat *et al*, 2015; Bhat *et al*, 2016).

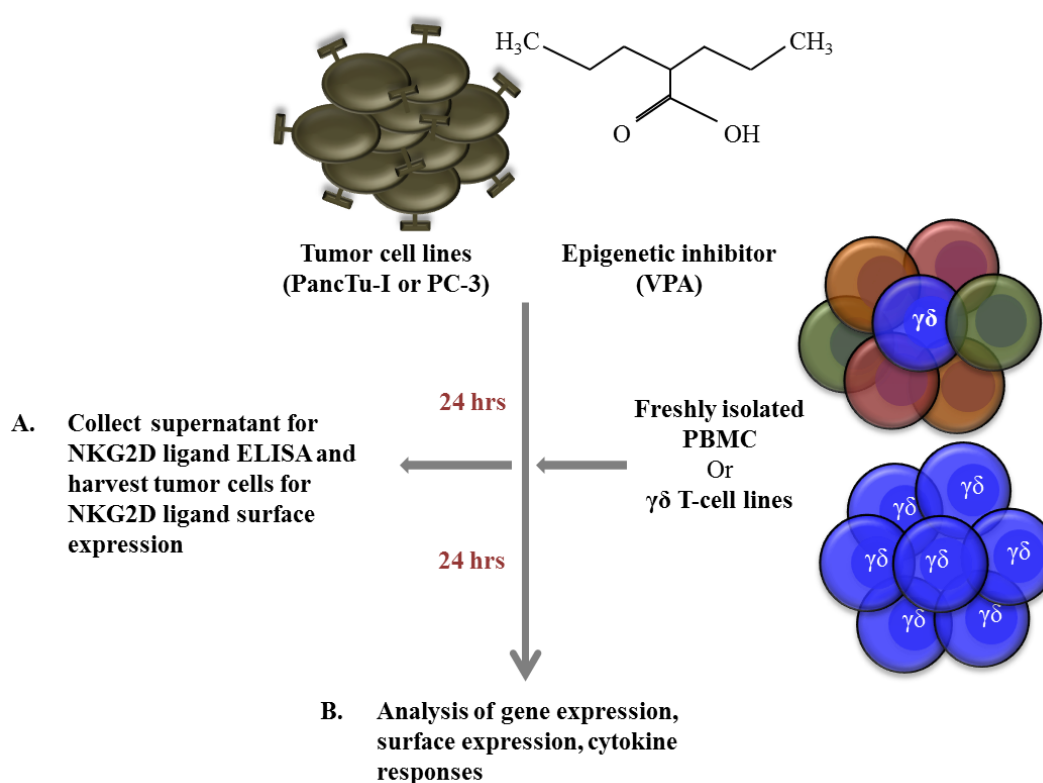


**Figure 5.2.1: Experimental strategy to analyze the modulation of NKG2D receptor - ligand mediated functional responses to epigenetic inhibitors.** NKG2D ligand (MICA, MICB, ULBP-1 and ULBP-2/5/6) expression and release from the pancreatic carcinoma cell line (PancTu-I) and prostate carcinoma cell line (PC-3) was measured after 24 hrs treatment with epigenetic modifiers. A) After 24 hrs, tumor cells were analyzed for NKG2D ligand expression and culture supernatants were collected to quantitate NKG2D ligands released from the same experiment. B) Otherwise, effector cells (freshly isolated PBMC or  $\gamma\delta$  T-cell lines) were added to tumor cells for co-culture at a 1:1 ratio. After 24 hrs of co-culture, effector and/or tumor cells were harvested and analyzed for NKG2D receptor expression by flow cytometry, or NKG2D receptor - ligand gene expression by qPCR.



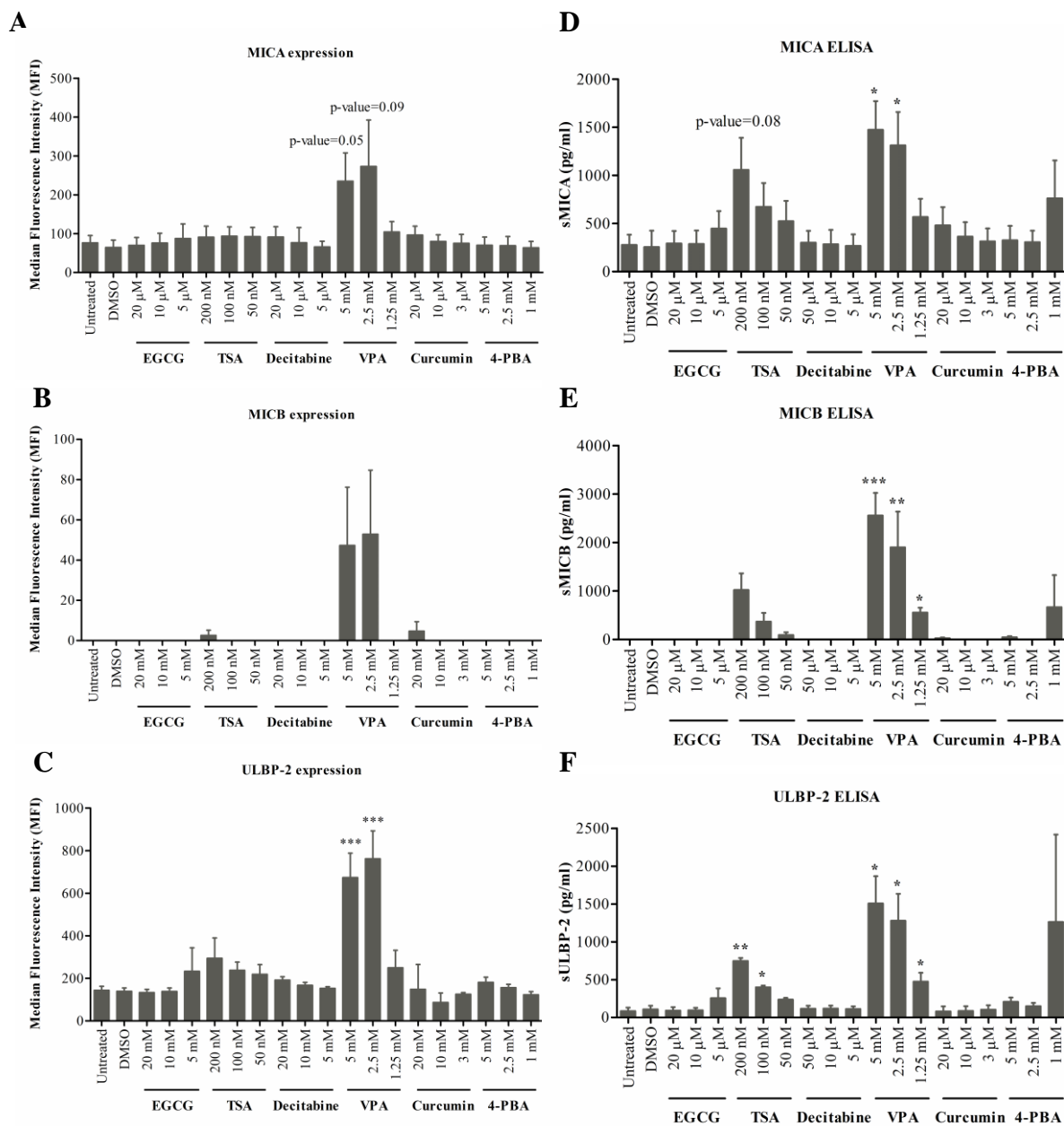


**Figure 5.2.2: Modulation of NKG2D ligand expression and release from pancreatic cancer cell line by epigenetic modifiers.** As schematically shown in figure 1,  $0.8 \times 10^6$  PancTu-I cells were treated with varying concentrations of inhibitors for HDACs, HATs and DNMTs. After 24 hrs, (A-C) cells were harvested for the analysis of MICA, MICB and ULBP-2 surface protein expression, respectively. (D-F) Culture supernatants from the same experiments were analyzed for the release of MICA, MICB and ULBP-2. Data represents mean values  $\pm$  S.E. of three independent experiments. Statistical significance with p-value  $<0.05$ ,  $0.01$  and  $0.001$  are indicated by \*, \*\* or \*\*\*, respectively.

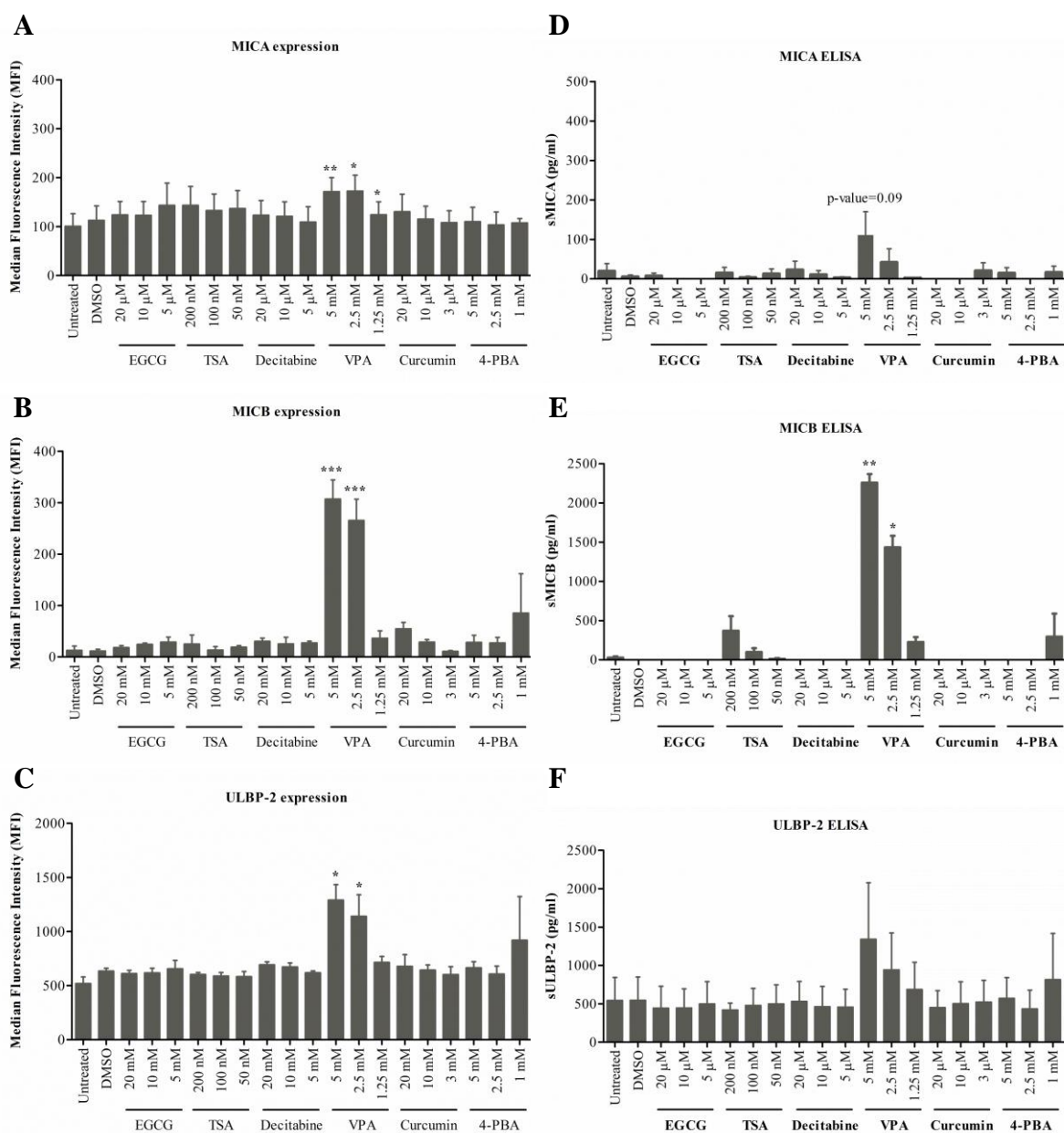


**Figure 5.2.3: Modulation of NKG2D ligands expressed and released from prostate cancer cell line by epigenetic inhibitors.** In a similar approach as shown for PancTu-I cells in figure 3, PC-3 cells were analyzed for MICA, MICB and ULBP-2 expression, respectively (A-C). (D-F) Culture supernatants were quantitated for respective soluble NKG2D ligand proteins. Data summarized as mean  $\pm$  S.E. from 3 independent experiments and p-values for 0.05, 0.01 and 0.001 shown as \*, \*\*, and \*\*\*, respectively.

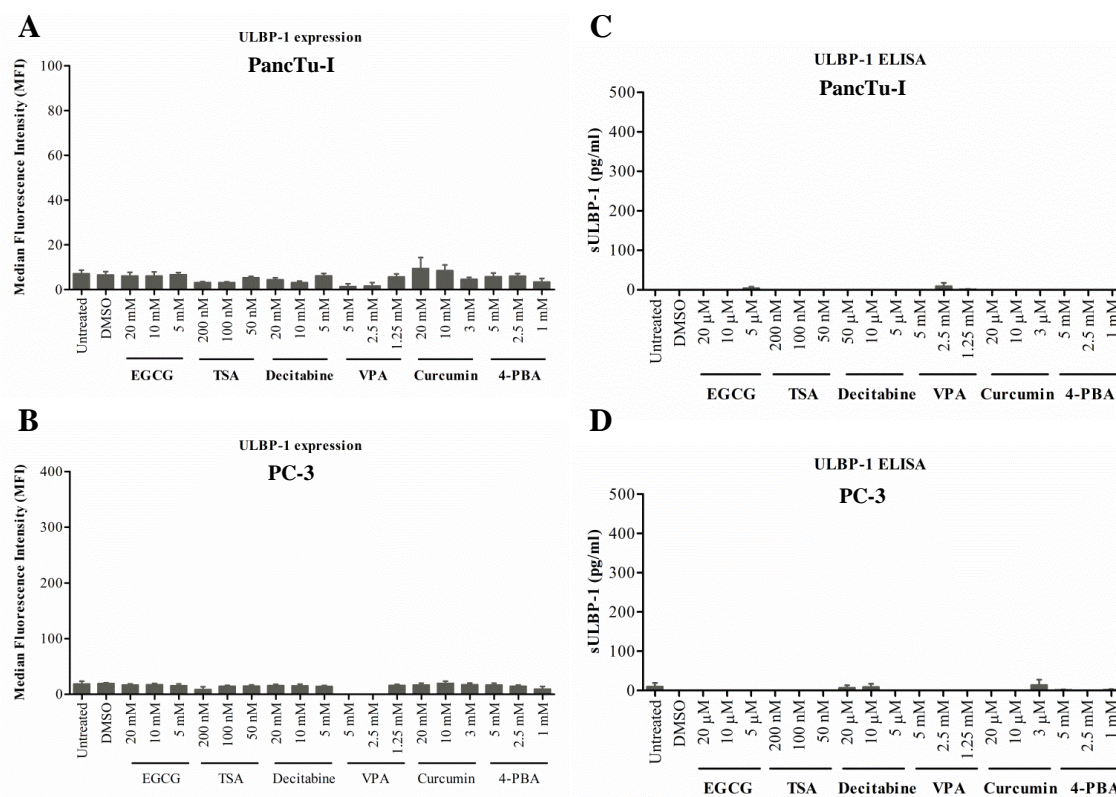


**Figure 5.2.4: Epigenetic modifiers do not modulate ULBP-1 expression and release from tumor cells.** PancTu-I and PC-3 cell lines were treated with different concentrations of epigenetic modifiers. After 24 hrs, PancTu-I (A) and PC-3 (B) cells were analyzed for cell surface ULBP-1 expression by flow cytometry, while the release of ULBP-1 from PancTu-I (C) and PC-3 (D) cells into culture supernatants was analyzed by ULBP-1 ELISA. Data displayed as mean values  $\pm$  S.E. of three independent experiments.

After 24 hours of VPA treatment at the concentration of 5 mM and 2.5 mM, PancTu-I cells showed a significant increase in MICA, MICB and ULBP-2/5/6 (also referred as ULBP-2) cell surface expression (Fig. 5.2.2A-C). Likewise PC-3 cells showed a significant expression of MICB and ULBP-2 but, increase in MICA was comparatively less after 5 mM and 2.5 mM VPA treatment (Fig. 5.2.3A-C). This was also evident from a shift in histograms after VPA treatment compared to untreated controls (data not shown). Analysis of soluble NKG2D ligands in culture supernatants by ELISA also showed a remarkable increase in the release from both cell lines after treatment with 5 and 2.5 mM VPA (Fig. 5.2.2D-F, 5.2.3D-F). In contrast to these results,

there was no increase in ULBP-1 cell surface expression (Fig. 5.2.4A-B) and release from PancTu-I and PC-3 cell lines upon treatment with epigenetic inhibitors (Fig. 5.2.4C-D). Treatment with the other HDAC inhibitor TSA also induced an increase in the release of MICA, MICB and ULBP-2/5/6 from PancTu-I cell culture supernatants, but not in surface expression of PancTu-I and no effect was observed in PC-3 cells. Of note, the epigenetic modifiers did not induce notable cell death at the concentration used (data not shown).

Thus, out of six total different epigenetic modifiers used, only VPA (an HDAC inhibitor) induced significant amount of shedding of MICA, MICB and ULBP-2 from both pancreatic carcinoma and prostate carcinoma cell lines irrespective of its allelic MICA variation.

### **5.2.2 VPA affects NKG2D receptor expression differentially on the cell surface of activated $\gamma\delta$ T-cells and freshly isolated PBMC**

Previous experiments showed that VPA treatment induces a significant increase (more than 3-4 fold) in MICA/B and ULBP-2 surface expression and release from tumor cells of different origin. Using a co-culture experiment setting, we tested the effect of VPA-induced NKG2D ligand shedding on effector cells, i.e. freshly isolated PBMC and short-term  $\gamma\delta$  T-cell lines obtained from zoledronate-stimulated PBMC. As expected,  $\gamma\delta$  T-cells down modulated NKG2D receptor expression upon co-culture with PancTu-I and PC-3 for 24 hrs. This effect was strikingly enhanced by VPA treatment of tumor cells before co-culture for 24 hrs (Fig. 5.2.5A, B). Down modulation of cell surface expression was evident from histograms presented in figure 5.2.5A and 5.2.5E (upper panel for untreated cells and lower panel for 2.5 mM VPA treatment). Interestingly, this effect was not seen in the co-culture with freshly isolated PBMC (Fig. 5.2.5E, F). In support of these observations and also to dissect the modulation of NKG2D receptor on effector cells ‘only’ by NKG2D ligands, but not by other tumor-derived proteins, we used a mixture of reconstituted NKG2D ligands as described in the materials and methods. sNKG2DL or imNKG2DL together with 2.5 mM VPA significantly decreased the expression of the NKG2D receptor on  $\gamma\delta$  T-cells (Fig. 5.2.5C, D), while in PBMC, the opposite effect was observed (Fig. 5.2.5G, H). One reason behind such selective downregulation of NKG2D on  $\gamma\delta$  T-cell might be the VPA treatment (Bhat *et al*, 2015). Nevertheless, it is interesting to note that NKG2D receptor expression on  $\gamma\delta$  T-cells and PBMC is differentially modulated by soluble versus immobilized NKG2D ligands.

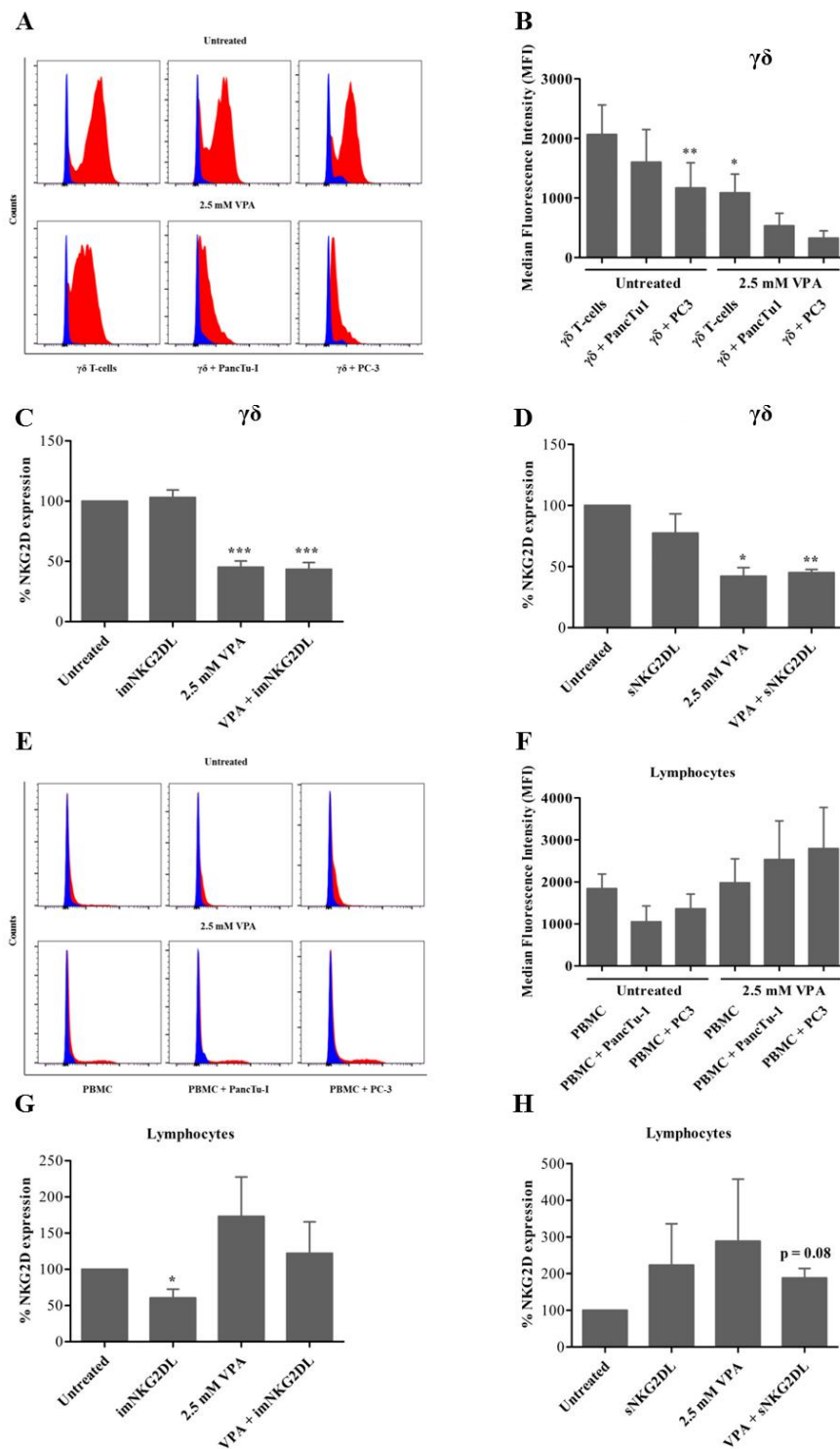


Figure 5.2.5: Effect of HDAC inhibitor on NKG2D receptor expression of effector cells. (Figure legend continued on the following page)

**Figure 5.2.5: Effect of HDAC inhibitor on NKG2D receptor expression of effector cells.** Effector cells, i.e. (A-B)  $\gamma\delta$  T cells from 12 day zoledronate-stimulated PBMC or (E-F) freshly isolated PBMC were co-cultured with PancTu-I and PC-3 cells at a 1:1 ratio in the presence or absence of 2.5 mM VPA, as described in figure 1. After 24 hrs of co-culture, effector cells were analyzed for NKG2D receptor expression by flow cytometry. In a control experiment,  $\gamma\delta$  T cells (C-D) or PBMC (G-H) were treated with or without 2.5 mM VPA in the presence or absence of soluble (sNKG2DL) or immobilized NKG2D ligands (imNKG2DL). After 24 hrs, cells were harvested and analyzed for NKG2D receptor expression by flow cytometry. In representative histograms, the upper panel represents the untreated effector cells or co-culture with PancTu-I or PC-3 and the lower panel represents 2.5 mM VPA treatment. Blue histograms represent isotype controls, while red histogram represents anti-human NKG2D PE staining. Median fluorescence intensity (MFI) was calculated by subtracting MFI of isotype controls from MFI of test antibodies. Percent NKG2D expression is calculated by setting MFI of untreated cells to 100. Mean values  $\pm$  S.E. of median fluorescence intensity (MFI) or percent NKG2D expression from 3-4 independent experiments are shown with statistical significant p-value <0.005, 0.01 or 0.05 as \*\*\*, \*\* or \*, respectively.

Taken together, these results support the previous notion that NKG2D binding induces down-modulation of NKG2D receptor cell surface expression, which is further regulated by HDAC inhibitors like VPA.

### 5.2.3 VPA regulates mRNA expression of the NKG2D receptor and its ligands

Using overexpression systems and biochemical approaches, Karimi *et al* (2014) recently showed that a truncated NKG2D isoform (Tr\_NKG2D) competitively interferes with full length form (FL\_NKG2D) resulting in decreased NKG2D cell surface receptor expression. Since we observed (Fig. 5.2.5) differential modulation of NKG2D receptor expression on the surface of  $\gamma\delta$  T-cells and PBMC in the presence of VPA, we next determined the role of Tr\_NKG2D at the gene expression level in the co-culture setting. In contrast to protein expression, VPA treatment of  $\gamma\delta$  T-cells had no impact on FL\_NKG2D and Both\_NKG2D (which constitutes both truncated and full length variants) gene expression level at 2.5 mM (Fig. 5.2.6A, upper panel). Interestingly, VPA treatment resulted in increased Tr\_NKG2D mRNA expression in  $\gamma\delta$  T-cells, whereas in PBMC both, FL\_NKG2D and Tr\_NKG2D transcript levels were increased. In  $\gamma\delta$  T-cells or PBMC co-cultured with PancTu-I, FL\_NKG2D and Tr\_NKG2D transcript were remarkably downregulated after treatment with 2.5 mM VPA. mRNA expression levels of NKG2D isoforms were relatively low in both effector cell populations co-cultured with PC-3 (Fig. 5.2.6A, B). In PBMC co-cultured with PC-3, it was even further decreased (Fig. 5.2.6B, upper panel), but that was not the case with  $\gamma\delta$  T-cells (Fig. 5.2.6A, upper panel).

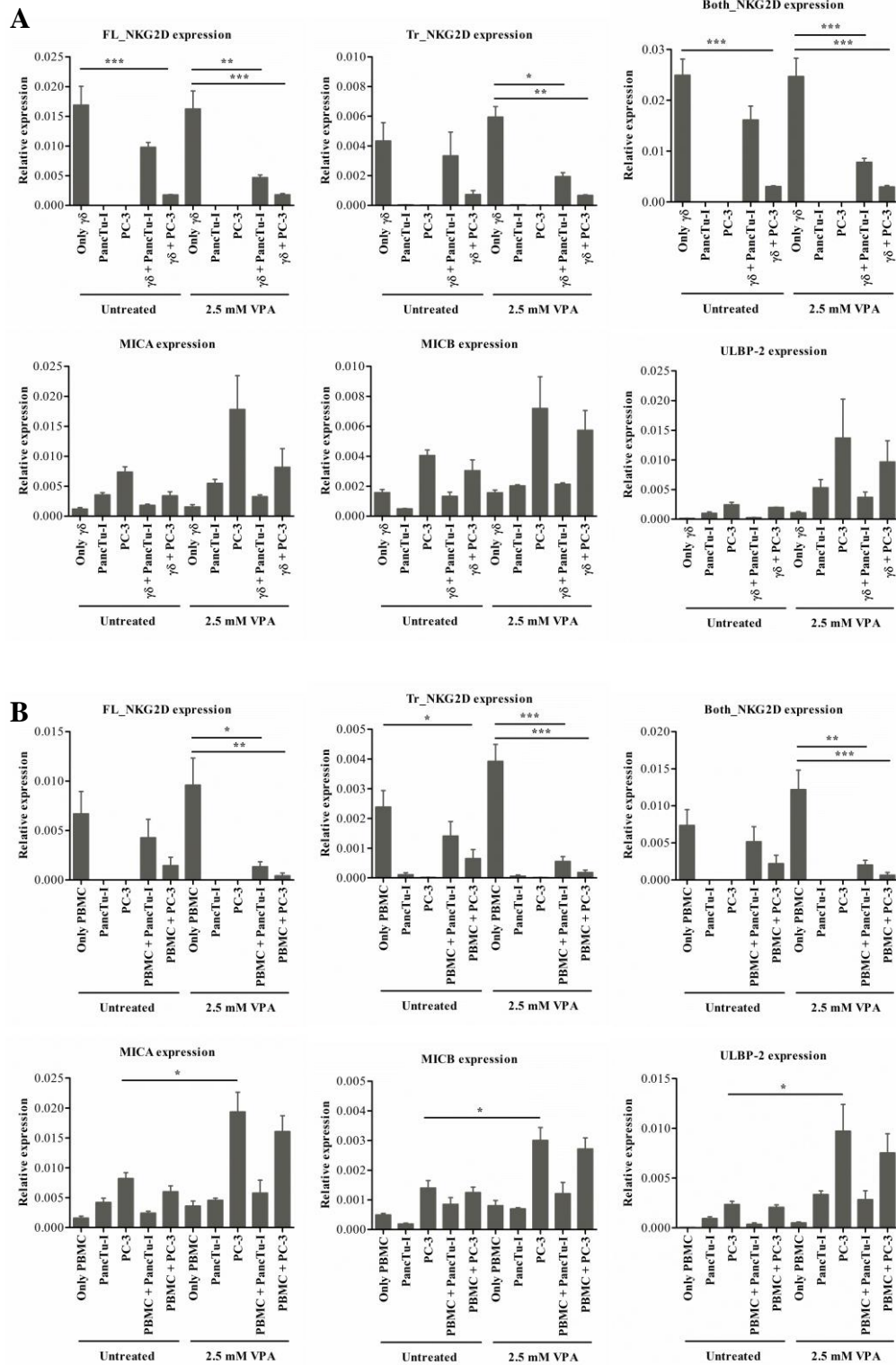
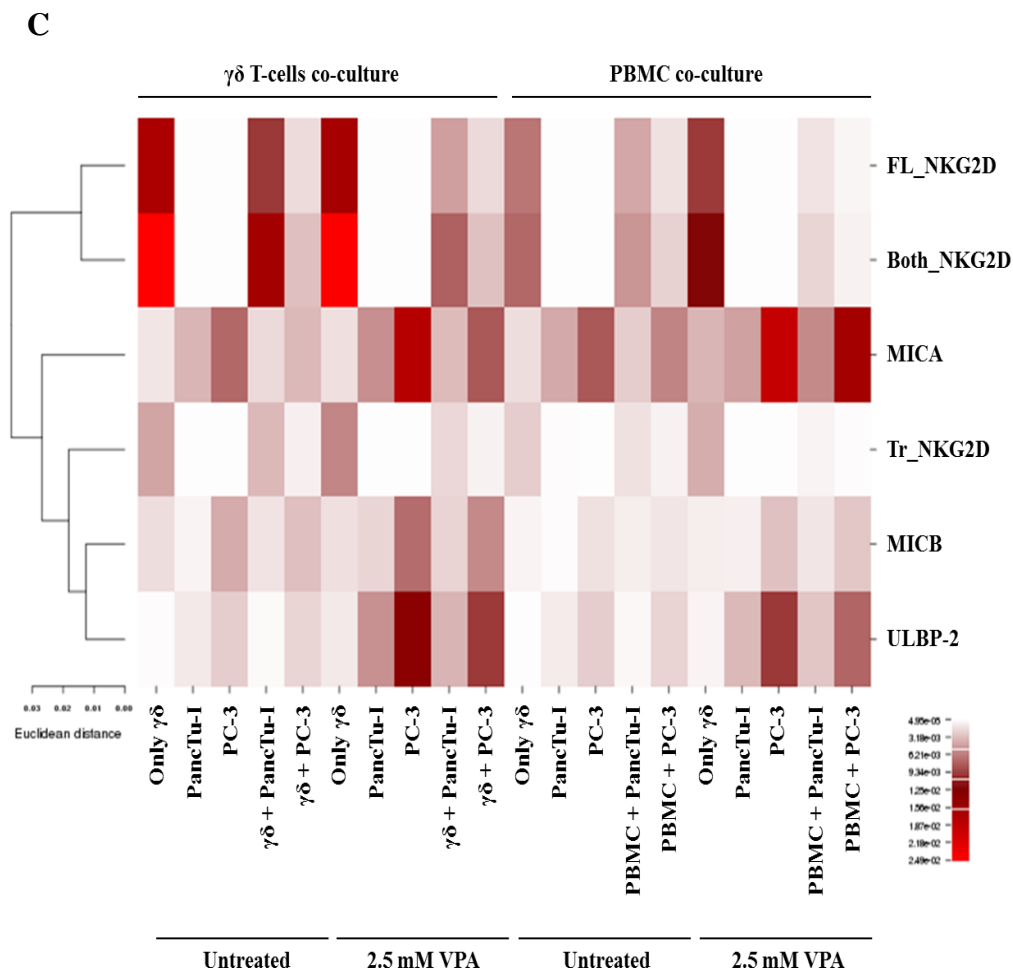


Figure 5.2.6: (Continued on the following page)





**Figure 5.2.6: Histone deacetylase inhibitor-mediated regulation of NKG2D receptor and ligand gene expression.** Within a similar set up of experiments as in figure 6, PBMC or  $\gamma\delta$  T cells were treated with 2.5 mM VPA or left untreated and co-cultured with and without PancTu-I and PC-3. After 24 hrs, the effector cells i.e. (A)  $\gamma\delta$  T cells and (B) PBMC from co-culture, or tumor cells from solo-culture (as an internal control) were harvested and analyzed for mRNA expression of full length NKG2D (FL\_NKG2D), truncated NKG2D (Tr\_NKG2D), sequences covering both the full length and truncated NKG2D gene (Both\_NKG2D), MICA, MICB and ULBP-2/5/6. mRNA levels were calculated as relative expression values compared to the mean Ct value of the housekeeping genes ( $\beta$ -actin,  $\beta$ 2-microglobulin and 18S). Graphs represented are mean values  $\pm$  S.E. of 3 independent experiments with p-values <0.001, 0.05, 0.01 as \*\*\*, \*\*, \*. (C) Based on the relative expression level the heatmap illustrates unsupervised clustering of respective mRNA for NKG2D receptor-ligands using Euclidian distance method with average linkage rule.



As our previous experiments showed substantial shedding of NKG2D ligands, i.e. MICA, MICB and ULBP-2, we also quantitated the expression of these genes in the same co-culture set up (Fig. 5.2.6A, B lower panel). Concomitant with the increased protein level, the gene expression of NKG2D ligands in both PancTu-I and PC-3 were also increased upon treatment of 2.5 mM VPA. Of note, the level of expression was comparatively low in PBMC or  $\gamma\delta$  T-cells co-cultured with untreated tumor cells, which was remarkably increased upon VPA treatment. As stated before, NKG2D ligand shedding and the truncated form of NKG2D receptor are shown to affect the expression and function of the NKG2D receptor on effector cells like NK cells. Hence, we performed statistical cluster analysis on genes with all the experimental conditions (Fig. 5.2.6C). Based on Euclidian distance method and average linkage rule, we found two distinct clusters, separating the full length NKG2D receptor and ligands, representing functionally related genes. To our surprise, the truncated form of NKG2D receptor did cluster with ligands for NKG2D. Thus, our results here demonstrate a distinct association of NKG2D receptor transcript variants (truncated versus full length), NKG2D ligand expression and regulation upon HDAC inhibitor treatment.

#### **5.2.4 Flow cytometric analysis of H3K9 acetylation at the single cell level**

VPA is a clinically used, FDA-approved short-chain fatty acid inhibitor (West *et al*, 2014; Gurvich *et al*, 2004). VPA effectively targets class I HDAC proteins and induces H3K9 acetylation in human  $\gamma\delta$  T cells (Bhat *et al*, 2015; Bhat *et al*, 2016), as shown by western blot. Considering the limitation in cell numbers and use of co-culture experiments, we addressed the combined effect of NKG2D ligand shedding and VPA-induced H3K9ac at the single cell level in  $\gamma\delta$  T cells and/or in freshly isolated PBMC using flow cytometry.

I thus established an epigenetic analysis method to investigate changes in protein expression associated with H3K9ac in  $\gamma\delta$  T cells based on previous reports (Watson *et al*, 2014; DiSpirito and Shen 2010). As expected, the highest concentration (0.1  $\mu\text{g/ml}$ ) of Pacific Blue-labelled H3K9ac antibody gave a higher background in untreated  $\gamma\delta$  T cells, which was decreased substantially with decreasing antibody concentrations (Fig. 5.2.7A). As analyzed by western blot, VPA decreased H3K9ac induction in a dose-dependent manner in  $\gamma\delta$  T cells (Fig. 5.2.7B). H3K9ac antibody at 0.01  $\mu\text{g/ml}$  concentration was chosen further based on ratio of median fluorescence intensity (MFI) between untreated and 5 mM VPA-treated  $\gamma\delta$  T cells. Our results

with VPA-dose-dependent decrease in H3K9ac protein determined by flow cytometry (Fig. 5.2.7C) further substantiated the use of 0.01  $\mu\text{g/ml}$  H3K9ac antibody, as this was not altered with 0.005  $\mu\text{g/ml}$  (data not shown). Hence, H3K9ac analysis by flow cytometry was highly correlated ( $R^2 = 0.72$ ,  $r = 0.85$ ,  $p\text{-value} = 0.0005$ ) with traditional western blot technique (Fig. 5.2.7D).

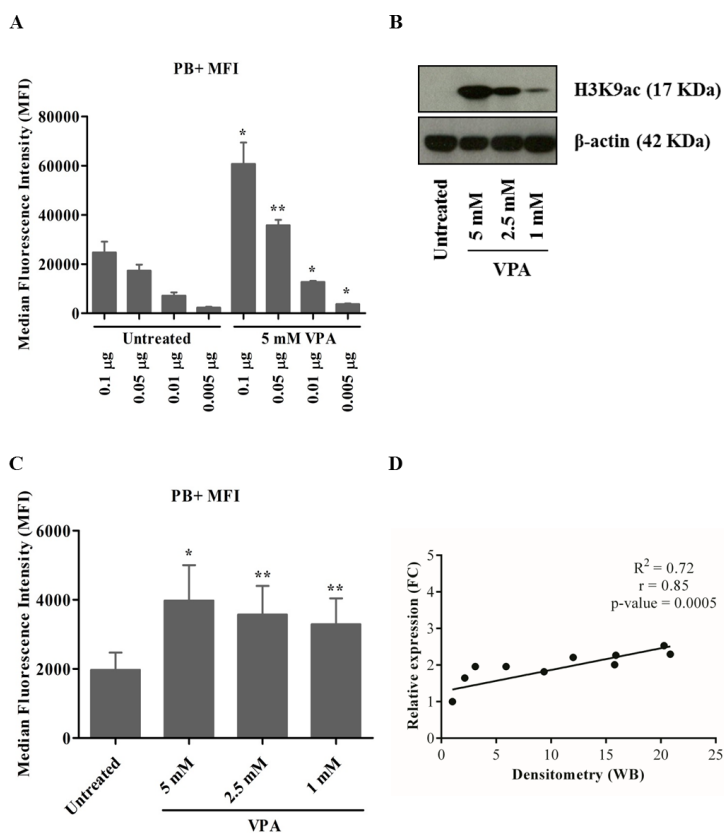


**Figure 5.2.7: Establishment of a flow cytometry-based analysis method of H3K9 acetylation.** Human  $\gamma\delta$  T cells were derived from PBMC stimulated with zoledronate and IL-2 for 12 days. (A)  $\gamma\delta$  T cells treated or not with 5 mM VPA were stained with titrated concentration of H3K9ac antibodies.  $\gamma\delta$  T cells were also treated with 5, 2.5 and 1 mM VPA for 24 hrs and harvested for analysis by western blot (B) or flow cytometry (C). For western blotting,  $\beta$ -actin was used as a loading control. For flow cytometry-based analysis, appropriate isotype control was used and median fluorescence intensity (MFI) was calculated. (D) A correlation between densitometric measurements from western blot (WB) of (B) and relative expression from flow cytometry (FC) of (C) was calculated for significance ( $p$ -value), correlation co-efficient ( $r$ ), the coefficient of determination ( $R^2$ ) and represented using the scatter plot. Plots represented in the figure are based on values from three independent experiments.  $P$ -value of significance for 0.05 and 0.01 are indicated by \* and \*\*.

To further validate the flow cytometry-based single cell epigenetic analysis, we performed control experiments to verify the specificity of the H3K9ac antibody. ImageStream cytometry was used to analyze the co-localization of H3K9ac with DRAQ5<sup>TM</sup> (DNA intercalating dye, which stains only living cells) in human  $\gamma\delta$  T cells treated or not with 5 mM VPA. Treatment with 5 mM VPA strikingly enhanced H3K9ac (Fig. 5.2.8). Moreover, co-localization H3K9ac and DNA was clearly seen only after treatment with VPA (Fig. 5.2.8A). 5 mM VPA-treated  $\gamma\delta$  T cells showed strong expression of H3K9ac compared to untreated cells (Fig. 5.2.8C). The weak expression of H3K9ac that was still observed in untreated  $\gamma\delta$  T cells (Fig. 5.2.8B) corresponds to the background staining as observed in flow cytometry (Fig. 5.2.8A). As a result, our  $\gamma\delta$  T cell-based single cell epigenetic analysis reveals specificity for nuclear H3K9 acetylation, as previously described for CD8 T cells (DiSpirito and Shen, 2010).

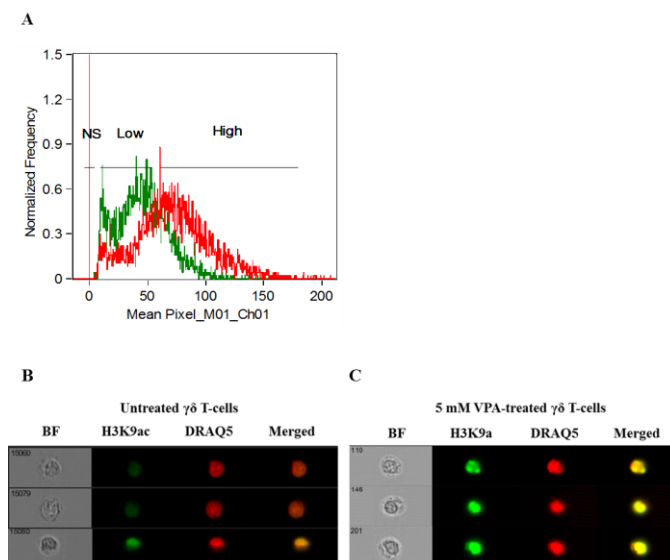


**Figure 5.2.8: ImageStream analysis showing binding specificity for the histone acetylation antibody.** Human  $\gamma\delta$  T cells were treated or not for 24 hrs with 5 mM VPA. Untreated and 5 mM VPA-treated  $\gamma\delta$  T cells were permeabilized and stained with Pacific Blue-conjugated H3K9ac antibody and 1  $\mu$ M DRAQ<sup>TM</sup> (a nuclear dye, staining live cells). Cells were measured immediately using an ImageStream cytometry device. The co-localization wizard was used for analysis. (A) Frequency plot represents change in fluorescence signal intensities for H3K9ac staining with three distinct fractions, ‘NS’ for no stained, ‘low’ for low stained cells and ‘high’ for significantly stained cells. (B) Untreated  $\gamma\delta$  T cells with minimal background staining for H3K9ac with living cells and (C) 5 mM  $\gamma\delta$  T cells clearly showing enhanced nuclear H3K9ac staining. 5000 cells were acquired in three independent experiments and three representative cells are shown in the image.

Taken together, the results clearly imply that NKG2D ligand shedding can be further modulated by using epigenetic inhibitors such as VPA, an inhibitor for HDAC and inducer of histone acetylation. The modulation in 'shedding' from tumors has a differential effect according to the origin of cancer. Interestingly, this leads to the distinct expression profile of the NKG2D receptor at the protein and the gene expression level, depending on the use of activated  $\gamma\delta$  T cells or freshly isolated PBMC in *in vitro* experimental read-outs. This successful establishment of single cell epigenetic method will help to investigate this phenomenon in more details.

### 5.3 Functional implications of epigenetic modulators on healthy human $\gamma\delta$ T cells: *Modulation of human $\gamma\delta$ T-cell activation and phenotype by histone deacetylase inhibitors*

*Associated publication:*

The results presented in this chapter are already published in the manuscript: **Jaydeep Bhat**, Hans-Heinrich Oberg and Dieter Kabelitz. (2015) Modulation of human gamma/delta T-cell activation and phenotype by histone deacetylase inhibitors. *Cellular Immunology*, 296(1):50-56.

Human  $\gamma\delta$  T cells have the unique ability to act against tumor cells of various origins via NKG2D and TCR molecules (Chitadze *et al*, 2016). Consequently, the potential impact of anti-tumor immune responses on their functional plasticity is also well documented (Lafont *et al*, 2014).  $\gamma\delta$  T-cells can actively modify the tumor microenvironment. This  $\gamma\delta$  T-cell-tumor interaction induces chemokine and cytokine expression (Di Carlo *et al*, 2013). In the same way, results from the previous section clearly showed that the use of valproic acid (VPA) significantly changes NKG2D ligand shedding in pancreatic ductal carcinoma and prostate carcinoma leading to defective functional responses of human  $\gamma\delta$  T cells. Of note, these VPA-induced effects were studied in the context of an *in vitro*  $\gamma\delta$  T-cell tumor co-culture set up. Apart from this, VPA is known as a short chain fatty acid, class I histone deacetylase inhibitor (Gurvich *et al*, 2004). Histone modification certainly affects molecular and cellular responses. In this section, I specifically addressed the modulation of functional responses of human  $\gamma\delta$  T-cells due to VPA.

#### 5.3.1 Dose-dependent inhibition of T-cell proliferation by VPA

$\alpha\beta$  T cells can be polyclonally activated by mitogens such as PHA (Ceuppens *et al*, 1988) or in a more restricted way by superantigens such as staphylococcal enterotoxins (Proft *et al*, 2003). V $\delta$ 2-expressing  $\gamma\delta$  T cells are selectively activated by phosphoantigens (Tanaka *et al*, 1995) and nitrogen-containing bisphosphonates in the presence of monocytes (Roelofs *et al*, 2009). In our first experiments, we studied the dose-dependent effects of VPA on the proliferation of T cells stimulated with superantigen, PHA, or phosphoantigens. Addition of VPA at the initiation of a 7 day stimulation of PBMC with zoledronate (Zol) plus IL-2 resulted in complete inhibition at 5 mM concentration (Fig. 5.3.1A). When added at day 6 of the 7 day culture period, VPA still significantly reduced  $^3\text{H-TdR}$  incorporation (Fig. 5.3.1B), even though inhibition was less pronounced. In a different setting, we established short-term  $\gamma\delta$  T-cell lines by stimulation of PBMC with zoledronate plus IL-2 for 18 days. Restimulation of such  $\gamma\delta$  T-cell lines with BrHPP

was also significantly inhibited by VPA at concentrations ranging from 5 to 1.25 mM (Fig. 5.3.1C).

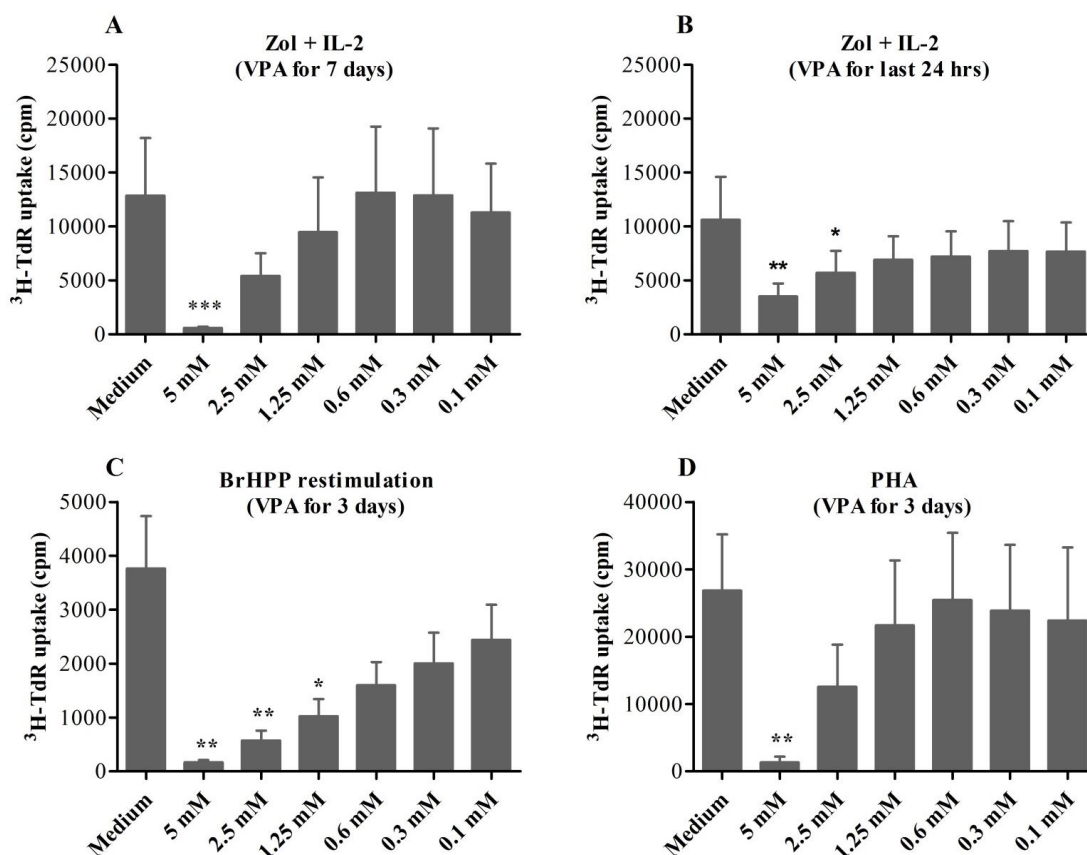


**Figure 5.3.1: Dose-dependent inhibition of T cell proliferation by VPA.** A) PBMC were stimulated with zoledronate (ZOL) plus IL-2 for 7 days, and titrated concentrations of VPA were added at the beginning of the cell culture as indicated. B) as in (A), but VPA was added only during the last 24 hrs of the 7 day culture period. C)  $\gamma\delta$  T cells from primary cell lines after 20 days were re-stimulated with BrHPP and IL-2 in the presence of VPA for 72 hrs. D) PMBC were stimulated with PHA for 72 hrs in the presence of VPA. In all experiments,  $^3\text{H-TdR}$  was added during the last 18 hrs of the culture period. Data shown here are mean cpm  $\pm$  S.E. of 3 independent experiments.

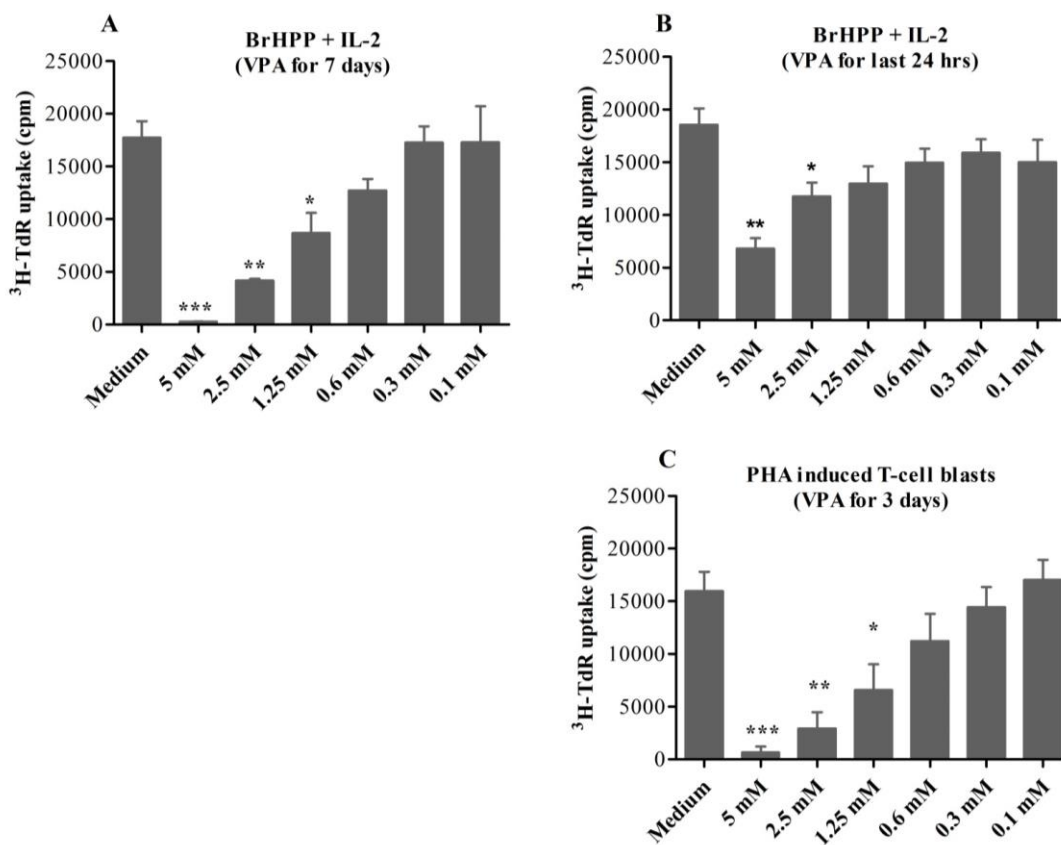


**Figure 5.3.2: VPA inhibits phosphoantigen- and mitogen-activated T-cell blast proliferation.** A) PBMC were stimulated with BrHPP for 7 days. VPA at the indicated concentrations was added at the initiation of cell cultures. B) as in (A), but VPA was present only during the last 24 hrs. C) PHA induced T-cell blasts were cultured for additional 3 days in the presence of IL-2 and the absence or presence of VPA. <sup>3</sup>H-TdR was added during last 18 hrs of experiment. Data represented here are mean  $\pm$  S.E. of 3 independent experiments.

Similar results were obtained when phosphoantigen BrHPP rather than zoledronate was used for stimulation of PBMC (Fig. 5.3.2A and B). Polyclonal mitogenic stimulation of PBMC with PHA showed similar inhibition by VPA at 5 mM and 2.5 mM concentrations when VPA was added at culture initiation (Fig. 5.3.1D). Furthermore, the IL-2-dependent proliferation of PHA blasts was significantly inhibited even at lower concentrations (1.25 mM) of VPA (Fig. 5.3.2C). Taken together, these experiments demonstrate that the inhibitory concentration of VPA for human T lymphocyte proliferation ranges between 5 and 1.25 mM, depending on the stimulation conditions.

### 5.3.2 Inhibitory concentrations of VPA induce cell death

The above experiments indicated strong inhibition of human  $\gamma\delta$  T-cell proliferation by VPA. Therefore we used combined Annexin V/PI staining and flow cytometry to analyze cell death upon VPA treatment. Etoposide was used as a positive control in these experiments.

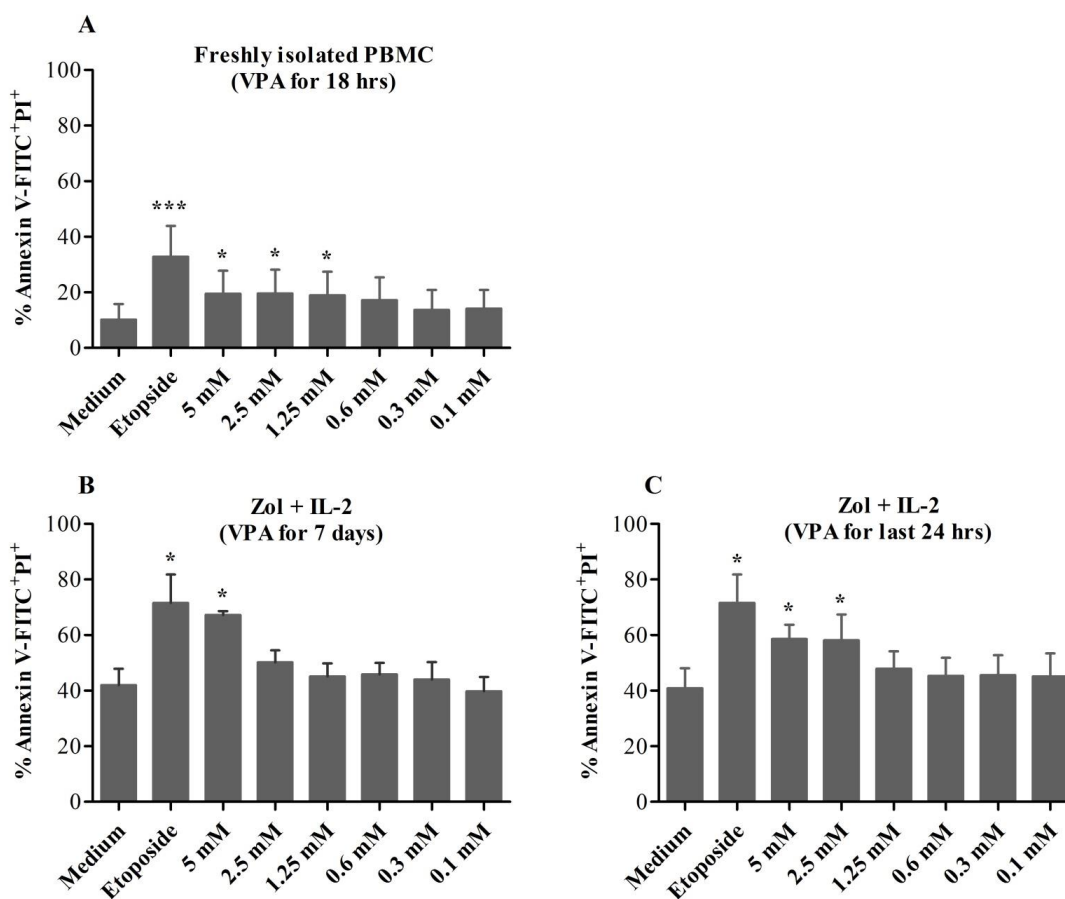


**Figure 5.3.3: Cell death analysis of stimulated or unstimulated PBMC.** A) Freshly isolated PBMC were treated with the indicated concentrations of VPA for 18 hrs. B) In another set up, PBMC were stimulated for 7 days with zoledronate (ZOL) with IL-2 in the presence of VPA. C) As in (B), but VPA was present only during the last 24 hrs of the 7 day culture period. Etoposide (0.425 mM) was used as a positive control. Cells were harvested at the end of the experiment and stained with annexin V FITC - PI and immediately acquired on the flow cytometer. Data represent mean  $\pm$  S.E. of 3 independent experiments.



As shown in Fig. 5.3.3A, VPA induced significant cell death in freshly isolated PBMC within 18 hrs. Furthermore, even more cell death was revealed when PBMC were cultured with zoledronate and IL-2 together with VPA for 7 days (Fig. 5.3.3B). Again, significant cell death was also induced when VPA was present only during the last 24 hours of the 7 day culture period with zoledronate (Fig. 5.3.3C). Similar levels of toxic effects of VPA were observed when we used BrHPP instead of zoledronate (data not shown). Therefore, these results clearly show that the inhibitory effect of VPA on human  $\gamma\delta$  T-cell proliferation is to a large extent due to the induction of cell death.

### 5.3.3 Subset specific cytotoxicity of VPA for human $\gamma\delta$ T cells

Since T-cell proliferation was strongly inhibited at higher concentrations of VPA, we sought to determine the immunophenotype of zoledronate or staphylococcal enterotoxin stimulated PBMC treated with VPA only for 24 hrs. Consistent with the proliferation and cell death data, the proportion of  $CD3^+V\delta 2^+$  T cells was significantly reduced at 5 mM of VPA even upon short-term treatment (Fig. 5.3.4A). Similar results were obtained when VPA was added from the beginning of zoledronate stimulation (Fig. 5.3.5).

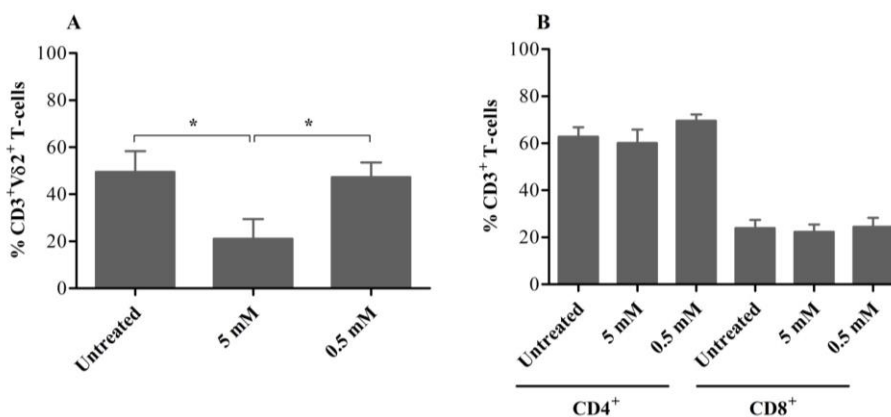


**Figure 5.3.4: Selective inhibition of human  $\gamma\delta$  T cells at toxic concentration of VPA.** PBMC were stimulated for 7 days in the presence of A) zoledronate plus IL-2, or B) staphylococcal enterotoxin mixture, each in the presence or absence of toxic (5 mM) and non-toxic (0.5 mM) concentrations of VPA during the last 24 hrs. At the end of the culture, cells were harvested and stained with PI combined with surface staining for A) CD3 and V $\delta$ 2, and B) CD3/CD4 and CD3/CD8. A gate was set on PI-negative cells which were further analyzed for subset markers. Data represent mean  $\pm$  S.E. of 3 independent experiments.

Activated  $\alpha\beta$  T cells can produce IL-2, required for cell survival, proliferation and further differentiation (Sojka *et al*, 2004), while  $\gamma\delta$  T-cells require exogenous supply of IL-2 for proliferation in response to zoledronate or phosphoantigens (Wesch *et al*, 1997). Hence, we analyzed similarly the short-term effect of VPA in PBMC stimulated with a mixture of staphylococcal enterotoxins. Interestingly, in contrast to the effect of zoledronate stimulation, we did not observe selective depletion of either  $CD4^+$  or  $CD8^+$  T-cells stimulated with staphylococcal enterotoxins (Fig. 5.3.4B).

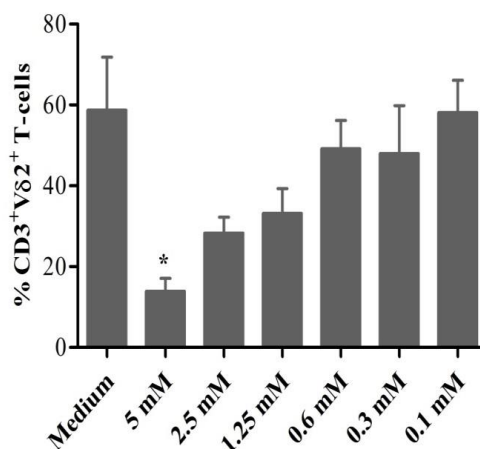


**Figure 5.3.5: Immunophenotyping of Vδ2 T-cells following treatment with various concentrations of VPA.** PBMC were cultured with titrated concentrations of VPA in the presence of zoledronate and IL-2 for 7 days. Thereafter, the proportion of  $CD3^+V\delta2^+$  T-cells was determined. Data represents mean  $\pm$  S.E. from 3 independent experiments.

Corresponding analysis of T-cell subsets (TCR  $\alpha\beta$  and TCR  $\gamma\delta$ ) were done exclusively on surviving cells by gating on the PI-negative population. Thus, results from these experiments clearly indicate selective survival of  $\alpha\beta$  T cells over  $\gamma\delta$  T cells upon VPA treatment.

#### 5.3.4 Toxic concentrations of VPA selectively down-regulate T-cell surface markers

Even though higher concentrations of VPA are clearly toxic to  $\gamma\delta$  T cells, not all T cells die in the cultures and 40-50 % of cells remain Annexin V/PI<sup>-</sup> in the presence of even 5 mM VPA. Therefore, we investigated the possible modulation of cell surface marker expression in the remaining viable T cells. PBMC cultured for 7 days with staphylococcal enterotoxin mixture or

with zoledronate plus IL-2 were treated with VPA for the last 24 hrs. Afterwards, we performed immunophenotypic analysis with two different sets of antibody panels against TCR $\alpha\beta$  or V $\delta$ 2 T-cell markers in the respective stimulation conditions. In the first panel, we analyzed CD25, CD95 and NKG2D, while in the second panel, antigen-presenting cell-associated markers like CD40, CD54, CD86, HLA-DR and CCR5 were determined. CD25 was unaffected on  $\alpha\beta$  T-cells, while the proportion of CD95<sup>+</sup> and NKG2D<sup>+</sup> cells was reduced in the presence of 5 mM VPA (Fig. 5.3.6A). In comparison, the proportion of CD95<sup>+</sup> and NKG2D<sup>+</sup> cells was even more strongly reduced in V $\delta$ 2 T cells (Fig. 5.3.6B).

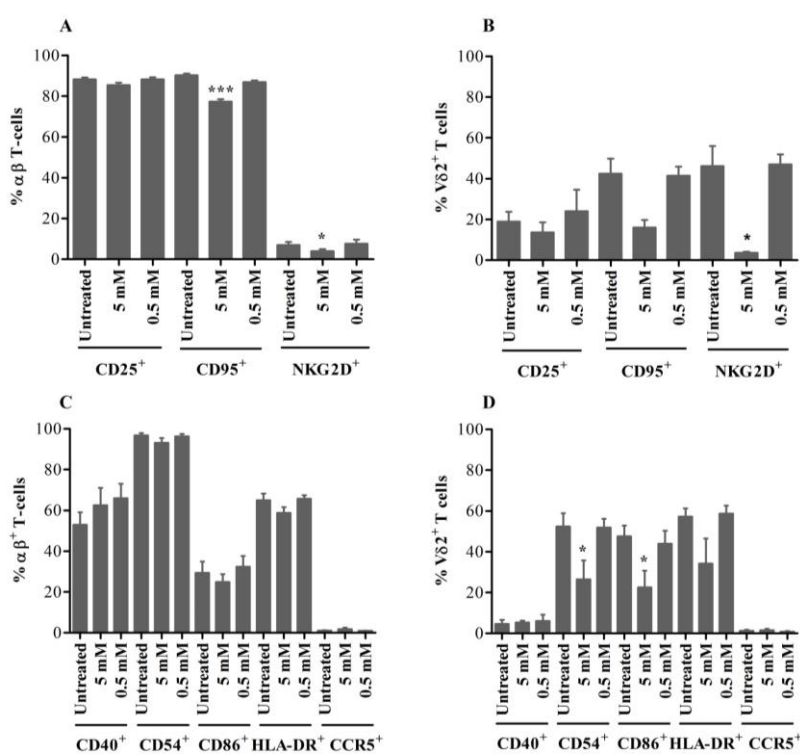


**Figure 5.3.6: Modulation of cell surface marker expression on T cells.** PBMC were stimulated with either staphylococcal enterotoxin mixture for 4 days (A, C) or with zoledronate plus IL-2 for 7 days (B, D). In each case, indicated concentrations of 5 mM or 0.5 mM VPA were added for last 24 hours. At the end of the experiment, cells were harvested and propidium iodide-negative cells were analyzed for surface expression of CD25, CD95, NKG2D receptors (A, B) and antigen presenting cell markers CD40, CD54, CD86, HLA-DR, CCR5 (C, D) together with TCR $\alpha\beta$  marker (A, C) or V $\delta$ 2 marker (B, D). Representative graphs are mean  $\pm$  S.E. from 2 independent experiments (A and B) or 3 independent experiments (C and D). Statistical significance shown by \* indicates p-values < 0.05 compared to untreated.

Striking differences were noted with respect to antigen presenting cell-associated markers. VPA had no effect on CD40, CD54, CD86 and HLA-DR expression on staphylococcal enterotoxin-stimulated  $\alpha\beta$  T cells, and additionally slightly increased CCR5 expression at 5 mM VPA concentration. In comparison, CD40 expression remained unaffected in  $\gamma\delta$  T cells (Fig. 5.3.6C). In striking contrast, the proportion of CD54<sup>+</sup>, CD86<sup>+</sup> and HLA-DR<sup>+</sup> cells was remarkably reduced in V $\delta$ 2 T cells surviving the 24 hrs presence of 5 mM VPA (Fig. 5.3.6D). Depending on the analyzed marker, the reduction in the proportion of positive cells as summarized in Fig. 6 was either due to lower expression on all cells (and thus a true down-modulation; e.g. NKG2D) or a biphasic expression where the remaining positive cells displayed similar fluorescence intensity as the control (e.g., CD95; data not shown). Like with  $\alpha\beta$  T cells, CCR5 cell surface expression on V $\delta$ 2 T cells was slightly increased at the higher concentration of VPA. Overall, these results reveal a differential modulation of cell surface marker expression by VPA on  $\alpha\beta$  versus  $\gamma\delta$  T cells.

### 5.3.5 Cell death-inducing concentrations of VPA modulate histone acetylation in human $\gamma\delta$ T-cells

The differential response of human  $\gamma\delta$  T cells at toxic concentrations of VPA led us to investigate the molecular function of VPA at the level of histone acetylation. To this end, we included valpromide (VPM), a carboxamide derivative of VPA also used in the treatment of epilepsy (Isoherranen *et al*, 2003). Since both inhibitors work in the same concentration range, we analyzed cell death induction in parallel by Annexin V and PI staining. This analysis clearly revealed equal effects of VPM and VPA at the level of Annexin V FITC<sup>+</sup> PI<sup>+</sup> cells, decreasing from 5 to 0.1 mM of VPM (data not shown).

Next, we treated short-term expanded V $\delta$ 2 T-cells for 24 h with 5 mM VPA or VPM and subsequently analyzed H3 acetylation by western blot. The western blot analysis revealed the Ac-H3 band at 17 KDa only in VPA treated samples, while it was absent in untreated, DMSO (solvent control for VPM) and VPM-pretreated  $\gamma\delta$  T-cells (Fig. 5.3.7). This clearly indicates that histone acetylation, a well-defined molecular function modified by VPA, is not affected even at toxic concentrations, thereby potentially modulating cellular responses of human  $\gamma\delta$  T-cells.

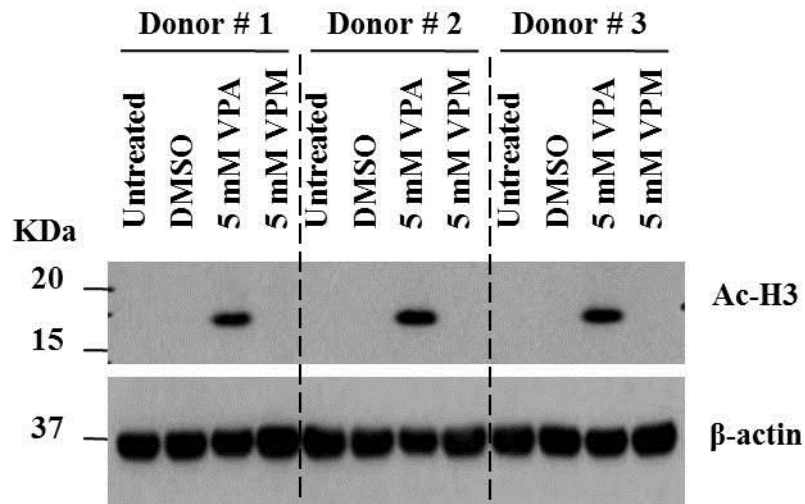


**Figure 5.3.7: VPA induces histone modification in  $\gamma\delta$  T cells.** Short-term  $\gamma\delta$  T-cell lines from 3 donors were left untreated or were treated with DMSO control, 5 mM VPA (HDAC inhibitor) or 5 mM VPM (structural analogue). Cells were harvested after 24 hours and lysed in lysis buffer. 10  $\mu$ g of protein was analyzed for acetylation of H3 marker (17 KDa) by SDS-PAGE.  $\beta$ -actin (37 KDa) served as a loading control.

## 5.4 Functional implications of epigenetic modulators on healthy human $\gamma\delta$ T-cells: *Generation of intracellular cytokine variants and association with cell death*

*Associated publication:*

The results presented in this chapter are already published in the manuscript: **Jaydeep Bhat**, Justyna Sosna, Jürgen Fritsch, Elgar Susanne Quabius, Stefan Schütze, Sebastian Zeissig, Ole Ammerpohl, Dieter Adam and Dieter Kabelitz. (2016) Expression of non-secreted IL-4 is associated with HDAC inhibitor-induced cell death, histone acetylation and c-Jun regulation in human gamma/delta T cells. *Oncotarget*, 7(40):64743-64756.

The previous results sections revealed that epigenetic modifiers like valproic acid (VPA), a HDAC inhibitor (HDACi), enhance NKG2D ligand shedding in PancTu-I and PC-3 cell lines. NKG2D ligand shedding and/or VPA primarily affect functional responses of human  $\gamma\delta$  T-cells. In continuation of these results, I specifically studied the modulation of  $\gamma\delta$  T-cell activation and phenotype by VPA. The observed modulation was differential and selective to specific cell surface markers on human  $\gamma\delta$  T-cells in a dose-dependent manner. With this background, I further studied the effect of VPA on  $\gamma\delta$  T cells at the level of intracellular cytokines and transcription factors. Expression of intracellular cytokines together with transcription factors are used to define various *in vitro* Th lineages.

### 5.4.1 HDACi induces IL-4 $\delta_{13}$ in human $\gamma\delta$ T cells

Epigenetic modifiers are known to modulate transcription factor and intracellular cytokine expression (Lal *et al*, 2009; Valapour *et al*, 2002). Here I analyzed intracellular IL-4 expression in activated and proliferating human  $\gamma\delta$  T-cells cultured for 24 hrs in the presence of HDACi. We used anti-IL-4 mAb 8D4-8 which specifically detects a non-secreted isoform with a 13 bp deletion (IL-4 $\delta_{13}$ ) that has been associated with apoptosis and age-dependent Th2 differentiation (Stein *et al*, 2000; Hebel *et al*, 2014; Ledru *et al*, 2003). As shown in Figure 5.4.1A, treatment with HDACi VPA and trichostatin A (TSA), but not with the hypomethylating agent decitabine, stimulated significant expression of IL-4 $\delta_{13}$  in surviving V $\delta$ 2 T cells. In comparison to V $\delta$ 2 T cells, only a very small amount of IL-4 $\delta_{13}$  expression was induced in surviving  $\alpha\beta$  T cells (Fig. 5.4.1B).

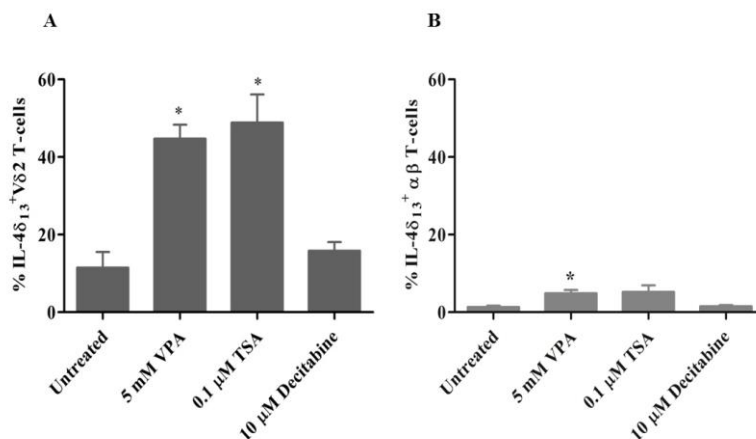


**Figure 5.4.1: Induction of IL-4δ<sub>13</sub> by HDACi treatment in human T cells.** γδ T-cell lines generated from PBMC stimulated for 12 d with zoledronate and IL-2 (A) or αβ T-cell lines generated from PBMC with a staphylococcal enterotoxin mixture (B) were treated for 24 hrs with the indicated concentrations of VPA, TSA, or decitabine. Thereafter, T cells were subjected to FACS analysis of T-cells co-expressing intracellular IL-4δ<sub>13</sub>. Dead cells were excluded based on live/dead fixable far-red dye staining. Data represent mean ± S.E. of 3 independent experiments. Statistical significance shown by \* indicates p-values < 0.05.

The sublethal concentration of VPA (5 mM), previously shown to modulate cell surface marker expression on surviving γδ T cells (results from previous section; Bhat *et al*, 2015), induced IL-4δ<sub>13</sub> and IL-4Rα as shown in a representative dot plot in Fig. 5.4.2A, but no significant IFN-γ expression in Vδ2 T cells. Results of 3 experiments are summarized in Fig. 5.4.2B. These results prompted us to study a possible intracellular co-localization of IL-4δ<sub>13</sub> and IL-4Rα by ImageStream cytometry. However, we failed to detect a significant degree of specific co-localization of IL-4δ<sub>13</sub> and IL-4Rα (Fig. 5.4.2C). Further analysis of mRNA levels for IFNγ and full-length IL-4 revealed opposite effects of VPA pretreatment, as expression levels of IFN-γ mRNA were up-regulated whereas those of mature IL-4 were down-regulated in Vδ2 T cells (Fig. 5.4.2D). This is not in contrast to the observed up-regulation of IL-4δ<sub>13</sub> at the protein level, as it is known that IL-4δ<sub>47</sub> (an alternative splice variant with a 47 bp deletion) also acts as a naturally occurring IL-4 antagonist (Vasiliev *et al*, 2003).

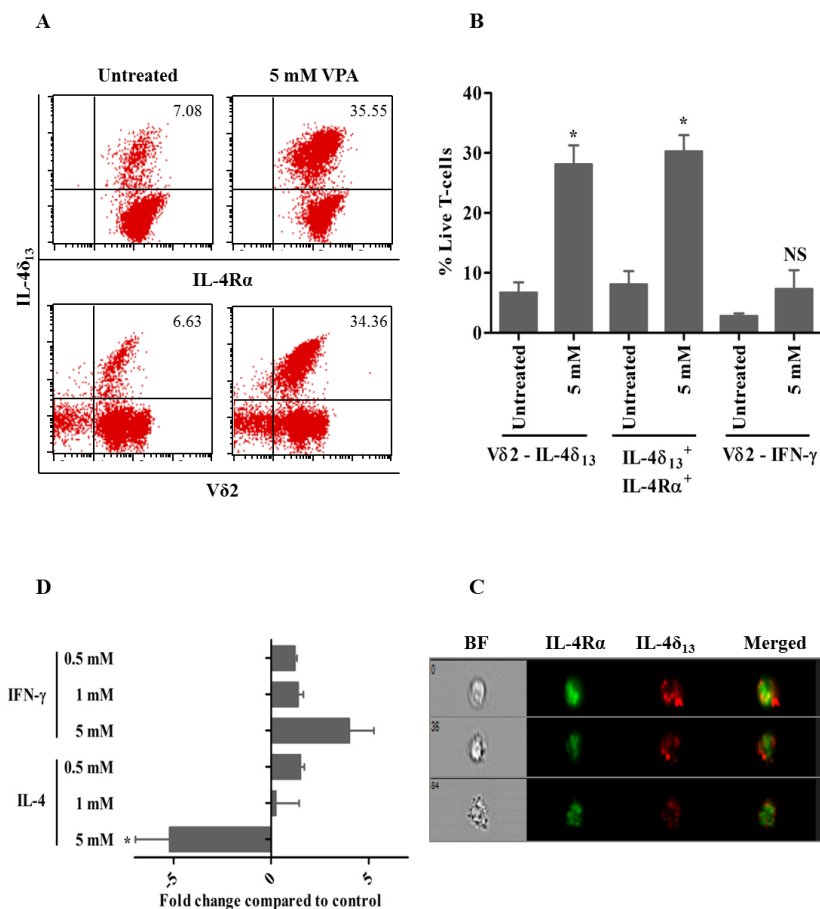


**Figure 5.4.2: VPA-regulated expression of intracellular cytokines in human  $\gamma\delta$  T cells.**  $\gamma\delta$  T-cell lines generated from PBMC stimulated for 12 days with zoledronate and IL-2 were treated for 24 hrs with 5 mM VPA, and monensin was added for the last 4 hrs. Thereafter, intracellular expression of IL4 $\delta_{13}$ , IL-4R $\alpha$  and IFN- $\gamma$  was determined by FACS. (A) Dot plot analysis of a representative experiment. The upper panel shows IL4 $\delta_{13}$  versus IL-4R $\alpha$ , the lower panel shows IL4 $\delta_{13}$  and V $\delta$ 2 expression. A combined gate was set on FSC versus SSC and the live/dead fixable far-red dye negative population. (B) Summary of 3 independent experiments. (C)  $\gamma\delta$  T cells were also analyzed by ImageStream cytometry for possible co-localization of IL-4 $\delta_{13}$  with IL-4R $\alpha$ . Images represented are live, single cell populations of 5 mM VPA-treated  $\gamma\delta$  T cells analyzed within focus, with marked column as bright field (BF), Alexa Fluor 488-labelled IL-4R $\alpha$ , PE-labelled IL-4 $\delta_{13}$  and both fluorochromes merged. Representative single cells from three independent experiments are shown. (D)  $\gamma\delta$  T cells obtained as above were treated for 24 hrs with the indicated concentrations of VPA. Thereafter, mRNA expression of IFN- $\gamma$  and IL-4 was quantified by real time PCR. All data represent mean  $\pm$  S.D. of 3 independent experiments. Data were analyzed using PrismGraph with student's t-test. \* indicates p-values <0.05.



### 5.4.2 Differential changes in secretory versus non-secretory forms of IL-4

In view of the reported down-regulation of the full length IL-4 transcript by the IL-4 $\delta_{47}$  isoform (Vasiliev *et al*, 2003), we tested whether IL-4 $\delta_{13}$  can also act as an IL-4 antagonist. To address this question, we used the anti-IL-4 antibody clone MP4-25D2, which specifically detects the mature form of IL-4 (Hebel *et al*, 2014). In line with mRNA regulation (Fig. 5.4.2C), we found a decrease in the intracellular expression of the mature form of IL-4 in V $\delta$ 2 T cells after treatment with 5 mM VPA (Fig. 5.4.3A, middle panel). Along with the significant increase in IL-4 $\delta_{13}$  expressing V $\delta$ 2 T cells (Fig. 5.4.3A, left panel), a slight increase in co-expression of both IL-4 and IL-4 $\delta_{13}$  was observed after 5 mM VPA treatment ( $p = 0.08$ ; Fig. 5.4.3A, right panel). The results presented in Fig. 5.4.3A summarize three independent experiments. Representative dot plots and histograms from a representative individual experiment (Fig. 5.4.3B) clearly illustrate the expression of IL-4 $\delta_{13}$  being associated with low TCR expression on V $\delta$ 2 T cells while expression of mature IL-4 was associated with high level TCR expression on V $\delta$ 2 T cells.

We further addressed the subcellular localization of IL-4 $\delta_{13}$  by a combined confocal and flow cytometry approach. Interestingly, ImageStream analysis of IL-4 $\delta_{13}$  consistently showed distinct punctuated localization in cytoplasmic granular structures of V $\delta$ 2 T cells which, however, failed to co-localize with CD107a (LAMP-1; lysosomal-associated membrane protein-1 and a marker for degranulation; Fig. 5.4.3C) or CD63 (a marker for intracellular vesicles; data not shown). Taken together, secretory and non-secretory forms of IL-4 seem to antagonize each other at the protein level. It may also be associated with the regulation of TCR surface expression on V $\delta$ 2 T cells and distinct subcellular localization.

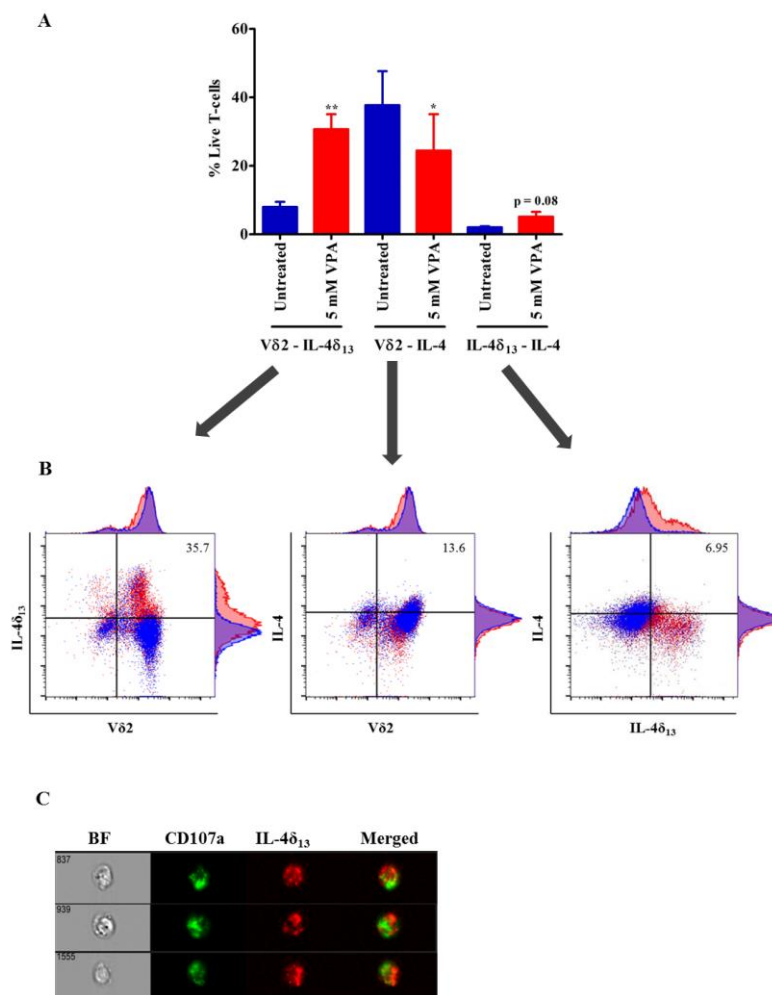


**Figure 5.4.3: Analysis of the non-secretory and mature form of IL-4 in  $\gamma\delta$  T cells.** (A) Short-term zoledronate-stimulated  $\gamma\delta$  T cells were treated with 5 mM VPA for 24 hrs. Afterwards, cells were harvested and analyzed by flow cytometry after staining with PE-IL4 $\delta_{13}$  (clone 8D4-8), FITC-V $\delta$ 2 and Brilliant Violet 605-IL-4 (clone MP4-25D2) and gating on live/dead fixable far-red dye negative cells. Graph of 4 independent experiments represents mean  $\pm$  S.E. Samples were acquired on BD LSR Fortessa and analyzed using FlowJo data analysis software. Statistical significance is shown by \* or \*\* for p-values < 0.05 or < 0.01, respectively. (B) Representative dot plots show overlay of untreated (blue color)  $\gamma\delta$  T-cells with 5 mM VPA (red color) treated cells expressing respective antibody staining. Numbers represented in dot plot indicate percentage of expressing population after 5 mM VPA treatment. (C) In a very similar approach to Figure 2C, ImageStream analysis was performed to analyze possible localization of CD107a and IL-4 $\delta_{13}$ . Live/dead far red dye negative 5 mM VPA-treated  $\gamma\delta$  T cells stained with FITC-CD107a and PE-IL-4 $\delta_{13}$ , are shown in single channels and in merged image, BF stands for bright field. Three representative cells from three independent experiments are shown.

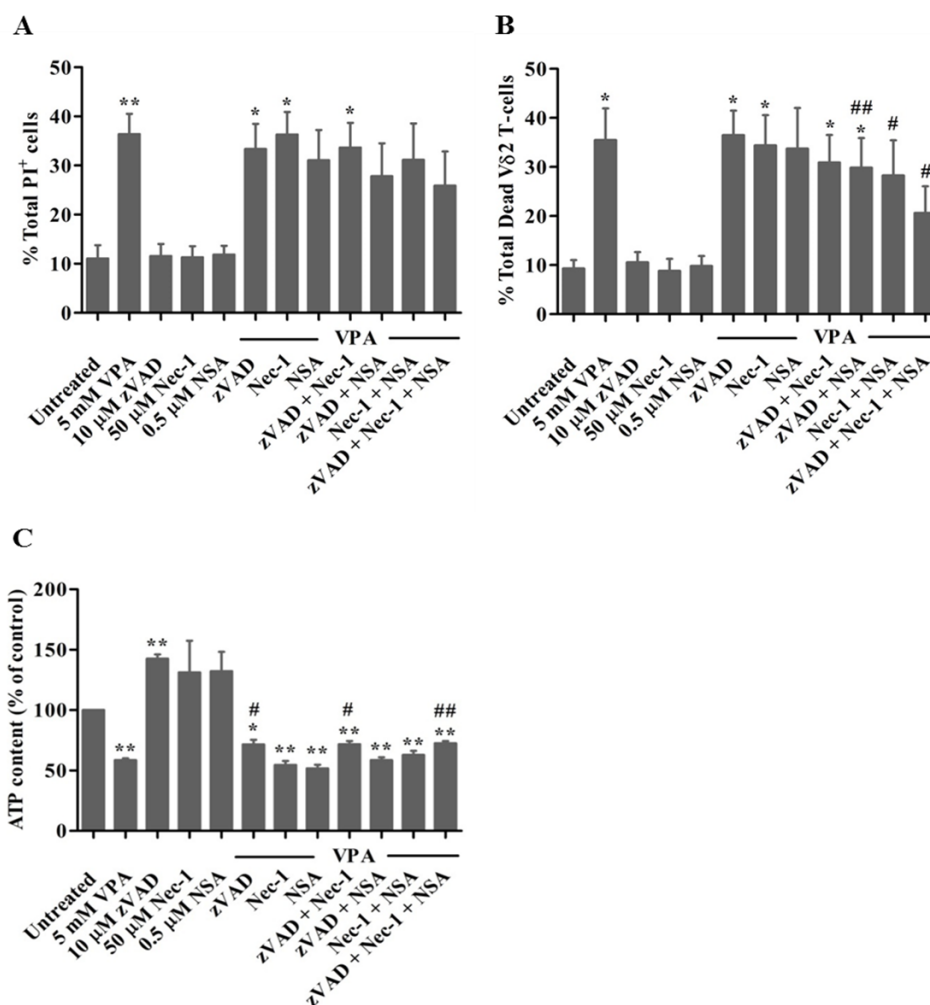


**Figure 5.4.4: Modulation of VPA-induced  $\gamma\delta$  T-cell death by cell death inhibitors.** Human short-term  $\gamma\delta$  T-cell lines were treated for 24 hrs with VPA and cell death inhibitors (Nec-1, NSA, zVAD). (A) After treatment cells were harvested and stained with annexin-V FITC and PI. Proportions of total PI positive cells are indicated. (B) Similarly, treated cells were harvested and stained for V $\delta$ 2 surface marker together with live/dead fixable dye. Samples were analyzed by gating on V $\delta$ 2 marker and distinguished as live or dead based on live/dead fixable dye labelling. Data represent mean  $\pm$  S.E. of 3 independent experiments. (C) Cells treated as previously described, were harvested and the ATP content was measured by Cell Titer-Glo Luminescent Cell Viability Assay and calculated relative to the untreated cells (set to 100%). Data were analyzed using PrismGraph with student's t-test. p values <0.05 were considered statistically significant and are displayed as \* or \*\* for p-values <0.05 or <0.01 (in relation to untreated medium control) and as # or ## for p-values <0.05 or <0.01 (in relation to 5 mM VPA treatment).

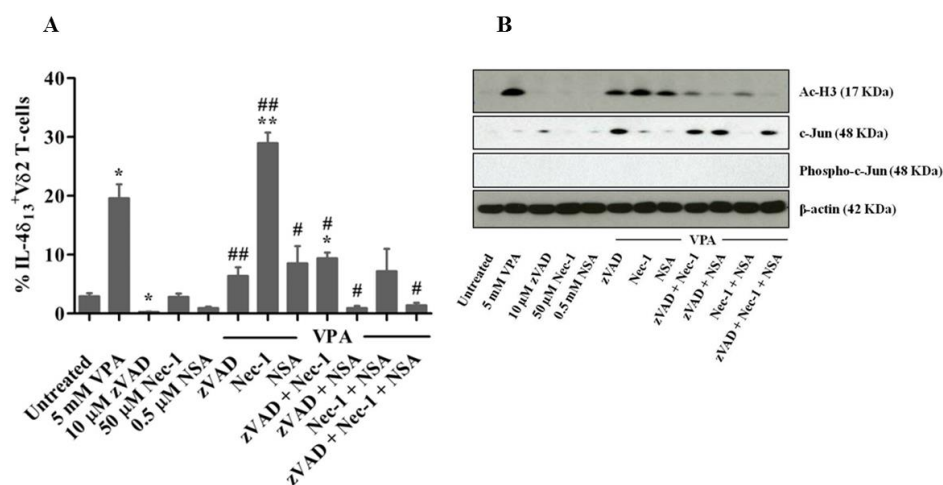


**Figure 5.4.5:** Modulation of IL-4δ<sub>13</sub>, c-Jun expression and histone H3 acetylation in γδ T-cells in response to VPA and cell death inhibitors. γδ T-cells obtained from zoledronate-stimulated PBMC were pre-treated for 30 min with zVAD, or for 2 hrs with Nec-1 or NSA, or were left untreated. Thereafter, VPA was added where indicated. (A) After 24 hrs, intracellular IL-4δ<sub>13</sub> expression was determined by FACS in gated Vδ2 T-cells. Dead cells were excluded based on live/dead fixable far-red dye staining. Data represents mean ± S.E. of 3 independent experiments. Data were analyzed using PrismGraph with student's t-test. p-values <0.05 were considered statistically significant and are displayed as \* or \*\* for p-values <0.05 or <0.01 (in relation to untreated medium control) and as # or ## for p-values <0.05 or <0.01 (in relation to 5 mM VPA treatment). (B) After 24 hrs, cells were lysed and 10 μg protein was subjected to western blot analysis for H3K9Ac (top panel), c-Jun (upper middle panel), phospho-c-Jun (lower middle panel) and β-actin (lower panel). One representative out of three experiments is shown.

### 5.4.3 Cell death pathway inhibitors modulate IL-4δ<sub>13</sub> induction and histone modification

IL-4δ<sub>13</sub> is known to be associated with induction of cell death (Stein *et al*, 2000). Also, VPA triggers diverse apoptotic and non-apoptotic cell death pathways (Schwartz *et al*, 2007; Bollino *et al*, 2015). We studied the effect of apoptosis (pan-caspase) inhibitor zVAD and inhibitors of programmed necrosis necrostatin-1 (Nec-1) and necrosulfonamide (NSA) on VPA-induced cell death and IL-4δ<sub>13</sub> induction. Inhibitor concentrations known to block apoptosis and necroptosis in established cell systems (Philip *et al*, 2015; Sosna *et al*, 2013) only moderately reduced cell death of VPA-treated Vδ2 T cells using three different read-outs (Fig. 5.4.4). Exogenous supply

of IL-4 has been shown to prevent T-cell apoptosis and to modulate cellular functions (Spinozzi *et al*, 1995; Mao *et al*, 2016). However, exogenous IL-4 did not rescue VPA-treated V $\delta$ 2 T cells from cell death (data not shown). zVAD, Nec-1 and NSA in combination prevented IL-4 $\delta$ <sub>13</sub> induction in VPA-treated live V $\delta$ 2 T cells (Fig. 5.4.5A), but not Nec-1 alone.

Next, we analyzed the modulation of global histone acetylation marker H3K9ac by VPA and cell death inhibitors (Fig. 5.4.5B, upper panel). We also analyzed Ac-H2Blys5, HDAC-1, HDAC-2 histone modifications; this resulted in similar patterns of protein expression as presented for H3K9ac (data not shown). However, HDAC2 expression was inconsistent in independent experiments with several donors (data not shown). Correlating with the modulation of IL-4 $\delta$ <sub>13</sub> expression, treatment with zVAD and Nec-1 (but not NSA) slightly reduced H3K9 acetylation induced by VPA. Combination of any two inhibitors further reduced acetylation, while complete loss of histone acetylation mark was observed when all three inhibitors were combined together. Thus, cell death inhibitors directly regulate IL-4 $\delta$ <sub>13</sub> and global H3K9 acetylation.

#### **5.4.4 Interplay of IL-4 $\delta$ <sub>13</sub> with c-Jun expression and histone acetylation**

H3K9 plays an important dual role in gene regulation. Acetylation of H3K9 correlates with active promoter and gene transcription, while methylation is associated with gene silencing (Karmodiya *et al*, 2012). Based on this information, we analyzed a number of transcription factors involved in regulation of IL-4, HDAC1 (the target of VPA), MLKL (the target for NSA) and CASP3 (the target for zVAD) genes, which had been identified from ChIP-seq experiments by the ENCODE project (Landt *et al*, 2012; <http://genome.ucsc.edu/ENCODE/index.html>). A list of transcription factors commonly ranked to be involved in the regulation of all four genes is listed in Table 5.1. String database analysis of this unique set of transcription factors revealed potential protein-protein interactions (Fig. 5.4.6A).

**Table 5.1:** List of unique candidate proteins derived from STRING database analysis for protein-protein interaction and association. Corresponding information is mentioned in the Table.

<b>Sr. No.</b>	<b>Symbol of the protein</b>	<b>Name and information of protein</b>	<b>Size (amino acids)</b>
1	CHD2	Chromodomain helicase DNA binding protein 2	1828
2	CTCF	CCCTC-binding factor (zinc finger protein)	727
3	EBF1	Early B-cell factor 1	591
4	EGR1	Early growth response 1	543
5	FOS	FBJ murine osteosarcoma viral oncogene homolog	380
6	FOXA1	Forkhead box A1	472
7	JUN	Jun oncogene	331
8	MAZ	MYC-associated zinc finger protein (purine-binding transcription factor)	493
9	MXI1	MAX interactor 1	295
10	MYC	v-myc myelocytomatosis viral oncogene homolog (avian)	454
11	PAX5	Paired box 5	391
12	POLR2A	Polymerase (RNA) II (DNA directed) polypeptide A, 220kDa	1970
13	POU2F2	POU class 2 homeobox 2	463
14	RELA	v-rel reticuloendotheliosis viral oncogene homolog A (avian)	551
15	REST	RE1-silencing transcription factor	1097
16	SIN3A	SIN3 homolog A, transcription regulator (yeast)	1273
17	SP1	Sp1 transcription factor	785
18	TAF1	TAF1 RNA polymerase II, TATA box binding protein (TBP)-associated factor, 250kDa	1872
19	TBP	TATA box binding protein	339
20	TCF12	Transcription factor 12	706

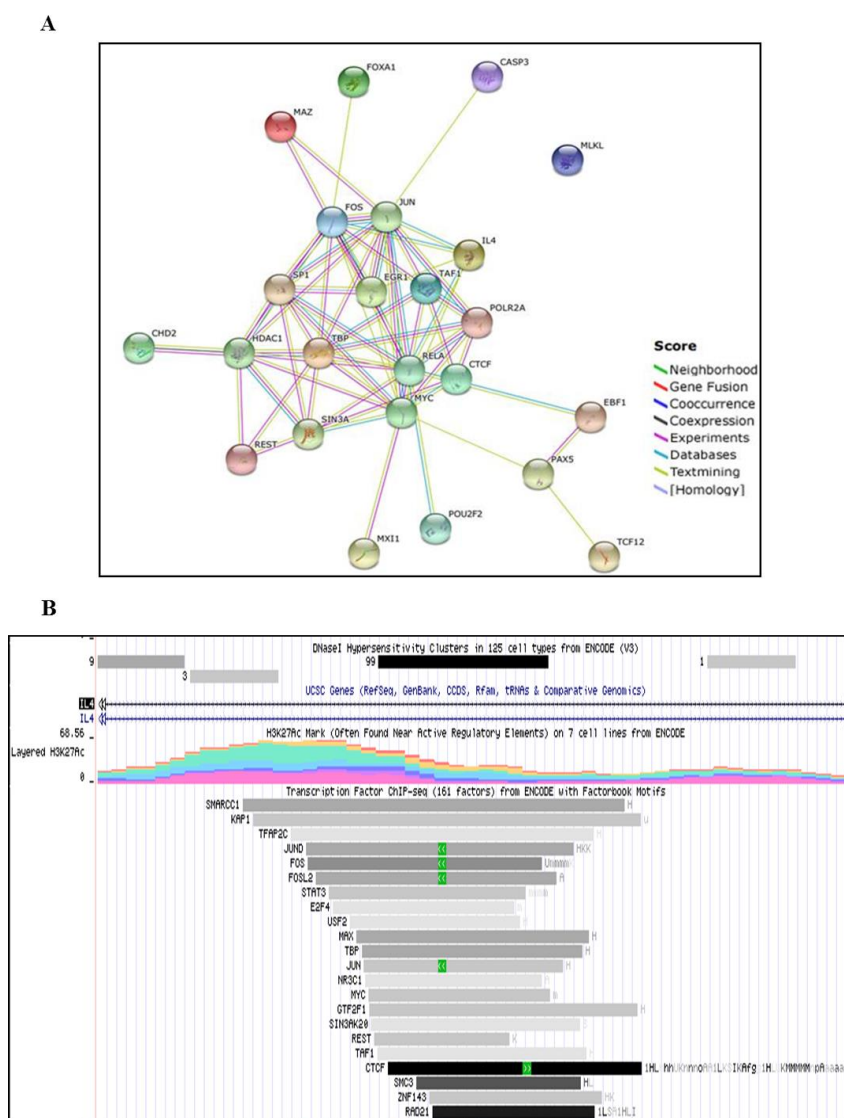


**Figure 5.4.6: Bioinformatic analysis of commonly occurring transcription factors in in silico IL-4 regulatory network.** (A) Sets of commonly occurring transcription factors (see Supplementary Table 1) were further analyzed for protein-protein interaction by STRING database. The absence of lines linking MLKL to other factors indicates that no such interactions have so far been described in the literature. (B) Bioinformatic analysis was done using the available ChIP-seq ENCODE transcription factors database. Representative image shows the number of transcription factors including c-Jun, found in IL-4 genomic region that are associated with H3K27ac mark.

Our bioinformatic analysis of the IL-4 gene using UCSC genome browser revealed putative binding sites of a subset of transcription factors, which are associated with H3K27ac marks often found near active regulatory elements (Fig. 5.4.6B). c-Jun was one of the unique transcription factors associated with all four genes. Hence, we chose to validate its role in this network at the protein level (Fig. 5.4.4B, middle panel). HDACi have been reported to suppress the induction of c-Jun (Yamaguchi *et al*, 2005). In line, we did not observe induction of c-Jun by VPA alone, but there was a striking up-regulation in the additional presence of zVAD. Whenever zVAD was present (together with VPA), enhanced c-Jun expression was observed, while NSA or Nec-1 had no effect (Fig. 5.4.5B, middle panel). The stimulatory effect of zVAD on c-Jun expression is in agreement with previous reports (Chen *et al*, 2011). Of note, phosphorylation of c-Jun was not detected (not shown), possibly due to the selected time point or reflecting the dispensability of c-Jun phosphorylation for T-cell proliferation (Yamaguchi *et al*, 2005). Most importantly, however, we found that the combination of zVAD, NSA and Nec-1 led to a complete loss of VPA-induced H3 acetylation mark (Fig. 5.4.5B, upper panel) which correlated with strongest inhibition of IL-4 $\delta_{13}$  induction (Fig. 5.4.5A) but marked c-Jun expression (Fig. 5.4.5B, middle panel). The absence of any histone mark observed here in the presence of a combination of cell death inhibitors has not been previously reported in the context of blockade of apoptosis (Fullgrabe *et al*, 2010). Thus, our results revealed a potential interrelation between epigenetic modification (H3K9ac), intracellular cytokine (IL-4 $\delta_{13}$ ) induction, transcription factor (c-Jun) expression and regulation by cell death inhibitors.



## 5.5 Comprehensive epigenetic landscape of human $\gamma\delta$ T-cells: *Chromatin accessibility, DNA methylation and total RNA analysis*

*Associated manuscript:*

The results presented in this chapter will be part of a manuscript (in preparation): **Jaydeep Bhat**, Johannes Helmuth, Matthias Hübenthal, Raheleh Sheibani-Tezerji, Svetlana Scheufele, Marcus Lettau, Anke Bergmann, Daniela Esser, Maren Falk-Paulsen, Christoph Kaleta, Reiner Siebert, Philip Rosenstiel, Andre Franke, Ole Ammerpohl, Martin Vingron and Dieter Kabelitz.

Compared to  $\alpha\beta$  T cells,  $\gamma\delta$  T cells possess diverse functional properties such as BTN3A1/CD277-dependent phosphoantigen recognition, stress surveillance capacity and antitumor potential. As shown in the previous results section, epigenetic inhibitor(s) such as HDAC inhibitor valproic acid (VPA) can significantly modulate this functional diversity. As an effect of HDAC inhibition, functional response and histone modification like H3K9ac are also induced in  $\gamma\delta$  T cells. Moreover, the dynamics of  $\gamma\delta$  T cell immune responses might be controlled by epigenetic regulations at multiple levels (Schmolka *et al*, 2013). Therefore, a comprehensive analysis of epigenetic regulations characteristic for  $\gamma\delta$  T cell, in comparison to CD4<sup>+</sup> $\alpha\beta$  T cells (hereafter referred to as CD4 T cells) and regulatory TCR  $\alpha\beta$ <sup>+</sup> T cells (hereafter referred to as Treg) and CD8<sup>+</sup> $\alpha\beta$  T cells (hereafter referred to as CD8 T cells) might help to unveil this complexity. With the aim to map the epigenetic landscape of human  $\gamma\delta$  T cells, the DNA methylation pattern, regulation of RNA expression (transcriptome and regulatory RNA including miRNA, long non-coding RNA/lncRNA) and chromatin accessibility were investigated using a systems immunology-approach.

### 5.5.1 DNA methylome segregates T-cell subsets

T cell lineage commitment is largely controlled by diverse epigenetic mechanisms. It is now evident that in  $\alpha\beta$  T cells the boundary between CD4 and CD8 T cells subsets is set by DNA methylation (Sellars *et al*, 2015; Feng and Rudensky, 2015). With this background and the information available from the literature, I sought to investigate the DNA methylation profile of freshly isolated  $\gamma\delta$  T cells in comparison to freshly isolated CD4, Treg and CD8 cells using 450k arrays. Due to the lack of a gold standard bioinformatic analysis pipeline, DNA methylation arrays were analyzed by two independent software packages. Also, both beta-values and M-values have been used to measure methylation levels (Du *et al*, 2010).

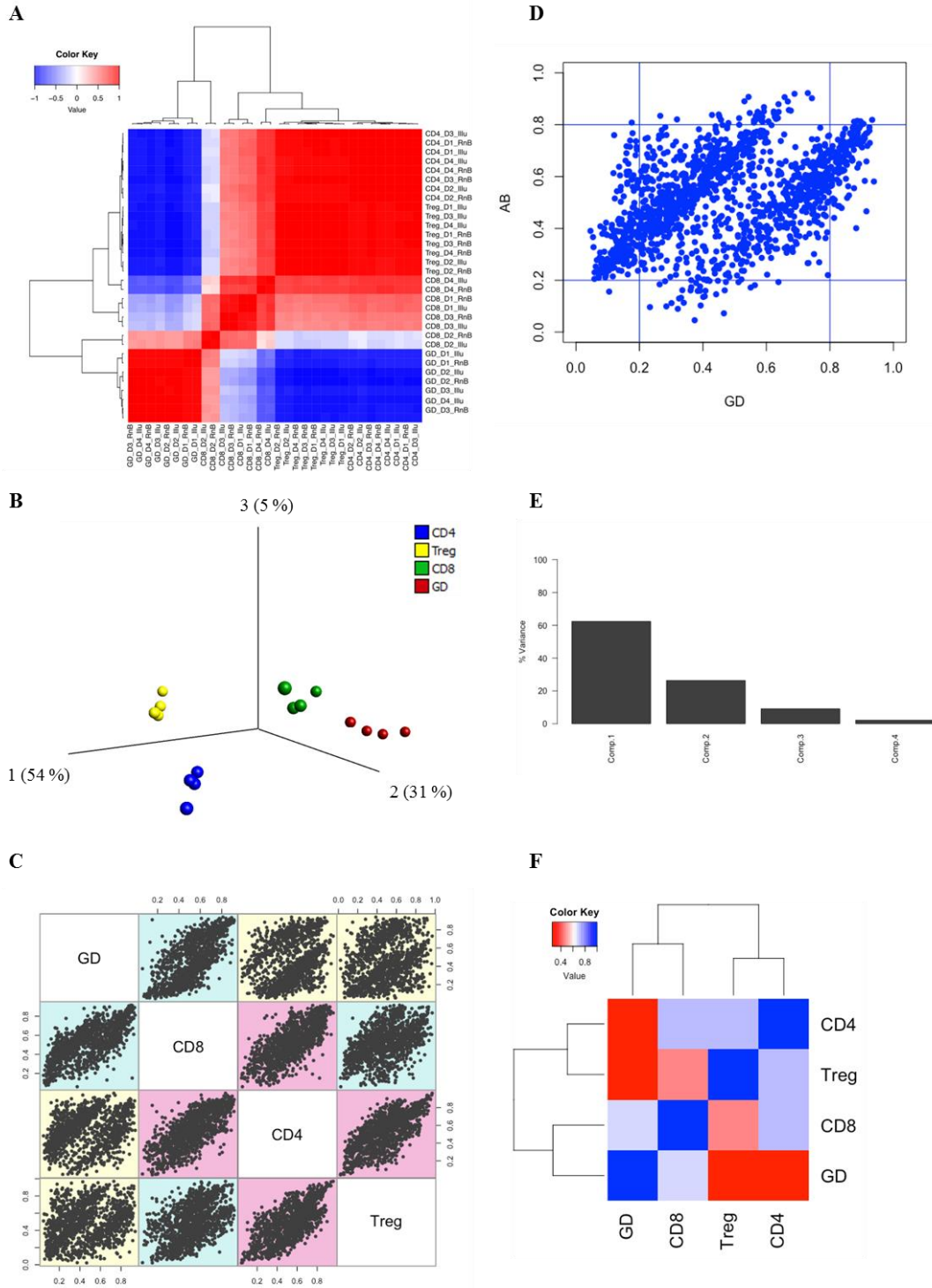


Figure 5.5.1: Principal component analysis separating  $\gamma\delta$  T cells from other  $\alpha\beta$  T-cell subsets at the DNA methylation level. (Figure legend continued on the following page)

**Figure 5.5.1: Principal component analysis separating  $\gamma\delta$  T cells from other  $\alpha\beta$  T-cell subsets at the DNA methylation level.** (A) GenomeStudio and Qlucore software-based bioinformatics pipeline was cross-validated with RnBeads package using  $\beta$ -values of top 100 CpG sites. (B) The 3D plot shows principal component analysis (PCA) on T-cell subsets. The plot was generated using Qlucore Omic Explorer software. PCA segregating all significant CpG sites is represented in the combined multiple scatter plots for all T-cell subsets (C) and using a scatter plot for the comparison between  $\alpha\beta$  and  $\gamma\delta$  T cells (D). (E) The simple bar plot explains percent variance as a number of components underlying T-cell methylome. (F) Heatmap using Pearson correlation method shows correlation between CD4, CD8, Treg and  $\gamma\delta$  T cells.

To address these issues, beta-values representing methylation levels from GenomeStudio software and from vanilla analysis mode of RnBeads package were compared for the 100 most differentially methylated CpG sites, which showed highly comparable and correlated results (Fig. 5.5.1A). M-values obtained from RnBeads were also highly correlated with beta values from GenomeStudio (data not shown). Thus, the DNA methylation data presented here is based on the beta-values of each CpG site from GenomeStudio tailored with Qlucore omic analysis software.

The principal component analysis (PCA) was used to find out the variation within CpG loci, between T-cell types and donor effects. The PCA clearly separated CD4, CD8, Treg and  $\gamma\delta$  T cells with no substantial effects from biological replicates (Figure 5.5.1B). The variation between CpG loci across the genome was clearly separated in all individual cell types (Figure 5.5.1B, C) and also within TCR group  $\gamma\delta$  and  $\alpha\beta$  (Fig. 5.5.1D). Overall, 4 components emerged from significant 1800 CpG sites analyzed (Fig. 5.5.1E), with a significant difference of about 63% variance in component 1 and 26% in component 2 (Fig. 5.5.1B). Of note, correlation analysis of T-cell subsets using the Pearson method revealed common clustering of CD4 - Treg and CD8 -  $\gamma\delta$  T cells (Fig. 5.5.1F), which supports the functional role of these T cell subsets. This functional role was further supported by the component 2, separating differentially methylated genes in  $\gamma\delta$ , including KLRG1, ADAP1, RUNX3, FBLN7 and SSBP3 in the opposite directions (data not shown). Altogether, the DNA methylome analyzed here indicates the epigenetic basis for the  $\gamma\delta$  T cell subset being more closely related to CD8 T cells than other subsets.

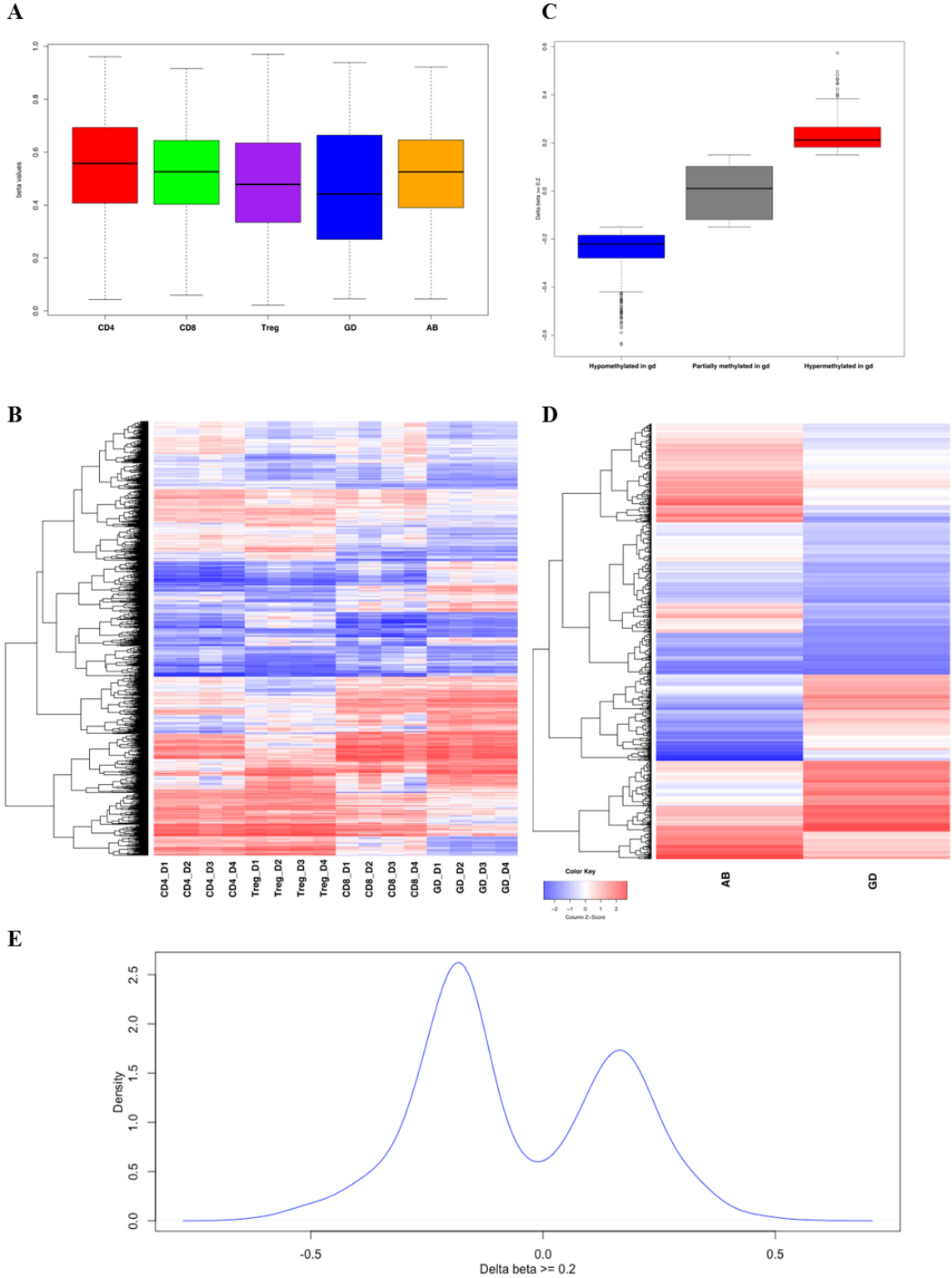


Figure 5.5.2:  $\gamma\delta$  T cell-specific methylation signature. (Figure legend continued on the following page)

**Figure 5.5.2:  $\gamma\delta$  T cell-specific methylation signature.** (A) Box-and-whisker-plot represents the overall methylation levels of CD4, CD8, Treg and  $\gamma\delta$  T cells. The methylation level for  $\alpha\beta$  T cells is calculated based on the mean of CD4, CD8 and Treg samples. (B) Unsupervised cluster analysis of all statistically significant CpG sites is presented via a heatmap. (C) Box plot depicts the distribution of differential methylation in  $\gamma\delta$  T cells. CpG sites were classified as ‘hypomethylated in  $\gamma\delta$ ’, ‘partially methylated in  $\gamma\delta$ ’ and ‘hypermethylated in  $\gamma\delta$ ’ based on delta beta values with  $\leq -0.15$ , between  $-0.15$  and  $0.15$ ,  $\geq 0.15$ , respectively. Delta beta value is the difference between mean of beta values of  $\gamma\delta$  and  $\alpha\beta$  T cell samples. (D) The heatmap represents the unsupervised cluster analysis of CpG sites between  $\gamma\delta$  and  $\alpha\beta$  T-cell groups, which are hypomethylated and hypermethylated in  $\gamma\delta$  T cells. (E) The density plot analysis based on delta beta values shows bimodal distribution due to hypomethylated and hypermethylated CpG sites in  $\gamma\delta$  T cells.

### 5.5.2 $\gamma\delta$ T cells share distinct DNA methylation patterns with $\alpha\beta$ T cells

With the preliminary information about the DNA methylation at hand, I studied the differential methylation between  $\gamma\delta$  and total  $\alpha\beta$  T cells (CD4, Treg and CD8 T cells together) in more detail. Overall methylation represented by beta-values showed a significantly low methylation level in  $\gamma\delta$  T cells (median beta-value 0.44) as compared to  $\alpha\beta$  T cells (median beta-value 0.53, adj.p-value =  $4.775468e-12$ ), while a comparatively less significant difference was observed between  $\gamma\delta$  T cells and Treg (median beta-value 0.47, adj.p-value =  $5.530386e-03$ ; Fig. 5.5.2A). The difference in the methylation level of  $\gamma\delta$  T cells with CD4 T cells (median beta-value 0.56) was even higher than with CD8 T cells (median beta-values 0.53). In total, 1512 CpG sites from all T-cell populations were methylated with the statistical significance of p-value 0.01 and q-value 0.01803 (Fig. 5.5.2B). 432 CpG sites were hypomethylated in  $\gamma\delta$ , 233 CpG sites were hypermethylated in  $\gamma\delta$  and the rest were partially methylated as the difference in methylation levels (delta-beta) of  $\gamma\delta$  and  $\alpha\beta$  T cells was between  $-0.15$  and  $+0.15$  (Fig. 5.5.2C, D). Unsupervised analysis of the DNA methylation profile showed differentially methylated CpG sites forming 3 distinct clusters (Fig. 5.5.2B, D). Out of all significantly methylated CpG loci in T cells, 75 % of CpG sites were annotated to one or more genes, while others might be located in non-coding regions of DNA or might be involved in the *trans*-regulation of gene expression. Moreover, the bimodal distribution of differentially methylated CpG sites in  $\gamma\delta$  T cells was more hypomethylated (Fig. 5.5.2E). Thus, the overall CpG hypomethylation in  $\gamma\delta$  T cells forms the basis for the DNA methylation signature.

### 5.5.3 Genomic and epigenomic features form the basis for the $\gamma\delta$ T-cell methylation pattern

To decipher the components responsible for CpG hypomethylation in  $\gamma\delta$  T cells, I studied the DNA methylation profile across the genomic and epigenomic features which regulate gene expression. The CpG island (CGI) densities and their location in the vicinity of transcription start site (TSS) distinguish transcriptionally repressive and permissive DNA methylation (Hughes *et al*, 2010). As expected, we found that more than 1000 CpG sites are located in the genomic body containing exons and introns. The number of CpG sites was more in distal promoter region (TSS1500) than proximal promoter region (TSS200; Fig. 5.5.3A). However, the delta beta value distribution reflecting differential methylation in  $\gamma\delta$  T cells was overall more hypomethylated (Fig. 5.5.3B). When the methylation levels (beta-values) of all T-cell subsets were plotted across genomic features, CD4 and CD8 cells had higher methylation than  $\gamma\delta$  and Treg cells (Fig. 5.5.3C). This is in agreement with previous results (Fig. 5.5.2A). Interestingly, beta-values of CD8 cells in the regions of transcriptional initiation (TSS200, 5'UTR and 1<sup>st</sup> Exon) were comparable to that of CD4 cells, but not to that of  $\gamma\delta$  T cells. But the beta values in Treg and  $\gamma\delta$  T cells at TSS200 region were nearly the same (Fig. 5.5.3C). Of note, methylation levels at TSS1500 (distal promoter region) had four different levels of methylation according to T-cell subsets, which might result in cell type-specific transcriptional regulation of genes. When  $\gamma\delta$  and  $\alpha\beta$  T cell groups were compared, the methylation levels were different at TSS1500, TSS200, 1stExon and gene body with statistical significance of adj.p-value 0.0491, 0.0409, 0.0001, 0.0287 and 5.626346e-10, respectively (Fig. 5.5.3D).

According to the traditional concept, island and shelf regions are described to regulate CpG methylation (Edgar *et al*, 2014). We found that the maximum number of CpG sites is located in the non-CGI region (also referred to as open sea or non-coding region) and then in N-shore (Fig. 5.5.3E). Nevertheless, as seen for genomic entities except for S shelf, the methylation pattern in  $\gamma\delta$  T cells as compared to  $\alpha\beta$  T cells was hypomethylated, but the distribution was notably wider in island and open sea regions (Fig. 5.5.3F). Thus,  $\gamma\delta$  T cells and other T-cell subsets possess characteristic DNA methylation patterns in respective genomic and epigenomic regions, which may potentially correlate with the functional role.

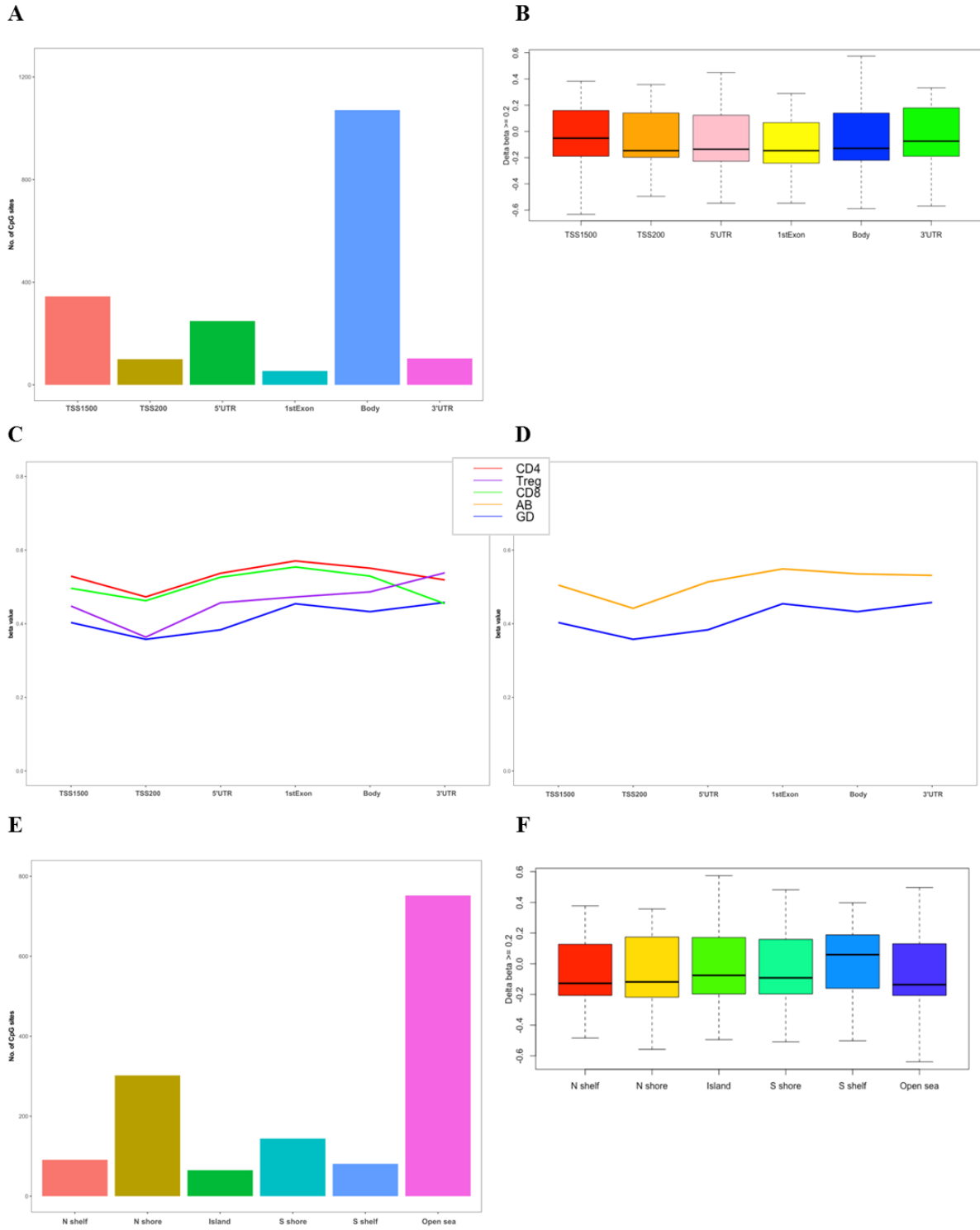


Figure 5.5.3: The DNA methylation pattern in T cells according to genomic and epigenomic entities. (Figure legend continued on the following page)

**Figure 5.5.3: The DNA methylation pattern in T cells according to genomic and epigenomic entities.** (A) Number of CpG sites according to specific (B) genomic- and (F) CpG Island (CGI)- features are presented after excluding unassigned CpG sites. DNA methylation levels as beta-value at each genomic region are illustrated for all four T-cell populations (C) and also only for  $\gamma\delta$  and  $\alpha\beta$  T cell group comparison (D). The box plot shows differential methylation between  $\gamma\delta$  and  $\alpha\beta$  T cells at (E) genomic regions such as promoter region (TSS1500, TSS200), gene body and untranslated regions (UTR), and at (G) CGI regions.

#### 5.5.4 Functional validation of T cell-specific DNA methylome

The CpG sites from the  $\gamma\delta$  T cell-specific DNA methylome are annotated to certain genes, which have diverse functional significance. However, the DNA methylome data was analyzed using 450k arrays. In the methylation arrays, predesigned probes are used to evaluate the differential methylation of particular bisulfite-converted DNA. Thus, the results obtained from arrays need to be validated by alternative methods. To validate our results, we performed CpG site-specific pyrosequencing. For pyrosequencing experiments, I randomly selected the 10 most differentially methylated CpG sites from the 450k array data. To exclude the effect of biological replicates, we performed pyrosequencing experiments on T-cell populations from 4 “old” samples (which were used for 450k arrays) and 4 newly prepared samples (which were used only for pyrosequencing). Finally, the percentage of methylation was obtained from pyrosequencing together with appropriate controls (fully (un)methylated DNA and non-bisulfite-converted genomic DNA) and then was compared with corresponding beta-values from 450k arrays. For 5 different CpG sites regulation of respective genes was significantly correlated with results obtained from 450k arrays and pyrosequencing (ranges for  $r=0.36 - 0.83$ ,  $R^2=0.38 - 0.69$ ; p-value ranged from 0.012 to  $<0.0001$ ; Fig. 5.5.4A-E). Moreover, the heatmap representing unsupervised cluster analysis on these selected genes showed largely similar association of clustering (Fig. 5.5.4F-G). The CpG site cg0447762 for the IL-6R gene was hypermethylated in  $\gamma\delta$  T cells and clustered separately from the hypomethylated CpG sites cg20235075, cg00014104, cg00344178, cg00556515 for EOMES, MAPK1, NMNAT2, TNFRSF1A, respectively.



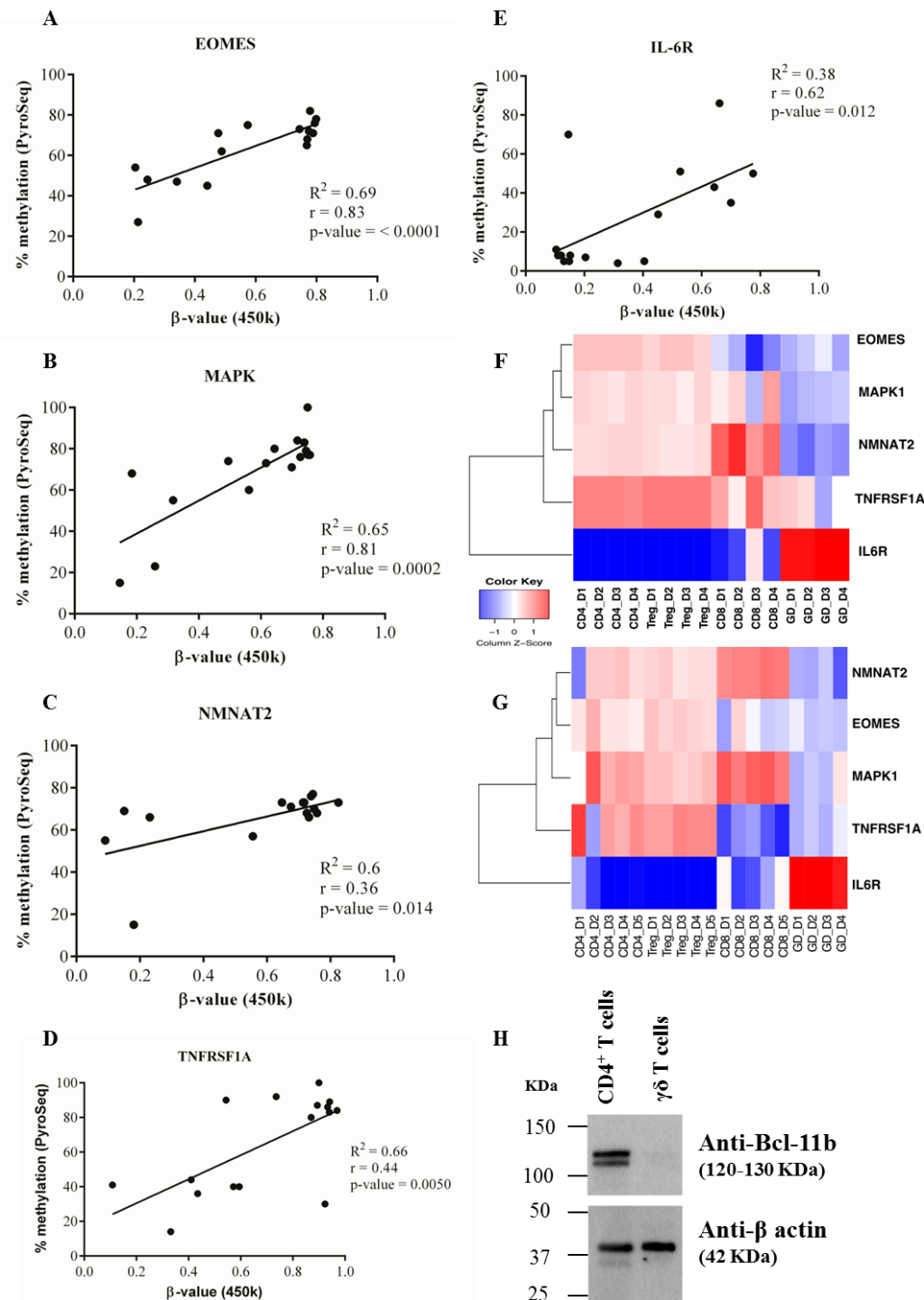


**Figure 5.5.4: Functional validation of HumanMethylation450 BeadChip (450k array) using pyrosequencing.**  
 (Figure legend continued on the following page)

**Figure 5.5.4: Functional validation of HumanMethylation450 BeadChip (450k array) using pyrosequencing.**

Five different CpG sites associated with indicated genes were quantitatively analyzed by methylation-specific pyrosequencing using the same samples that were used for the 450k arrays and also using additional new samples. (A-E) Scatter plot represents correlation analysis between % methylation value from pyrosequencing and beta value from 450k arrays. Unsupervised clustering of five CpG sites shows clear separation based on differential methylation in  $\gamma\delta$  T cells derived from 450k arrays (F) and pyrosequencing (G). (H) 10  $\mu$ g of cell lysate from CD4 and  $\gamma\delta$  T cell under the reducing conditions was analyzed by western blot. Upper panel shows protein detected by anti-human Bcl-11b mAb (120-130 KDa; Cell Signaling Technology) and the lower panel shows anti-human  $\beta$ -actin mAb (42 KDa; Sigma-Aldrich). The blot represented here is one out of the three independent experiments.

DNA methylation was also validated at the protein level. Though 5 out of 10 CpG sites could not be validated by pyrosequencing, protein expression analysis for one of the selected CpG sites was still performed considering the functional importance of this gene in T cell development. Western blot analysis clearly showed expression of the Bcl-11b protein only in CD4 cells, but not in  $\gamma\delta$  T cells (Fig. 5.5.4H). Furthermore, previous results from our group have already shown that 90 % of CD4 T cells and 46 % on CD8 T cells expressed IL-6R, but only 11 %  $\gamma\delta$  T cells (Oberge *et al*, 2006) which is well in line with our methylation analysis. Taken together, our technical validation clearly supports DNA methylation signature of  $\gamma\delta$  T cells with functionally characteristic features.

**5.5.5 Gene expression profile represents differential regulation of  $\gamma\delta$  T cells**

Accumulating evidence suggests that DNA methylation plays an indispensable role in the expression of genes responsible for T-cell development, function and survival (Lee *et al*, 2001 Immunity). The direct association of DNA methylation and protein expression observed in our functional validation also supports this fact. However, the differential gene expression itself is a complex molecular event, which is further regulated by different RNA subspecies like microRNA (miRNA) and long non-coding RNA (lncRNA). Additionally, there has not been any study published so far using a whole-genome RNA sequencing approach to understand the differential regulation of  $\gamma\delta$  T cells compared to  $\alpha\beta$  T cells in an integrated and comprehensive view of the epigenetic landscape. Hence, we first generated the differential expression gene (DEG) profile of  $\gamma\delta$  T cells and compared it with  $\alpha\beta$  T cells (CD4, CD8 and Treg).

The protocols for RNA purification were optimized with regard to quality and quantity in a way that maximum deep coverage of sequencing was possible, resulting in the analysis of all

subspecies of RNA i.e. miRNA and lncRNA in addition to transcriptome. RNA-sequencing to analyze transcriptome and lncRNA generated an average 26 million 125-nt paired-end reads for each sample. The RNA-seq-based transcriptome analysis showed a clear separation of T-cell subsets (CD4, Treg, CD8 and  $\gamma\delta$ ). To our surprise, we observed a strong influence in % variance based on gender differences, but still separating  $\gamma\delta$  T cells and  $\alpha\beta$  T cells (Fig. 5.5.5A). Hence after excluding the only female donor, the remaining male donors in T cell biological replicates grouped together with minimal variance. The transcriptome of  $\gamma\delta$  compared to other T-cell subsets possesses two components with around 74% and 8% variance (Fig. 5.5.5B). Of note, CD8 T cells were closer to  $\gamma\delta$  T cells than to CD4 T cells. Treg were highly distant from  $\gamma\delta$  T cells, separating principal component horizontally. Hence, we performed all transcriptome analyses with three male donors, excluding the female donor. The MA plot analysis clearly showed significant differences in mean transcript expression and  $\log_2$ FoldChange, which is the  $\log_2$  ratio of fold difference between  $\gamma\delta$  and  $\alpha\beta$  T cells (Fig. 5.5.5C). With high stringency in analysis (adj. p-value  $\leq 0.01$  and  $\log_2$ FoldChange 1.5), we obtained 569 differentially expressed genes, of which 120 were upregulated and 449 were downregulated. The top 50 most differentially regulated genes presented in a heatmap showed a distinct pattern of gene clustering (Fig. 5.5.5D). Out of the upregulated genes in  $\gamma\delta$  T cells, TCR  $\gamma$  and  $\delta$  chain genes were separately clustered from other genes such as DTX3, BANK1 and CD22. Other well-known genes, which were downregulated in  $\gamma\delta$  T cells, included CCR7, LEF1, RCAN3 and TCR  $\alpha$  and  $\beta$  chain genes. Thus, our transcriptome analyses showed that  $\gamma\delta$  T cells possess very distinct gene expression patterns, when compared to  $\alpha\beta$  T cells.

### 5.5.6 $\gamma\delta$ T cells share a discrete regulatory RNA (miRNA and lncRNA) profile

Transcriptional regulation of genes is an orchestrated phenomenon. Differential expression of genes (DEG) is widely described to be regulated by miRNA (Orang *et al*, 2014) and lncRNA (Wang and Chang, 2011) Even though we have identified the DEG signature for  $\gamma\delta$  T cells, we went one step ahead to decipher the involvement of both miRNA and lncRNA responsible for this DEG. We used a RNA-seq-based miRNA profiling approach. The same biological samples of T-cell subsets from healthy donors were used for a second run of RNA-seq. Thus, DEG, differentially expressed miRNA and lncRNA analysis was performed on the same T-cell

populations from the very same healthy donors, to explore the three different layers of gene regulation in the epigenetic landscape.

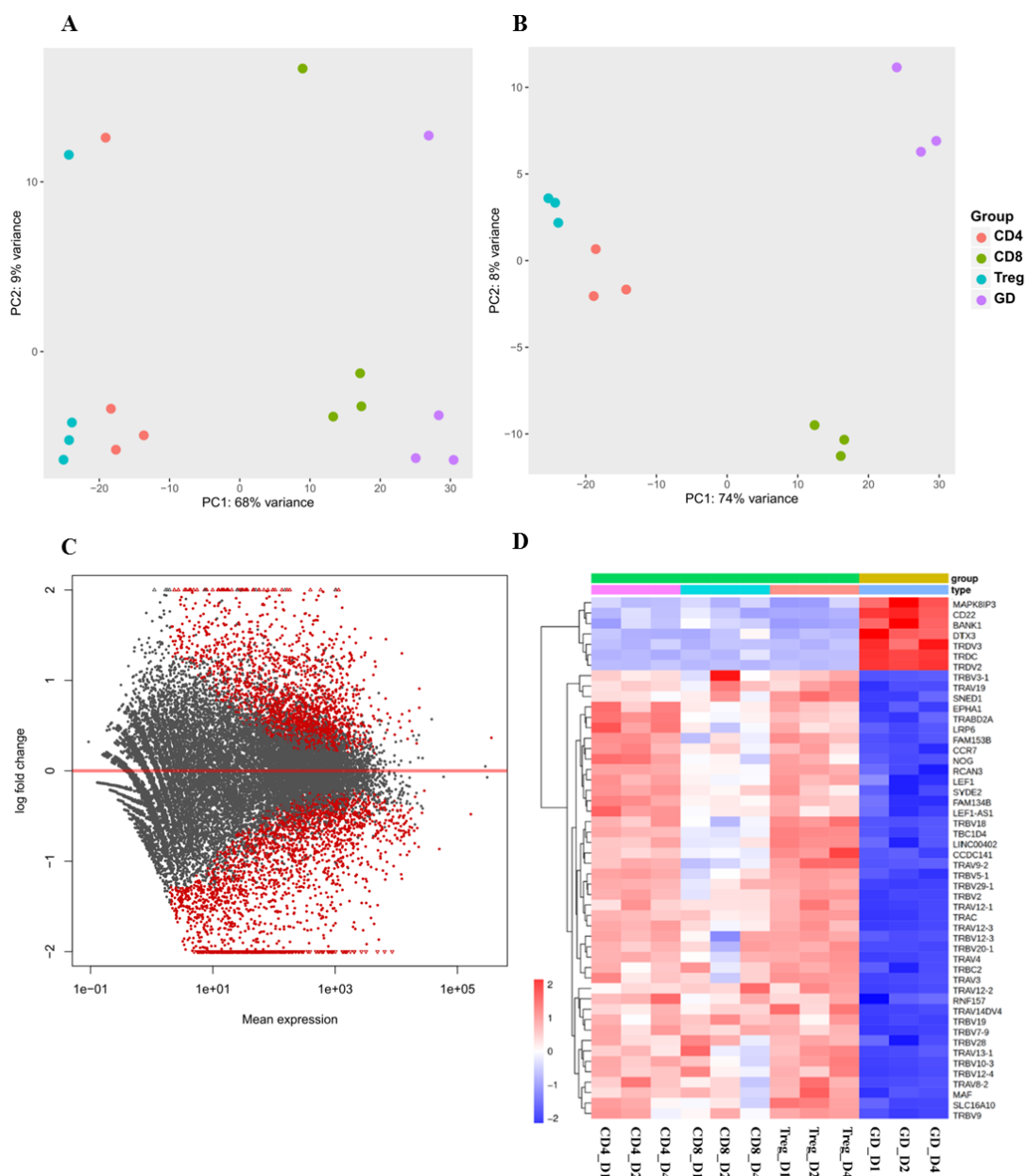


**Figure 5.5.5: RNA-seq-based transcriptome analysis of  $\gamma\delta$  T cells and  $\alpha\beta$  T cell subsets.** (A-B) The PCA separates individual donors according to cell type. (C) The MA plot shows differential gene expression as a measure of  $\log_2$  fold change and mean expression. (D) The heatmap presents the 50 most differentially expressed genes with adjusted p-value  $\leq 0.01$  and  $\log_2$ FoldChange.

As it was observed before (Fig. 5.5.5A), the variation in miRNA profile of T-cell subsets was consistent as an effect of gender (the female, donor marked by ‘F’ in the plot). However, as displayed in the MDS plot (Fig. 5.5.6A),  $\gamma\delta$  T cells were also closely related to CD8 and equally far distantly related to CD4 and Treg cells. The miRNA profile of  $\gamma\delta$  T cells and Treg revealed a remarkable heterogeneity within donors, which is in line with a previous report (Durek *et al*, 2016). The quality control (QC) report based on 301 miRNA of T cells using a box-whisker plot showed nearly the same total normalized count of Treg and  $\gamma\delta$  as for CD4 and CD8 T cells, but with a wider distribution of counts in Treg cells (data not shown). We obtained 301 differentially expressed miRNA using variance-stabilizing transformation method (Fig. 5.5.6B). Top upregulated miRNA include has-miR-509-3p (targets NTRK3 gene), has-miR-424-5p (targets CCNF), while downregulated miRNA include has-miR-4772-3p (targets RAB40B) and has-miR-9-5p (targets MMP13).

Although the in-depth analysis of this data is ongoing, our exploratory analysis has revealed a list of miRNA specific for certain T-cell subsets (Table 5.2). For instance, 75 miRNA are involved in the regulation of CD4<sup>+</sup> and  $\gamma\delta$  T cells. Out of these, 36 miRNA are also involved in the regulation of CD8 and  $\gamma\delta$  T cells. Thus, the miRNA profile specific for  $\gamma\delta$  T cell function is generated.

**Table 5.2:** Number of significantly differentially expressed miRNAs overlapping between comparisons of cell types

	<b>Treg vs <math>\gamma\delta</math></b>	<b>CD4 vs <math>\gamma\delta</math></b>	<b>CD8 vs Treg</b>	<b>CD4 vs CD8</b>	<b>CD8 vs <math>\gamma\delta</math></b>	<b>CD4 vs Treg</b>
<b>Treg vs <math>\gamma\delta</math></b>	85	57	43	29	34	22
<b>CD4 vs <math>\gamma\delta</math></b>		75	37	32	36	20
<b>CD8 vs Treg</b>			54	27	26	18
<b>CD4 vs CD8</b>				45	21	16
<b>CD8 vs <math>\gamma\delta</math></b>					42	18
<b>CD4 vs Treg</b>						30

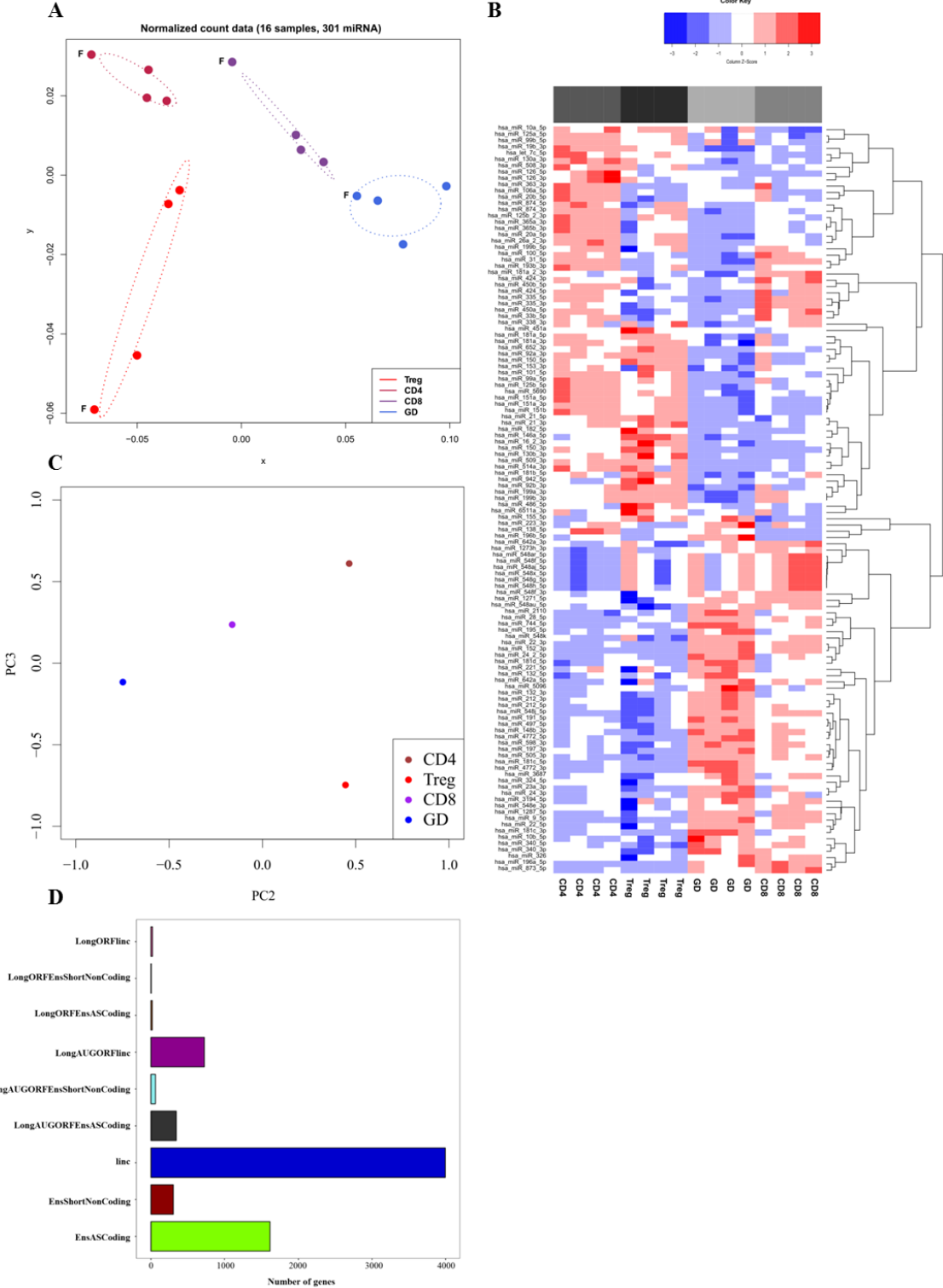


Figure 5.5.6: Differential expression of miRNA and lncRNA in  $\gamma\delta$  T cells in comparison to  $\alpha\beta$  T cells. (Figure legend continued on the following page)

**Figure 5.5.6: Differential expression of miRNA and lncRNA in  $\gamma\delta$  T cells in comparison to  $\alpha\beta$  T cells.** (A) Multidimensional scaling (MDS) plot shows normalized count data. Ellipses tracing bivariate normal density contours are added to illustrate the distribution of each group. Cell types are color-coded and female samples are marked with 'F'. (B) Expression patterns of significantly differentially expressed miRNAs are represented. Heatmap are generated using a distance based on Spearman correlation. Dendrograms are constructed employing complete linkage. (C) The PCA plot showing component 2 vs component 3 shows distribution of lncRNA in T-cell population groups. (D) Number of different sub-species of lncRNA found in T cell epigenome.

Looking at the regulation of DEG by lncRNA, the PCA plot with component 1 vs 2 showed clear separation of  $\gamma\delta$  and other T cells only on vertical axis (data not shown). However, the pattern of T-cell subset distribution influencing differences was very similar, but with better separation of T cells by components (Fig. 5.5.6C). Also, we detected several different subspecies of lncRNA. The predominant subspecies of lncRNA found were long intervening/intergenic RNA of more than 200 nucleotide in length (for  $\sim 4000$  genes) and natural antisense transcript (NAT or EnsASCoding; for  $\sim 1500$  genes; Fig. 5.5.6D). In total, 202659 detected transcripts were mapped to genes. Depending on the genomic location, one or several lncRNA were annotated to a gene. The maximum expression level of the transcript (as described by FPKM count, Fragments Per Kilobase of transcript per Million mapped reads) were used to identify differentially expressed lncRNA (collectively for all subspecies) in  $\gamma\delta$  T cells compared to other T-cell subsets. Upregulated lncRNA was found to regulate functionally important genes, including NKG7 (CD4 = 15.27, CD8 = 512.62, Treg = 1.15,  $\gamma\delta$  = 928.94), CCL5 (CD4 = 37.36, CD8 = 538.37, Treg = 4.54,  $\gamma\delta$  = 862.90) and GNLY (CD4 = 15.4, CD8 = 214.21, Treg = 0.82,  $\gamma\delta$  = 648.71). The downregulated transcripts included CCR7 (CD4 = 83.83, CD8 = 38.52, Treg = 59.22,  $\gamma\delta$  = 3.34), JUN (CD4 = 535.18, CD8 = 377.34, Treg = 577.31,  $\gamma\delta$  = 275.23), FOS (CD4 = 153.97, CD8 = 81.58, Treg = 122.64,  $\gamma\delta$  = 54.55), JUNB (CD4 = 1068.89, CD8 = 699.34, Treg = 845.88,  $\gamma\delta$  = 462.44) and CD8A (CD4 = 0.11, CD8 = 193.7, Treg = 0.147,  $\gamma\delta$  = 5.82). Of note, DEG level from transcriptome analysis was also found to be downregulated in  $\gamma\delta$  T cells for  $-1.05$  fold in JUNB expression,  $-1.14$  fold in FOS expression and  $-3.95$  fold in CCR7 expression. Taken together, lncRNA regulating genes and other transcription factors are likely involved in differential expression of  $\gamma\delta$  T-cell protein-coding genes.

### 5.5.7 Nucleosome positioning and differential chromatin accessibility support $\gamma\delta$ T-cell subset specification

Differential gene expression is an orchestrated process mediated by RNA polymerase II (pol II), transcription factors and associated binding complexes. The chromatin accessibility and nucleosome positioning facilitate free DNA to be subjected to active gene expression in this orchestrated process. Thus, this adds an additional layer of regulation to the control of differential gene expression (DEG). Hence, after generating  $\gamma\delta$  T cell-specific expression profiles supported by miRNA and lncRNA, ATAC-seq enabled us to address the role of chromatin accessibility, nucleosome positioning and transcription factor footprint. Though this approach to fully characterize the  $\gamma\delta$  T cell epigenetic landscape is in major parts still ongoing, I could provide some insights on some preliminary results in continuation of the previously studied epigenetic processes.

According to the method described by Buenrostro *et al* (2013), Tn5 transposases can be used, as they independently transposed to freely accessible DNA. The paired-end reads generate sequenced fragments of periodicity of about 200 bp size. This fragment distribution from T-cell chromatin resembled to the multiples of nucleosomes or nucleosome positioning (data not shown). Thus, based on this distribution of size, all mapped fragments with sizes up to 100 bp were nucleosome free regions (NFR) and between 180 to 247 bp were mononucleosome region. The region spanning the start and end of DNA fragment thus represented the region involved in gene expression. Furthermore the read counts were quantified from 1000 bp non-overlapping region and used for analysis. As it can be seen in the MDS plot upon nucleosome positioning, the individual T-cell subsets were separated in nucleosome free DNA (Fig. 5.5.7A), but not in mononucleosomal regions (Fig. 5.5.7B). However, a strong variance was observed only in biological samples of Treg cells. The Pearson's method-based cluster analysis showed positive correlation within all T-cell subsets from all the donors. The cluster analysis clearly showed that CD4 and Treg cells clustered together, while CD8 were more similar to V $\delta$ 1 than to V $\delta$ 2 T cells (Fig. 5.5.7C). With the feasibility to perform ATAC-seq on hundreds of T cells, we additionally analyzed the chromatin accessibility map of between V $\delta$ 1 and V $\delta$ 2 T cells. Considering immunologically significant differences between the subsets of  $\gamma\delta$  T cells, V $\delta$ 1 and V $\delta$ 2 were nicely separated as indicated by the NFR (Fig. 5.5.7D). Interestingly, the subset based separation



of  $\gamma\delta$  T-cell population was not seen in mononucleosomal regions (Fig. 5.5.7B). The clustering in T-cell ATAC-seq was mostly seen between donor 1 and donor 4, who are age-matched female healthy individuals. The differential accessibility within T cell populations was also evident from nucleosome positioning. It was represented by GAPDH (house-keeping gene), other T-cell function-specific genes including IFNG, IL-4, IL-13, KLRK1 (gene for NKG2D), DOCK5 and GAS7 (Fig. 5.5.7E) and also for the genes (e.g. TET2) involved in epigenetic processes.

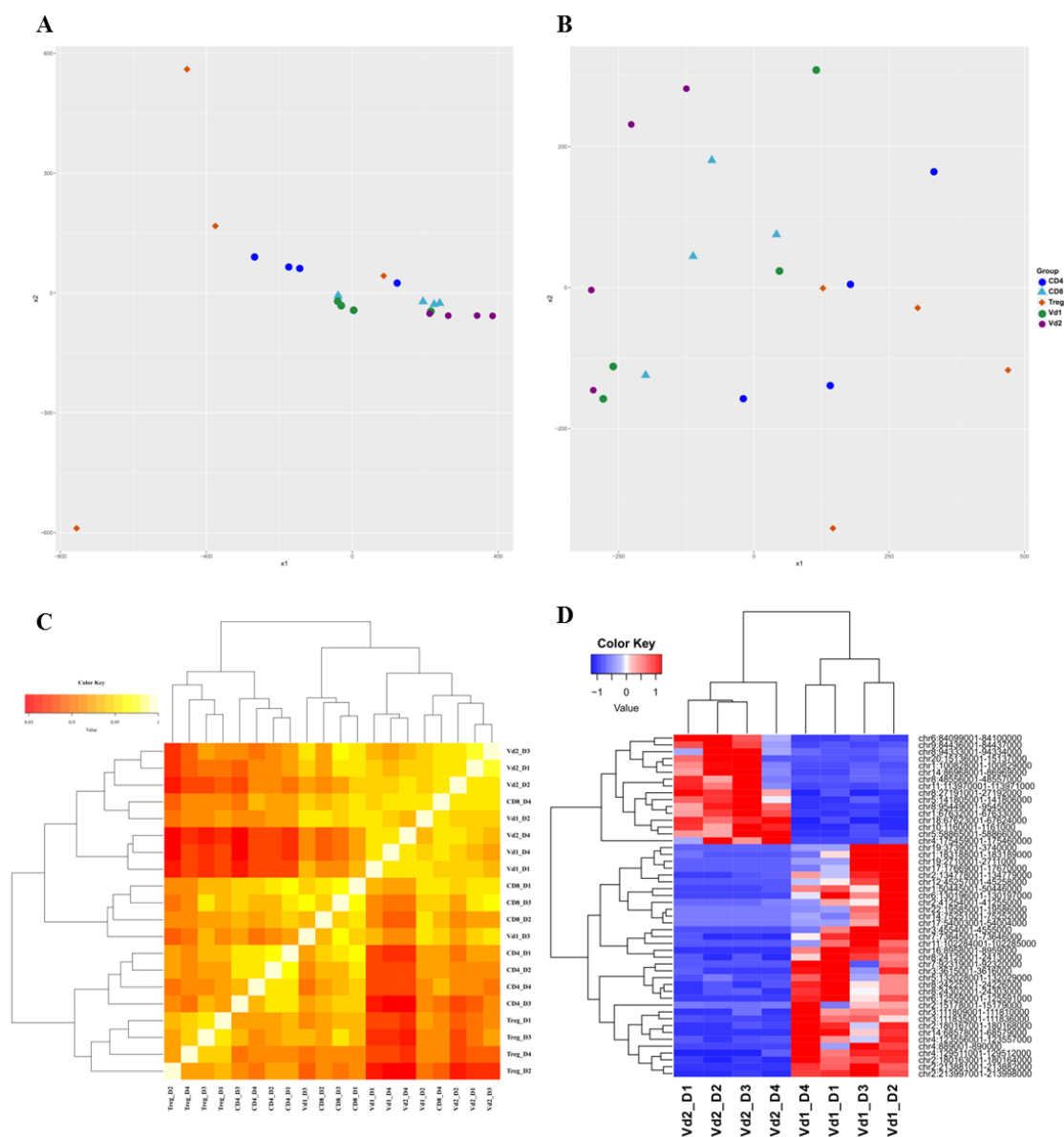
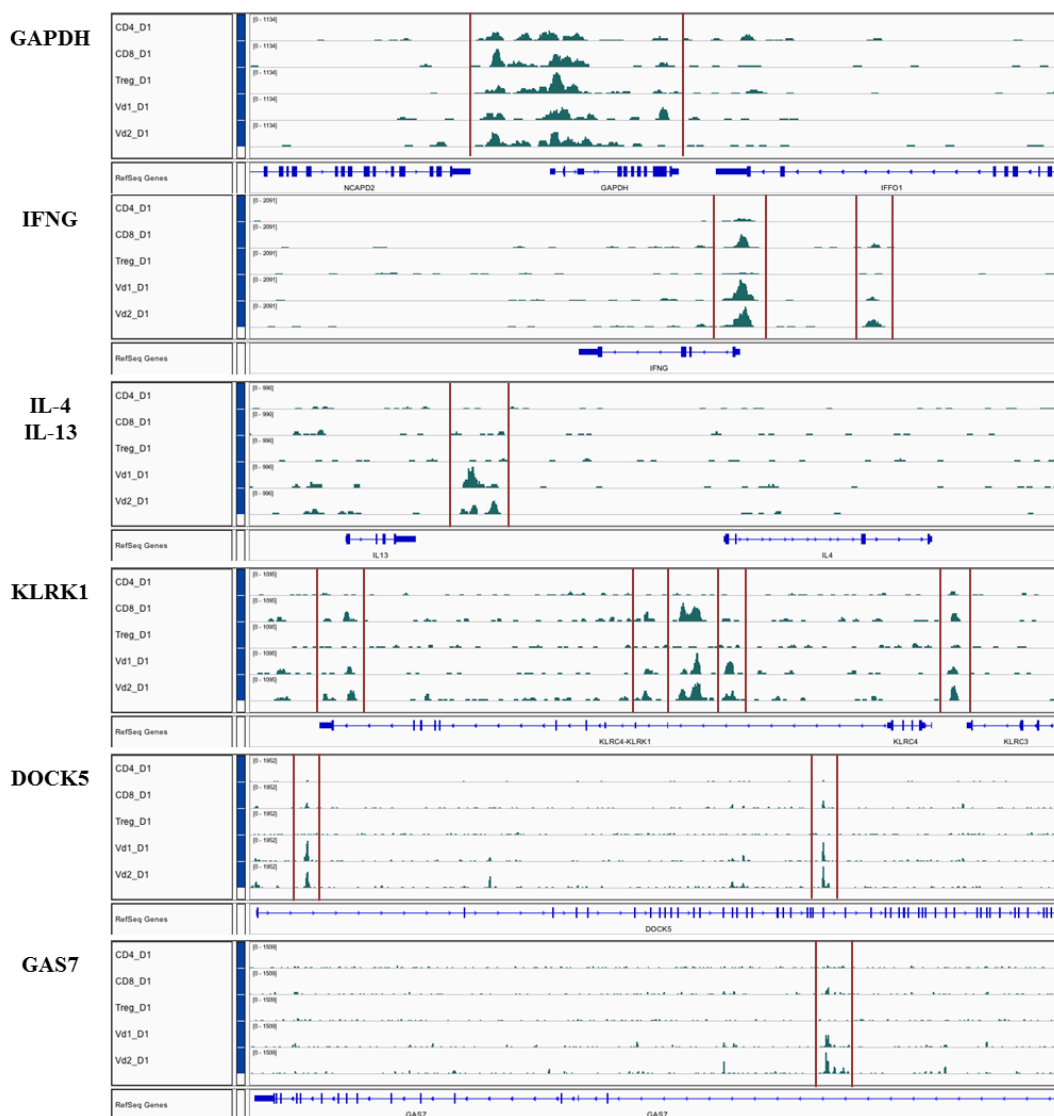


Figure 7: (Continued on the following page)

E



**Figure 5.5.7: Assay for transposase-accessible chromatin using sequencing (ATAC-seq) of human T-cell populations.** The mapped DNA fragments with sizes between 147 bp and 247 bp were referred to as mononucleosome and with fragment sizes below 100 bp were nucleosome-free regions (NFR). The MDS plot represents the distribution of T cells from four donors, based on the counts generated from 1000bp non-overlapping window of the NFR (A) and the mononucleosomal regions (B). (C) The Pearson's correlation analysis showed the relation between CD4, CD8, Treg, Vδ1 and Vδ2 T cells obtained from different donors. (D) The heatmap clustering samples and variable (DNA region) represents the top 50 most differentially accessible regions (1000 bp size). (E) A representative image of accessible DNA from one donor is explored by Integrated Genome Viewer (IGV). The chromatin accessibility for respective genomic location are shown by dark green peaks marked by vertical red bars for the samples CD4\_D1, CD8\_D1, Treg\_D1, Vδ1\_D1 and Vδ2\_D1. 'D1' is noted for donor number 1.

Therefore, the results presented here clearly show that  $\gamma\delta$  T cells (or even V $\delta$ 1 and V $\delta$ 2 subsets) carry a characteristic feature by possessing differentially accessible chromatin and nucleosome remodeling.

### **5.5.8 A set of genes integrating $\gamma\delta$ T cell-specific DNA methylation and the RNA expression profile forms the basis for $\gamma\delta$ T cell immune function**

After having successfully generated a  $\gamma\delta$  T-cell-specific -omics signature, we analyzed the potential in the co-ordination of all these multiple epigenetic processes in an integrated multiomic approach. As of now, the analysis of miRNA and ATAC-seq data is ongoing, so I performed the integrated analysis with human T cells ( $\gamma\delta$  and  $\alpha\beta$ ) datasets from DNA methylation, transcriptome and lncRNA analyses. From the respective epigenomic data, the correlation was done based on their gene symbol (hg19, UCSC genome database). For DNA methylation, statistically significant differentially methylated CpG sites (p-value = 0.01, q = 0.01803, n = 1,149) annotated with respective gene symbols were used, while for lncRNA, the statistically significant transcripts (n = 202,659) annotating to the respective gene were used. DEG with adj. p-value  $\leq 0.01$  and  $\log_2$ FoldChange 1.5 (n = 569) were used for analysis (Fig. 5.5.8A). To find out the association of multiple genomic datasets, the Fitting Linear Model was used. For the common variables (n = 54), which were found in differentially expressed genes (DEG) and differentially methylated genes (DMG), adjusted  $R^2$  was 0.1709 with statistical significant p-value of 0.0003. For 825 variables commonly occurring between DMG and differentially expressed lncRNA (DE lncRNA) datasets, adjusted  $R^2$  was 0.00008 with p-value of 0.1667. For 503 variables commonly found in DEG and DE lncRNA, adjusted  $R^2$  was 0.02645 with p-value of 2.20e-16. However, notable distribution in QQ plot due to non-fitting variables (data not shown) was observed.

Next, PCA on these datasets showed variance between two components of DEG and DMG due to the strong influence of genes like ADAP1, DOCK5, FBLN7 (Fig. 5.5.9A) with a negative Pearson correlation of -0.4281 (Fig. 5.5.9B). PCA between DMG and lncRNA datasets showed nearly no variance in the components, possibly due to SNORD17 and SNORA63 (small nuclear RNA) resulting as a confounding factor (Fig. 5.5.9C), but the correlation of 0.0867 (Fig. 5.5.9D). Comparing DEG and lncRNA, the orthogonal components showed a negative correlation of

–0.02235 (Fig. 5.5.9E-F). Interestingly, major players in separating these components of DEG and lncRNA were TCR chain expression genes. Thus, the differential correlation between different epigenomic datasets for  $\gamma\delta$  T cells supports complexity for multiple levels of gene expression.

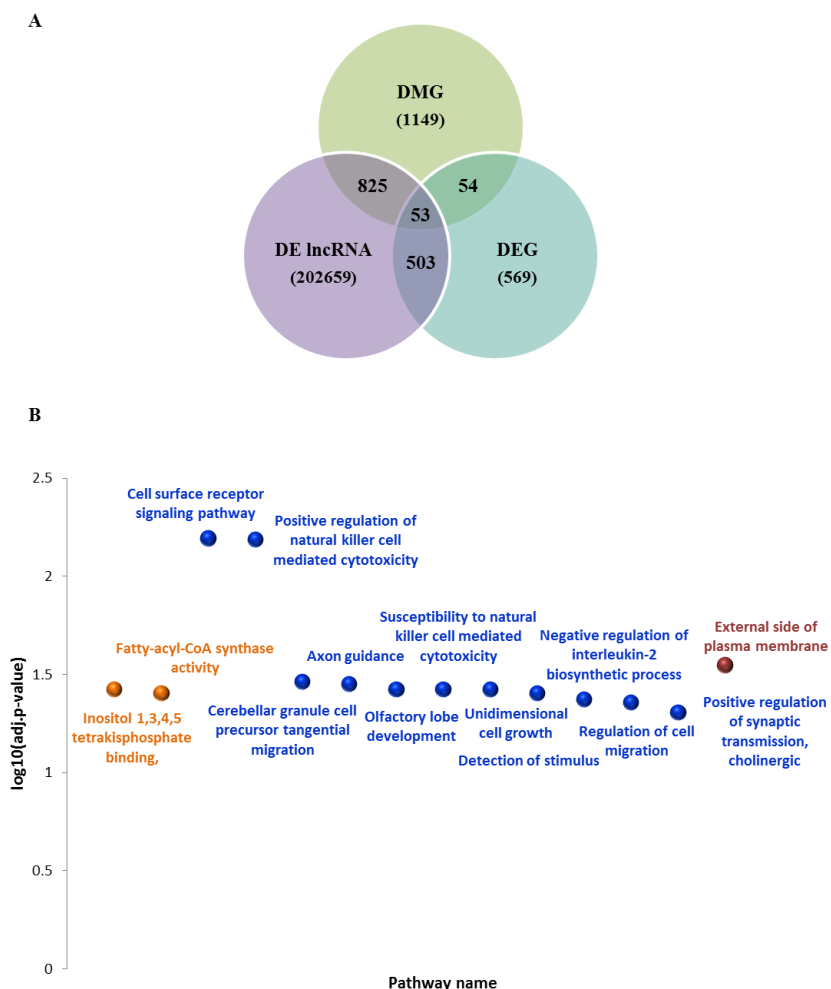


**Figure 5.5.8: Integrated analysis of differentially expressed genes (DEG), differentially methylated genes (DMG) and differentially expressed lncRNA (DE lncRNA) in human  $\gamma\delta$  T cells.** (A) After merging genes using “gene symbols” from the respective datasets, 53 unique genes were found. (B) Functional annotation of upregulated genes from these 53 unique genes was done. The color coded ball shows statistically significant (Benjamini-Hochberg, adj. p-value  $\leq 0.05$ ) Gene Ontology (GO) terms. Orange color balls represent GO association with molecular function, while blue and red colors represent biological processes and cellular components, respectively.

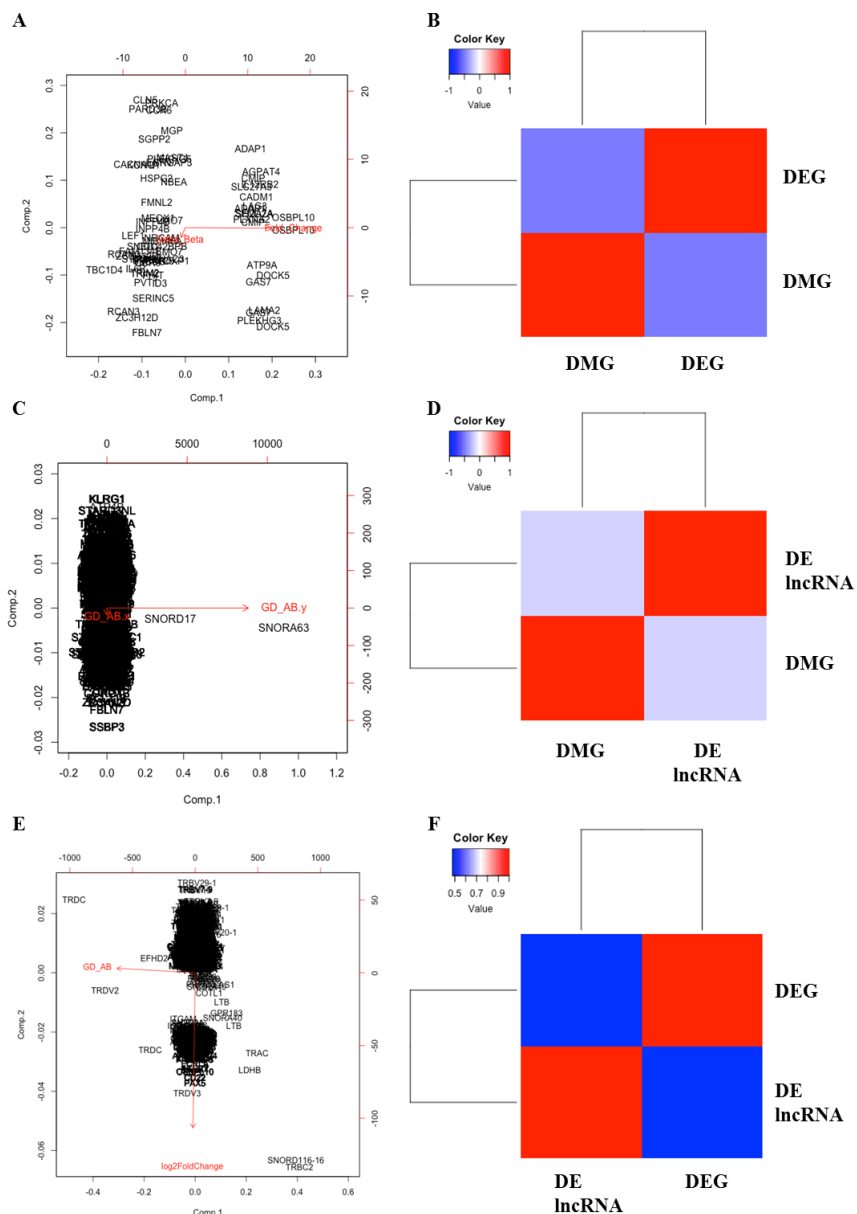


**Figure 5.5.9: PCA and correlation analysis of epigenomic datasets.** (A), (C) and (E) are the scatter plots representing PCA. Red color arrows indicate the direction of the both components. Sample groups are displayed in red, while black color gene names are commonly occurring variables from each dataset. In PCA plots, delta beta and GD\_AB.x stand for differential methylation values from DNA methylation profiles; fold change and log2FoldChange are the differential expression values from transcriptome analyses. GD\_AB.y and GD\_AB stands for the differential expression values from IncRNA profiles. (B, D, F) The color coded correlation plots were generated based on Pearson correlation with complete linkage. The following abbreviations are used: DEG,

differentially expressed genes; DMG, differentially methylated genes and DE lncRNA, differentially expressed lncRNA.

Moreover, we looked at the expression levels of these 53 unique genes derived from the integrated analysis. Out of 53, 16 genes were upregulated in  $\gamma\delta$  T cells, while 37 genes were downregulated in  $\gamma\delta$  T cells compared to  $\alpha\beta$  T cells (as listed in Table 5.3). Therefore, it was interesting to look at the functional association of these genes. So, using the Gene ontology (GO) approach, we identified functionally associated GO terms in relation to these differentially expressed genes (Fig. 5.5.8B). Though GO terms in InnateDB database were not significantly enriched for downregulated genes, a significant association of upregulated gene was found by adjusting the false discovery rate (FDR) using the Benjamini-Hochberg method. Some of the notable processes included cell surface receptor signaling, regulation of NK cell-mediated cytotoxicity and genes regulating external side of plasma membrane.

**Table 5.3: The list of genes derived from integrated epigenomic analysis of  $\gamma\delta$  T cells**

Gene symbol	log2 Fold Change	Adj. p-value	Regulation in $\gamma\delta$ T cells
OSBPL10	3.270693	1.46E-10	Upregulated
DOCK5	2.471913	1.60E-05	Upregulated
LAMA2	2.137432	3.10E-09	Upregulated
ATP9A	2.032507	0.001451	Upregulated
AGPAT4	1.982552	4.10E-09	Upregulated
PLEKHG3	1.939356	4.31E-06	Upregulated
IL12RB2	1.929912	0.000337	Upregulated
GAS7	1.894028	0.00718	Upregulated
CADM1	1.789074	0.000744	Upregulated
LAG3	1.735829	0.005223	Upregulated
SH2D2A	1.71346	0.000505	Upregulated
SEMA7A	1.703205	0.000742	Upregulated
CMIP	1.664077	0.000475	Upregulated
PLXNA2	1.608247	0.006273	Upregulated
SLC27A3	1.596834	0.001961	Upregulated

ADAP1	1.548616	0.009557	Upregulated
FOXP1	-1.49788	1.36E-06	Downregulated
NBEA	-1.49799	0.000532	Downregulated
SRGAP3	-1.55005	0.007346	Downregulated
MAST4	-1.56673	0.001755	Downregulated
MGP	-1.59342	0.007261	Downregulated
LMO7	-1.65388	8.55E-08	Downregulated
PLEKHG5	-1.68723	0.000115	Downregulated
NRCAM	-1.97032	0.006488	Downregulated
CDC42BPB	-1.97144	0.000314	Downregulated
PRKCA	-2.00782	1.12E-10	Downregulated
ID3	-2.05019	0.001095	Downregulated
LAYN	-2.11166	0.001258	Downregulated
CCR6	-2.11369	0.000276	Downregulated
MEOX1	-2.12545	0.002704	Downregulated
FMNL2	-2.18445	0.000638	Downregulated
HSPG2	-2.19744	0.001359	Downregulated
ICOS	-2.29034	7.43E-07	Downregulated
SGPP2	-2.29386	0.000117	Downregulated
SERINC5	-2.30363	1.12E-11	Downregulated
FHIT	-2.31197	0.00032	Downregulated
ST6GALNAC3	-2.31935	0.000156	Downregulated
INPP4B	-2.33594	4.26E-08	Downregulated
CCR9	-2.52736	2.76E-05	Downregulated
FBLN7	-2.54405	0.00022	Downregulated
PARD3B	-2.55062	3.69E-05	Downregulated
PVT1	-2.59435	1.04E-08	Downregulated
TRIM2	-2.64797	2.18E-05	Downregulated
CLN5	-2.66119	6.73E-10	Downregulated

KCNQ1	-2.71782	1.16E-08	Downregulated
SNED1	-2.72444	5.02E-13	Downregulated
FAM134B	-2.83195	1.81E-17	Downregulated
ZC3H12D	-2.94784	2.58E-07	Downregulated
IL6R	-3.00467	1.18E-06	Downregulated
CACNA1I	-3.08184	1.38E-10	Downregulated
LEF1	-3.11278	2.14E-13	Downregulated
RCAN3	-3.4826	1.06E-21	Downregulated
TBC1D4	-4.25768	6.87E-19	Downregulated

Taken together, our systemic approach to understand the complex epigenetic regulation revealed  $\gamma\delta$  T cell-specific signatures in the regulation of genes responsible for functional immune responses.



## 5.6 Epigenetic modification of human $\gamma\delta$ T-cells in malignancy: A case report of an hepatosplenic gamma/delta T-cell lymphoma patient responding to Interferon- $\alpha$ treatment

*Associated manuscript:*

The results presented in this chapter will be part of a manuscript (in preparation): **Jaydeep Bhat\***, Anke Bergmann\*, Christoph Nerl, Silvio Waschina, Christoph Kaleta, Reiner Siebert, Ole Ammerpohl, and Dieter Kabelitz (shared first authors).

The previous result sections focused on the involvement of diverse epigenetic mechanisms that might govern the  $\gamma\delta$  T-cell signature and form the basis for their functional responses under *in vitro* conditions. Along with other epigenetic regulations, the stable and reversible modification of DNA methylation synergistically controls HDAC activity. After describing distinct features of the healthy  $\gamma\delta$  T-cell methylome, it would be interesting to perform similar studies in malignant  $\gamma\delta$  T cells. The differential DNA methylation signature of cancer has emerged as a characteristic clinical feature in cancer biology which correlates with disease progression, prognosis and drug responses. Thus in this last result section of the PhD thesis, the importance of epigenetic regulation of  $\gamma\delta$  T cells will be extended to study the changes in DNA methylation in an example case of human  $\gamma\delta$ -hepatosplenic T-cell lymphoma (HSTCL) patients during the course of therapy.

### 5.6.1 Clinical representation of a $\gamma\delta$ -HSTCL patient

A 39-years-old female patient had a chronic lymphocytosis with 22,300/ $\mu$ l white blood cell counts with 95% lymphocytes and 99% of  $\gamma\delta$  T-cell clonal phenotype. At diagnosis, the patient presented with mild hepatosplenomegaly, severe anemia with hemoglobin (Hb) 6.9 g/dl, haptoglobin < 5 mg/dl, LDH 300 U/ml with distinct Coombs-positive hemolysis. Though no peripheral, intrathoracic or abdominal lymph node enlargements were seen, the skin showed multiple vitiligo-like lesions with lymphocyte infiltration. The bone marrow also revealed histologically lymphocyte infiltrates with pathological features. The expanded circulating lymphocytes showed resemblance with large granular lymphocytes (LGL) with TCR $\gamma\delta$  surface expression (Metzger *et al*, 1992; Hinz *et al*, 1996). The patient was treated with Interferon- $\alpha$ 2c (IFN $\alpha$ 2c) over the period of 6 years with daily administration. During these 6 years, the patient had been followed up at 5 different intermittent time points, where she represented an increase in Hb level (from 6.9 to 12 g/dl) and a steady decrease in the leukocyte count (from 22,300/ $\mu$ l to

7,200/ $\mu$ l). The hematological parameters and PBMC phenotyping were identical before and after the first visit upon IFN $\alpha$ 2c treatment initiation (Table 3, materials and methods chapter; Metzger *et al*, 1992). This patient thus responded to IFN $\alpha$ 2c therapy with remission in disease progression.

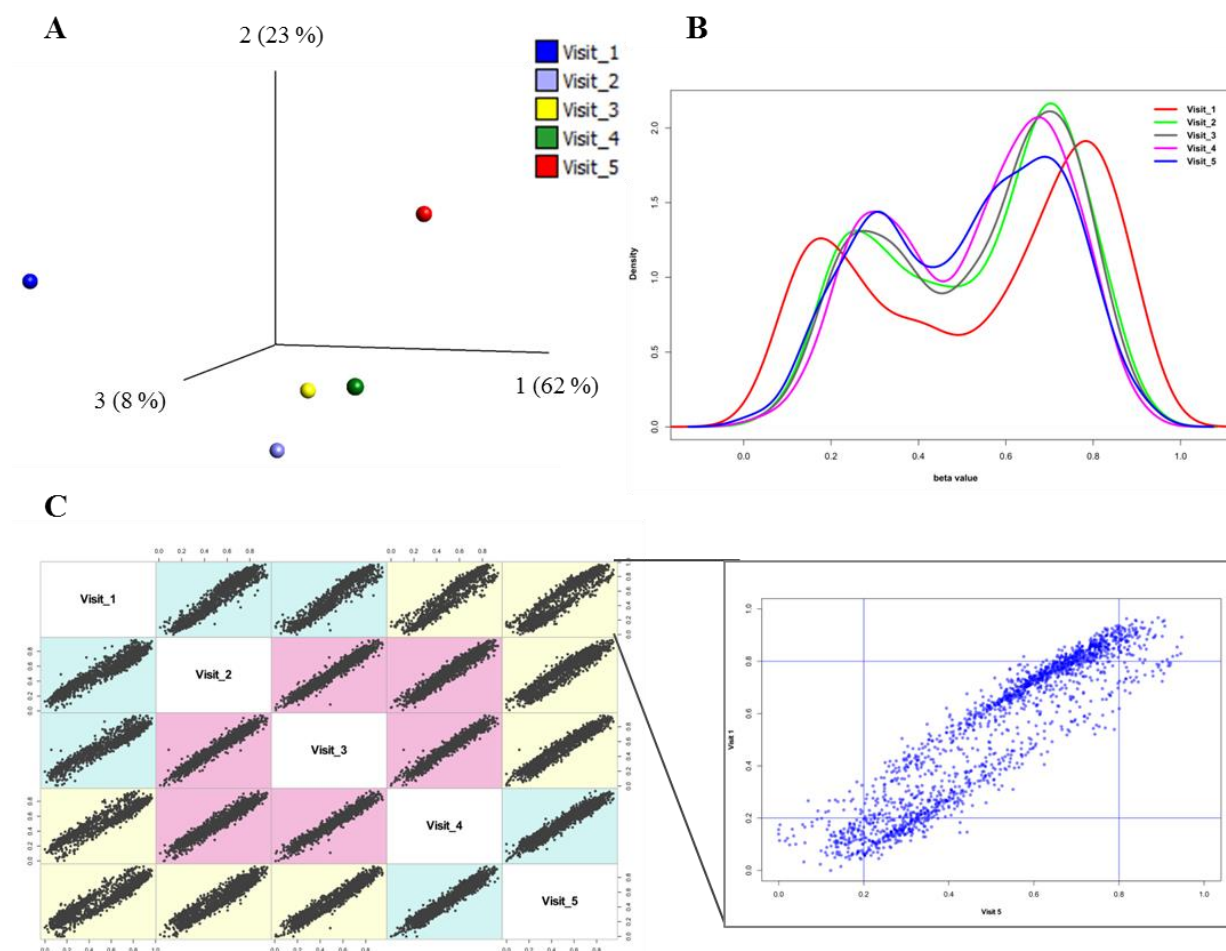


**Figure 5.6.1: Principal component analysis (PCA) of a  $\gamma\delta$ -HSTCL patient undergoing IFN $\alpha$ 2c therapy.** (A) The 3D plot shows PCA on samples collected during each visit of the patient. (B) PCA on all CpG sites according to visits of the patients in a time-course manner. The variables are ordered and colored by correlation. The magnified view of PCA between visit 1 and visit 5 is shown by scatter plot.

### 5.6.2 Time-dependent changes in DNA methylation

In a retrospective study with frozen PBMC from this  $\gamma\delta$ -HSTCL patient, I sought to investigate the DNA methylation pattern in a time course-dependent manner as a response to the IFN $\alpha$ 2c treatment. Thus, DNA methylation analysis using 450k arrays were performed on PBL drawn from the  $\gamma\delta$ -HSTCL patient during five subsequent visits after IFN $\alpha$ 2c therapy. The 3D plot for principal component analysis (PCA) clearly showed the separation of overall DNA methylation of the  $\gamma\delta$ -HSTCL patient PBL according to visits (1 to 5) during IFN $\alpha$ 2c therapy. Primary component (PC1) showed a variance of 62%, in addition to 23% and 8% (Fig. 5.6.1A). We performed PCA analysis on all significant CpG sites during all five visits of this  $\gamma\delta$ -HSTCL patient. Consistent with the PCA on samples, PCA on all CpG sites showed a distinct distribution of CpG sites for visit 1 and visit 5. Using density plot, a typical bimodal distribution of beta-values from CpG loci was observed, reflecting hypo- and hyper- methylated CpG sites (Fig. 5.6.1B-C). Therefore, the primary analysis showed that IFN $\alpha$ 2c treatment results in striking changes in the genome-wide methylation of  $\gamma\delta$ -HSTCL patient PBL over time.

### 5.6.3 Interferon- $\alpha$ therapy induces differential methylation over time

After finding out changes in the global methylation level in a time-dependent manner during IFN $\alpha$ 2c treatment, we performed an in depth analysis of DNA methylation. Our preliminary analysis clearly showed a significant reduction in the overall methylation level between visit 1 to 5 using Wilcox test (adj. p-value = 0.000006) for total 1797 CpG sites (Fig. 5.6.2A). Out of these 1797, 21 CpG sites were hypomethylated on visit 5, 26 were hypermethylated on visit 5 and the rest were considered as partially methylated on visit 5 (Fig. 5.6.2B). For the differential methylation between visit 5 and 1, delta beta values ranged between  $-0.2418$  to  $+0.2963$ , with a median of  $-0.06954$ . Hence, based on these delta beta values, the heatmap showed differential methylation (Fig. 5.6.2C). As it was observed that the patient achieved remission on visit 5 during therapy and also the absolute white blood cell count were substantially decreased, we compared the CpG methylation of visit 1 and visit 5 of  $\gamma\delta$ -HSTCL patient PBL, and of healthy  $\gamma\delta$  T cells. Surprisingly, a remarkable difference was observed between visit 5 of  $\gamma\delta$ -HSTCL patient PBL and healthy  $\gamma\delta$  T cells, when compared with visit 1 of  $\gamma\delta$ -HSTCL patient PBL. Altogether, though the Interferon- $\alpha$  therapy significantly changed the whole-methylome, the patient PBL mainly carried an aberrant DNA methylation pattern different from healthy  $\gamma\delta$  T cells.

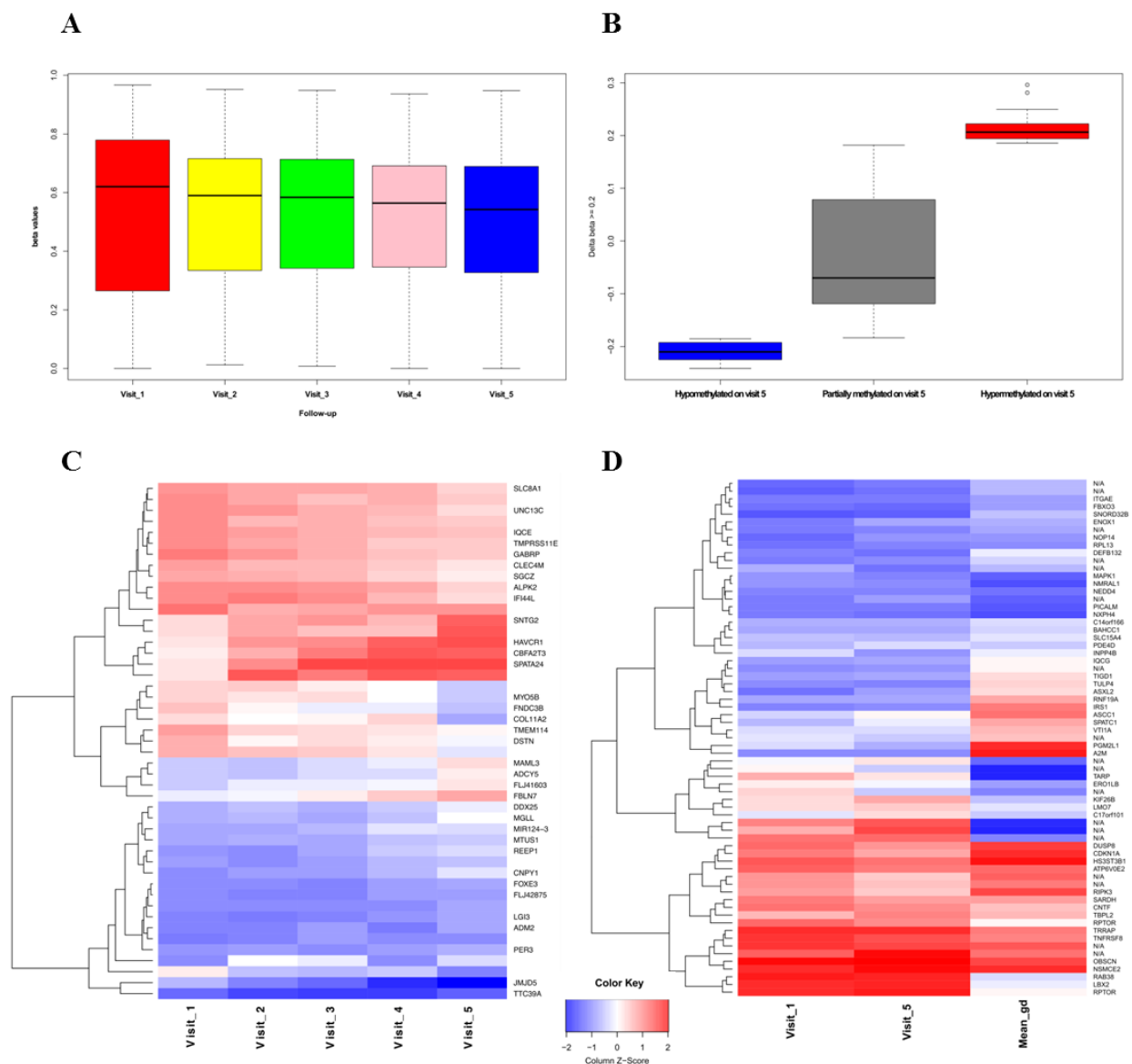


**Figure 5.6.2: Differential methylation profile of  $\gamma\delta$ -HSTCL patient PBL undergoing Interferon- $\alpha$  therapy.** (A) Overall changes in the methylation level are represented during each follow-up, referred to as visit (1-5). (B) All significant 1797 CpG sites with 0.25 variance criteria were shown to define differential methylation based on delta beta values ( $|\Delta\beta|$ ) and designated as ‘hypomethylated on visit 5’, ‘partially methylated on visit 5’ and ‘hypermethylated on visit 5’. (C) The heatmap showed differential methylation with delta beta values ( $|\Delta\beta| \geq 0.2$ ). (D) Comparative analysis of CpG sites involved in visit 1, visit 5 and of healthy  $\gamma\delta$  T cells from mean of four individuals (labelled as ‘Mean\_gd’).

#### 5.6.4 Genomic- and CpG Island (CGI)- features support changes in malignant $\gamma\delta$ T cell DNA methylome due to Interferon- $\alpha$ therapy

Next, using the Illumina HumanMethylation450 annotation available from UCSC Genome Browser database (hg19), we analyzed genomic- and CGI- features of each CpG site (Kent *et al*, 2002). With the possibility of one CpG site regulating multiple genomic features, each genomic feature was split and assigned to each CpG site unique for corresponding genomic features. First as expected, we found that more than 800 CpG sites were placed on the gene body constituting exons and introns and TSS1500 (region 1500 bp upstream of TSS) representing promoter region (Fig. 5.6.3A). But the median differential methylations of TSS1500 and 5'UTR were not much affected (Fig. 5.6.3B). When the methylation level represented by beta-values was analyzed in detail during each visit of the patient, substantial changes were observed on all these genomic regions (Fig. 5.6.3C). However, the statistically significant increase in methylation was observed on visit 5 compared to visit 1 of  $\gamma\delta$ -HSTCL patient PBL only in the respective TSS200 (adj. p-value = 0.0225; region 200 bp upstream of TSS), genomic body (adj. p-value = 5.92e-06; probably due to the maximum number of CpG sites involved) and 3'UTR (adj. p-value = 2.2467e-02) regions. Of note, when differential methylation between visit 1 and 5 was considered, there was not a single CpG site found in the 3'UTR region and no difference in the methylation at the genomic body (data not shown). Thus, TSS200, core promoter region plays an important role in the regulation of the methylation level as an effect of Interferon- $\alpha$  treatment in the PBL of this  $\gamma\delta$ -HSTCL patient.

Furthermore, the modulation of CpG sites associated with CGI and non-CGI was addressed. The CpG sites, which were in the non-CGI region, were referred to as 'open sea' region. The analysis of these features revealed a significant number of CpG sites located in the open sea and in the island region (Fig. 5.6.3D). The differential regulation of methylation was observed in all the CGI features, except for the shore region (Fig. 5.6.3E). This observation was also supported by the statistical analysis for N shelf, island, S shelf and open sea regions in visit 5 as compared to visit 1 of  $\gamma\delta$ -HSTCL patient PBL with adj. p-value 0.03187, 0.0059, 0.0345 and 1.70e-10, respectively. Taken together, CGI-associated shelf and island, and non-CGI-associated CpG sites (open sea) are affected in the malignant  $\gamma\delta$  T-cell clones during Interferon- $\alpha$  therapy leading to clinical remission.

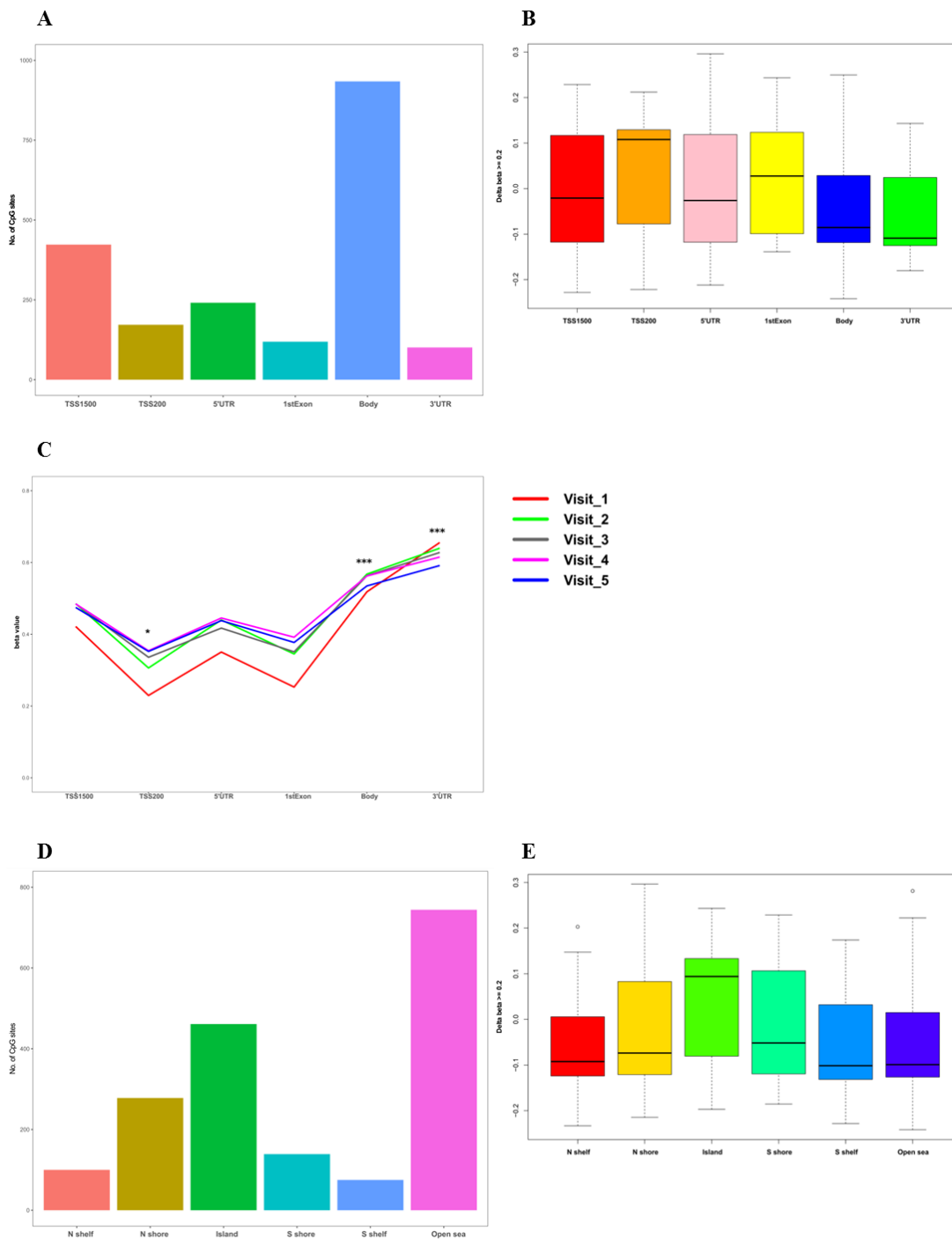


**Figure 5.6.3: Methylation analysis of genomic and CGI-features from a  $\gamma\delta$ -HSTCL patient during IFN $\alpha$ 2c treatment.** (Figure legend continued on the following page)

**Figure 5.6.3: Methylation analysis of genomic and CGI-features from a  $\gamma\delta$ -HSTCL patient during IFN $\alpha$ 2c treatment.** The number of CpG sites located in genomic regions and CGI/non-CGI regions are represented in (A) and (D), respectively. Differential methylation for genomic regions (B) and CGI/non-CGI regions (E) are represented based on the calculation of delta beta values ( $|\Delta\beta| = 0.2$ ) between visit 5 and visit 1 of the  $\gamma\delta$ -HSTCL patient PBL. (C) Changes in the methylation level ( $\beta$ -value) according to visits of the  $\gamma\delta$ -HSTCL patient and their corresponding genomic features are represented to understand involvement of various genomic regions in the regulation of DNA methylation. The statistical significance was calculated between visit 5 and visit 1 of the patient using Wilcox test with FDR and shown by p-value  $<0.05$ ,  $<0.01$  and  $<0.001$  with \*, \*\*, \*\*\*, respectively.

### 5.6.5 Biological association of differential methylation pattern upon IFN $\alpha$ 2c-treatment

After the analysis of DNA methylation pattern in this  $\gamma\delta$ -HSTCL patient, the biological significance of CpG sites regulating particular genes was studied. Out of 47 CpG sites, which were differentially methylated, only 37 CpG sites were annotated to one or multiple genes. Hence, we used 15 hypomethylated genes and 19 hypermethylated genes for gene ontology (GO) analysis of biological association. To this end, we used different functional annotation tools. None of the tools resulted in the statistical significant association of GO function. However, the analysis using the PANTHER database (v1.1) revealed positive fold enrichment for the biological process. Table 5.4 describes GO features and their GO terms regulating gene expression.

Hypomethylated genes on visit 5 of the  $\gamma\delta$ -HSTCL patient, such as DSTN, MYO5B and GABRP were annotated for molecular function like structural molecule activity (GO:0005198) and signal transducer activity (GO:0004871), biological process like biogenesis or cellular component organization (GO:0071840). MYO5B gene (unconventional myosin-VB is G-protein modulator actin binding motor protein) was found to be associated with cell junction (GO:0030054) category of GO termed cellular component. From the set of hypermethylated genes, metabolic process (GO:0008152) and extracellular region (GO:0005576) were overrepresented. The genes responsible for these functional features include transcription factors like FOXE3, MAML3. TRANSFAC and JASPAR based transcription factor analysis using Enrichr database revealed significant association (adj. p-value = 0.03146) of FBLN7, REEP1, DDX25, MAML3, CBFA2T3, MGLL, PUS3, PER3, PRDM16 and CNPY1 genes with ARNT and MTF1 transcription factors. Importantly, all these genes were hypermethylated on visit 5 of PBL from  $\gamma\delta$ -HSTCL patient during the IFN $\alpha$ 2c therapy.

Using the example of the  $\gamma\delta$ -HSTCL patient treated with interferon- $\alpha$ , I herein presented therapy induced changes in DNA methylation amongst several other epigenetic mechanisms. This differential regulation of DNA methylation certainly modulates transcriptional activity of related genes. This modulation of gene expression through epigenetic processes is highly cell-type specific and depends on healthy versus disease state of an individual.

**Table 5.4: Gene ontology analysis of differentially methylated genes ( $|\Delta\beta| = 0.2$ ) using PANTHER database.**

GO feature(s) different for hypo- and hyper-methylated genes are marked in red.

	<i>Hypomethylated genes</i>		<i>Hypermethylated genes</i>	
<b>Gene Ontology</b>	<b>Category</b>	<b>No. of genes (%)</b>	<b>Category</b>	<b>No. of genes (%)</b>
<b>Molecular Function</b>	binding (GO:0005488)	20.00%	binding (GO:0005488)	50.00%
	receptor activity (GO:0004872)	20.00%	catalytic activity (GO:0003824)	28.60%
	<b>structural molecule activity (GO:0005198)</b>	<b>20.00%</b>	receptor activity (GO:0004872)	14.30%
	catalytic activity (GO:0003824)	20.00%	transporter activity (GO:0005215)	7.10%
	<b>signal transducer activity (GO:0004871)</b>	<b>10.00%</b>	-	-
	transporter activity (GO:0005215)	10.00%	-	-
<b>Biological Process</b>	cellular process (GO:0009987)	26.10%	<b>metabolic process (GO:0008152)</b>	<b>32.10%</b>
	developmental process (GO:0032502)	13.00%	cellular process (GO:0009987)	28.60%
	<b>cellular component organization or biogenesis (GO:0071840)</b>	<b>13.00%</b>	biological regulation (GO:0065007)	10.70%



	multicellular organismal process (GO:0032501)	13.00%	response to stimulus (GO:0050896)	7.10%
	localization (GO:0051179)	8.70%	developmental process (GO:0032502)	7.10%
	response to stimulus (GO:0050896)	8.70%	biological adhesion (GO:0022610)	3.60%
	immune system process (GO:0002376)	8.70%	multicellular organismal process (GO:0032501)	3.60%
	biological adhesion (GO:0022610)	4.30%	localization (GO:0051179)	3.60%
	biological regulation (GO:0065007)	4.30%	immune system process (GO:0002376)	3.60%
<b>Cellular Component</b>	membrane (GO:0016020)	33.30%	cell part (GO:0044464)	38.50%
	cell part (GO:0044464)	22.20%	organelle (GO:0043226)	30.80%
	organelle (GO:0043226)	22.20%	macromolecular complex (GO:0032991)	15.40%
	macromolecular complex (GO:0032991)	11.10%	membrane (GO:0016020)	7.70%
	cell junction (GO:0030054)	11.10%	extracellular region (GO:0005576)	7.70%

**6. Discussion and conclusion****6.1 Release of NKG2D ligands from tumor cells: *Exosomes versus shedding***

Due to their broad anti-tumor activity, human  $\gamma\delta$  T cells have become one of the potential candidates for cell-based cancer immunotherapy. Activating NK receptors expressed on  $\gamma\delta$  T cells play a crucial role in the recognition of tumor cells via NKG2D ligands like MICA and ULBPs (Cosman *et al*, 2001; Girlanda *et al*, 2005). However, soluble MICA has been detected in serum of multiple myeloma patients undergoing phase I clinical trial with zoledronate-activated V $\gamma$ 9V $\delta$ 2 T cells (Abe *et al*, 2009). Clinical studies from multiple myeloma and other cancer patients have revealed a negative correlation between NKG2D expression and soluble MICA, becoming a poor prognostic factor (Rebmann *et al*, 2007; Kumar *et al*, 2012; Li *et al*, 2013; Chen *et al*, 2016).

NKG2D ligand shedding is mediated by matrix metalloproteinases (MMP) and “a disintegrin and metalloproteinase” (ADAM) proteases (Salih *et al*, 2002; Waldhauer *et al*, 2008). ADAM10 and ADAM17 play an important role in the shedding of ectodomains. Typically, ADAMs cleave cell surface proteins within a membrane proximal stalk region. Substrate specificity hardly relies on the recognition of certain consensus sites, but is rather guided by secondary structure elements regulating the accessibility of the stalk region (Mochizuki and Okada, 2007). The regulation of ADAM activity is not yet understood in detail, although trafficking, glycosylation, phosphorylation (upon treatment with PMA that stimulates ADAM activity) and interactions with accessory molecules might play important roles (Seals and Courtneidge, 2003). PMA stimulation can enhance shedding activity by ADAM17. But PMA-mediated activity is largely controlled by specificity and kinetics of ADMA17 or other related subsets of sheddases (Huovila *et al*, 2005). Our results failed to detect significant changes in modulation of MICA release by PMA stimulation.

Both MICA and MICB are highly polymorphic, with 84 allelic variants of MICA and 35 allelic variants of MICB described so far (<http://www.ebi.ac.uk/imgt/hla/>) (Robinson *et al*, 2011). The differences in the primary structure mainly apply to single amino acid substitutions within the extracellular part that in principle might already affect the secondary structure and thus the recognition by ADAM proteases. However, several allelic variants of MICA including MICA\*008, MICA\*023, MICA\*028 and MICA\*054 are associated with a certain micro-satellite

polymorphism (A5.1) within exon 5. Five GCT repeats encode alanines within the transmembrane domain and an additional guanine causes a frameshift that result in an altered transmembrane (TM) domain and a substantially truncated intracellular part. This applies to the most frequent allelic variant in caucasians, MICA\*008 (Ashiru *et al*, 2010; Huovila *et al*, 2005). Interestingly, in HeLa cells and transfected CHO cells, full-length MICA\*008 was described to be enriched in detergent-resistant membrane microdomains and constitutively released in exosomes (Ashiru *et al*, 2010). This is in line with our observation that the truncated MICA variant expressed in PC-3 cells is released as full-length molecule in association with exosomes and is not proteolytically processed.

In support of previous reports and the biochemical system established by us, MICA protein clearly showed differences in size in different tumor cells (PancTu-I and PC-3) that reflect MICA allelic variation. In addition, this distinction can be seen after deglycosylation of immunoprecipitated MICA using clone-specific anti-human MICA antibody used to detect truncated form. MIC proteins are highly glycosylated (Huovila *et al*, 2005) and the effect of glycosylation on the overall structure might also influence the accessibility of the cleavage site. MIC proteins are also palmitoylated at cysteine residues in the membrane proximal cytoplasmic part and this palmitoylation is prerequisite for both the localization to detergent-resistant membrane microdomains and the subsequent shedding (Gooz 2010). These cysteines are missing in MICA\*008-like molecules and this might facilitate exosomal release. It has been described that not only the lipid composition of the plasma membrane but also posttranslational modifications such as glycosylation and palmitoylation may be altered in a given tumor cell (Aguera-Gonzalez *et al*, 2011; Dall'olio *et al*, 2012; Mashima *et al*, 2009).

Soluble NKG2D ligands are discussed as key component involved in tumor immune evasion, resulting in the modulation of the functional activity of NK cells and T-cell subsets (Marten *et al*, 2006; Waldhauer *et al*, 2006; Ashiru *et al*, 2010). In future, it would be interesting to investigate the possible role of epigenetic mechanisms regulating NKG2D ligand shedding from tumor cells and associated effector cell functions. Along this line, use of inhibitors for epigenetic 'writers', 'readers' and 'erasers', which are already in clinic or in experimental systems, will be studied in detail.

## 6.2 Epigenetic modulation of NKG2D receptor and ligands: *Mechanism of NKG2D ligand release and functional effects*

Ligands for NKG2D (NKG2DL) are known to be expressed on a number of tumor types, including carcinomas, leukemia and lymphoma, multiple myeloma and gliomas (Spear *et al*, 2013). NKG2D ligand expression can be modulated by the use of proteasome inhibitors (Butler *et al*, 2009), inhibitors for HSP90 chaperone proteins (Fionda *et al*, 2009), HDAC inhibitors (Armeanu *et al*, 2005), GSK3 inhibitors (Fionda *et al*, 2013), the DNA damage response pathway (Lam *et al*, 2014), the ERK signaling pathway (Wu *et al*, 2012) and miRNA (Cado *et al*, 2014). In addition to the regulation of NKG2D ligand expression by these cellular, molecular and epigenetic pathways, heterogeneity in the mechanism of shedding within NKG2D ligand family members are found based on the type of membrane-association that can rely on Glycosylphosphatidylinositol (GPI)-anchors and/or transmembrane domains (Fernandez-Messina *et al*, 2010; Chitadze *et al*, 2013). As an example, MICA\*008 is GPI-anchored and acquires truncated MICA allelic feature, which is released through exosomes (Ashiru *et al*, 2013; Chitadze *et al*, 2013). Similarly, ULBP-2 can be expressed with or without a GPI-anchor (Fernandez-Messina *et al*, 2011).

As discussed in the last section, others and we have related allelic polymorphisms of MICA to the differential mechanism of NKG2DL release. Using epigenetic inhibitors, its effect on possible NKG2D ligand shedding was further investigated. When we targeted proteins involved in histone and DNA modifications, we found that only inhibition of HDACs from the family of epigenetic ‘erasers’ modulated NKG2D ligand expression and release. The heterogeneity in the release of NKG2D ligands based on tumor of origin was also observed after treatment with the HDAC inhibitor, VPA. Genotype analysis of MICA showed that PC-3 is heterozygous for MICA\*008:01:01 (A5.1) and MICA\*012:01 (A4) allelic polymorphism. Interestingly, PC-3 was found to release MICA directly in culture supernatant after VPA treatment at 5 mM, 2.5 mM and very slightly at 1 mM. This substantial change in the mechanism of MICA release might be due to the heterozygous nature of PC-3. However, previous reports (Huang *et al*, 2011; Armeanu *et al*, 2005) have not described such change in the release of MICA after treatment with VPA and its association with heterozygous MICA expression. Chitadze *et al* (2013) showed that shedding of MICA/B from PancTu-I is mediated by metalloproteases (MP). But, at this point it is not clear

whether VPA-induced NKG2D ligand release is due to ADAM-10/17- or MP-mediated proteolysis. In addition to heterozygosity of MICA and possible mechanism of proteolytic cleavage, the origin of tumor cells might also play an important role in the response to VPA. For instance, in human ovarian and cervical cancer cell lines, Trichostatin A (TSA) and sodium butyrate showed a similar effect on MICA/B induction, while VPA was the least effective (Huang *et al*, 2011). But as in human hepatoma cells (Armeanu *et al*, 2005), the effect of VPA was consistent in pancreatic and prostate cancer cells from our study.

VPA has been used to study *in vitro* functional responses at concentrations ranging from 0.5 to 10 mM (Greenblatt *et al*, 2008; Yagi *et al*, 2010; Grabarska *et al*, 2014). To study the modulation of MICA expression and release from tumor cells, Armeanu *et al* (2005) used 1 mM VPA for human hepatoma cells. Their results showed a differential induction of NKG2D ligands by VPA on malignant and non-malignant cells. In contrast, our study revealed only minor changes in the shedding of MICA by PancTu-I cells and no changes at all by PC-3 cells after treatment with 1 mM VPA. In fact, NKG2D ligand (MICA/B and ULBP-2) gene expression was remarkably induced with 2.5 mM VPA both on malignant (PancTu-I and PC-3) and non-malignant cells (PBMC and  $\gamma\delta$  T cells). The use of 2.5 mM VPA concentration to induce MICA protein is in line with a previous study performed with Hodgkin lymphoma cells (Zocchi *et al*, 2012).

DNA damage by genotoxic agents like VPA or irradiation is known to induce NKG2D ligands, specifically MICA/B and ULBPs through ATM/ATR-mediated signaling pathways. However, ULBP-1 expression is known to be associated with proteasome regulation (Butler *et al*, 2009). Notably, VPA also failed to induce ULBP-1 expression on PancTu-I and PC-3 cells. In the scope of this study, we didn't address induction of ULBP-3 and ULBP-4, which is of future interest. Nevertheless, treatment of melanoma cells with 1 mM VPA has been shown to induce only MICA, MICB and ULBP-2 mediated by the ERK pathway (Wu *et al*, 2012), which is also consistent with our results with PancTu-I and PC-3 cells. Of note, mRNA quantitation showed NKG2D ligand induction in  $\gamma\delta$  T cells and PBMC upon treatment with VPA. Thus, it would be interesting to further study the involvement of cytotoxicity-associated molecules like perforin, granzyme in PBMC and  $\gamma\delta$  T cells, and important components of signaling pathways like ERK1/2 and AKT in PancTu-I and PC-3 upon VPA treatment.

Another important facet of our study is the downregulation of NKG2D receptors at the level of both proteins and genes. It has been noted that NKG2D ligand shedding down modulates NKG2D receptor expression on effector cells, such as NK cells (Groh *et al*, 2002), while in contrast Deng and coworkers (2015) showed increased NKG2D receptor expression. At the protein level, coculture experiments showed downregulation of NKG2D receptor on  $\gamma\delta$  T cells, but the expression was maintained on lymphocyte-gated freshly isolated PBMC. Downregulation of the full-length form of the NKG2D receptor and ligands was corroborated well at the level of gene expression. Karimi *et al* (2014) have shown that the truncated NKG2D receptor plays an important role to downregulate the expression of the NKG2D receptor, which is also a feature of NKG2D ligand-mediated shedding. Of note, this functional similarity is further strongly supported by the cluster analysis, which grouped the truncated form of the NKG2D receptor and all NKG2D ligands together. This observation provides a hint that the truncated NKG2D form may be involved in the modulation of VPA-induced NKG2D receptor expression in coculture with PBMC and  $\gamma\delta$  T cells.

The use of epigenetic modulators like VPA is of importance for tumor immunology, not only because of their clinical significance, but also for their potential to induce global histone modification. Epigenetic methods like ChIP assays for H3K9ac, methylation-specific PCR are already used to study epigenetic mechanism responsible for NKG2D gene regulation in CD8 T cells and NK cells (Fernandez-Sanchez *et al*, 2013). Methods such as single cell epigenetic analysis will allow for combined analysis of histone modification and other relevant proteins in a given single cell, irrespective of its malignant and non-malignant origin. In this study, flow cytometry-based H3K9ac analysis in  $\gamma\delta$  T cells has been established. Thus, here we report for the first time the technical feasibility to investigate H3K9ac in a single  $\gamma\delta$  T cell using techniques like multicolor flow cytometry and ImageStream cytometry. This open possibility to investigate the modulation of NKG2D receptor expression and other intracellular cytokines, transcription factors in relation to epigenetic processes in a single cell from *in vitro* cocultures and/or from blood and other clinical material of patients.

Results of this section underscore the differential regulation of NKG2D receptor expression on  $\gamma\delta$  T cells as an effect of NKG2D ligand release additionally modulated by the HDAC inhibitor, valproic acid (VPA). Therefore, in the next section, I will address the impact of VPA on the

modulation of NKG2D receptor expression and other important surface markers expressed on  $\gamma\delta$  T cells in comparison to  $\alpha\beta$  T cells, which are essential for immune cell functions such as antigen-presentation.

### 6.3 Functional implications of epigenetic modulators on healthy human $\gamma\delta$ T-cells: *Modulation of human $\gamma\delta$ T-cell activation and phenotype by histone deacetylase inhibitors*

Our results and previous reports have repeatedly shown that human  $\gamma\delta$  T cells are affected by the tumor microenvironment (Di Carlo *et al*, 2013). Numerous approaches have suggested to enhance the cytotoxic potential of human  $\gamma\delta$  T cells (Kabelitz, 2016). However, the use of selective epigenetic modulators surprisingly enhances shedding of NKG2D ligands from tumor cells. At the same time, the epigenetic machinery of not only tumor cells, but also of human  $\gamma\delta$  T-cells is potentially affected. Thus, it is important to understand the functional implications of epigenetic modulators (here VPA, a clinically used HDAC inhibitor) on healthy human  $\gamma\delta$  T-cells mediated by key surface receptor proteins.

As stated above, several recent reports suggest a substantial potential for  $\gamma\delta$  T cells in cancer immunotherapy. So far, such strategies have been based on the adoptive transfer of  $\gamma\delta$  T cells and/or the *in vivo* activation of  $\gamma\delta$  T cells with zoledronate plus IL-2 (Kabelitz *et al*, 2007; Fisher *et al*, 2014). Zoledronate, like other nitrogen-containing bisphosphonates, has anti-resorptive activity and is a licensed drug for the treatment of osteoporosis and other bone fragility disorders. Upon treatment with bisphosphonates, tumor cells are recognized by V $\gamma$ 9V $\delta$ 2 T cells resulting in tumor cell lysis (Das *et al*, 2001). It has been previously shown that different tumor cells are susceptible to lysis by  $\gamma\delta$  T-cells, variably mediated by TCR-dependent and/or by NKG2D receptor-dependent recognition (Wrobel *et al*, 2007). Another report studied the effects of VPA on hepatocellular carcinoma cells and their killing by NK cells (Armeanu *et al*, 2005). These authors found that sensitization by VPA induced NKG2D ligand expression, which triggered the corresponding receptors on NK cells for antitumor activity. In the present study, we observed reduced CD25, CD95 and particularly NKG2D receptor expression on  $\gamma\delta$  T cells surviving the exposure to 5 mM VPA, in contrast to similarly treated  $\alpha\beta$  T cells. The strongly reduced NKG2D expression on VPA-treated  $\gamma\delta$  T cells suggests that their recognition of tumor cells might be severely compromised, a notion which requires further experimental investigation.

Several HDAC inhibitors have been used to study apoptosis or other forms of cell death in various leukemic T-cell lines. In line with our results, all epigenetic modulators induce different levels of cell death in different cell types (Morales *et al*, 2010). While we observed significant toxic effects of VPA on freshly isolated PBMC, more cell death was induced in activated T cells.



In fact, a mouse study has shown differential effects of various VPA concentrations on distinct T-cell subsets (Lv *et al*, 2012). Furthermore, HDACi were found to modulate murine T-cell polarization both *in vitro* and *in vivo* (Glauben *et al*, 2014). Our immunophenotyping also showed preferential modulatory effects of VPA on V $\delta$ 2 T cells in a dose-dependent manner, while  $\alpha\beta$  T cells were less affected. This prompted us to look in more detail at other V $\delta$ 2 cell functional features, since  $\gamma\delta$  T cells can function as regulatory cells, antigen presenting cells and memory cells (Kabelitz and He 2012; Brandes *et al*, 2009; Himoudi *et al*, 2012; Peters *et al*, 2014). In all experiments, treatment with higher concentrations (i.e. 5 mM) VPA caused nearly 40-50 % cell death. In order to study the modulation of cell surface markers, we excluded dead cells and analyzed only the PI-negative populations. Unlike  $\alpha\beta$  T cells, V $\delta$ 2 T cells underwent differential modulation of cell surface markers associated with antigen-presenting cells following VPA treatment. It is presently unclear why the expression of certain surface molecules is differentially affected by VPA in  $\alpha\beta$  versus  $\gamma\delta$  T cells. In general, epigenetic modulators affect a wide range of molecules and consequently functional responses. The interplay between acetylation and deacetylation spans from minutes to hours and may differ between  $\alpha\beta$  and  $\gamma\delta$  T cells. In any case, further experiments are required to investigate the functional consequences of the phenotypic alterations observed in the present study.

VPM, a carboxamide derivative of VPA, is also used for the treatment of epilepsy (Isoherranen *et al*, 2003). Even though the clinical usage is the same, VPM lacks histone deacetylase activity (Harikrishnan *et al*, 2008) and works through other yet unknown molecular mechanisms. Our results on the effect of VPA versus VPM on histone acetylation in  $\gamma\delta$  T cells are consistent with the literature. VPA is known to inhibit HDAC1 and at the same time induces acetylation of histone (H3, H4) proteins, which was also clearly revealed in our experiment with  $\gamma\delta$  T cells by comparing VPA and VPM. So far, we have only looked at the H3 acetylation process. Future analysis will address particular transcription factor(s) and/or gene(s) in detail. The cellular response to VPA mainly leads to two totally different effects. At non-toxic concentrations, cells undergo acetylation, while effects at the level of cell death together with induction of acetylation are only induced with higher concentrations (Luchenko *et al*, 2014). A potential scenario for the dose-dependent modulation of  $\gamma\delta$  T-cell activation by VPA is displayed in Fig. 6.1.

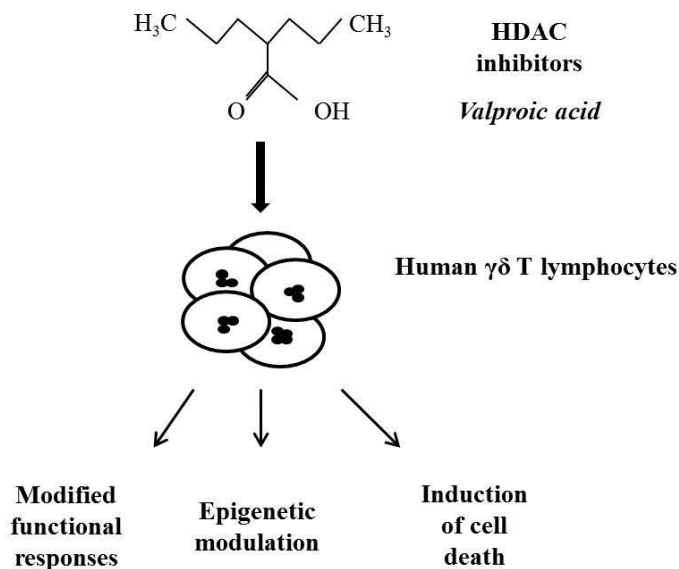


**Figure 6.1:** A scenario of possible effects of histone deacetylase inhibitors on human  $\gamma\delta$  T-cells. HDAC inhibitors are known to upregulate expression of NKG2D ligands on tumor cells sensitizing them for NK cells and  $\gamma\delta$  T-cell mediated killing. However, treatment with valproic acid at the same concentration results in certain extent of cell death while simultaneously modulating the functional activity and histone acetylation in surviving cells.

Cell death-inducing concentrations make HDAC inhibitors such as VPA potent candidates to consider for therapeutic strategies. High concentrations will kill certain tumor cells, but will also delete certain peripheral blood cells, for instance  $\gamma\delta$  T cells. On the other hand, VPA modulates histone acetylation and thereby the functional program in surviving cells. Therefore, our future investigation will focus on VPA-induced functional epigenetic consequences in  $\gamma\delta$  T cells. Currently many diseases including especially cancer are considered for epigenetic therapy (Yoo and Jones, 2006). In recent studies, VPA together with other chemotherapeutic agents was shown to be safe, tolerable and efficacious in a prostate cancer clinical trial (Goyal and Rodriguez, 2013). On the other hand, however, a study in a murine leukemia model revealed unwanted effects of VPA as an accelerator of tumorigenesis (Santoro *et al*, 2013). HDACi thus play a dual role in oncogenesis and also oncosuppression.

In conclusion, previous reports and our present study clearly imply that epigenetic drugs like histone deacetylase inhibitors emerge as a suitable regimen for future treatment strategies. However, divergent roles of epigenetic modulators must be considered according to disease and

cell type, dose-dependency and applicability for combination- and/or mono- therapy. Considering this possibility, I particularly focused on the impact of epigenetic drugs on the generation of intracellular cytokines and transcription factors in  $\gamma\delta$  T cells in the following section. This will provide detail insights altogether into clinical efficacy, underlying regulation of the signaling networks and compelling players involved *in vitro*  $\gamma\delta$  T-cell differentiation.

#### 6.4 Functional implications of epigenetic modulators on healthy human $\gamma\delta$ T-cells: *Generation of intracellular cytokine variants and association with cell death*

VPA is widely used as a mood stabilizer and anti-epileptic drug. Apart from its recently identified inhibitory activity on histone deacetylase, it has been shown to directly target Gamma Amino Butyrate (GABA) transaminobutyrate and ion channels (Chateauvieux *et al*, 2010). VPA is also tested in various clinical trials for cancer therapy (NCT01182285 and NCT00302159; <http://clinicaltrials.gov>; West *et al*, 2014). The clinical dosage varies substantially in different cancer types and with the treatment protocol, depending on whether it is used as monotherapy or in combination therapy (Atmaca *et al*, 2007; Sharma *et al*, 2008; Munster *et al*, 2009; Su *et al*, 2011; Avallone *et al*, 2014). Under *in vitro* conditions, VPA has been shown to modulate diverse functional responses at concentrations ranging from 0.5 mM to 10 mM (Greenblatt *et al*, 2008; Yagi *et al*, 2010; Grabarska *et al*, 2010).

In the previous section, I showed that HDAC inhibition by VPA modulates the expression of certain cell surface proteins (results from previous sections; Bhat *et al*, 2015). Apart from VPA, EGCG (HAT and DNMT inhibitor), TSA (HDAC inhibitor) and decitabine (DNMT inhibitor) have been reported to modulate expression of intracellular cytokines and transcription factors (Lal *et al*, 2009; Valapour *et al*, 2002). Valapour *et al*, (2002) reported that IL-4 production by activated peripheral blood T-cells is enhanced by TSA. Hence, we analyzed intracellular expression of IL-4 in human  $\gamma\delta$  T-cells upon treatment with inhibitors for HDAC and DNMT by flow cytometry following appropriate exclusion of dead cells. The IL-4 protein can be expressed in different isoforms. In our experiments, we used different antibodies to monitor IL-4 expression, specifically the 8D4-8 clone, which detects the unglycosylated, non-secreted form of IL-4 (IL-4 $\delta_{13}$ , 13 bp deleted form) and the MP4-25D2 clone which detects the mature form of IL-4 (Stein *et al*, 2000; Hebel *et al*, 2014; Ledru *et al*, 2003). Treatment with VPA and TSA enhanced the expression of IL-4 $\delta_{13}$ . “Toxic” concentrations of VPA (5 mM) significantly induced expression of IL-4 $\delta_{13}$  and decreased the expression of mature IL-4, but did not modulate IFN- $\gamma$  cytokine. The increase in IL-4 $\delta_{13}$  was associated with an increase in intracellular IL-4R. On the contrary, the mature form of IL-4 mRNA expression was down regulated. It is already known that IL-4 $\delta_2$  (an alternative splice variant with a 47 bp deletion) acts like a naturally occurring human IL-4 antagonist (Vasiliev *et al*, 2003). We failed to reveal a significant

interaction of IL-4 $\delta_{13}$  with the  $\alpha$  chain of IL-4R, which is in contrast to IL-4 $\delta_2$  signaling pathway (Vasiliev *et al*, 2003). We also attempted to characterize the subcellular localization of IL-4 $\delta_{13}$ , but we observed only partial co-localization with CD107a and CD63. It seems that IL-4 $\delta_{13}$  is neither secreted in exosomes nor undergoes lysosomal degradation and is packaged in specialized vesicles.

Different signaling pathways are involved in the regulation of cell death. Such regulated cell death may trigger inflammation and induces signaling cascades (Linkermann *et al*, 2014). The role of distinct signaling pathways can be addressed through specific inhibitors. Previous reports already showed that the expression of IL-4 $\delta_{13}$  is associated with programmed cell death, notably apoptosis (Stein *et al*, 2000; Ledru *et al*, 2003). In recent years, however, it has been realized that caspase-independent non-apoptotic cell death pathways (programmed necrosis) are equally important in the regulation of cell death and survival (Linkermann *et al*, 2014). VPA is also known to execute diverse cell death mechanisms, other than apoptosis in multiple myeloma and neuronal cells (Schwartz *et al*, 2007; Bollino *et al*, 2015). In our experiments, we used cell death inhibitors to explore a potential role of distinct cell death pathways using pan-caspase inhibitor zVAD (to block apoptosis) and additionally Nec1, NSA (to block programmed necrosis). Pre-treatment of  $\gamma\delta$  T cells with zVAD, Nec1 and NSA substantially modulated VPA-induced IL-4 $\delta_{13}$  expression. It should be noted that using various experimental read-out systems, these inhibitors when used alone or even in combination did not completely rescue VPA-treated cells from cell death. Similarly, exogenous IL-4 did not prevent VPA-induced cell death of  $\gamma\delta$  T cells. A possible explanation might be that VPA induces diverse cell death pathways, some of which might not be influenced by the inhibitors used here. Although not analyzed in detail, VPA might have induced a 'mixed' type of cell death in  $\gamma\delta$  T cells.

In the same experimental set up, we analyzed the induction of histone acetylation. In line with the modulation of IL-4 $\delta_{13}$  expression, treatment with zVAD, Nec1 and NSA modulated H3K9Ac leading to complete loss of histone acetylation marks induced by VPA. Furthermore, location of c-Jun transcription factor interaction site on IL-4 gene was associated with H3K27 marks. Our network analysis was validated at the protein level by expression of c-Jun transcription factor. Previous reports suggested that HDAC inhibitors block c-Jun transcription (Yamaguchi *et al*, 2005), while c-Jun phosphorylation is not required for T-cell proliferation or differentiation, but

for thymocyte apoptosis (Behrens *et al*, 2001). Our protein analysis by western blot revealed very similar results in terms of HDAC inhibitor treatment and c-Jun phosphorylation.

The characteristic features of apoptosis are histone degradation, chromatin condensation and DNA fragmentation. Absence of any histone mark has not been reported with blockade of apoptosis (Fullgrabe *et al*, 2010). Available reports showed that serine proteases like granzyme A could induce histone proteolysis and increase accessibility of cellular DNA to nucleases (Zhang *et al*, 2001). Also, it has been suggested that the apoptotic effects of HDACi are predominantly elicited through their impact on gene expression rather than on histone acetylation (Th'ng *et al*, 2001). However, IL-4 $\delta_{13}$  may act as a survival signal to cells undergoing differentiation. It would be interesting to further investigate such a potential Th2 bias effect associated with histone modification in  $\gamma\delta$  T cells from neonates and adult individuals. Moreover, in an autoimmune encephalitis mouse model, Lv and coworkers observed a role of non-toxic doses of VPA in maintaining immune homeostasis through induction of apoptosis in activated T-cells (Lv *et al*, 2012). But evidence for an induction of the non-secreted form of IL-4 in any disease, except HIV pathogenesis, is completely missing. Primate models are the most suitable experimental system for both HIV disease and human  $\gamma\delta$  T-cell research, because they share the V $\gamma$ 9V $\delta$ 2 TCR required for recognition of microbial pyrophosphates (Eberl *et al*, 2003; Gober *et al*, 2003). Interestingly, evolutionary studies in primates of genes involved in HIV pathogenesis have also identified IL-4 as one of the proteins undergoing diverse positive selection (Ortiz *et al*, 2009; Koyanagi *et al*, 2010). As a result of such evolutionary processes, IL-4 $\delta_{13}$  is expressed at the protein level, but the cellular and molecular significance have not been defined.

Our present study depicts the potential role of c-Jun transcription factor in correlation with IL-4 $\delta_{13}$  expression and histone acetylation (Fig. 6.2) and previous reports show that various isoforms of IL-4 share potential crosstalk regulating mature IL-4 expression. Future experiments will focus on analyzing functional genomic features of the 13 bp deletion in comparison to IL-4 $\delta_{47}$  and full length form of IL-4. In summary, the expression of novel IL-4 $\delta_{13}$  may emerge as a 'combined marker' for cell death, epigenetic modification and  $\gamma\delta$  T-cell differentiation. Regulation of IL4 gene appears as one of the important candidate to investigate cellular and molecular discrepancy between  $\gamma\delta$  and  $\alpha\beta$  T cells upon cellular activation. However, it must be

noted that differential regulation of intracellular cytokine and transcription factors in antigen activated T cells was observed only in the presence of epigenetic modifier (like VPA). Therefore, in the next section, I investigated differences between resting human  $\alpha\beta$  (CD4, CD8, Treg) and  $\gamma\delta$  T cells without TCR/antigen activation and in the absence of epigenetic inhibitors by multiple levels of endogenous epigenetic processes. This would provide a mechanistic view of the epigenetic basis for T-cell subset specification.

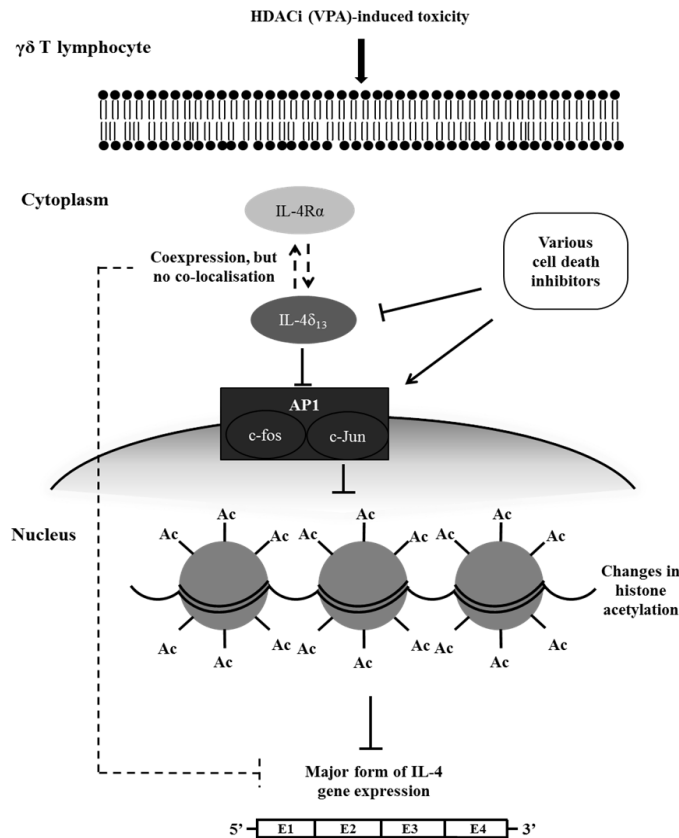


**Figure 6.2: Schematic diagram of proposed regulatory interplay between VPA-induced toxicity, induction of IL-4 $\delta_{13}$  and c-Jun, histone acetylation, and modulation by cell death inhibitors.** When human  $\gamma\delta$  T cells are treated with VPA at sublethal concentrations, non-secreted form of IL-4 (described as IL-4 $\delta_{13}$ ) and intracellular IL-4R $\alpha$  are induced, which however fail to directly interact. Cell death inhibitors modulate c-Jun transcription factor and IL-4 $\delta_{13}$  expression as well as active histone acetylation global mark. In parallel to induced protein expression of IL-4 $\delta_{13}$  and IL-4R $\alpha$ , this signaling cascade might down-regulate gene expression of the major form of IL-4.

### 6.5 Comprehensive epigenetic landscape of human $\gamma\delta$ T-cells: *Chromatin accessibility, DNA methylation and total RNA analysis*

In comparison to other immune cells,  $\gamma\delta$  T cells are distinct with respect to their developmental pathway, functional plasticity, tissue distribution and additionally their potential applicability for cell-mediated immunotherapy. The lineage commitment and functional response of T cells is governed by epigenetic modifications regulating gene expression. Thus, a precise knowledge of the diverse processes involved allows us, to study epigenetic regulation as a key to understand the cellular and molecular features of  $\gamma\delta$  T cells.  $\alpha\beta$  T cells, particularly CD4 T cells have been studied widely in this regard, but a systems immunology-approach to understand epigenetic regulation of  $\gamma\delta$  T cells is largely missing. A genome-wide epigenetic landscape for histone methylation and acetylation in mouse  $\gamma\delta$  T cells was presented by Schmolka *et al*, 2013. However, this epigenetic analysis in mice was focused on the comparison of IL-17 vs IFN- $\gamma$ -producing  $\gamma\delta$  T cells, which is relevant for  $\gamma\delta$  T cell development in mice. In this thesis, I described for the first time the epigenetic regulation of human  $\gamma\delta$  T cells compared to  $\alpha\beta$  T cells (CD4, Treg and CD8) at multiple levels.

As discussed before, DNA methylation plays an important role in the control of gene expression and expression of cellular proteins. Overall, the  $\gamma\delta$  T cell genome is less methylated compared to other T-cell subsets. We also observed remarkable promoter methylation and methylation of CpG loci across non-CpG islands (non-CGI), which are often referred to as CpG loci located in regulatory regions such as enhancers. This observation however is well supported by previous reports on CD4 T cells (Zilbauer *et al*, 2013). Moreover, Treg and  $\gamma\delta$  T cells have nearly the same level of overall methylation and promoter methylation. Along this line, we found a close association in Treg and  $\gamma\delta$  T cell miRNA counts as well. Since in-depth analysis of microRNA (miRNA) profiling is still ongoing, our preliminary analysis showed  $\gamma\delta$  T cell-specific miRNA signatures. When we looked at the integrated analysis of DNA methylation and the transcriptome, only 4% of the genes were differentially methylated and also negatively regulated. Thus, DNA methylation might have very little impact on the overall regulation of  $\gamma\delta$  T-cell gene expression.

Gene expression profiling of  $\gamma\delta$  T cells has been already performed (Pont *et al*, 2012). However, the study by Pont *et al* (2012) has a limitation, as they used microarray for genome-wide



analysis. Additionally, they analyzed phosphoantigen-activated  $\gamma\delta$  T cells, which certainly differ from non-activated peripheral  $\gamma\delta$  T cells used in the present study. The  $\gamma\delta$  T-cell gene signatures were reported to reflect a hybrid state of  $\alpha\beta$  T cells and NK cells (even more NK-like). They also showed the same level of B-cell CLL/Lymphoma 11b (Bcl-11b) expression in human  $\alpha\beta$  and  $\gamma\delta$  T-cells, which is in contrast to our RNA-seq transcriptome analysis. In fact, our DNA methylation analysis showed kind of a hybrid state, but not gene expression analysis. The differential expression of genes was substantiated by the corresponding miRNA and long non-coding RNA (lncRNA) profiles. The downregulation of some of the candidate genes, including JUNB, FOS and CCR7, might be due to downregulation in their corresponding lncRNA. Though expression of MMP13 was not detected in transcriptome, miRNA miR-9-5p targeting MMP13 was found. It is not clear whether differential expression of genes and their respective miRNA and/or lncRNA modulate gene expression, as we did not provide direct functional evidences in our study. Thus, based on the non-coding RNA profiles of  $\gamma\delta$  T cells, we are in the process of identifying such target genes. Apart from RNA species, gene expression is also regulated by transcription factors. It is known that active gene expression is often marked by transcription factor footprint. An important feature of ATAC-seq is transcription factor footprint analysis. Although ATAC-seq analysis of  $\gamma\delta$  T cells is currently still ongoing, we will eventually combine this footprint analysis with  $\gamma\delta$  T cell gene expression features.

At this point, a few issues should be considered. Our integrated analysis is based on the use of UCSC hg19 gene symbols. The use of gene symbols for DNA methylation 450k arrays and RNA-seq-based lncRNA database is critical, especially considering the nucleotide length of CpG sites and lncRNA. Thus, the correct approach would be to utilize the sequence information (e.g. genomic locations) for data integration. Also while generating the comprehensive epigenetic landscape of  $\gamma\delta$  T cells, we should consider to use more powerful statistical analysis tools and to recruit more healthy individuals in the future. The integrated analysis was done according to the Fitting Linear Model and was further supplemented by simple correlation analysis. Considering the complexity of data and multiple variables as potential influencing factors, the use of multivariate analysis and other models like Bayesian approaches might be helpful (Conesa *et al*, 2016). Another interesting result of this study is the change in the genomic pattern within T-cell subsets based on gender differences. After excluding the female donor, it was more evident that

the whole transcriptome or miRNA would shift the pattern. It can also be seen in the chromatin accessibility of  $\gamma\delta$  T cell subsets (V $\delta$ 1 and V $\delta$ 2). Inheritance of genetic variability in CD4 T cells and, also human individuality and variation in personal regulomes of primary CD4 T cells fundamentally support our gender based difference in chromatin accessibility and gene expression (Qu *et al*, 2015). Thus, with larger cohorts, such gender-specific differences can be excluded to set up an unbiased comprehensive picture of the  $\gamma\delta$  T cell epigenetic landscape.

The gene ontology (GO) analysis has helped us to understand the meaning behind the processes involved in the epigenetic regulation of  $\gamma\delta$  T cells. GO analysis on each -omic dataset could give us the functional process related to the respective individual epigenomic processes. However, we performed GO analysis on the set of genes, which are unique and derived from integrated analysis. Thus, they will provide information about processes/functions regulated by core genes. GO analysis showed enrichment of terms, which are associated with  $\gamma\delta$  T-cell function. For instance, positive regulation of NK cell mediated cytotoxicity.  $\gamma\delta$  T cells are known for their cytotoxicity against a broad range of tumor cells (Silva-Santos *et al*, 2015; Wrobel *et al*, 2007). It is also reported that  $\gamma\delta$  T cell facilitate NK-cell mediated cytotoxicity of tumors (Maniar *et al*, 2010). In this NK-cell mediated cytotoxicity, the mechanism requires priming of NK cells by human immunoglobulin G1 and costimulation through CD137L expressed on activated  $\gamma\delta$  T cells, which leads to increase in NKG2D expression on the NK-cell surface. Another important GO feature is the enrichment of term 'external side of plasma membrane' in the GO category of cellular component reflecting cellular location of functional protein product of genes. With regard to  $\gamma\delta$  T cell activation, recognition of phosphoantigens mediated by BTN3A1/CD277 molecule occurs through these receptors expressed on cell membrane.

The data imply that the peripheral  $\gamma\delta$  T cells exhibit an epigenetic signature specifying a sequential thymic T cell differentiation and development process and also regulating phosphoantigen-reactive  $\gamma\delta$  T cell activation genes. The schematic illustration of this hypothesis is shown in the Fig. 6.3.

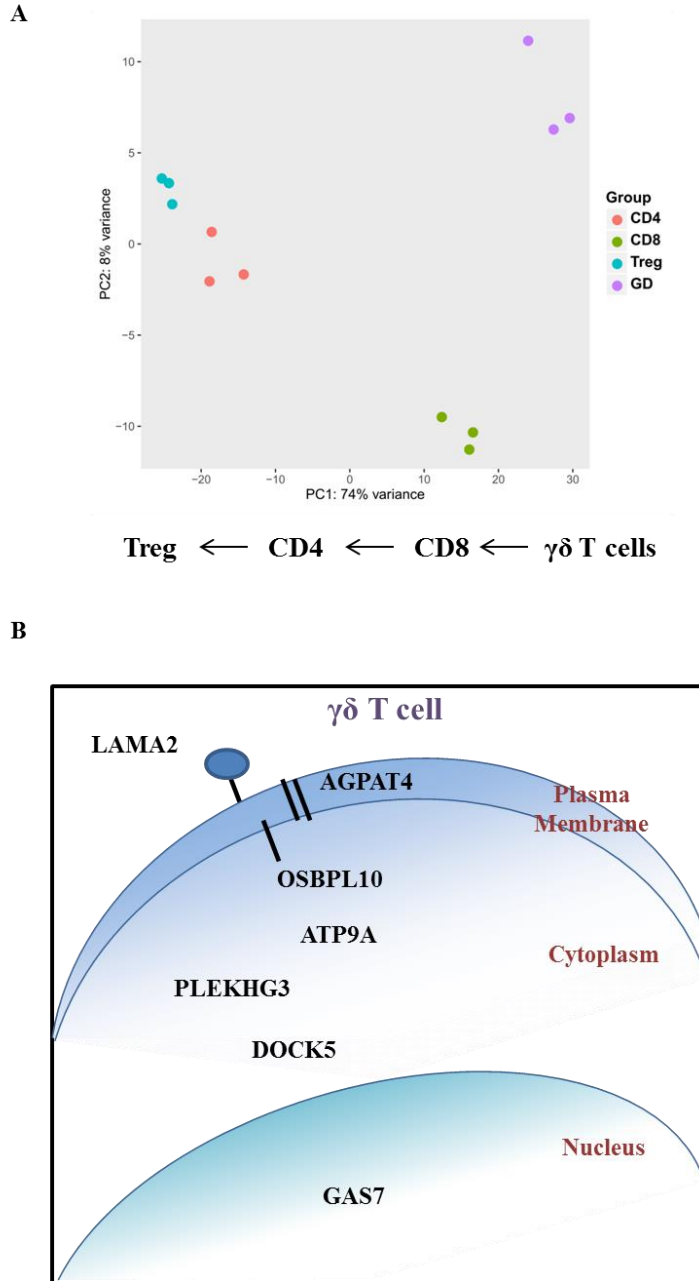


**Figure 6.3:** Proposed hypothetical model for the epigenetic regulation of human  $\gamma\delta$  T cells. (A) The representative PCA plot from transcriptome analysis showing  $\gamma\delta$  T cells are closely related to CD8, than CD4 and Treg cells. The PCA plot is used here to schematically represent the hypothetical sequence of T-cell development and its relation to  $\gamma\delta$  T cells. (B) The core set of genes obtained by integrating all the three epigenetic mechanisms is vital for  $\gamma\delta$  T-cell activation. The location of protein activity of some of these genes is shown based on the information available from GeneCards® The human Gene Database.

The epigenomic analyses of T cells showed overall similar patterns of T-cell distribution on the principal component analysis (PCA) or MDS plots.  $\gamma\delta$  T cells are functionally more similar to CD8, then CD4 and Treg cells (Fig. 6.3A). Similarly, memory CD4 T cell differentiation pattern has been shown using epigenomic profiling approach (Durek *et al*, 2016). Thus peripheral  $\gamma\delta$  T cells might carry the epigenetic signature of T-cell development that has followed in the sequence of events:  $\gamma\delta \rightarrow \text{CD8} \rightarrow \text{CD4} \rightarrow \text{Treg}$  cells. In this sequence of T-cell development,  $\gamma\delta$  T cells originate from DN, ISP or early DP stage (introduced in section 1.1.2 of the thesis), whereas Treg cells are generated as part of the central tolerance mechanism after the successful generation of CD4 cells. Also, Treg cells are generated upon TCR and low-affinity self-peptide MHC ligand interaction (Xing and Hogquist, 2012). This is further supported by the signal strength model of  $\gamma\delta$  T-cell development. According to this model, stronger pre-TCR signal leads to  $\gamma\delta$  T cell development, while weaker signal leads to  $\alpha\beta$  T cells. In fact, selective and differential involvement of ID3, LEF1 and ERK/MAPK signaling molecules in the choice of  $\alpha\beta$  vs  $\gamma\delta$  T-cell lineage commitment have been an important component of this model (Hayes *et al*, 2003; Kreslavsky *et al*, 2010; Lauritsen *et al*, 2006). Thus, consecutively, our epigenetic analysis is strongly supported through this signal strength model, specifically because of the DNA methylation profile showing regulation of some of these genes, hypomethylation of MAPK1, hypermethylation of Bcl-11b. Moreover, additional observations such as the differential chromatin accessibility of KLRK1, hypomethylation of KLRG1 and IFNG in  $\gamma\delta$  T cells as well as CD8 cells compared to CD4 and Treg, clearly support shared properties of  $\gamma\delta$  T cells with CD8 cells.

Another interesting result of our epigenetic analysis of  $\gamma\delta$  T cells is the expression and regulation of RNA. Apart from the expression of several TCR  $\gamma$  and  $\delta$  chain variants, we observed the expression of genes related to B cell function (e.g. CD19, CD22), Th1 differentiation (e.g. IL12RB2) and Th2 differentiation (e.g. CMIP), which reflects the  $\gamma\delta$  T-cell potential for functional plasticity on an epigenomic level. However, the differentially expressed genes, which were regulated by DNA methylation and lncRNA, were more related to  $\gamma\delta$  T-cell activation pathways. For example, as per information available from GeneCards<sup>®</sup> Human Gene Database, LAMA2 is the extracellular basement membrane protein, a receptor for integrins which mediates the attachment and interaction with other cells; AGPAT4 is the integral membrane protein,

which converts lysophosphatidic acid to phosphatidic acid; the OSBPL10 protein belong to intracellular lipid receptors and has the ability to bind to phosphatidylserine of the plasma membrane; PLEKHG3 and DOCK5 proteins are related to the Rho guanyl-nucleotide exchange factor activity; ATP9A protein is related to nucleotide binding and cation-transporting ATPase activity; ADAP1 protein is a GTPase-activating protein for the ADP ribosylation factors, involved in Arf6 signaling and PI3K signaling events; protein product of GAS7 gene is associated with transcription factor activity and also in sequence-specific DNA binding and actin filament binding, predominantly localized in the nucleus. In the context of T cells, protein products of these genes are shown to play an exclusive role in direct or indirect T cell activation. In this context, there are several supporting reports available in the literature. Thus,  $\gamma\delta$  T-cell activation was described in response to binding of vitronectin receptor, an Integrin to the extracellular matrix (Sturmhoefel *et al*, 1995). In case of CD8 T cells, phosphatidylserine externalization mediated by flippase is linked to potent T cell activation and immune synapse formation (Fischer *et al*, 2006). Additionally, the ATP9A is shown to possess phospholipid flippase activity and also functions as cargo machinery within cell organelles (Tanaka *et al*, 2016). Recently, Sebestyen *et al* (2016) showed that  $\gamma\delta$  T cell activation is modulated by tumor cells expressing RhoB GTPase and BTN3A1 molecules, supporting the proposed “outside-in model” of  $\gamma\delta$  T-cell activation (introduced in section 1.1.3 of the thesis). Finally, our integrated epigenetic analysis also showed regulation of genes, whose protein products are components of the cholesterol and lipid biosynthesis pathway, and its transport up to the external side of the plasma membrane of  $\gamma\delta$  T cells that might lead to their activation (as depicted in Fig. 6.3B).

It is tempting to speculate that peripheral  $\gamma\delta$  T cells carry a stable DNA methylation signature of thymic T cell development, while RNA expression and its regulation carry signatures for expression of functional TCR  $\gamma\delta$  chains and  $\gamma\delta$  T-cell activation, as part of the stress immune surveillance or primary response to microbial phosphoantigens. Nonetheless, the hypothesis proposed on the basis of our systems immunology-approach, needs functional proof, perhaps using  $\gamma\delta$  T cell functional assays, which will be addressed in the future.

### 6.6 Epigenetic modification of human $\gamma\delta$ T-cells in malignancy: A case report of an hepatosplenic gamma/delta T-cell lymphoma patient responding to Interferon- $\alpha$ treatment

Epigenetic regulations form the basis for individual cellular identity and functional responses of cells to environmental stimuli, nutrition, etiological factors and therapeutic agents. Concordantly, one of the main characteristics of  $\gamma\delta$ -HSTCL is the inactive cytotoxicity and the clonal TCR gene rearrangement. Previously, a case was reported that a patient with  $\gamma\delta$ -HSTCL showed NK cell-like cytotoxic activity. But, the malignant cell clones had V $\gamma$ 3, V $\gamma$ 9 and V $\delta$ 1 chain expression (Weidmann *et al*, 2000). Like-wise the malignant cells from the patient of the present study also lacked cytotoxic potential. Though additional V $\gamma$ 3 and V $\gamma$ 9 TCR chain non-functional gene rearrangement occurred, the malignant clones expressed fully functional V $\gamma$ 4, V $\gamma$ 5 and V $\delta$ 1 TCR chains detected by flow cytometry (Metzger *et al*, 1992; Hinz *et al*, 1996).

Interferon- $\alpha$  treatment is known to target Janus kinase (JAK-STAT) pathway, particularly STAT3 and STAT5, and suppressor of cytokine signaling (SOCS) pathways (Wang *et al*, 2000). Of note, the  $\gamma\delta$ -HSTCL patient studied in the present clinical case report carried STAT3 mutation (Bergmann *et al*, unpublished data), which may not be the possible mechanism of action. Another mode of action for IFN $\alpha$ 2c is to induce proapoptotic gene expression (Kiladjian *et al*, 2011), which should cause the elimination of malignant T-cell blasts. With this possible mechanism of action of Interferon- $\alpha$  therapy, the  $\gamma\delta$ -HSTCL patient showed substantial decrease in  $\gamma\delta$  T-cell lymphoblast count over the course of treatment, but the proportion of  $\gamma\delta$  T cells (90-90%) did not change. Instead, the steady decrease in absolute leukocyte count leading to remission and recovery of hemoglobin level were seen. Thus, it is tempting to speculate that the phenotypic characteristic of PBL blasts of the  $\gamma\delta$ -HSTCL patient remained same, while altering functional immune response. However, these functional responses do not seem to involve proliferative capacity or NK cell-like direct cytotoxic potential (Metzger *et al*, 1992). In this regard, biological association of hypomethylated genes points towards the possible involvement of other cellular functions like active immune cell synapse formation and reduction in metabolic processes. For instance, MYO5B, which was one of the hypomethylated genes on visit 5, is involved in the protein trafficking in the cell (Swiatecka-Urban *et al*, 2007).

Our DNA methylation analysis clearly support the fact that epigenomic characteristics were not altered, even after reaching remission (visit 5), as observed by no gain of DNA methylome

profile resembling healthy  $\gamma\delta$  T-cell methylome. Though  $\gamma\delta$ -HSTCL is genotypically characterized by chromosomal abnormality, we observed slight enrichment of the methylation levels of chromosome 1, 2 and 16 (data not shown). Another important asset of our analysis of the patient is the significant changes in methylation on core promoter, non-CGI/open sea and island, shelf of CGI region due to disease progression and Interferon- $\alpha$  treatment. With respect to the CGI feature, our whole-genome methylation analysis supports the traditional view of gene silencing through the presence of CpG Islands on promoter region and dynamic methylation patterns on CGI shelves and in open sea/non-CGI regions (Edgar *et al*, 2014; Zilbauer *et al*, 2013). In contrast to the initial overall analysis at each visit of  $\gamma\delta$ -HSTCL patient showing a significant decrease in the methylation level, the increase in methylation on TSS200, 5'UTR and 1<sup>st</sup> exon region in follow-up dependent manner was observed. This might be due to three possibilities: first, one CpG loci might be annotated to more than one genomic feature, which certainly would affect overall methylation analysis. Second, to investigate involvement of each genomic feature, CpG sites were separately assigned to multiple genomic features. Thus, more CpG sites were considered. Thus, this would certainly affect methylation levels during extended IFN $\alpha$ 2c therapy. Third possibility is the methylated CpG site carry no genomic features at all, which were excluded from later genomic feature analysis. Nevertheless, the promoter methylation proximal to TSS plays an important role in transcriptional regulation (Moarii *et al*, 2015).

The exploratory analysis of DNA methylation in this  $\gamma\delta$ -HSTCL patient sheds light on the involvement of some transcription factors such as MAML3 (a transcriptional activator for NOTCH proteins) and ARNT (a transcriptional regulator of hypoxia-inducible factor-1). An epigenetically important candidate gene JMJD5, a transcriptional activator, was also hypomethylated on visit 5 of the  $\gamma\delta$ -HSTCL patient. JMJD5 is known to modulate the G2/M phase of cell cycle progression and the expression of the CCNA1 gene that regulates cancer cell proliferation (He *et al*, 2016). Thus, the role of JMJD5 should be examined in more detail, as it can serve as a potential biomarker of drug response or a suitable candidate for personalized medicine.

**7. Future perspectives**

With the knowledge on the epigenetic regulation specific for  $\gamma\delta$  T cells compared to other T-cell subsets, a more systematic analysis of  $\gamma\delta$  T cells under different conditions should be performed. This includes the impact of epigenetic drugs on antigen-activated human  $\gamma\delta$  T cell in a multi-omic-approach. Additionally, more insight on the epigenomic basis of phosphoantigen recognition and  $\gamma\delta$  T-cell activation will be advantageous. Thus, the information on combined epigenetic profiles of  $\gamma\delta$  T cells with and without phosphoantigen-stimulation in the presence or absence of epigenetic drugs might refine the design of improved treatment strategies to augment clinical outcomes. This approach is very important for  $\gamma\delta$  T cell-mediated immunotherapy. We presented first example of changes in DNA methylation of a  $\gamma\delta$ -HSTCL patient treated with Interferon- $\alpha$ 2c leading to clinical remission. Beyond Interferon- $\alpha$ 2c treatment, other additional strategies might include chemotherapeutics or antibody constructs in addition to epigenetic drugs. In fact, the differentially regulated epigenetic targets emerging from such systems immunology studies can also be beneficial for personalized medicine. Therefore, based on all these considerations, we believe that the treatment of cancer patients with epigenetic drugs combined with the adoptive transfer of in vitro expanded  $\gamma\delta$  T cells currently holds the best promise for a useful liaison.



## 8. Summary

Human  $\gamma\delta$  T-cells have emerged as key players in diverse immune responses both in health and disease. Such a dynamic functional diversity of cells is controlled at various levels of (epi)genetic regulation in an orchestrated manner. However, a comprehensive overview of epigenetic mechanisms dictating human  $\gamma\delta$  T-cell development, regulation and molecular function is largely missing. The present thesis aims at elucidating the epigenetic landscape of human  $\gamma\delta$  T-cells by mainly two distinct approaches. In a first approach based on in vitro culture, the NKG2D ligand expression and release, and its further implications on NKG2D receptor expression by epigenetic inhibitors such as histone deacetylase inhibitor valproic acid, a drug widely used in the clinic, was studied. The modulation of NKG2D receptor expression and function of  $\gamma\delta$  T cells in co-culture with pancreatic carcinoma and prostate carcinoma tumor cell lines were addressed. Additionally, the effect on functional responses of  $\gamma\delta$  T-cells upon treatment with valproic acid provided new insight into  $\gamma\delta$  T-cell subset-specific responses. Specifically, valproic acid induced changes in molecular and cellular responses of human  $\gamma\delta$  T-cells, specifically by enhanced expression of the non-secretory form of IL-4, regulation of cell death and induction of global histone acetylation (H3K9ac).

In a second approach, the “endogenous” molecular regulation of peripheral  $\gamma\delta$  T-cells in comparison to  $\alpha\beta$  T-cells were deciphered using highly sensitive assays for chromatin accessibility, DNA methylation and RNA expression. Next generation sequencing-based preliminary results showed differential expression of genes clearly distinguishing  $\gamma\delta$  T-cells from other T-cell subsets. The mRNA expression profile of  $\gamma\delta$  T cells was analyzed in parallel to assess the involvement of regulatory RNA i.e. miRNA and lncRNA that control the transcriptional signature of  $\gamma\delta$  T cells. The RNA expression and regulation was further complemented by analyses of DNA methylation and chromatin accessibility. Moreover, the integration of all these multiple layers of epigenetic regulations resulted in a unique set of genes clearly separating  $\gamma\delta$  T cells from CD4, Treg and CD8 T cells.  $\gamma\delta$  T-cell signatures were mainly associated with  $\gamma\delta$  T-cell development and activation pathways. Our research based on (epi)genetic mechanisms will broaden the characterization of human  $\gamma\delta$  T-cells and thereby contribute to a better understanding of basic features of  $\gamma\delta$  T cells especially with respect to immunotherapeutic application.

### 9. Zusammenfassung

$\gamma\delta$  T Zellen sind sowohl bei Gesunden als auch in Patienten als wichtige zelluläre Komponente der Immunantwort identifiziert worden. Die dynamische funktionelle Plastizität von Zellen wird auf unterschiedlichen Ebenen, insbesondere aber auf epigenetischer Ebene reguliert. Bisher fehlte allerdings eine genaue Charakterisierung der epigenetischen Mechanismen, welche die Entwicklung, Differenzierung und Funktion von  $\gamma\delta$  T-Zellen steuern. Das Ziel dieser Dissertation war die Aufklärung der epigenetischen „Landschaft“ von human  $\gamma\delta$  T-Zellen auf zwei Wegen. Zum einen sollte in in vitro Kultursystemen die epigenetische Regulation der NKG2D-Rezeptor und -Ligand Expression sowie des NKG2D Ligand „Sheddings“ durch Verwendung des Histon-Deazetylase-Inhibitors Valproinsäure (VPA) untersucht werden. VPA wird bereits therapeutisch in der Klinik eingesetzt. Die Modulation des NKG2D-Rezeptors und die Funktion von  $\gamma\delta$  T-Zellen nach Behandlung mit VPA wurden in Kokulturen mit Prostata- und Pankreas-Tumorzellen untersucht. Ferner wurden Untersuchungen zum Einfluss von VPA auf Marker-Expression und Funktion von  $\gamma\delta$  T-Zellen durchgeführt. Dabei zeigte sich, dass VPA Veränderungen von  $\gamma\delta$  T-Zellen auf molekularer und zellulärer Ebene induzierte und insbesondere die Expression einer nicht-sezernierten IL-4 Variante sowie die Regulation von Zelltod und globaler Histon-Azetylierung (H3K9ac) modulierte.

In einem weiteren Teil wurde die „endogene“ molekulare Regulation von peripheren Blut  $\gamma\delta$  T-Zellen im Vergleich zu  $\alpha\beta$  T-Zellen mittels hochsensitiver Methoden zur Analyse des Chromatin-Zugänglichkeit, der DNA-Methylierung sowie der RNA-Expression untersucht. Next-generation-sequencing (NGS)-basierte vorläufige Ergebnisse konnten eindeutig die Expression und Regulation bestimmter Gene identifizieren, welche  $\gamma\delta$  T-Zellen klar von anderen T-Zellpopulationen abgrenzen. Parallel zu dem mRNA-Expressionsprofil von  $\gamma\delta$  T-Zellen wurden auch regulatorische RNAs wie miRNA und lncRNA untersucht, welche die transkriptionelle Signatur von  $\gamma\delta$  T-Zellen kontrollieren. Zusätzlich zur RNA-Expression und Regulation wurden auch DNA-Methylierung sowie die Chromatin-Zugänglichkeit untersucht. Die bioinformatische Integration dieser unterschiedlichen Regulationsebenen ergab Hinweise auf die Expression und Regulation spezifischer Gene, welche  $\gamma\delta$  T-Zellen eindeutig von anderen T-Zellpopulationen wie CD4, CD8 und Treg abgrenzen. Diese  $\gamma\delta$  T-Zell- „Signaturen“ waren u.a. mit  $\gamma\delta$  T-Zell-Entwicklung und -Aktivierung assoziiert. Diese Ergebnisse tragen entscheidend

## **Zusammenfassung**

zur weiteren Charakterisierung der Besonderheiten humaner  $\gamma\delta$  T-Zellen bei. Ferner erlauben die Ergebnisse eine bessere Klassifizierung von  $\gamma\delta$  T-Zellen, was insbesondere für die weitere therapeutische Anwendung von  $\gamma\delta$  T-Zellen von großer Bedeutung ist.

**10. References**

1. (1939). An Introduction to Modern Genetics. By C. H. Waddington. Proceedings of the Royal Entomological Society of London. Series A, General Entomology 14, 82.
2. Abe, Y., Muto, M., Nieda, M., Nakagawa, Y., Nicol, A., Kaneko, T., Goto, S., Yokokawa, K., and Suzuki, K. (2009). Clinical and immunological evaluation of zoledronate-activated Vgamma9gammadelta T-cell-based immunotherapy for patients with multiple myeloma. *Experimental hematology* 37, 956-968.
3. Aguera-Gonzalez, S., Gross, C.C., Fernandez-Messina, L., Ashiru, O., Estes, G., Hang, H.C., Reyburn, H.T., Long, E.O., and Vales-Gomez, M. (2011). Palmitoylation of MICA, a ligand for NKG2D, mediates its recruitment to membrane microdomains and promotes its shedding. *European journal of immunology* 41, 3667-3676.
4. Allis, C.D., and Jenuwein, T. (2016). The molecular hallmarks of epigenetic control. *Nature reviews. Genetics* 17, 487-500.
5. Ammerpohl, O., Haake, A., Kolarova, J., and Siebert, R. (2016). Quantitative DNA Methylation Profiling in Cancer. *Methods in molecular biology* 1381, 75-92.
6. Anders, S., Pyl, P.T., and Huber, W. (2015). HTSeq--a Python framework to work with high-throughput sequencing data. *Bioinformatics* 31, 166-169.
7. Andrews, F.H., Strahl, B.D., and Kutateladze, T.G. (2016). Insights into newly discovered marks and readers of epigenetic information. *Nature chemical biology* 12, 662-668.
8. Angelini, C., and Costa, V. (2014). Understanding gene regulatory mechanisms by integrating ChIP-seq and RNA-seq data: statistical solutions to biological problems. *Frontiers in cell and developmental biology* 2, 51.
9. Annunziato, A.T. (2008). DNA Packaging: Nucleosomes and Chromatin. *Nature Education* 1.
10. Araki, Y., Wang, Z., Zang, C., Wood, W.H., 3rd, Schones, D., Cui, K., Roh, T.Y., Lhotsky, B., Wersto, R.P., Peng, W., et al. (2009). Genome-wide analysis of histone methylation reveals chromatin state-based regulation of gene transcription and function of memory CD8<sup>+</sup> T cells. *Immunity* 30, 912-925.
11. Armeanu, S., Bitzer, M., Lauer, U.M., Venturelli, S., Pathil, A., Krusch, M., Kaiser, S., Jobst, J., Smirnow, I., Wagner, A., et al. (2005). Natural killer cell-mediated lysis of hepatoma cells via specific induction of NKG2D ligands by the histone deacetylase inhibitor sodium valproate. *Cancer research* 65, 6321-6329.
12. Ashiru, O., Boutet, P., Fernandez-Messina, L., Aguera-Gonzalez, S., Skepper, J.N., Vales-Gomez, M., and Reyburn, H.T. (2010). Natural killer cell cytotoxicity is suppressed by exposure to the

- human NKG2D ligand MICA\*008 that is shed by tumor cells in exosomes. *Cancer research* 70, 481-489.
13. Ashiru, O., Lopez-Cobo, S., Fernandez-Messina, L., Pontes-Quero, S., Pandolfi, R., Reyburn, H.T., and Vales-Gomez, M. (2013). A GPI anchor explains the unique biological features of the common NKG2D-ligand allele MICA\*008. *The Biochemical journal* 454, 295-302.
  14. Assenov, Y., Muller, F., Lutsik, P., Walter, J., Lengauer, T., and Bock, C. (2014). Comprehensive analysis of DNA methylation data with RnBeads. *Nature methods* 11, 1138-1140.
  15. Atmaca, A., Al-Batran, S.E., Maurer, A., Neumann, A., Heinzl, T., Hentsch, B., Schwarz, S.E., Hovelmann, S., Gottlicher, M., Knuth, A., and Jager, E. (2007). Valproic acid (VPA) in patients with refractory advanced cancer: a dose escalating phase I clinical trial. *British journal of cancer* 97, 177-182.
  16. Avallone, A., Piccirillo, M.C., Delrio, P., Pecori, B., Di Gennaro, E., Aloj, L., Tatangelo, F., D'Angelo, V., Granata, C., Cavalcanti, E., et al. (2014). Phase 1/2 study of valproic acid and short-course radiotherapy plus capecitabine as preoperative treatment in low-moderate risk rectal cancer-V-shoRT-R3 (Valproic acid--short Radiotherapy--rectum 3rd trial). *BMC cancer* 14, 875.
  17. Bannister, A.J., and Kouzarides, T. (2011). Regulation of chromatin by histone modifications. *Cell research* 21, 381-395.
  18. Bansal, R.R., Mackay, C.R., Moser, B., and Eberl, M. (2012). IL-21 enhances the potential of human gammadelta T cells to provide B-cell help. *European journal of immunology* 42, 110-119.
  19. Barski, A., Cuddapah, S., Cui, K., Roh, T.Y., Schones, D.E., Wang, Z., Wei, G., Chepelev, I., and Zhao, K. (2007). High-resolution profiling of histone methylations in the human genome. *Cell* 129, 823-837.
  20. Basher, F., Jeng, E.K., Wong, H., and Wu, J. (2016). Cooperative therapeutic anti-tumor effect of IL-15 agonist ALT-803 and co-targeting soluble NKG2D ligand sMIC. *Oncotarget* 7, 814-830.
  21. Behrens, A., Sabapathy, K., Graef, I., Cleary, M., Crabtree, G.R., and Wagner, E.F. (2001). Jun N-terminal kinase 2 modulates thymocyte apoptosis and T cell activation through c-Jun and nuclear factor of activated T cell (NF-AT). *Proceedings of the National Academy of Sciences of the United States of America* 98, 1769-1774.
  22. Benjamini, Y., and Hochberg, Y. (1995). Controlling the False Discovery Rate: A Practical and Powerful Approach to Multiple Testing. *Journal of the Royal Statistical Society. Series B (Methodological)* 57, 289-300.

23. Bernstein, B.E., Mikkelsen, T.S., Xie, X., Kamal, M., Huebert, D.J., Cuff, J., Fry, B., Meissner, A., Wernig, M., Plath, K., et al. (2006). A bivalent chromatin structure marks key developmental genes in embryonic stem cells. *Cell* 125, 315-326.
24. Bhat, J., and Kabelitz, D. (2015). gammadelta T cells and epigenetic drugs: A useful merger in cancer immunotherapy? *Oncoimmunology* 4, e1006088.
25. Bhat, J., Oberg, H.H., and Kabelitz, D. (2015). Modulation of human gamma/delta T-cell activation and phenotype by histone deacetylase inhibitors. *Cellular immunology* 296, 50-56.
26. Bhat, J., Sosna, J., Fritsch, J., Quabius, E.S., Schutze, S., Zeissig, S., Ammerpohl, O., Adam, D., and Kabelitz, D. (2016). Expression of non-secreted IL-4 is associated with HDAC inhibitor-induced cell death, histone acetylation and c-Jun regulation in human gamma/delta T-cells. *Oncotarget* 7, 64743-64756.
27. Bibikova, M., Barnes, B., Tsan, C., Ho, V., Klotzle, B., Le, J.M., Delano, D., Zhang, L., Schroth, G.P., Gunderson, K.L., et al. (2011). High density DNA methylation array with single CpG site resolution. *Genomics* 98, 288-295.
28. Birzele, F., Fauti, T., Stahl, H., Lenter, M.C., Simon, E., Knebel, D., Weith, A., Hildebrandt, T., and Mennerich, D. (2011). Next-generation insights into regulatory T cells: expression profiling and FoxP3 occupancy in Human. *Nucleic acids research* 39, 7946-7960.
29. Bollino, D., Balan, I., and Aurelian, L. (2015). Valproic acid induces neuronal cell death through a novel calpain-dependent necroptosis pathway. *Journal of neurochemistry* 133, 174-186.
30. Boyle, A.P., Davis, S., Shulha, H.P., Meltzer, P., Margulies, E.H., Weng, Z., Furey, T.S., and Crawford, G.E. (2008). High-resolution mapping and characterization of open chromatin across the genome. *Cell* 132, 311-322.
31. Brandes, M., Willmann, K., Bioley, G., Levy, N., Eberl, M., Luo, M., Tampe, R., Levy, F., Romero, P., and Moser, B. (2009). Cross-presenting human gammadelta T cells induce robust CD8+ alphabeta T cell responses. *Proceedings of the National Academy of Sciences of the United States of America* 106, 2307-2312.
32. Breuer, K., Foroushani, A.K., Laird, M.R., Chen, C., Sribnaia, A., Lo, R., Winsor, G.L., Hancock, R.E., Brinkman, F.S., and Lynn, D.J. (2013). InnateDB: systems biology of innate immunity and beyond--recent updates and continuing curation. *Nucleic acids research* 41, D1228-1233.
33. Brown, S.W. (1966). Heterochromatin. *Science* 151, 417-425.
34. Buenrostro, J.D., Giresi, P.G., Zaba, L.C., Chang, H.Y., and Greenleaf, W.J. (2013). Transposition of native chromatin for fast and sensitive epigenomic profiling of open chromatin, DNA-binding proteins and nucleosome position. *Nature methods* 10, 1213-1218.

35. Buenrostro, J.D., Wu, B., Chang, H.Y., and Greenleaf, W.J. (2015). ATAC-seq: A Method for Assaying Chromatin Accessibility Genome-Wide. *Current protocols in molecular biology* 109, 21 29 21-29.
36. Buenrostro, J.D., Wu, B., Littenburger, U.M., Ruff, D., Gonzales, M.L., Snyder, M.P., Chang, H.Y., and Greenleaf, W.J. (2015). Single-cell chromatin accessibility reveals principles of regulatory variation. *Nature* 523, 486-490.
37. Butler, J.E., Moore, M.B., Presnell, S.R., Chan, H.W., Chalupny, N.J., and Lutz, C.T. (2009). Proteasome regulation of ULBP1 transcription. *Journal of immunology* 182, 6600-6609.
38. Caccamo, N., Todaro, M., La Manna, M.P., Sireci, G., Stassi, G., and Dieli, F. (2012). IL-21 regulates the differentiation of a human gammadelta T cell subset equipped with B cell helper activity. *PloS one* 7, e41940.
39. Cavill, R., Jennen, D., Kleinjans, J., and Briede, J.J. (2016). Transcriptomic and metabolomic data integration. *Briefings in bioinformatics* 17, 891-901.
40. Ceuppens, J.L., Baroja, M.L., Lorre, K., Van Damme, J., and Billiau, A. (1988). Human T cell activation with phytohemagglutinin. The function of IL-6 as an accessory signal. *Journal of immunology* 141, 3868-3874.
41. Chateavieux, S., Morceau, F., Dicato, M., and Diederich, M. (2010). Molecular and therapeutic potential and toxicity of valproic acid. *Journal of biomedicine & biotechnology* 2010.
42. Chen, J., Xu, H., and Zhu, X.X. (2016). Abnormal expression levels of sMICA and NKG2D are correlated with poor prognosis in pancreatic cancer. *Therapeutics and clinical risk management* 12, 11-18.
43. Chen, S.Y., Chiu, L.Y., Maa, M.C., Wang, J.S., Chien, C.L., and Lin, W.W. (2011). zVAD-induced autophagic cell death requires c-Src-dependent ERK and JNK activation and reactive oxygen species generation. *Autophagy* 7, 217-228.
44. Chen, T., Hao, Y.J., Zhang, Y., Li, M.M., Wang, M., Han, W., Wu, Y., Lv, Y., Hao, J., Wang, L., et al. (2015). m(6)A RNA methylation is regulated by microRNAs and promotes reprogramming to pluripotency. *Cell stem cell* 16, 289-301.
45. Chen, X., Shen, Y., Draper, W., Buenrostro, J.D., Littenburger, U., Cho, S.W., Satpathy, A.T., Carter, A.C., Ghosh, R.P., East-Seletsky, A., et al. (2016). ATAC-seq reveals the accessible genome by transposase-mediated imaging and sequencing. *Nature methods* 13, 1013-1020.
46. Chitadze, G., Bhat, J., Lettau, M., Janssen, O., and Kabelitz, D. (2013). Generation of soluble NKG2D ligands: proteolytic cleavage, exosome secretion and functional implications. *Scandinavian journal of immunology* 78, 120-129.

47. Chitadze, G., Lettau, M., Bhat, J., Wesch, D., Steinle, A., Furst, D., Mytilineos, J., Kalthoff, H., Janssen, O., Oberg, H.H., and Kabelitz, D. (2013). Shedding of endogenous MHC class I-related chain molecules A and B from different human tumor entities: heterogeneous involvement of the "a disintegrin and metalloproteases" 10 and 17. *International journal of cancer* 133, 1557-1566.
48. Choudhuri, K., Kearney, A., Bakker, T.R., and van der Merwe, P.A. (2005). Immunology: how do T cells recognize antigen? *Current biology : CB* 15, R382-385.
49. Chowdhury, D., and Novina, C.D. (2005). Potential roles for short RNAs in lymphocytes. *Immunology and cell biology* 83, 201-210.
50. Christman, J.K. (2002). 5-Azacytidine and 5-aza-2'-deoxycytidine as inhibitors of DNA methylation: mechanistic studies and their implications for cancer therapy. *Oncogene* 21, 5483-5495.
51. Codo, P., Weller, M., Meister, G., Szabo, E., Steinle, A., Wolter, M., Reifenberger, G., and Roth, P. (2014). MicroRNA-mediated down-regulation of NKG2D ligands contributes to glioma immune escape. *Oncotarget* 5, 7651-7662.
52. Conesa, A., Madrigal, P., Tarazona, S., Gomez-Cabrero, D., Cervera, A., McPherson, A., Szczesniak, M.W., Gaffney, D.J., Elo, L.L., Zhang, X., and Mortazavi, A. (2016). A survey of best practices for RNA-seq data analysis. *Genome biology* 17, 13.
53. Correia, D.V., Fogli, M., Hudspeth, K., da Silva, M.G., Mavilio, D., and Silva-Santos, B. (2011). Differentiation of human peripheral blood Vdelta1+ T cells expressing the natural cytotoxicity receptor Nkp30 for recognition of lymphoid leukemia cells. *Blood* 118, 992-1001.
54. Cosman, D., Mullberg, J., Sutherland, C.L., Chin, W., Armitage, R., Fanslow, W., Kubin, M., and Chalupny, N.J. (2001). ULBPs, novel MHC class I-related molecules, bind to CMV glycoprotein UL16 and stimulate NK cytotoxicity through the NKG2D receptor. *Immunity* 14, 123-133.
55. Creyghton, M.P., Cheng, A.W., Welstead, G.G., Kooistra, T., Carey, B.W., Steine, E.J., Hanna, J., Lodato, M.A., Frampton, G.M., Sharp, P.A., et al. (2010). Histone H3K27ac separates active from poised enhancers and predicts developmental state. *Proceedings of the National Academy of Sciences of the United States of America* 107, 21931-21936.
56. Dall'Olio, F., Malagolini, N., Trinchera, M., and Chiricolo, M. (2012). Mechanisms of cancer-associated glycosylation changes. *Frontiers in bioscience* 17, 670-699.
57. Dar, A.A., Patil, R.S., and Chiplunkar, S.V. (2014). Insights into the Relationship between Toll Like Receptors and Gamma Delta T Cell Responses. *Frontiers in immunology* 5, 366.
58. Das, H., Wang, L., Kamath, A., and Bukowski, J.F. (2001). Vgamma2Vdelta2 T-cell receptor-mediated recognition of aminobisphosphonates. *Blood* 98, 1616-1618.



59. Davis, M.M. (2002). A new trigger for T cells. *Cell* 110, 285-287.
60. Deng, W., Gowen, B.G., Zhang, L., Wang, L., Lau, S., Iannello, A., Xu, J., Rovis, T.L., Xiong, N., and Raulet, D.H. (2015). Antitumor immunity. A shed NKG2D ligand that promotes natural killer cell activation and tumor rejection. *Science* 348, 136-139.
61. Derrien, T., Johnson, R., Bussotti, G., Tanzer, A., Djebali, S., Tilgner, H., Guernec, G., Martin, D., Merkel, A., Knowles, D.G., et al. (2012). The GENCODE v7 catalog of human long noncoding RNAs: analysis of their gene structure, evolution, and expression. *Genome research* 22, 1775-1789.
62. Di Carlo, E., Bocca, P., Emionite, L., Cilli, M., Cipollone, G., Morandi, F., Raffaghello, L., Pistoia, V., and Prigione, I. (2013). Mechanisms of the antitumor activity of human Vgamma9Vdelta2 T cells in combination with zoledronic acid in a preclinical model of neuroblastoma. *Molecular therapy : the journal of the American Society of Gene Therapy* 21, 1034-1043.
63. Dispirito, J.R., and Shen, H. (2010). Histone acetylation at the single-cell level: a marker of memory CD8+ T cell differentiation and functionality. *Journal of immunology* 184, 4631-4636.
64. Dokmanovic, M., Clarke, C., and Marks, P.A. (2007). Histone deacetylase inhibitors: overview and perspectives. *Molecular cancer research : MCR* 5, 981-989.
65. Du, P., Zhang, X., Huang, C.C., Jafari, N., Kibbe, W.A., Hou, L., and Lin, S.M. (2010). Comparison of Beta-value and M-value methods for quantifying methylation levels by microarray analysis. *BMC bioinformatics* 11, 587.
66. Duan, X., Deng, L., Chen, X., Lu, Y., Zhang, Q., Zhang, K., Hu, Y., Zeng, J., and Sun, W. (2011). Clinical significance of the immunostimulatory MHC class I chain-related molecule A and NKG2D receptor on NK cells in pancreatic cancer. *Medical oncology* 28, 466-474.
67. Dunn, G.P., Old, L.J., and Schreiber, R.D. (2004). The three Es of cancer immunoediting. *Annual review of immunology* 22, 329-360.
68. Durek, P., Nordstrom, K., Gasparoni, G., Salhab, A., Kressler, C., de Almeida, M., Bassler, K., Ulas, T., Schmidt, F., Xiong, J., et al. (2016). Epigenomic Profiling of Human CD4+ T Cells Supports a Linear Differentiation Model and Highlights Molecular Regulators of Memory Development. *Immunity* 45, 1148-1161.
69. Eberl, M., Hintz, M., Reichenberg, A., Kollas, A.K., Wiesner, J., and Jomaa, H. (2003). Microbial isoprenoid biosynthesis and human gammadelta T cell activation. *FEBS letters* 544, 4-10.
70. Edgar, R., Tan, P.P., Portales-Casamar, E., and Pavlidis, P. (2014). Meta-analysis of human methylomes reveals stably methylated sequences surrounding CpG islands associated with high gene expression. *Epigenetics & chromatin* 7, 28.

71. Espinoza, J.L., Takami, A., Yoshioka, K., Nakata, K., Sato, T., Kasahara, Y., and Nakao, S. (2012). Human microRNA-1245 down-regulates the NKG2D receptor in natural killer cells and impairs NKG2D-mediated functions. *Haematologica* 97, 1295-1303.
72. Falk, M., Ussat, S., Reiling, N., Wesch, D., Kabelitz, D., and Adam-Klages, S. (2004). Caspase inhibition blocks human T cell proliferation by suppressing appropriate regulation of IL-2, CD25, and cell cycle-associated proteins. *Journal of immunology* 173, 5077-5085.
73. Falkenberg, K.J., and Johnstone, R.W. (2014). Histone deacetylases and their inhibitors in cancer, neurological diseases and immune disorders. *Nature reviews. Drug discovery* 13, 673-691.
74. Fazzari, M.J., and Grealley, J.M. (2004). Epigenomics: beyond CpG islands. *Nature reviews. Genetics* 5, 446-455.
75. Feng, Y., and Rudensky, A.Y. (2015). DNA methylation secures CD4(+) and CD8(+) T cell lineage borders. *Nature immunology* 16, 681-683.
76. Fernandez-Messina, L., Ashiru, O., Boutet, P., Aguera-Gonzalez, S., Skepper, J.N., Reyburn, H.T., and Vales-Gomez, M. (2010). Differential mechanisms of shedding of the glycosylphosphatidylinositol (GPI)-anchored NKG2D ligands. *The Journal of biological chemistry* 285, 8543-8551.
77. Fernandez-Sanchez, A., Baragano Raneros, A., Carvajal Palao, R., Sanz, A.B., Ortiz, A., Ortega, F., Suarez-Alvarez, B., and Lopez-Larrea, C. (2013). DNA demethylation and histone H3K9 acetylation determine the active transcription of the NKG2D gene in human CD8+ T and NK cells. *Epigenetics* 8, 66-78.
78. Fionda, C., Malgarini, G., Soriani, A., Zingoni, A., Cecere, F., Iannitto, M.L., Ricciardi, M.R., Federico, V., Petrucci, M.T., Santoni, A., and Cippitelli, M. (2013). Inhibition of glycogen synthase kinase-3 increases NKG2D ligand MICA expression and sensitivity to NK cell-mediated cytotoxicity in multiple myeloma cells: role of STAT3. *Journal of immunology* 190, 6662-6672.
79. Fionda, C., Soriani, A., Malgarini, G., Iannitto, M.L., Santoni, A., and Cippitelli, M. (2009). Heat shock protein-90 inhibitors increase MHC class I-related chain A and B ligand expression on multiple myeloma cells and their ability to trigger NK cell degranulation. *Journal of immunology* 183, 4385-4394.
80. Fionda, C., Soriani, A., Zingoni, A., Santoni, A., and Cippitelli, M. (2015). NKG2D and DNAM-1 Ligands: Molecular Targets for NK Cell-Mediated Immunotherapeutic Intervention in Multiple Myeloma. *BioMed research international* 2015, 178698.

81. Fischer, K., Voelkl, S., Berger, J., Andreesen, R., Pomorski, T., and Mackensen, A. (2006). Antigen recognition induces phosphatidylserine exposure on the cell surface of human CD8+ T cells. *Blood* 108, 4094-4101.
82. Fisher, J.P., Heuijerjans, J., Yan, M., Gustafsson, K., and Anderson, J. (2014). gammadelta T cells for cancer immunotherapy: A systematic review of clinical trials. *Oncoimmunology* 3, e27572.
83. Friedlander, M.R., Mackowiak, S.D., Li, N., Chen, W., and Rajewsky, N. (2012). miRDeep2 accurately identifies known and hundreds of novel microRNA genes in seven animal clades. *Nucleic acids research* 40, 37-52.
84. Frigoul, A.L., Marie-Paule (2005). MICA: standardized IMGT allele nomenclature, polymorphisms and diseases. *Recent Research Developments in Human Genetics* 3, 50.
85. Fritsch, J., Stephan, M., Tchikov, V., Winoto-Morbach, S., Gubkina, S., Kabelitz, D., and Schutze, S. (2014). Cell fate decisions regulated by K63 ubiquitination of tumor necrosis factor receptor 1. *Molecular and cellular biology* 34, 3214-3228.
86. Fullgrabe, J., Hajji, N., and Joseph, B. (2010). Cracking the death code: apoptosis-related histone modifications. *Cell death and differentiation* 17, 1238-1243.
87. Gangadharan, S., Mularoni, L., Fain-Thornton, J., Wheelan, S.J., and Craig, N.L. (2010). DNA transposon Hermes inserts into DNA in nucleosome-free regions in vivo. *Proceedings of the National Academy of Sciences of the United States of America* 107, 21966-21972.
88. Gentles, A.J., Newman, A.M., Liu, C.L., Bratman, S.V., Feng, W., Kim, D., Nair, V.S., Xu, Y., Khuong, A., Hoang, C.D., et al. (2015). The prognostic landscape of genes and infiltrating immune cells across human cancers. *Nature medicine* 21, 938-945.
89. Girlanda, S., Fortis, C., Belloni, D., Ferrero, E., Ticozzi, P., Sciorati, C., Tresoldi, M., Vicari, A., Spies, T., Groh, V., et al. (2005). MICA expressed by multiple myeloma and monoclonal gammopathy of undetermined significance plasma cells Costimulates pamidronate-activated gammadelta lymphocytes. *Cancer research* 65, 7502-7508.
90. Glaubien, R., Sonnenberg, E., Wetzel, M., Mascagni, P., and Siegmund, B. (2014). Histone deacetylase inhibitors modulate interleukin 6-dependent CD4+ T cell polarization in vitro and in vivo. *The Journal of biological chemistry* 289, 6142-6151.
91. Gober, H.J., Kistowska, M., Angman, L., Jeno, P., Mori, L., and De Libero, G. (2003). Human T cell receptor gammadelta cells recognize endogenous mevalonate metabolites in tumor cells. *The Journal of experimental medicine* 197, 163-168.

92. Godderis, L., Schouteden, C., Tabish, A., Poels, K., Hoet, P., Baccarelli, A.A., and Van Landuyt, K. (2015). Global Methylation and Hydroxymethylation in DNA from Blood and Saliva in Healthy Volunteers. *BioMed research international* 2015, 845041.
93. Goldberg, A.D., Allis, C.D., and Bernstein, E. (2007). Epigenetics: a landscape takes shape. *Cell* 128, 635-638.
94. Gooz, M. (2010). ADAM-17: the enzyme that does it all. *Critical reviews in biochemistry and molecular biology* 45, 146-169.
95. Grabarska A, D.-G.M., Jeleniewicz W, Kielbus M, Nowosadzka E, Rivero-Muller A, Polberg K, Stepulak A (2014). Valproic acid suppresses growth and enhances cisplatin cytotoxicity to larynx cancer cells. *Head Neck Oncol* 6, 7.
96. Greenblatt, D.Y., Cayo, M.A., Adler, J.T., Ning, L., Haymart, M.R., Kunnimalaiyaan, M., and Chen, H. (2008). Valproic acid activates Notch1 signaling and induces apoptosis in medullary thyroid cancer cells. *Annals of surgery* 247, 1036-1040.
97. Groh, V., Wu, J., Yee, C., and Spies, T. (2002). Tumour-derived soluble MIC ligands impair expression of NKG2D and T-cell activation. *Nature* 419, 734-738.
98. Gurvich, N., Tsygankova, O.M., Meinkoth, J.L., and Klein, P.S. (2004). Histone deacetylase is a target of valproic acid-mediated cellular differentiation. *Cancer research* 64, 1079-1086.
99. Haig, D. (2004). The (dual) origin of epigenetics. *Cold Spring Harbor symposia on quantitative biology* 69, 67-70.
100. Haig, D. (2007). Weismann Rules! OK? Epigenetics and the Lamarckian temptation. *Biology & Philosophy* 22, 415-428.
101. Han, Q., Bagheri, N., Bradshaw, E.M., Hafler, D.A., Lauffenburger, D.A., and Love, J.C. (2012). Polyfunctional responses by human T cells result from sequential release of cytokines. *Proceedings of the National Academy of Sciences of the United States of America* 109, 1607-1612.
102. Harikrishnan, K.N., Karagiannis, T.C., Chow, M.Z., and El-Osta, A. (2008). Effect of valproic acid on radiation-induced DNA damage in euchromatic and heterochromatic compartments. *Cell cycle* 7, 468-476.
103. Harly, C., Guillaume, Y., Nedellec, S., Peigne, C.M., Monkkonen, H., Monkkonen, J., Li, J., Kuball, J., Adams, E.J., Netzer, S., et al. (2012). Key implication of CD277/butyrophilin-3 (BTN3A) in cellular stress sensing by a major human gammadelta T-cell subset. *Blood* 120, 2269-2279.
104. Hayes, S.M., Shores, E.W., and Love, P.E. (2003). An architectural perspective on signaling by the pre-, alphabeta and gammadelta T cell receptors. *Immunological reviews* 191, 28-37.

105. He, Z., Wu, J., Su, X., Zhang, Y., Pan, L., Wei, H., Fang, Q., Li, H., Wang, D.L., and Sun, F.L. (2016). JMJD5 (Jumonji Domain-containing 5) Associates with Spindle Microtubules and Is Required for Proper Mitosis. *The Journal of biological chemistry* 291, 4684-4697.
106. Hebel, K., Weinert, S., Kuropka, B., Knolle, J., Kosak, B., Jorch, G., Arens, C., Krause, E., Braun-Dullaeus, R.C., and Brunner-Weinzierl, M.C. (2014). CD4+ T cells from human neonates and infants are poised spontaneously to run a nonclassical IL-4 program. *Journal of immunology* 192, 5160-5170.
107. Hedlund, M., Nagaeva, O., Kargl, D., Baranov, V., and Mincheva-Nilsson, L. (2011). Thermal- and oxidative stress causes enhanced release of NKG2D ligand-bearing immunosuppressive exosomes in leukemia/lymphoma T and B cells. *PLoS one* 6, e16899.
108. Heinz, S., Benner, C., Spann, N., Bertolino, E., Lin, Y.C., Laslo, P., Cheng, J.X., Murre, C., Singh, H., and Glass, C.K. (2010). Simple combinations of lineage-determining transcription factors prime cis-regulatory elements required for macrophage and B cell identities. *Molecular cell* 38, 576-589.
109. Hezroni, H., Koppstein, D., Schwartz, M.G., Avrutin, A., Bartel, D.P., and Ulitsky, I. (2015). Principles of long noncoding RNA evolution derived from direct comparison of transcriptomes in 17 species. *Cell reports* 11, 1110-1122.
110. Hilpert, J., Grosse-Hovest, L., Grunebach, F., Buechele, C., Nuebling, T., Raum, T., Steinle, A., and Salih, H.R. (2012). Comprehensive analysis of NKG2D ligand expression and release in leukemia: implications for NKG2D-mediated NK cell responses. *Journal of immunology* 189, 1360-1371.
111. Himoudi, N., Morgenstern, D.A., Yan, M., Vernay, B., Saraiva, L., Wu, Y., Cohen, C.J., Gustafsson, K., and Anderson, J. (2012). Human gammadelta T lymphocytes are licensed for professional antigen presentation by interaction with opsonized target cells. *Journal of immunology* 188, 1708-1716.
112. Hinz, T., Marx, S., Nerl, C., and Kabelitz, D. (1996). Clonal expansion of gamma delta T cells expressing two distinct T-cell receptors. *British journal of haematology* 94, 62-64.
113. Holdenrieder, S., Stieber, P., Peterfi, A., Nagel, D., Steinle, A., and Salih, H.R. (2006). Soluble MICA in malignant diseases. *International journal of cancer* 118, 684-687.
114. Holdenrieder, S., Stieber, P., Peterfi, A., Nagel, D., Steinle, A., and Salih, H.R. (2006). Soluble MICB in malignant diseases: analysis of diagnostic significance and correlation with soluble MICA. *Cancer immunology, immunotherapy* : CII 55, 1584-1589.
115. Holtmeier, W., and Kabelitz, D. (2005). gammadelta T cells link innate and adaptive immune responses. *Chemical immunology and allergy* 86, 151-183.

116. Hughes, T., Webb, R., Fei, Y., Wren, J.D., and Sawalha, A.H. (2010). DNA methylome in human CD4<sup>+</sup> T cells identifies transcriptionally repressive and non-repressive methylation peaks. *Genes and immunity* 11, 554-560.
117. Huovila, A.P., Turner, A.J., Pelto-Huikko, M., Karkkainen, I., and Ortiz, R.M. (2005). Shedding light on ADAM metalloproteinases. *Trends in biochemical sciences* 30, 413-422.
118. Isoherranen, N., Yagen, B., and Bialer, M. (2003). New CNS-active drugs which are second-generation valproic acid: can they lead to the development of a magic bullet? *Current opinion in neurology* 16, 203-211.
119. Jatinder Goyal, R.R. (2013). Evidence from clinical trials for the use of valproic acid in solid tumors: focus on prostate cancer. *Clinical Investigation* 3, 12.
120. Jinushi, M., Hodi, F.S., and Dranoff, G. (2006). Therapy-induced antibodies to MHC class I chain-related protein A antagonize immune suppression and stimulate antitumor cytotoxicity. *Proceedings of the National Academy of Sciences of the United States of America* 103, 9190-9195.
121. Joachims, M.L., Chain, J.L., Hooker, S.W., Knott-Craig, C.J., and Thompson, L.F. (2006). Human alpha beta and gamma delta thymocyte development: TCR gene rearrangements, intracellular TCR beta expression, and gamma delta developmental potential--differences between men and mice. *Journal of immunology* 176, 1543-1552.
122. Jonkers, I., and Lis, J.T. (2015). Getting up to speed with transcription elongation by RNA polymerase II. *Nature reviews. Molecular cell biology* 16, 167-177.
123. Kabelitz, D. (2016). Human gammadelta T cells: From a neglected lymphocyte population to cellular immunotherapy: A personal reflection of 30years of gammadelta T cell research. *Clinical immunology* 172, 90-97.
124. Kabelitz, D., and He, W. (2012). The multifunctionality of human Vgamma9Vdelta2 gammadelta T cells: clonal plasticity or distinct subsets? *Scandinavian journal of immunology* 76, 213-222.
125. Kabelitz, D., Kalyan, S., Oberg, H.H., and Wesch, D. (2013). Human Vdelta2 versus non-Vdelta2 gammadelta T cells in antitumor immunity. *Oncoimmunology* 2, e23304.
126. Kabelitz, D., Wesch, D., and He, W. (2007). Perspectives of gammadelta T cells in tumor immunology. *Cancer research* 67, 5-8.
127. Karimi, M.A., Aguilar, O.A., Zou, B., Bachmann, M.H., Carlyle, J.R., Baldwin, C.L., and Kambayashi, T. (2014). A truncated human NKG2D splice isoform negatively regulates NKG2D-mediated function. *Journal of immunology* 193, 2764-2771.

128. Karmodiya, K., Krebs, A.R., Oulad-Abdelghani, M., Kimura, H., and Tora, L. (2012). H3K9 and H3K14 acetylation co-occur at many gene regulatory elements, while H3K14ac marks a subset of inactive inducible promoters in mouse embryonic stem cells. *BMC genomics* 13, 424.
129. Kent, W.J., Sugnet, C.W., Furey, T.S., Roskin, K.M., Pringle, T.H., Zahler, A.M., and Haussler, D. (2002). The human genome browser at UCSC. *Genome research* 12, 996-1006.
130. Kiladjian, J.J., Mesa, R.A., and Hoffman, R. (2011). The renaissance of interferon therapy for the treatment of myeloid malignancies. *Blood* 117, 4706-4715.
131. Kornberg, R.D. (1974). Chromatin structure: a repeating unit of histones and DNA. *Science* 184, 868-871.
132. Kouzarides, T. (2007). Chromatin modifications and their function. *Cell* 128, 693-705.
133. Kowalczyk, M.S., Higgs, D.R., and Gingeras, T.R. (2012). Molecular biology: RNA discrimination. *Nature* 482, 310-311.
134. Koyanagi, M., Kerns, J.A., Chung, L., Zhang, Y., Brown, S., Moldoveanu, T., Malik, H.S., and Bix, M. (2010). Diversifying selection and functional analysis of interleukin-4 suggests antagonism-driven evolution at receptor-binding interfaces. *BMC evolutionary biology* 10, 223.
135. Kreslavsky, T., Gleimer, M., Garbe, A.I., and von Boehmer, H. (2010). alphabeta versus gammadelta fate choice: counting the T-cell lineages at the branch point. *Immunological reviews* 238, 169-181.
136. Kuleshov, M.V., Jones, M.R., Rouillard, A.D., Fernandez, N.F., Duan, Q., Wang, Z., Koplev, S., Jenkins, S.L., Jagodnik, K.M., Lachmann, A., et al. (2016). Enrichr: a comprehensive gene set enrichment analysis web server 2016 update. *Nucleic acids research* 44, W90-97.
137. Kulis, M., Merkel, A., Heath, S., Queiros, A.C., Schuyler, R.P., Castellano, G., Beekman, R., Raineri, E., Esteve, A., Clot, G., et al. (2015). Whole-genome fingerprint of the DNA methylome during human B cell differentiation. *Nature genetics* 47, 746-756.
138. Kumar, V., Yi Lo, P.H., Sawai, H., Kato, N., Takahashi, A., Deng, Z., Urabe, Y., Mbarek, H., Tokunaga, K., Tanaka, Y., et al. (2012). Soluble MICA and a MICA variation as possible prognostic biomarkers for HBV-induced hepatocellular carcinoma. *PloS one* 7, e44743.
139. Laad, A.D., Thomas, M.L., Fakhri, A.R., and Chiplunkar, S.V. (1999). Human gamma delta T cells recognize heat shock protein-60 on oral tumor cells. *International journal of cancer* 80, 709-714.
140. Lafont, V., Sanchez, F., Laprevotte, E., Michaud, H.A., Gros, L., Eliaou, J.F., and Bonnefoy, N. (2014). Plasticity of gammadelta T Cells: Impact on the Anti-Tumor Response. *Frontiers in immunology* 5, 622.

141. Lal, G., and Bromberg, J.S. (2009). Epigenetic mechanisms of regulation of Foxp3 expression. *Blood* 114, 3727-3735.
142. Lam, A.R., Le Bert, N., Ho, S.S., Shen, Y.J., Tang, M.L., Xiong, G.M., Croxford, J.L., Koo, C.X., Ishii, K.J., Akira, S., et al. (2014). RAE1 ligands for the NKG2D receptor are regulated by STING-dependent DNA sensor pathways in lymphoma. *Cancer research* 74, 2193-2203.
143. Landt, S.G., Marinov, G.K., Kundaje, A., Kheradpour, P., Pauli, F., Batzoglou, S., Bernstein, B.E., Bickel, P., Brown, J.B., Cayting, P., et al. (2012). ChIP-seq guidelines and practices of the ENCODE and modENCODE consortia. *Genome research* 22, 1813-1831.
144. Langmead, B., and Salzberg, S.L. (2012). Fast gapped-read alignment with Bowtie 2. *Nature methods* 9, 357-359.
145. Lanier, L.L. (2015). NKG2D Receptor and Its Ligands in Host Defense. *Cancer immunology research* 3, 575-582.
146. Lauritsen, J.P., Haks, M.C., Lefebvre, J.M., Kappes, D.J., and Wiest, D.L. (2006). Recent insights into the signals that control alphabeta/gammadelta-lineage fate. *Immunological reviews* 209, 176-190.
147. Ledru, E., Fevrier, M., Lecoeur, H., Garcia, S., Boullier, S., and Gougeon, M.L. (2003). A nonsecreted variant of interleukin-4 is associated with apoptosis: implication for the T helper-2 polarization in HIV infection. *Blood* 101, 3102-3105.
148. Lee, P.P., Fitzpatrick, D.R., Beard, C., Jessup, H.K., Lehar, S., Makar, K.W., Perez-Melgosa, M., Sweetser, M.T., Schlissel, M.S., Nguyen, S., et al. (2001). A critical role for Dnmt1 and DNA methylation in T cell development, function, and survival. *Immunity* 15, 763-774.
149. Legube, G., and Trouche, D. (2003). Regulating histone acetyltransferases and deacetylases. *EMBO reports* 4, 944-947.
150. Lenschow, D.J., Walunas, T.L., and Bluestone, J.A. (1996). CD28/B7 system of T cell costimulation. *Annual review of immunology* 14, 233-258.
151. Leoni, C., Vincenzetti, L., Emming, S., and Monticelli, S. (2015). Epigenetics of T lymphocytes in health and disease. *Swiss medical weekly* 145, w14191.
152. Li, J.J., Pan, K., Gu, M.F., Chen, M.S., Zhao, J.J., Wang, H., Liang, X.T., Sun, J.C., and Xia, J.C. (2013). Prognostic value of soluble MICA levels in the serum of patients with advanced hepatocellular carcinoma. *Chinese journal of cancer* 32, 141-148.
153. Linkermann, A., Stockwell, B.R., Krautwald, S., and Anders, H.J. (2014). Regulated cell death and inflammation: an auto-amplification loop causes organ failure. *Nature reviews. Immunology* 14, 759-767.



154. Liu, G., Atteridge, C.L., Wang, X., Lundgren, A.D., and Wu, J.D. (2010). The membrane type matrix metalloproteinase MMP14 mediates constitutive shedding of MHC class I chain-related molecule A independent of A disintegrin and metalloproteinases. *Journal of immunology* 184, 3346-3350.
155. Love, M.I., Huber, W., and Anders, S. (2014). Moderated estimation of fold change and dispersion for RNA-seq data with DESeq2. *Genome biology* 15, 550.
156. Luchenko, V.L., Litman, T., Chakraborty, A.R., Heffner, A., Devor, C., Wilkerson, J., Stein, W., Robey, R.W., Bangiolo, L., Levens, D., and Bates, S.E. (2014). Histone deacetylase inhibitor-mediated cell death is distinct from its global effect on chromatin. *Molecular oncology* 8, 1379-1392.
157. Lv, J., Du, C., Wei, W., Wu, Z., Zhao, G., Li, Z., and Xie, X. (2012). The antiepileptic drug valproic acid restores T cell homeostasis and ameliorates pathogenesis of experimental autoimmune encephalomyelitis. *The Journal of biological chemistry* 287, 28656-28665.
158. Mangino, M., Roederer, M., Beddall, M.H., Nestle, F.O., and Spector, T.D. (2017). Innate and adaptive immune traits are differentially affected by genetic and environmental factors. *Nature communications* 8, 13850.
159. Maniar, A., Zhang, X., Lin, W., Gastman, B.R., Pauza, C.D., Strome, S.E., and Chapoval, A.I. (2010). Human gammadelta T lymphocytes induce robust NK cell-mediated antitumor cytotoxicity through CD137 engagement. *Blood* 116, 1726-1733.
160. Mao, Y., Yin, S., Zhang, J., Hu, Y., Huang, B., Cui, L., Kang, N., and He, W. (2016). A new effect of IL-4 on human gammadelta T cells: promoting regulatory Vdelta1 T cells via IL-10 production and inhibiting function of Vdelta2 T cells. *Cellular & molecular immunology* 13, 217-228.
161. Mardis, E.R. (2008). Next-generation DNA sequencing methods. *Annual review of genomics and human genetics* 9, 387-402.
162. Marten, A., von Lilienfeld-Toal, M., Buchler, M.W., and Schmidt, J. (2006). Soluble MIC is elevated in the serum of patients with pancreatic carcinoma diminishing gammadelta T cell cytotoxicity. *International journal of cancer* 119, 2359-2365.
163. Martin, M. (2011). Cutadapt removes adapter sequences from high-throughput sequencing reads. 2011 17.
164. Mashima, T., Seimiya, H., and Tsuruo, T. (2009). De novo fatty-acid synthesis and related pathways as molecular targets for cancer therapy. *British journal of cancer* 100, 1369-1372.
165. Maston, G.A., Evans, S.K., and Green, M.R. (2006). Transcriptional regulatory elements in the human genome. *Annual review of genomics and human genetics* 7, 29-59.

166. Medina-Rivera, A., Defrance, M., Sand, O., Herrmann, C., Castro-Mondragon, J.A., Delerce, J., Jaeger, S., Blanchet, C., Vincens, P., Caron, C., et al. (2015). RSAT 2015: Regulatory Sequence Analysis Tools. *Nucleic acids research* 43, W50-56.
167. Metzger, R., Heckl-Ostreicher, B., Nerl, C., Schondelmaier, S., and Kabelitz, D. (1992). Immunological studies of gamma delta T cells in a case of large granular lymphocyte (LGL) leukemia: leukemic gamma delta+ T cells are resistant to growth stimulation in vitro but respond to interferon-alpha treatment in vivo. *Leukemia research* 16, 1087-1095.
168. Metzker, M.L. (2010). Sequencing technologies - the next generation. *Nature reviews. Genetics* 11, 31-46.
169. Meyer, C.A., and Liu, X.S. (2014). Identifying and mitigating bias in next-generation sequencing methods for chromatin biology. *Nature reviews. Genetics* 15, 709-721.
170. Mi, H., Huang, X., Muruganujan, A., Tang, H., Mills, C., Kang, D., and Thomas, P.D. (2017). PANTHER version 11: expanded annotation data from Gene Ontology and Reactome pathways, and data analysis tool enhancements. *Nucleic acids research* 45, D183-D189.
171. Michie, A.M., and Zuniga-Pflucker, J.C. (2002). Regulation of thymocyte differentiation: pre-TCR signals and beta-selection. *Seminars in immunology* 14, 311-323.
172. Moarii, M., Boeva, V., Vert, J.P., and Reyal, F. (2015). Changes in correlation between promoter methylation and gene expression in cancer. *BMC genomics* 16, 873.
173. Mochizuki, S., and Okada, Y. (2007). ADAMs in cancer cell proliferation and progression. *Cancer science* 98, 621-628.
174. Morales, J.C., Ruiz-Magana, M.J., Carranza, D., Ortiz-Ferron, G., and Ruiz-Ruiz, C. (2010). HDAC inhibitors with different gene regulation activities depend on the mitochondrial pathway for the sensitization of leukemic T cells to TRAIL-induced apoptosis. *Cancer letters* 297, 91-100.
175. Morris, T.J., and Beck, S. (2015). Analysis pipelines and packages for Infinium HumanMethylation450 BeadChip (450k) data. *Methods* 72, 3-8.
176. Munster, P., Marchion, D., Bicaku, E., Lacevic, M., Kim, J., Centeno, B., Daud, A., Neuger, A., Minton, S., and Sullivan, D. (2009). Clinical and biological effects of valproic acid as a histone deacetylase inhibitor on tumor and surrogate tissues: phase I/II trial of valproic acid and epirubicin/FEC. *Clinical cancer research : an official journal of the American Association for Cancer Research* 15, 2488-2496.
177. Nedellec, S., Sabourin, C., Bonneville, M., and Scotet, E. (2010). NKG2D costimulates human V gamma 9V delta 2 T cell antitumor cytotoxicity through protein kinase C theta-dependent

- modulation of early TCR-induced calcium and transduction signals. *Journal of immunology* 185, 55-63.
- 178.** Ness-Schwickerath, K.J., Jin, C., and Morita, C.T. (2010). Cytokine requirements for the differentiation and expansion of IL-17A- and IL-22-producing human Vgamma2Vdelta2 T cells. *Journal of immunology* 184, 7268-7280.
- 179.** Nguyen, M.L., Jones, S.A., Prier, J.E., and Russ, B.E. (2015). Transcriptional Enhancers in the Regulation of T Cell Differentiation. *Frontiers in immunology* 6, 462.
- 180.** Nie, Z., Hu, G., Wei, G., Cui, K., Yamane, A., Resch, W., Wang, R., Green, D.R., Tessarollo, L., Casellas, R., et al. (2012). c-Myc is a universal amplifier of expressed genes in lymphocytes and embryonic stem cells. *Cell* 151, 68-79.
- 181.** Oberg, H.H., Wesch, D., Grussel, S., Rose-John, S., and Kabelitz, D. (2006). Differential expression of CD126 and CD130 mediates different STAT-3 phosphorylation in CD4+CD25- and CD25high regulatory T cells. *International immunology* 18, 555-563.
- 182.** Ortiz, M., Guex, N., Patin, E., Martin, O., Xenarios, I., Ciuffi, A., Quintana-Murci, L., and Telenti, A. (2009). Evolutionary trajectories of primate genes involved in HIV pathogenesis. *Molecular biology and evolution* 26, 2865-2875.
- 183.** Pai, A.A., Cain, C.E., Mizrahi-Man, O., De Leon, S., Lewellen, N., Veyrieras, J.B., Degner, J.F., Gaffney, D.J., Pickrell, J.K., Stephens, M., et al. (2012). The contribution of RNA decay quantitative trait loci to inter-individual variation in steady-state gene expression levels. *PLoS genetics* 8, e1003000.
- 184.** Passarge, E. (1979). Emil Heitz and the concept of heterochromatin: longitudinal chromosome differentiation was recognized fifty years ago. *American journal of human genetics* 31, 106-115.
- 185.** Patten, P., Yokota, T., Rothbard, J., Chien, Y., Arai, K., and Davis, M.M. (1984). Structure, expression and divergence of T-cell receptor beta-chain variable regions. *Nature* 312, 40-46.
- 186.** Pegram, H.J., Andrews, D.M., Smyth, M.J., Darcy, P.K., and Kershaw, M.H. (2011). Activating and inhibitory receptors of natural killer cells. *Immunology and cell biology* 89, 216-224.
- 187.** Pekowska, A., Benoukraf, T., Ferrier, P., and Spicuglia, S. (2010). A unique H3K4me2 profile marks tissue-specific gene regulation. *Genome research* 20, 1493-1502.
- 188.** Peters, C., Oberg, H.H., Kabelitz, D., and Wesch, D. (2014). Phenotype and regulation of immunosuppressive Vdelta2-expressing gammadelta T cells. *Cellular and molecular life sciences : CMLS* 71, 1943-1960.
- 189.** Petty, E., and Pillus, L. (2013). Balancing chromatin remodeling and histone modifications in transcription. *Trends in genetics : TIG* 29, 621-629.

190. Philipp, S., Sosna, J., Plenge, J., Kalthoff, H., and Adam, D. (2015). Homoharringtonine, a clinically approved anti-leukemia drug, sensitizes tumor cells for TRAIL-induced necroptosis. *Cell communication and signaling : CCS* 13, 25.
191. Plongthongkum, N., Diep, D.H., and Zhang, K. (2014). Advances in the profiling of DNA modifications: cytosine methylation and beyond. *Nature reviews. Genetics* 15, 647-661.
192. Pont, F., Familiades, J., Dejean, S., Fruchon, S., Cendron, D., Poupot, M., Poupot, R., L'Faqihi-Olive, F., Prade, N., Ycart, B., and Fournie, J.J. (2012). The gene expression profile of phosphoantigen-specific human gammadelta T lymphocytes is a blend of alphabeta T-cell and NK-cell signatures. *European journal of immunology* 42, 228-240.
193. Prabakaran, S., Lippens, G., Steen, H., and Gunawardena, J. (2012). Post-translational modification: nature's escape from genetic imprisonment and the basis for dynamic information encoding. *Wiley interdisciplinary reviews. Systems biology and medicine* 4, 565-583.
194. Proft, T., and Fraser, J.D. (2003). Bacterial superantigens. *Clinical and experimental immunology* 133, 299-306.
195. Qu, K., Zaba, L.C., Giresi, P.G., Li, R., Longmire, M., Kim, Y.H., Greenleaf, W.J., and Chang, H.Y. (2015). Individuality and variation of personal regulomes in primary human T cells. *Cell systems* 1, 51-61.
196. Quabius, E.S., Ossenkop, L., Harder, S., and Kern, M. (2012). Dental implants stimulate expression of Interleukin-8 and its receptor in human blood--an in vitro approach. *Journal of biomedical materials research. Part B, Applied biomaterials* 100, 1283-1288.
197. Quinn, J.J., and Chang, H.Y. (2016). Unique features of long non-coding RNA biogenesis and function. *Nature reviews. Genetics* 17, 47-62.
198. Ramachandran, S., and Henikoff, S. (2016). Nucleosome dynamics during chromatin remodeling in vivo. *Nucleus* 7, 20-26.
199. Ramirez, F., Dundar, F., Diehl, S., Gruning, B.A., and Manke, T. (2014). deepTools: a flexible platform for exploring deep-sequencing data. *Nucleic acids research* 42, W187-191.
200. Ranzani, V., Rossetti, G., Panzeri, I., Arrigoni, A., Bonnal, R.J., Curti, S., Gruarin, P., Provasi, E., Sugliano, E., Marconi, M., et al. (2015). The long intergenic noncoding RNA landscape of human lymphocytes highlights the regulation of T cell differentiation by linc-MAF-4. *Nature immunology* 16, 318-325.
201. Raulet, D.H. (2003). Roles of the NKG2D immunoreceptor and its ligands. *Nature reviews. Immunology* 3, 781-790.

202. Raulet, D.H., Gasser, S., Gowen, B.G., Deng, W., and Jung, H. (2013). Regulation of ligands for the NKG2D activating receptor. *Annual review of immunology* 31, 413-441.
203. Rebmann, V., Schutt, P., Brandhorst, D., Opalka, B., Moritz, T., Nowrouzian, M.R., and Grosse-Wilde, H. (2007). Soluble MICA as an independent prognostic factor for the overall survival and progression-free survival of multiple myeloma patients. *Clinical immunology* 123, 114-120.
204. Rhodes, D.A., Stammers, M., Malcherek, G., Beck, S., and Trowsdale, J. (2001). The cluster of BTN genes in the extended major histocompatibility complex. *Genomics* 71, 351-362.
205. Riano, F., Karunakaran, M.M., Starick, L., Li, J., Scholz, C.J., Kunzmann, V., Olive, D., Amslinger, S., and Herrmann, T. (2014). Vgamma9Vdelta2 TCR-activation by phosphorylated antigens requires butyrophilin 3 A1 (BTN3A1) and additional genes on human chromosome 6. *European journal of immunology* 44, 2571-2576.
206. Ritchie, M.D., Holzinger, E.R., Li, R., Pendergrass, S.A., and Kim, D. (2015). Methods of integrating data to uncover genotype-phenotype interactions. *Nature reviews. Genetics* 16, 85-97.
207. Roberts, S., and Girardi, M. (2008). Conventional and Unconventional T Cells. In *Clinical and Basic Immunodermatology*, A.A. Gaspari, and S.K. Tyring, eds. (London: Springer London), pp. 85-104.
208. Robinson, J., Mistry, K., McWilliam, H., Lopez, R., Parham, P., and Marsh, S.G. (2011). The IMGT/HLA database. *Nucleic acids research* 39, D1171-1176.
209. Roelofs, A.J., Jauhainen, M., Mönkkönen, H., Rogers, M.J., Mönkkönen, J., and Thompson, K. (2009). Peripheral blood monocytes are responsible for  $\gamma\delta$  T cell activation induced by zoledronic acid through accumulation of IPP/DMAPP. *British journal of haematology* 144, 245-250.
210. Salih, H.R., Rammensee, H.G., and Steinle, A. (2002). Cutting edge: down-regulation of MICA on human tumors by proteolytic shedding. *Journal of immunology* 169, 4098-4102.
211. Sandstrom, A., Peigne, C.M., Leger, A., Crooks, J.E., Konczak, F., Gesnel, M.C., Breathnach, R., Bonneville, M., Scotet, E., and Adams, E.J. (2014). The intracellular B30.2 domain of butyrophilin 3A1 binds phosphoantigens to mediate activation of human Vgamma9Vdelta2 T cells. *Immunity* 40, 490-500.
212. Santoro, F., Botrugno, O.A., Dal Zuffo, R., Pallavicini, I., Matthews, G.M., Cluse, L., Barozzi, I., Senese, S., Fornasari, L., Moretti, S., et al. (2013). A dual role for Hdac1: oncosuppressor in tumorigenesis, oncogene in tumor maintenance. *Blood* 121, 3459-3468.
213. Schmolka, N., Serre, K., Grosso, A.R., Rei, M., Pennington, D.J., Gomes, A.Q., and Silva-Santos, B. (2013). Epigenetic and transcriptional signatures of stable versus plastic differentiation of proinflammatory gammadelta T cell subsets. *Nature immunology* 14, 1093-1100.

214. Schones, D.E., Cui, K., Cuddapah, S., Roh, T.Y., Barski, A., Wang, Z., Wei, G., and Zhao, K. (2008). Dynamic regulation of nucleosome positioning in the human genome. *Cell* 132, 887-898.
215. Schubeler, D. (2009). Epigenomics: Methylation matters. *Nature* 462, 296-297.
216. Schwartz, C., Palissot, V., Aouali, N., Wack, S., Brons, N.H., Leners, B., Bosseler, M., and Berchem, G. (2007). Valproic acid induces non-apoptotic cell death mechanisms in multiple myeloma cell lines. *International journal of oncology* 30, 573-582.
217. Scotet, E., Martinez, L.O., Grant, E., Barbaras, R., Jenou, P., Guiraud, M., Monsarrat, B., Saulquin, X., Maillet, S., Esteve, J.P., et al. (2005). Tumor recognition following Vgamma9Vdelta2 T cell receptor interactions with a surface F1-ATPase-related structure and apolipoprotein A-I. *Immunity* 22, 71-80.
218. Seals, D.F., and Courtneidge, S.A. (2003). The ADAMs family of metalloproteases: multidomain proteins with multiple functions. *Genes & development* 17, 7-30.
219. Sebestyén, Z., Scheper, W., Vyborova, A., Gu, S., Rychnavska, Z., Schiffler, M., Cleven, A., Cheneau, C., van Noorden, M., Peigne, C.M., et al. (2016). RhoB Mediates Phosphoantigen Recognition by Vgamma9Vdelta2 T Cell Receptor. *Cell reports* 15, 1973-1985.
220. Sellars, M., Huh, J.R., Day, K., Issuree, P.D., Galan, C., Gobeil, S., Absher, D., Green, M.R., and Littman, D.R. (2015). Regulation of DNA methylation dictates Cd4 expression during the development of helper and cytotoxic T cell lineages. *Nature immunology* 16, 746-754.
221. Sen, D.R., Kaminski, J., Barnitz, R.A., Kurachi, M., Gerdemann, U., Yates, K.B., Tsao, H.W., Godec, J., LaFleur, M.W., Brown, F.D., et al. (2016). The epigenetic landscape of T cell exhaustion. *Science* 354, 1165-1169.
222. Sharma, S., Symanowski, J., Wong, B., Dino, P., Manno, P., and Vogelzang, N. (2008). A Phase II Clinical Trial of Oral Valproic Acid in Patients with Castration-Resistant Prostate Cancers Using an Intensive Biomarker Sampling Strategy. *Translational oncology* 1, 141-147.
223. Silva-Santos, B., Serre, K., and Norell, H. (2015). gammadelta T cells in cancer. *Nature reviews. Immunology* 15, 683-691.
224. Song, H., Kim, J., Cosman, D., and Choi, I. (2006). Soluble ULBP suppresses natural killer cell activity via down-regulating NKG2D expression. *Cellular immunology* 239, 22-30.
225. Sosna, J., Voigt, S., Mathieu, S., Kabelitz, D., Trad, A., Janssen, O., Meyer-Schwesinger, C., Schutze, S., and Adam, D. (2013). The proteases HtrA2/Omi and UCH-L1 regulate TNF-induced necroptosis. *Cell communication and signaling : CCS* 11, 76.

226. Spear, P., Wu, M.R., Sentman, M.L., and Sentman, C.L. (2013). NKG2D ligands as therapeutic targets. *Cancer immunity* 13, 8.
227. Spinozzi, F., Nicoletti, I., Agea, E., Belia, S., Moraca, R., Migliorati, G., Riccardi, C., Grignani, F., and Bertotto, A. (1995). IL-4 is able to reverse the CD2-mediated negative apoptotic signal to CD4-CD8- alpha beta and/or gamma delta T lymphocytes. *Immunology* 86, 379-384.
228. Spits, H. (2002). Development of alphabeta T cells in the human thymus. *Nature reviews. Immunology* 2, 760-772.
229. Stein, G.M., Pfuller, U., Schietzel, M., and Bussing, A. (2000). Expression of interleukin-4 in apoptotic cells: stimulation of the type-2 cytokine by different toxins in human peripheral blood mononuclear and tumor cells. *Cytometry* 41, 261-270.
230. Strahl, B.D., and Allis, C.D. (2000). The language of covalent histone modifications. *Nature* 403, 41-45.
231. Sturmhofel, K., Brando, C., Martinon, F., Shevach, E.M., and Coligan, J.E. (1995). Antigen-independent, integrin-mediated T cell activation. *Journal of immunology* 154, 2104-2111.
232. Su, J.M., Li, X.N., Thompson, P., Ou, C.N., Ingle, A.M., Russell, H., Lau, C.C., Adamson, P.C., and Blaney, S.M. (2011). Phase 1 study of valproic acid in pediatric patients with refractory solid or CNS tumors: a children's oncology group report. *Clinical cancer research : an official journal of the American Association for Cancer Research* 17, 589-597.
233. Swiatecka-Urban, A., Talebian, L., Kanno, E., Moreau-Marquis, S., Coutermarsh, B., Hansen, K., Karlson, K.H., Barnaby, R., Cheney, R.E., Langford, G.M., et al. (2007). Myosin Vb is required for trafficking of the cystic fibrosis transmembrane conductance regulator in Rab11a-specific apical recycling endosomes in polarized human airway epithelial cells. *The Journal of biological chemistry* 282, 23725-23736.
234. Szklarczyk, D., Franceschini, A., Wyder, S., Forslund, K., Heller, D., Huerta-Cepas, J., Simonovic, M., Roth, A., Santos, A., Tsafou, K.P., et al. (2015). STRING v10: protein-protein interaction networks, integrated over the tree of life. *Nucleic acids research* 43, D447-452.
235. Tak, Y.G., and Farnham, P.J. (2015). Making sense of GWAS: using epigenomics and genome engineering to understand the functional relevance of SNPs in non-coding regions of the human genome. *Epigenetics & chromatin* 8, 57.
236. Talbert, P.B., and Henikoff, S. (2017). Histone variants on the move: substrates for chromatin dynamics. *Nature reviews. Molecular cell biology* 18, 115-126.

237. Tanaka, Y., Morita, C.T., Tanaka, Y., Nieves, E., Brenner, M.B., and Bloom, B.R. (1995). Natural and synthetic non-peptide antigens recognized by human gamma delta T cells. *Nature* 375, 155-158.
238. Tanaka, Y., Ono, N., Shima, T., Tanaka, G., Katoh, Y., Nakayama, K., Takatsu, H., and Shin, H.W. (2016). The phospholipid flippase ATP9A is required for the recycling pathway from the endosomes to the plasma membrane. *Molecular biology of the cell* 27, 3883-3893.
239. Th'ng, J.P. (2001). Histone modifications and apoptosis: cause or consequence? *Biochemistry and cell biology = Biochimie et biologie cellulaire* 79, 305-311.
240. Trapnell, C., Roberts, A., Goff, L., Pertea, G., Kim, D., Kelley, D.R., Pimentel, H., Salzberg, S.L., Rinn, J.L., and Pachter, L. (2012). Differential gene and transcript expression analysis of RNA-seq experiments with TopHat and Cufflinks. *Nature protocols* 7, 562-578.
241. Tsagaratou, A., Aijo, T., Lio, C.W., Yue, X., Huang, Y., Jacobsen, S.E., Lahdesmaki, H., and Rao, A. (2014). Dissecting the dynamic changes of 5-hydroxymethylcytosine in T-cell development and differentiation. *Proceedings of the National Academy of Sciences of the United States of America* 111, E3306-3315.
242. Tsompana, M., and Buck, M.J. (2014). Chromatin accessibility: a window into the genome. *Epigenetics & chromatin* 7, 33.
243. Tullai, J.W., Schaffer, M.E., Mullenbrock, S., Sholder, G., Kasif, S., and Cooper, G.M. (2007). Immediate-early and delayed primary response genes are distinct in function and genomic architecture. *The Journal of biological chemistry* 282, 23981-23995.
244. Uldrich, A.P., Le Nours, J., Pellicci, D.G., Gherardin, N.A., McPherson, K.G., Lim, R.T., Patel, O., Beddoe, T., Gras, S., Rossjohn, J., and Godfrey, D.I. (2013). CD1d-lipid antigen recognition by the gammadelta TCR. *Nature immunology* 14, 1137-1145.
245. Valapour, M., Guo, J., Schroeder, J.T., Keen, J., Cianferoni, A., Casolaro, V., and Georas, S.N. (2002). Histone deacetylation inhibits IL4 gene expression in T cells. *The Journal of allergy and clinical immunology* 109, 238-245.
246. Valinezhad Orang, A., Safaralizadeh, R., and Kazemzadeh-Bavili, M. (2014). Mechanisms of miRNA-Mediated Gene Regulation from Common Downregulation to mRNA-Specific Upregulation. *International journal of genomics* 2014, 970607.
247. van Eijk, K.R., de Jong, S., Boks, M.P., Langeveld, T., Colas, F., Veldink, J.H., de Kovel, C.G., Janson, E., Strengman, E., Langfelder, P., et al. (2012). Genetic analysis of DNA methylation and gene expression levels in whole blood of healthy human subjects. *BMC genomics* 13, 636.



- 248.** Vanhille, L., Griffon, A., Maqbool, M.A., Zacarias-Cabeza, J., Dao, L.T., Fernandez, N., Ballester, B., Andrau, J.C., and Spicuglia, S. (2015). High-throughput and quantitative assessment of enhancer activity in mammals by CapStarr-seq. *Nature communications* 6, 6905.
- 249.** Vantourout, P., and Hayday, A. (2013). Six-of-the-best: unique contributions of gammadelta T cells to immunology. *Nature reviews. Immunology* 13, 88-100.
- 250.** Vasiliev, A.M., Vasilenko, R.N., Kulikova, N.L., Andreev, S.M., Chikileva, I.O., Puchkova, G.Y., Kosarev, I.V., Khodyakova, A.V., Khlebnikov, V.S., Ptitsyn, L.R., et al. (2003). Structural and functional properties of IL-4delta2, an alternative splice variant of human IL-4. *Journal of proteome research* 2, 273-281.
- 251.** Vavassori, S., Kumar, A., Wan, G.S., Ramanjaneyulu, G.S., Cavallari, M., El Daker, S., Beddoe, T., Theodossis, A., Williams, N.K., Gostick, E., et al. (2013). Butyrophilin 3A1 binds phosphorylated antigens and stimulates human gammadelta T cells. *Nature immunology* 14, 908-916.
- 252.** Venkatesh, S., and Workman, J.L. (2015). Histone exchange, chromatin structure and the regulation of transcription. *Nature reviews. Molecular cell biology* 16, 178-189.
- 253.** Viaud, S., Terme, M., Flament, C., Taieb, J., Andre, F., Novault, S., Escudier, B., Robert, C., Caillat-Zucman, S., Tursz, T., et al. (2009). Dendritic cell-derived exosomes promote natural killer cell activation and proliferation: a role for NKG2D ligands and IL-15Ralpha. *PloS one* 4, e4942.
- 254.** Vroom, T.M., Scholte, G., Ossendorp, F., and Borst, J. (1991). Tissue distribution of human gamma delta T cells: no evidence for general epithelial tropism. *Journal of clinical pathology* 44, 1012-1017.
- 255.** Waddington (1942). The epigenotype. *Endeavour* 1, 3.
- 256.** Waldhauer, I., Goehlsdorf, D., Gieseke, F., Weinschenk, T., Wittenbrink, M., Ludwig, A., Stevanovic, S., Rammensee, H.G., and Steinle, A. (2008). Tumor-associated MICA is shed by ADAM proteases. *Cancer research* 68, 6368-6376.
- 257.** Walker, D.L., Bhagwate, A.V., Baheti, S., Smalley, R.L., Hilker, C.A., Sun, Z., and Cunningham, J.M. (2015). DNA methylation profiling: comparison of genome-wide sequencing methods and the Infinium Human Methylation 450 Bead Chip. *Epigenomics* 7, 1287-1302.
- 258.** Wang, K.C., and Chang, H.Y. (2011). Molecular mechanisms of long noncoding RNAs. *Molecular cell* 43, 904-914.
- 259.** Wang, Q., Miyakawa, Y., Fox, N., and Kaushansky, K. (2000). Interferon-alpha directly represses megakaryopoiesis by inhibiting thrombopoietin-induced signaling through induction of SOCS-1. *Blood* 96, 2093-2099.

- 260.** Wang, Y.C., Peterson, S.E., and Loring, J.F. (2014). Protein post-translational modifications and regulation of pluripotency in human stem cells. *Cell research* 24, 143-160.
- 261.** Watson, M., Chow, S., Barsyte, D., Arrowsmith, C., Shankey, T.V., Minden, M., and Hedley, D. (2014). The study of epigenetic mechanisms based on the analysis of histone modification patterns by flow cytometry. *Cytometry. Part A : the journal of the International Society for Analytical Cytology* 85, 78-87.
- 262.** Weber, C.M., and Henikoff, S. (2014). Histone variants: dynamic punctuation in transcription. *Genes & development* 28, 672-682.
- 263.** Weidmann, E., Hinz, T., Klein, S., Schui, D.K., Harder, S., Kriener, S., Kabelitz, D., Hoelzer, D., and Mitrou, P.S. (2000). Cytotoxic hepatosplenic gammadelta T-cell lymphoma following acute myeloid leukemia bearing two distinct gamma chains of the T-cell receptor. *Biologic and clinical features. Haematologica* 85, 1024-1031.
- 264.** Wesch, D., Glatzel, A., and Kabelitz, D. (2001). Differentiation of resting human peripheral blood gamma delta T cells toward Th1- or Th2-phenotype. *Cellular immunology* 212, 110-117.
- 265.** Wesch, D., Marx, S., and Kabelitz, D. (1997). Comparative analysis of  $\alpha\beta$  and  $\gamma\delta$  T cell activation by *Mycobacterium tuberculosis* and isopentenyl pyrophosphate. *European journal of immunology* 27, 952-956.
- 266.** West, A.C., and Johnstone, R.W. (2014). New and emerging HDAC inhibitors for cancer treatment. *The Journal of clinical investigation* 124, 30-39.
- 267.** Wrobel, P., Shojaei, H., Schitteck, B., Gieseler, F., Wollenberg, B., Kalthoff, H., Kabelitz, D., and Wesch, D. (2007). Lysis of a broad range of epithelial tumour cells by human gamma delta T cells: involvement of NKG2D ligands and T-cell receptor- versus NKG2D-dependent recognition. *Scandinavian journal of immunology* 66, 320-328.
- 268.** Wu, C., and Morris, J.R. (2001). Genes, genetics, and epigenetics: a correspondence. *Science* 293, 1103-1105.
- 269.** Wu, J.D., Higgins, L.M., Steinle, A., Cosman, D., Haugk, K., and Plymate, S.R. (2004). Prevalent expression of the immunostimulatory MHC class I chain-related molecule is counteracted by shedding in prostate cancer. *The Journal of clinical investigation* 114, 560-568.
- 270.** Wu, X., Tao, Y., Hou, J., Meng, X., and Shi, J. (2012). Valproic acid upregulates NKG2D ligand expression through an ERK-dependent mechanism and potentially enhances NK cell-mediated lysis of myeloma. *Neoplasia* 14, 1178-1189.
- 271.** Xing, Y., and Hogquist, K.A. (2012). T-cell tolerance: central and peripheral. *Cold Spring Harbor perspectives in biology* 4.

- 272.** Yagi, Y., Fushida, S., Harada, S., Kinoshita, J., Makino, I., Oyama, K., Tajima, H., Fujita, H., Takamura, H., Ninomiya, I., et al. (2010). Effects of valproic acid on the cell cycle and apoptosis through acetylation of histone and tubulin in a scirrhous gastric cancer cell line. *Journal of experimental & clinical cancer research* : CR 29, 149.
- 273.** Yamaguchi, K., Lantowski, A., Dannenberg, A.J., and Subbaramaiah, K. (2005). Histone deacetylase inhibitors suppress the induction of c-Jun and its target genes including COX-2. *The Journal of biological chemistry* 280, 32569-32577.
- 274.** Yang, X.J., and Seto, E. (2007). HATs and HDACs: from structure, function and regulation to novel strategies for therapy and prevention. *Oncogene* 26, 5310-5318.
- 275.** Yoo, C.B., and Jones, P.A. (2006). Epigenetic therapy of cancer: past, present and future. *Nature reviews. Drug discovery* 5, 37-50.
- 276.** Yoshikai, Y., Kimura, N., Toyonaga, B., and Mak, T.W. (1986). Sequences and repertoire of human T cell receptor alpha chain variable region genes in mature T lymphocytes. *The Journal of experimental medicine* 164, 90-103.
- 277.** Zafirova, B., Wensveen, F.M., Gulin, M., and Polic, B. (2011). Regulation of immune cell function and differentiation by the NKG2D receptor. *Cellular and molecular life sciences : CMLS* 68, 3519-3529.
- 278.** Zaina, S., Perez-Luque, E.L., and Lund, G. (2010). Genetics talks to epigenetics? The interplay between sequence variants and chromatin structure. *Current genomics* 11, 359-367.
- 279.** Zhang, D., Pasternack, M.S., Beresford, P.J., Wagner, L., Greenberg, A.H., and Lieberman, J. (2001). Induction of rapid histone degradation by the cytotoxic T lymphocyte protease Granzyme A. *The Journal of biological chemistry* 276, 3683-3690.
- 280.** Zhang, J., Basher, F., and Wu, J.D. (2015). NKG2D Ligands in Tumor Immunity: Two Sides of a Coin. *Frontiers in immunology* 6, 97.
- 281.** Zhang, Y., Liu, T., Meyer, C.A., Eeckhoute, J., Johnson, D.S., Bernstein, B.E., Nusbaum, C., Myers, R.M., Brown, M., Li, W., and Liu, X.S. (2008). Model-based analysis of ChIP-Seq (MACS). *Genome biology* 9, R137.
- 282.** Zilbauer, M., Rayner, T.F., Clark, C., Coffey, A.J., Joyce, C.J., Palta, P., Palotie, A., Lyons, P.A., and Smith, K.G. (2013). Genome-wide methylation analyses of primary human leukocyte subsets identifies functionally important cell-type-specific hypomethylated regions. *Blood* 122, e52-60.
- 283.** Ziller, M.J., Hansen, K.D., Meissner, A., and Aryee, M.J. (2015). Coverage recommendations for methylation analysis by whole-genome bisulfite sequencing. *Nature methods* 12, 230-232.

## References

- 284.** Zocchi, M.R., Catellani, S., Canevali, P., Tavella, S., Garuti, A., Villaggio, B., Zunino, A., Gobbi, M., Fraternali-Orcioni, G., Kunkl, A., et al. (2012). High ERp5/ADAM10 expression in lymph node microenvironment and impaired NKG2D ligands recognition in Hodgkin lymphomas. *Blood* 119, 1479-1489.
- 285.** Zorca, C.E., Kim, L.K., Kim, Y.J., Krause, M.R., Zenklusen, D., Spilianakis, C.G., and Flavell, R.A. (2015). Myosin VI regulates gene pairing and transcriptional pause release in T cells. *Proceedings of the National Academy of Sciences of the United States of America* 112, E1587-1593.

### 11. Appendix

#### 11.1 Acknowledgements

Finishing the PhD is a landmark in the life of every researcher and it is my honor to say “thank you” to all those people who contributed to achieve this landmark. First of all, I would like to thank Prof. Dr. Dieter Kabelitz for giving me the opportunity to do my PhD in his institute. I am thankful for his trust, support, care, guidance and constant enthusiasm, especially when I needed it most. Being an international student, it was a very big thing. Thanks for making it much easier! I am grateful to Prof. Thomas Bosch for being first examiner on the thesis committee, Prof. Hinrich Schulenburg and Prof. Andre Franke for being my doctoral committee members. I wish to express my deepest gratitude to Prof. Andreas Radbruch, Prof. Shubhada Chiplunkar, Prof. Dr. Rajiv Sarin, Dr. Narendra Joshi, Prof. Milind Gore and Prof. Raghunath Mahajan for being my referee and supporting me during stepping up the ladders of professional life.

My special thanks are due to PD Dr. Marcus Lettau and Dr. Guranda Chitadze being with me from the time of arrival in Kiel until this moment. Marcus, I am very lucky to have a chance to work with you. It’s really great that I started and will end working with you, though on different projects! Also thanks for thesis corrections, discussions and many more things. You are definitely not only my mentor. Guranda, thank you for your great friendship in personal and professional life, your constant support, motivation during ups-and-downs of my ‘exciting’ German life and listening to my crazy theories, hypotheses and ideas of science about real life.

I owe big thanks to Frau Birgit Schlenga and Frau Doreen Eckert for helping me through all the German bureaucracy and day-to-day institutional affairs.

The biggest contribution to my success is from all my collaborators. I thank you all, especially Prof. Martin Vingron and Johannes Helmuth for exciting turn in the life of ATAC-seq project. Johannes, your last minute help is also very much appreciated. Equally special thanks for the help and guidance to Matthias Hübenthal for miRNA project, Dr. Justyna Sosna for cell death project and Dr. Jürgen Fritsch for ImageStream experiments. Prof. Dr. Christoph Kaleta, Daniela Esser, Dr. Silvio Waschina and Peer Aramillo Irizar, I would like to thank you all for being my true neighbors. Whenever I knocked on your door for help, you guys were there with full-hearted support. Thanks for this amazing help! You all are not just collaborators, I found young, highly motivated, dedicated, genuine researchers in you. I thank Prof. Ole Ammerpohl for the help with

## Acknowledgements

organization of the epigenetic experiments, fruitful discussions and useful suggestions on every step of the epigenetics project.

Samuel Dubin and Alexandra Danenberg (aka Allie), thanks for being my official students. Your hard work was a great help. Thank you so much!

My sincere thanks to former members of the Institute of Immunology, especially Dr. Benjamin Schönbeck and Dr. Henriette Ebsen for becoming my friends at work, Dr. Juliane Fazio and Dr. Malte Puchert for being with me during the initial exciting German life. You all made it very memorable for me! I am thankful to all the current members of the Institute of Immunology, especially Ina Martens and Sandra Ussat for your technical help and Prof. Stefan Schütze for great support in the absence of Dieter and members of the AG Schütze for sharing lively moments, Marie Dowds for sharing interesting scientific and non-scientific discussions.

I owe big thanks to all friends outside lab/work... to my Indian friends, especially Deepak Mishra, Archana Akella and Vedant Tiwari for the frequent Berlin visits and fun time together; Marathi mitra mandal tumche khup abhar! Spaciba to Alexandra Afanasieva and Anastasia Zhuravleva for introducing me to Russian culture and language; Danke to Yvonne Sender for nice talks, Hanna Sender for being my anti-depressant; Heidi Kalbe for preparing extra food during my thesis writing marathon; and Nelli Betke for everything!

I must say 'thanks' to Dr. Sabine Milde, the Graduate Center people and Frau Daniela Suhr, the Cluster office people for friendly support through finances, courses and other activities. My big big thanks to all those people, who directly or indirectly helped me... maybe I missed your name, but my thanks are always for you!

I also met some incredible '*nette Leute*'. My few words for you His-/Her- Highness, 'you pelted stones on me, but I used them to build the house'. You never let me forget that I am a traveler. Thank you so much for being 'statistically significant' part of my success!

Last but not least is thanks to my family for your endless, unconditional love. Because of whom I can see this day and who means the whole world for me! I am lucky to have two families, German and Indian. Thank you so much to my German family, Heike (my German mom!) and Moni (your cowboy!) for being with me. All my life belongs to my parents, sisters (Swapna and Jyotsna), brother-in-laws (Yogesh and Sushil) and on top of everything, my love - my niece and nephews (Swara, Aagam and Swayam)... 'Thank you' is a very small word in return to say!

## 11.2 Curriculum vitae

Name: Jaydeep Bhat  
Address: Institute of Immunology,  
Arnold-Heller-Str. 3,  
UKS-H, Kiel 24105  
Birthdate: 24.09.1985  
Birthplace: Jalgaon (MS), India  
Marital status: Single  
Nationality: Indian

### Education:

since September 2011                      Doctorate of Philosophy (PhD) candidate  
Institute for Immunology, University of Kiel, Kiel,  
Germany  
2006 - 2008                                      Master of Science (Biotechnology)  
North Maharashtra University, Jalgaon, India  
2003 - 2006                                      Bachelor of Science (Biotechnology)  
North Maharashtra University, Jalgaon, India

### Publications (associated with PhD)

1. Bhat J, Sosna J, Fritsch J, Quabius ES, Schuetze S, Zeissig S, Ammerpohl O, Adam D and Kabelitz D. (2016) Expression of non-secreted IL-4 is associated with HDAC inhibitor-induced cell death, histone acetylation and c-Jun regulation in human gamma/delta T-cells. *Oncotarget* 7(40):64743-64756.
2. Bhat J and Kabelitz D. (2015)  $\gamma\delta$  T cells and epigenetic drugs: An useful merger in cancer immunotherapy? *Oncoimmunology*, 4(6):e1006088.
3. Bhat J, Oberg H-H, Kabelitz D. (2015) Modulation of human gamma/delta T-cell activation and phenotype by histone deacetylase inhibitors. *Cellular Immunology*, 296(1):50-56.
4. Chitadze G\*, Lettau M\*, Bhat J, Wesch D, Steinle A, Fuerst D, Mytilineos J, Kalthoff H, Janssen O, Oberg H-H\* and Kabelitz D\*. (2013) Shedding of endogenous MHC class I-related chain molecules A and B from different human tumor entities: Heterogeneous

involvement of the “a disintegrin and metalloproteases” 10 and 17. *International Journal of Cancer*, 133: 1557-1567. (\*equal contribution)

5. Chitadze G, Bhat J, Lettau M, Janssen O and Kabelitz D. (2013) Generation of Soluble NKG2D Ligands: Proteolytic Cleavage, Exosome Secretion and Functional Implications. *Scandinavian Journal of Immunology*, 78: 120-129.

### Associated manuscript(s) ('in preparation')

1. Jaydeep Bhat, Johannes Helmuth, Matthias Hübenthal, Raheleh Sheibani-Tezerji, Swetlana Scheufele, Marcus Lettau, Anke Bergmann, Daniela Esser, Maren Falk-Paulsen, Christoph Kaleta, Reiner Siebert, Philip Rosenstiel, Andre Franke, Ole Ammerpohl, Martin Vingron and Dieter Kabelitz. Epigenetic landscape of human  $\gamma\delta$  T-cells.
2. Jaydeep Bhat\*, Anke Bergmann\*, Christoph Nerl, Silvio Waschina, Christoph Kaleta, Reiner Siebert, Ole Ammerpohl, and Dieter Kabelitz. A case report of an hepatosplenic gamma/delta T-cell lymphoma patient responding to Interferon- $\alpha$  treatment (shared first authors)
3. Jaydeep Bhat, Samuel Dubin, Alexandra Dananberg, Elgar Susanne Quabius, Guranda Chitadze, Jürgen Fritsch, Marie Dowds, Marcus Lettau and Dieter Kabelitz. Epigenetic modulation of NKG2D receptor and ligands: Mechanism of NKG2D ligand release and functional effects.

### Conference presentations

1. Oral presentation: 'Epigenetic landscape of human  $\gamma\delta$  T cells'. 7<sup>th</sup> International Gamma Delta T-cell conference at the King's college in London on June 16 - 19, 2016
2. Poster presentation: 'Generation of non-secreted isoform of IL-4 in human  $\gamma\delta$  T-cells: Interplay between cell death and epigenetic modification' in 4th European Congress of Immunology (ECI) on September 6 - 9, 2015
3. Poster presentation: 'Differential modulation of normal  $\gamma\delta$  T-cells versus tumor cells by HDAC inhibitors' in 11th Spring School on Immunology, German Immunology Society (DGfI), Ettal, Bavaria, Germany, held on March 8 - 13, 2015



4. Poster presentation: 'Molecular and cellular response of human  $\gamma\delta$  T lymphocytes to HDAC inhibitors' in 6th International Gamma-Delta T cell conference, University of Illinois College of Medicine, Chicago, Illinois, USA on May 16 - 18, 2014
5. Poster presentation: 'Dose-dependent effect of HDAC inhibitor on functional responses of human  $\gamma\delta$  T lymphocytes' in 43rd Annual meeting German Immunology Society (DGfI), University of Mainz, Mainz, Germany on September 11 - 13, 2013
6. Oral presentation: 'Mechanisms and implications of NKG2D ligand shedding' in 4th Autumn School of Immunology German Immunology Society (DGfI), Bad Schandau, Germany, on September 30 - October 5, 2012

**11.3 Declaration**

I hereby declare that apart from the supervisor's guidance, the content and design of the thesis is all my own work. This thesis has not been either partially or wholly submitted elsewhere. All sections have been published before or submitted for publication, if not, they remains unpublished. At the beginning of each chapter, it is indicated which experiments were done by the author of this thesis and who else contributed to the presented work. The thesis has been prepared subjected to the Rules of Good Scientific Practice of the German Research Foundation (DFG).

-----

Signature

-----

Date